Molecular Studies on Peptide Deformylase and Methionine Aminopeptidase from *Mycobacterium tuberculosis*

THESIS SUBMITTED TO
THE UNIVERSITY OF KERALA
FOR THE AWARD OF THE DEGREE OF

DOCTOR OF PHILOSOPHY
IN
BIOTECHNOLOGY

UNDER THE FACULTY OF APPLIED SCIENCE

By

SAI SHYAM N

UNDER THE SUPERVISION OF
DR. K. MADHAVAN NAMPOOTHIRI

BIOTECHNOLOGY DIVISION
NATIONAL INSTITUTE FOR INTERDISCIPLINARY SCIENCE AND TECHNOLOGY (NIIST), CSIR, TRIVANDRUM – 695 019
KERALA, INDIA

2011

DEDICATED AT

THY LOTUS FEET OF

BHAGWAN SRI SATHYA

SAI BABA

National Institute for Interdisciplinary Science and Technology (NIIST)

Council of Scientific & Industrial Research (CSIR)
(Department of Scientific & Industrial Research, Ministry of S&T, Govt. of India)
Industrial Estate P.O., Trivandrum - 695 019
Kerala, INDIA

K Madhavan Nampoothiri, *PhD*
Scientist
Biotechnology Division

Tel:+91-471-2515 366
Fax:+91-471-24 91 712
Tel/fax:+91-471-24 95 949
E-mail: madhavan85@hotmail.com

5 th July, 2011

CERTIFICATE

This is to certify that the work embodied in the thesis entitled, ***"Molecular Studies on Peptide Deformylase and Methionine Aminopeptidase from Mycobacterium tuberculosis"*** is based on the original research work carried out by Mr. Sai Shyam N under my supervision in Biotechnology Division, NIIST (CSIR), Trivandrum-19, and that no part of this work has been submitted previously for the award of any degree.

Dr. K Madhavan Nampoothiri

Research Supervisor

Declaration

I hereby declare that the Ph. D. thesis entitled, **"Molecular Studies on Peptide Deformylase and Methionine Aminopeptidase from *Mycobacterium tuberculosis*"** is an independent work carried out by me at the Biotechnology Division, National Institute for Interdisciplinary Science and Technology-CSIR, Trivandrum, under the supervision of Dr. K. Madhavan Nampoothiri and it has not been submitted elsewhere for any other degree, diploma or title.

In keeping with the general practice of reporting scientific observations, due acknowledgements have been made wherever the work described is based on the findings of other investigators.

Thiruvanthapuram **Sai Shyam N**

July 2011

ACKNOWLEDGEMENTS

This thesis arose in part out of years of research that has been done since I joined National Institute for Interdisciplinary Science and Technology (NIIST), CSIR, Thiruvananthapuram in 2005. During this period a great number of people who have contributed in assorted ways to the research and making of this thesis deserve special mention. It is a pleasure to convey my gratitude to all of them in my humble acknowledgment.

First and foremost I would like to express my love, respect and gratitude towards my research supervisor, Dr. K. Madhavan Nampoothiri for introducing me into this topic of research with contemporary relevance and into many aspects of recombinant DNA technology. I sincerely thank him for providing me constant supervision, advice, and guidance from the very early stage of this research until the last day of making this thesis. He was an unflinching source of encouragement in pursuing many endeavors during this period. In person, he was more than a friend, supporting me through the toughest times in my pursuit of Ph.D. His passion for science and his scientific intuitions have inspired and enriched my growth as a researcher. I am indebted to him in more ways than he knows.

I am happy to acknowledge my debt to Professor Ashok Pandey, Head, Biotechnology Division, NIIST for his constant encouragement and support during my tenure in the division as a research student. I consider it to be a great honour to have associated with a scientist of his stature which has provided me opportunities to interact and collaborate with many eminent personalities of both national and international stature in science. Apart from providing wonderful environment and facilities to work, he has always extended his personal care in making the system in place in division. I am

grateful to him in every possible way for nourishing my intellectual maturity that I will benefit from for a long time to come.

I express my gratitude to Dr Suresh Das, Director NIIST for providing me the necessary facilities and infrastructure to carry out my research work at NIIST. Thanks are also due to former Directors of NIIST during my tenure, Professor T.K. Chandrasekhar and Dr. B. C Pai, for providing me all facilities at the laboratory.

I express my heart-felt gratitude to Professor M. V. George, Emeritus Professor, Photosciences Division, NIIST for having come down to my level and encouraged me all through out my research work. His unending passion and curiosity for science and scientific topics have made the association with him an unforgettable one.

I record my gratitude to Professor Ramachandran Murugesan, Emeritus Professor, School of chemistry, Madurai Kamaraj University (MKU) for his collaborative support on molecular dynamics simulation and molecular docking works. I take this opportunity to thank Mr. Pandian Sokkar, MKU for all his assistance in performing molecular modelling experiments and for his invaluable contributions in publishing this study. I am deeply indebted to Professor P. Gunasekharan, Head, School of Biological Sciences, MKU for selecting me as a visting fellow in his laboratory and for taking me through various aspects of molecular biology during this time. Thanks are due to Dr. Rajendran, for guiding me in these aspects of molecular biology. I express my gratitude to Mr. Rajesh, Dr. Gobi, Mr. Ponraj and Mr. Ganesh Babu, MKU for their support during my stay.

I thank Dr. Rajeev K. Sukumaran, Scientist, NIIST for all the fruitful discussions we had together on various topics. I thank him for kindly granting me his time even for answering some of my unintelligent questions about various topics. I deeply acknowledge the technical supports provided the technical staffs of the division, Dr. Vijayalekshmi Amma, Mr. SivankuttyNair and Mr. Prakash. I also wish to remember the

timely help rendered by Dr. Sindhu, Dr. Binod, Mr. Kiran Kumar, Dr. Syed Dastagar and Dr.Sudheer kumar Singh during different stages of the study. At this point I remember the affection and care shown to me by late Dr. P. Prema, former senior scientist in the division.

I thank Mr. Jino George, Photo sciences division and Dr. Praveen, inorganic chemistry division for their kind help in performing CD spectroscopy and Atomic absorption spectroscopy, respectively.

Friends in biotechnology division and other divisions have been an integral part of my life during this period of time. The unforgettable associations with many of them will be cherished all through out my life. I owe my sincere thanks to my senior colleagues, Dr. Babita, Dr. Rojan, Dr. Dhanya, Ms. Reeta. R Singhania, Dr.Syed U.Ahamed, Mrs. Sumantha A, Dr. Shwetha S, Dr. Anil Patel, Dr. Anisha Dr. Nila and Dr. Nicemol, for all the timely support and valuable suggestions provided throughout my work. Special thanks are due to Mr. Shyam Krishna for his friendship and timely help during the preparation of this thesis. I wish to remember the wonderful moments shared along with late Mr. Rubex, who lives in our heart forever. I thank all the project students, Ajeena, Anjana, Salma, Sumi and Brintha, who have contributed to various aspects of this thesis. I am deeply grateful to Ms. Arya Nandan S for her excellent support in performing many of the studies in my thesis. I extend my gratitude towards Mr. Vipin, Mr. Kiran, Mr. Kuttiraja, Mr. Abrham and Mr. Nobel for their association with me at various stages of this work. I am grateful for time the spent with my friends, Aswathy, Bindu, Raji, Nisha, Nimisha, Ushasree, Vidya, Deepthy Anu, Deepa, Anusree, Varsha, Janu, Lalitha, Divya Gincy, Sajna, and thank them for their loving company, encouragement and moral support throughout. I extend my warm thanks to all other friends in the division for making the lab a wonderful place to work. I express my love and gratitude towards Jathish, Jino, Sankar, Akhil, Prashanth, Ramakrishnan, Anas,

Sreejith, Anupama, Divya, Sarin, Lijin, Ranjith,Shajesh and other friends in NIIST. I also acknowledge the support from the staffs from the administration wing, library and all other non-scientific staffs at NIIST.

I am grateful and dedicated my life to my wife, Jyothi, who during my years of study had believed in me and provided all the emotional support. This thesis, in part, is the result of her understanding, sacrifice and moral support that could only stem from a loved one. I thank her profusely for being with me at hard times as a refuge to solve all my personal and research frustrations.

I am deeply grateful to my parents and my other family members for their constant love and care that have been a great motivation for these successful efforts.

I thank DBT and CSIR for their financial support in the form of research fellowships.

Lastly, but above all, I express my love and gratitude to my lord and spiritual guru, Bhagwan Sri Sathya Sai Baba for what he has provided me in my life, for now for future.

Sai Shyam N

PREFACE

Mycobacterium tuberculosis (Mtb), the causative agent of tuberculosis (TB), has plagued mankind since the beginning of medical history. The discovery of anti-tuberculosis agents that target new pathways is crucial for effective short-term therapy against multi drug-resistant (MDR) and extensively drug-resistant (XDR) strains of *Mycobacterium tuberculosis* and latent tuberculosis (TB). In prokaryotic translation, the initiator methionine is always formylated, leading to the formylation of all nascent polypeptides at the amino-terminal end. Generally, the N-terminal methionine has to be cleaved of following translation for majority of the polypeptides for their maturation and folding. Peptide deformylase (PDF) catalyzes the removal of formyl group from the initiator methionine followed by the N-terminal methionine excision (NME) by the second enzyme Methionine Aminopeptidases (MAP). Since deformylation and NME are vital for survival of bacteria PDF and MAP are considered as potent drug target for developing next generation antimicrobials.

In the present study, we have cloned and expressed the recombinant PDF (*def* / Rv0429c) and two MAPs (*map*A / Rv0734 and *map*B / Rv2861c) of *M. tuberculosis* (MtbPDF and MtbMAPs) to characterize these enzymes at molecular level to bring out their salient structural and biochemical features, which might be useful in developing specific inhibitors against these enzymes. The study brought out the amino acid sequence variations in MtbPDF with other well characterized bacterial PDFs and mitochondrial PDFs and suggested possible structural and biochemical significance of these variations. Similarly, the study revealed the significant differences in enzyme activity and metal ion preferences of the two hypothetical MtbMAP proteins. The structure-function relationships of both MtbMAP proteins were analyzed by site-directed mutagenesis to

bring out the relevance of each residue in activity and stability of MAPs in *M. tuberculosis*.

The thesis has been framed into seven chapters. Chapter 1 gives an introduction about TB, TB drugs and current treatment of TB, emphasizing on the need for novel TB-drugs due to the emergence of multidrug resistant strains. This is followed by a detailed review of literature on novel genomic drug targets in *M. tuberculosis*, pertaining mainly to NME enzymes such as PDF and MAP involved in the peptide processing- the development of NME enzymes as drug targets, the current set of inhibitors available against them and the need for detailed characterization of these enzymes to improve the current set of inhibitors into TB-drugs. Chapter 2 describes the general experimental methodologies and protocols used in the study. Chapter 3 describes the cloning of *def* gene of *M. tuberculosis* into *E. coli* expression vectors, its recombinant expression, purification, biochemical and biophysical characterizations. Chapter 4 describes the construction and characterization of relevant site-directed mutants of MtbPDF to bring out their structural and functional role in activity and stability of the enzyme. This chapter also brings out the relevance of glycine residue in motif III of MtbPDF structure by biochemical and molecular modeling studies. Chapter 5 describes the molecular cloning, recombinant expression, purification and biochemical characterization of MtbMAP A and MtbMAP B enzymes of *M. tuberculosis*. Chapter 6 deals with the construction and characterization of substitution mutants corresponding to the metal binding residues and residues lining the substrate binding pocket of MtbMAP B protein. Importance of a Mycobacterium specific insertion region in the structure of MtbMAP A for its activity and stability has been characterized by deletion mutagenesis. Chapter 7 summarizes the entire work and the conclusions drawn from the study towards the future directions. This is followed by a bibliographic section. Finally, two annexure are

attached. List of the major equipments used is included in annexure 1 and the list of publications, honours and awards are attached as annexure 2.

Sai Shyam N

****

CONTENTS

LIST OF TABLES

****

LIST OF FIGURES

****

ABBREVIATIONS

%	Percentage
Δ164-176	Deletion of amino acids from position 164 to 176
° C	Degree celsius
µ	Micro
µg	Microgram
µg / ml	Microgram per microlitre
µl	Microlitre
µM	Micro molar
aa	Amino acid
AAS	Atomic absorption chromatography
BCIP/NBT	5-Bromo-4-Chloro-3'-Indolyl Phosphate *p*-Toluidine /Nitro-Blue Tetrazolium Chloride
bp	Base pair
BSA	Bovine serum albumin
CD	Circular Dichroism
Co^{2+}	Divalent cobalt
DMSO	Dimethyl Sulphoxide
DNA	Deoxyribo Nucleic acid
dNTP	Deoxynecleotide phosphate
DOTS	Directly observed treatment, short-course
DTT	Dithiothreitol
EDTA	Ethylene diamine tetraacetic acid
Fe^{2+}	Divalent Iron

g	Gram
G151D	Glycine 151 to Asparatate
h	Hour
H_2O_2	Hydrogen peroxide
IgG	Immunoglobulin G
IPTG	Isopropylβ-D-1-thiogalactopyranoside
Kan	Kanamycin
K_{cat}	Catalytic turn-over number
kDa	Kilo Dalton
K_m	Michealis-Menten constant
LB	Luria Bertani
mA	Milli amperes
MDR-TB	Multiple drug resistant-Tuberculosis
mg	Milligram
mg/ ml	Milligram per millilitre
min	Minute
ml	Millilitre
mM	Milli molar
MtbMAP	*Mycobacterium tuberculosis* methionine aminopeptidases
MtbPDF	*Mycobacterium tuberculosis* Peptide deformylase
N-f-M	*N*-formyl-Met
N-f-MAS	*N*-formyl-Met-Ala-Ser
N-f-MLF	*N*-formyl-Met-Leu-Phe
ng	Nano gram
Ni^{2+}	Divalent nickel
nM	Nano molar

NME	N-terminal methionine excision
NTA	Nitrilotriacetic acid
OD	Optical density
PCR	Polymerase Chain Reaction
PDB	Protein Data Bank
pH	Hydrogen ion concentration
PMSF	Phenyl methane sulphonyl fluoride
*p*NA	*para*-Nitro aniline
ps	Pico second
s	Second
SDS-PAGE	Sodium dodecyl sulfate polyacrylamide gel electrophoresis
TNBSA	2, 4, 6-Trinitrobenzenesulfonic acid
V_{max}	Velocity maximum of an enzyme reaction
XDR-TB	Extensively drug resistant-Tuberculosis
θ	Mean residue ellipticty

****

CHAPTER 1

Introduction and Review of Literature

CHAPTER 1

Introduction and Review of Literature

1.1 Introduction

Tuberculosis (TB) still remains as one of the major threats to many lives all over the world. It is caused by *Mycobacterium tuberculosis*, the most dreadful bacterial pathogen in the history of mankind. The disease affects 1.8 billion people per year which is equal to one-third of the entire world population (Wirth et al., 2008). The World Health Organization predicts that between 2002 and 2020, 36 million people would have died from tuberculosis. TB is on the increase in recent years, largely owing to human immunodeficiency viral (HIV) infections, decline in the socio economic and moral standards, immigration, increased trade (WHO, 2005).

M. tuberculosis is highly successful pathogen with its remarkable ability to persist intracellularly even in the presence of an intact immune system. The current treatment for TB was established over 30 years ago with a set of drugs developed in 1940s. This ‘‘short-course’’ regimen comprises multiple drugs to be taken daily for at least six months (Lamichhane, 2011).When strictly followed, this chemotherapy program has proven to be effective; however, the inconvenience of this drug course has precluded rigorous adherence and has led to the development of multidrug-resistant (MDR) strains of *M. tuberculosis*. Nearly 50 million people all around the world have already been infected with drug-resistant TB (WHO, 2005). For treating MDR-TB, a set of second line drugs were formulated, which are more toxic, less active and more expensive and it

prolong the treatment time compared to the standard first-line drugs. Any mismanagement of treatment of MDR-TB leads to extensively drug-resistant tuberculosis (XDR-TB), which is too difficult to cure with the current set of drugs (Onyebujoh et al., 2005).

Another unsolved problem with *M. tuberculosis* infection is its latency, which is an asymptomatic state that can persist for many years in the host, requiring only a weakened immune response to get activated to cause active TB (Zhang, 2004). It is estimated that among the approximately 2 billion persons throughout the world with latent TB infection, between 100 and 200 million will develop active disease during their lifetimes. The current antibiotics show only slight activity against persistent organisms that are in the dormant phase and they do not eliminate all the dormant populations (Zhang, 2005). Developments of efficient drugs for treatment of latent TB infections have been deemed essential to the elimination of tuberculosis in low-incidence countries such as the United States (O'brien and Nunn, 2001).

Active immunization or vaccination appear to be an essential component in controlling of tuberculosis, although current vaccine strategies have been ineffective in bringing the disease under control. To date, well over one billion people have been vaccinated with Bacillus Calmette-Guérin (BCG) since the first inoculation given in 1921 (Reed et al., 2003). BCG vaccine was not effective in reducing the incidence of infectious pulmonary cases in adults, even though the vaccine showed prevention of childhood TB. Any live vaccine would cause concerns in immune-compromised populations like HIV infected patients (Styblo K and Meijer J, 1976).

There is an urgent need and significant interest in developing new TB drugs (Global Alliance for Tuberculosis Drug Development, 2001; O'brien and Nunn, 2001). Over past 40 years no new effective drugs for treating tuberculosis has been discovered (Khasnobis *et al.*, 2002). To achieve global control of this epidemic, the new TB drugs should be able to: (1) shorten treatment duration (2) target MDR or XDR strains (3) simplify treatment by reducing the daily pill burden (4) lower dosing frequency (5) reduce the burden of both active as well as dormant bacterial load and (6) be co-administered with HIV medications (Koul et al., 2011). In developing new TB drugs, it is crucial to identify the best drug targets in the tubercle bacillus. Current TB drugs inhibit particular targets in DNA synthesis, RNA synthesis, cell wall synthesis and energy metabolism pathways (Zhang, 2005). In view of drug resistant TB problems, new drugs that inhibit novel targets, different from currently used drugs, are needed (Zhang and Amzel, 2002). Any new target for TB drug development should be gene products involved in at least some of the vital physiological aspects such as growth and viability, various metabolism, survival or persistence of the bug.

The availability of the complete genome sequence of H37Rv (laboratory strain) and CDC1551 (clinical strain) strains of *M. tuberculosis* (Cole et al., 1998; Fleischmann et al., 2002) has opened new avenues for TB drug discovery in the new millennium. Contemporary completion of the human genome project (International Human Genome Sequencing Consortium, 2001) has paved ways to compare the genomes of host and pathogen and list out potential gene products that might be essential for the survival of pathogen and non-essential for the host cells. Advances in some functional genomics

tools like targeted gene knock outs, transposon mutagenesis, conditional mutagenesis, genomic and transcriptomic analysis have aided researchers in validating some of these genes as drug targets in *M. tuberculosis* (Warner and Mizrahi, 2004).

In post-genomic era, comparative genomics approach between *M. tuberculosis* and closely related species, both pathogenic like *M. leprae* and *M. bovis* (http://www.sanger.ac.uk) and non-pathogenic like *M. smegmatis* and *M. marinum* (http://www.tigr.org) have helped in further refining the list of genes comprising the essential virulence gene set. This would be useful in restricting targets to those unique mycobacterial genes whose inactivation will not adversely affect the normal intestinal flora（Warner and Mizrahi, 2004). These approaches have produced a list of *M. tuberculosis* specific drug targets which mostly includes growth-essential genes with no close homologs in host or host gut flora. This list includes mainly enzymes involved in Mycobacterial cell wall biosynthesis (eg. *kasA*, *kasB*), Mycobacterial two-component systems (eg. *devR-devS*), some virulence factors (eg. fibronectin-binding proteins) etc. (Chopra et al., 2003; Hasan et al., 2006). Many non-essential genes in the *in vitro* screening have been reported to be essential for survival of the bug *in vivo* in mice models. Some of these genes like isocitrate lyase (*icl)* (McKinney et al., 2000) and methyl transferases (*pcaA*) (Glickman et al., 2000) have been considered as potent persistant related drug target, which would potentially eliminate the persistent bacilli *in vivo* (Chopra et al., 2003; Hasan et al., 2006).

Apart from these *M. tuberculosis* specific drug targets, another list of "druggable enzymes" are available as a result of genome wide scanning of different pathogenic

microbes. They are classified under the broad category of metabolic drug targets. This list includes enzymes involved in essential check-point reactions in vital metabolic pathways, whose function cannot be compensated for by another enzyme homolog in the organism (Yeh et al., 2004). These enzymes may not be specific to *M. tuberculosis*, but some of these enzymes might have been proven successful as drug target in the treatment of other infectious disease with identified druggable molecules inhibiting them. It would be worth considering and characterizing these enzymes as potential drug targets in *M. tuberculosis* (Robertson, 2005). This kind of approach will be advantageous in accelerating the drug discovery process for TB, since there are druggable targets and drug-like molecules already available and the researchers only need to characterize their *M. tuberculosis* homologs to identify salient structural and functional features so as to modify the drug-like molecule to specifically suit the target in *M. tuberculosis*. It is highly essential to consider both biological druggability (essentiality for survival) and chemical druggability (availability of drug like molecules) of a drug target in order to accelerate the drug discovery process (Kinnings et al., 2010). Comparing the KEGG (Kyoto Encyclopedia of Genes and Genomes) (Kanehisa et al., 2002) metabolic pathway database for *M. tuberculosis* and *Homo sapiens* suggested many unique metabolic pathways in pathogens which do not appear in the host (Anishetty et al., 2005). Potential metabolic drug targets were suggested from pathways related to lipid metabolism, carbohydrate metabolism, amino acid metabolism, energy metabolism, vitamin and cofactor biosynthetic pathways and nucleotide metabolism (Anishetty et al., 2005; White et al., 2004).

The most fertile source of antibacterial targets in any bacteria has been the protein biosynthesis machinery, especially the ribosome (Sutcliffe, 2005). Apart from ribosome, other enzymes required for efficient and accurate protein synthesis has been investigated and identified as suitable drug targets (Pohlmann and Brotz-Oesterhelt, 2004). The protein synthesis involves three sequential steps such as the initiation, elongation and termination. Although the process exhibits overall similarity between eukaryotes and prokaryotes, subtle differences occur at the translation initiation step. In eukaryotes, except in organelles (mitochondria and chloroplast), the first amino acid incorporated during polypeptide biosynthesis has been shown to be methionine. On the other hand, in prokaryotes the process in initiated with N-formyl-Methionyl-tRNA leading to the formylation of all nascent polypeptides at the N-terminal. This difference has led to variations in the first co-translation step on the nascent polypeptide. The co-translational peptide processing or N-terminal methionine excision is an important step in protein biosynthesis where the initiator methionine is cleaved from vast majority of the nascent polypeptides (Meinnel et al., 1993). Since the N-terminal peptidases cleaving the initiator methionine have been found to be unable to use formylated peptides as substrates, their removal has been a mandatory step in prokaryotes for mature polypeptide synthesis (Solbiati et al., 1999). The peptide deformylase (PDF) enzyme catalyzes the deformylation of N-formyl-methionine of the nascent polypeptides in prokaryotes. Since the NME process is a mandatory step for proper folding and localization of polypeptide, the importance of deformylation has been envisaged long ago (Adams, 1968). The deformylated polypeptides form substrates for the subsequent enzyme in NME,

methionine aminopeptidase (MAP), which is a ubiquitous enzyme involved in cleaving the initiator methionine in all compartments of protein synthesis (Bradshaw et al., 1998). Gene inactivation experiments on genes encoding PDF (*def*) and MAP (*map*) in many eubacteria like *Escherichia coli*, *Salmonella typhimurium* and *Thermus thermophilus* (Chang et al., 1989; Miller et al., 1989; Meinnel and Blanquet, 1994) have proved these enzymes to be essential for cell survival in bacteria. Both *def* and *map* genes are part of the ~300-gene minimal genome requirement of eubacteria (Hutchison et al., 1999). In the advent of genome sequencing, both these genes were reported from the genome of many pathogens like *Streptococcus*, *Pseudomonas* and *Mycobacterium tuberculosis* (Mazel et al., 1997). Nuclear-encoded *def* genes with mitochondrial target sequences have been identified from many eukaryotes including human (Giglione et al., 2000). Interestingly, many of the PDF inhibitors have already been reported to affect bacterial growth, without any toxic effects for human cells (Nguyen et al., 2003; Serero et al., 2003). The NME enzymes have never been used as a target for antibiotics in human therapeutics and have therefore never been subject to selection pressure and the development of resistance (Giglione et al., 2000). For these reasons, it is worth characterizing these enzymes as drug targets in bacteria.

Except for a few reports, no detailed biochemical characterizations of the NME enzymes from *M. tuberculosis* have been carried out. In the present study, we attempt to characterize both these enzymes involved in the peptide processing or NME pathway at their molecular level, in order to bring out their salient catalytic and biochemical properties prior to validating their use as drug targets for anti-TB drug discovery.

1.2 Objectives

To characterize the enzymes, peptide deformylase (PDF) and methionine aminopeptidases (MAP) involved in the peptide processing of *M. tuberculosis* by,

a) Cloning of peptide deformylase gene (*def,* Rv0429c) of *Mycobacterium tuberculosis* H37Rv.
b) Cloning of methionine aminopeptidase genes (*map*A, Rv0734), (*map*B, Rv2861c) of *M. tuberculosis* H37Rv.
c) Expression of MtbPDF, MtbMAP A and MtbMAP B proteins in *E. coli* as recombinant proteins.
d) Purification and biochemical characterization of MtbPDF and MtbMAPs expressed in *E. coli.*
e) Site-directed mutagenesis studies on *def*, *map*A and *map*B genes of *M. tuberculosis* H37Rv.

1.3 Review of literature

1.3.1 Tuberculosis (TB) - a recent update

In 1882, Robert Koch identified *Mycobacterium tuberculosis* as the causative agent of tuberculosis (TB). *Mycobacteria* belong to the family *Mycobacteriaceae* and are members of the CMN group (*Corynebacteria, Mycobacteria and Nocardia*). The family *Mycobacteriaceae* is grampositive, nonmotile, catalase-positive, have a rodlike to filamentous morphology and can be pleomorphic. Mycobacteria are acid-fast rods of variable appearance, approximately 0.2-0.6 by 1-10 μm. *M. tuberculosis*, a slow growing obligate aerobe, is a facultative intracellular parasite, usually of macrophages, and has a

slow generation time 15-20 h, a physiological characteristic that may contribute to its virulence (*http://www.textbookofbacteri ology.net/tuberculosis.html)*.

The genus Mycobacterium consists of 127 species according to the latest approved list of bacterial species. Mycobacteria other than *M. tuberculosis* are commonly referred to as atypical or non-tuberculous mycobacteria (NTM). However, *M. leprae, M. ulcerans,* which often cause disease in normal hosts are often not regarded as NTM. The remaining species are considered nonpathogenic or opportunistic pathogens and cause disease when host-defences are compromised

TB kills nearly two million people annually and has been a major health threat for centuries (WHO report, 2009). For the previous year (2010), it was anticipated that there will be about 9.8 million new cases, more than in any other year in the history (Dye and Williams, 2010). This situation highlights the relative shortcomings of the current treatment strategies for TB and the limited effectiveness of public health systems, particularly in resource-poor countries where the main TB burden lies (Koul et al., 2011). The current treatment of TB was established over 30 years ago using drugs that were developed as early as the 1940s. This ‘‘short-course’’ regimen comprises multiple drugs like isoniazid (INH), rifampicin(RIF), pyrazinamide (PZA) and ethambutol (EMB) to be taken daily for at least six months (Blumberg et al., 2003). Although *M. tuberculosis* replicates at a slower rate than most bacteria, the current treatment scheme of four drugs over six months renders this pathogen particularly prone to developing resistance. Currently, 10–20% of all TB cases in each region are of the MDR type (resistant to INH and RIF) and that by now, XDR-TB, which is resistant to virtually all the effective anti-

TB drugs, has been reported in 55 countries across the globe (Parida and Kaufmann, 2010; WHO report, 2009a). The world's two most populous countries, India and China, account for more than 50% of the world's MDR-TB cases and as such these countries are encountering a high and increasing TB disease burden (WHO report, 2009). Half a centaury of chemotherapy has left one-third of the world's population with asymptomatic dormant or latent form of *M. tuberculosis* (**Fig 1.1**) with a life long risk of disease reactivation (Barry et al., 2009). The hope of eradicating TB was shattered by the emerging HIV/AIDS crisis. Reactivation of latent TB is a high risk factor for disease development particularly in HIV/AIDS cases, on an anti-tumor necrosis factor therapy or with diabetes (Barry et al., 2009; Parida and Kaufmann, 2010). Today, one-eighth of the two million deaths caused by TB occur in individuals co-infected with HIV and *M. tuberculosis* (Parida and Kaufmann, 2010). Drug–drug interactions of available TB drugs with certain anti-HIV treatments or diabetes drugs have made the situation worse (Koul et al., 2011).

All these challenges and obstacles have to be surpassed in the future drug discovery efforts for bringing out novel drugs for TB. The situation is further hampered by the unfavourable economics of TB drug development and the lack of proper policy incentives.

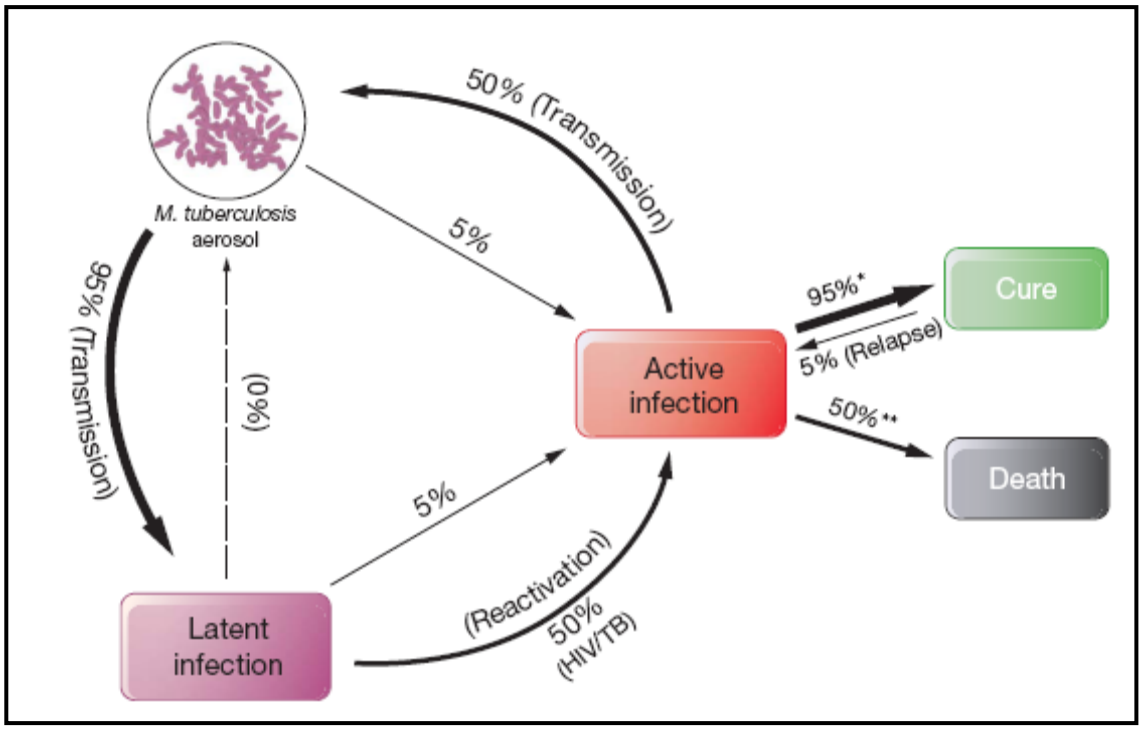

Fig 1.1: Stages in *M. tuberculosis* infection (Adopted from Koul et al., 2011)

1.3.2 Current TB therapy - Problems of drug resistance and persistence

The current TB chemotherapy evolved from numerous experimental and clinical studies primarily conducted between the 1950s and 1970s (Fox et al., 1999). The current recommended standard TB chemotherapy, called DOTS (directly observed treatment, short-course), is a six month therapy consisting of an initial two-month phase of treatment with four drugs, INH, RIF, PZA, and EMB (**Fig 1.2**), followed by a continuation phase of treatment with INH and RIF for another four months (Blumberg et al., 2003). Strictly followed, DOTS can cure up to 95% of TB cases. The lengthy six month therapy makes patient compliance difficult, and noncompliance is a frequent source of drug-resistant

strains. MDR-strains are at least resistant to INH and RIF (Oyenbujoh et al., 2005) and in cases of high incidence of MDR-TB the cure rate for DOTS is less than 50%. WHO recommends DOT-Plus, which includes second-line TB drugs for treatment of MDR-TB (WHO report, 2005). The second-line drugs include kanamycin, amikacin, capreomycin, cycloserine, *para*-amino salicylic acid, ethionamide / prothionamide, thiacetazone and flouroquinones (Zhang, 2005; Oyenbujoh et al., 2005). However, treatment of MDR-TB with DOTS-Plus takes up to 24 months and is highly costly and has significant toxicity (Zhang, 2005). Resistance development during DOT-Plus leads to extensively drug resistant form of TB (XDR-TB), which is difficult to cure with current drugs (Burman, 2010).

Genetic resistance to an anti-tuberculosis drug is due to spontaneous chromosomal mutations at a frequency of 10^{-6} to 10^{-8} mycobacterial replications. INH resistance is the most common form of anti-TB drug resistance encountered, whether in isolation or in combination with other drugs (WHO report, 2009). Resistance against most of the first and second line drugs are observed at various levels in MDR and XDR-TB cases. Researchers have characterized the molecular mechanism of drug actions and resistance development in *M. tuberculosis* against most of these drugs (Zhang and Yew, 2009). The mechanisms of drug resistance in *M. tuberculosis* against various drugs are summarized in **Table 1.1** (Zhang and Yew, 2009).

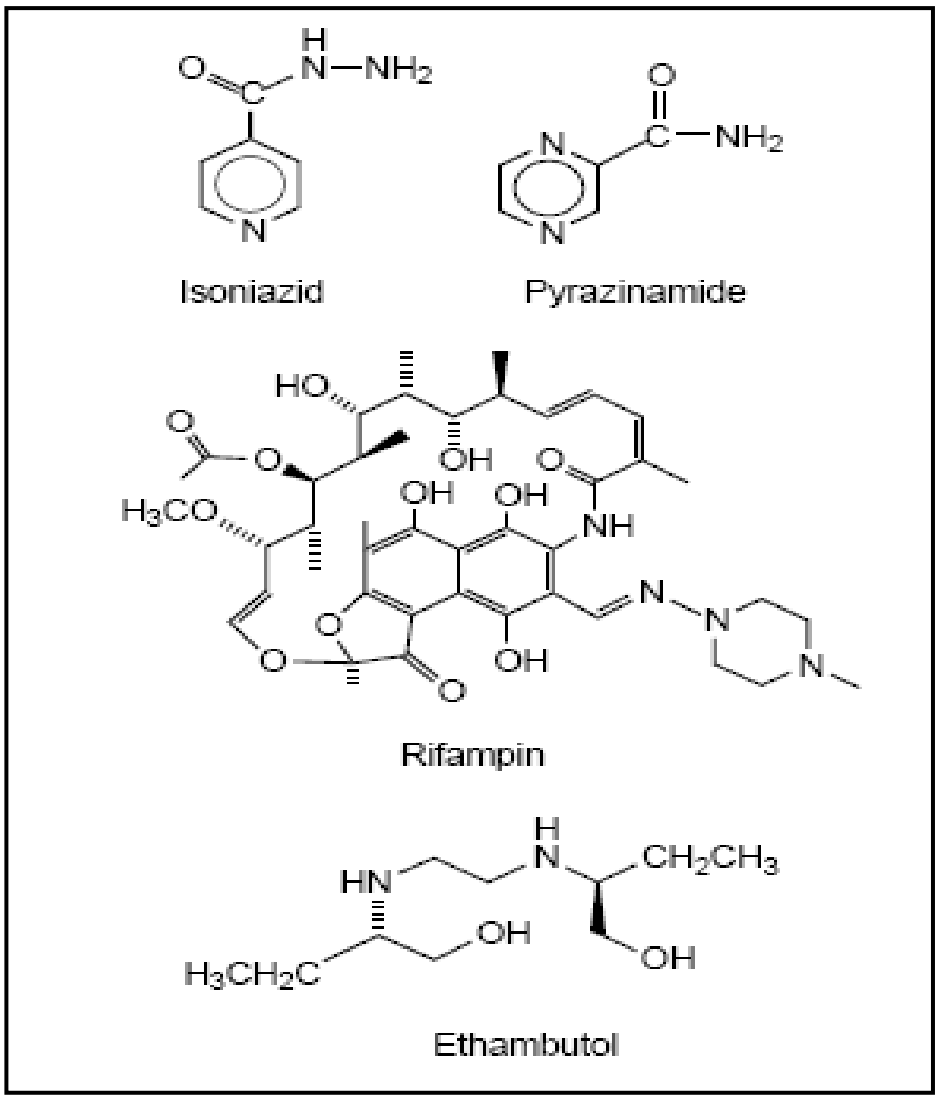

Fig 1.2: Structures of frontline TB drugs

Table 1.1 Mechanisms of drug resistance in *M. tuberculosis*

Drug (year of discovery)	MIC µg/ml	Gene(s) involved in resistance	Gene function	Role	Mechanism of action	Mutation frequency %
Isoniazid (1952)	0.02–0.2	*kat*G *inh*A	Catalase-peroxidase Enoyl ACP reductase	Pro-drug conversion Drug target	Inhibition of mycolic acid biosynthesis and other multiple effects	50–95 8–43
Rifampicin (1966)	0.05–1	*rpo*B	β subunit of RNA polymerase	Drug target	Inhibition of RNA synthesis	95
Pyrazinamide (1952)	16–50 (pH 5.5)	*pnc*A	Nicotinamidase/pyrazinamidase	Pro-drug conversion	Depletion of membrane energy	72–97
Ethambutol (1961)	1–5	*emb*B	Arabinosyl transferase	Drug target	Inhibition of arabinogalactan synthesis	47–65
Streptomycin (1944)	2–8	*rps*L *rrs* *gid*B	S12 ribosomal protein 16S rRNA rRNA methyltransferase (G527 in 530 loop)	Drug target Drug target Drug target	Inhibition of protein synthesis	52–59 8–21 ?
Amikacin/kanamycin (1957)	2–4	*rrs*	16S rRNA 16S rRNA	Drug target	Inhibition of protein synthesis	76
Capreomycin (1960)		*tly*A	2′-O-methyltransferase			
Quinolones (1963)	0.5–2.5	*gyr*A *gyr*B	DNA gyrase subunit A DNA gyrase subunit B	Drug target	Inhibition of DNA gyrase	75–94
Ethionamide (1956)	2.5–10	*eta*A/*eth*A *inh*A	Flavin monooxygenase	Prodrug conversion Drug target	Inhibition of mycolic acid synthesis	37 56
PAS (1946)	1–8	*thy*A	Thymidylate synthase	Drug activation?	Inhibition of folic acid and iron metabolism?	36

MIC = minimum inhibitory concentration; ACP = acyl carrier protein; PAS = para-aminosalicylic acid.

Antibiotics are active against growing bacteria but are ineffective against non-growing bacteria. There are at least three types of non-growing bacteria that are phenotypically resistant to antibiotics: (a) the stationary phase bacteria (b) residual survivors or persisters not killed during antibiotic exposure when a growing culture is treated with antibiotics and (c) dormant bacteria. Although all three types of phenotypic resistance may share some common mechanism, the mechanism of phenotypic resistance in *M. tuberculosis* is unknown (Zhang, 2005; Hasan et al., 2006).

According to Mitchison (1979), tubercle bacilli in lesions consist of at least four different subpopulations: (a) those that are actively growing, which are killed primarily by INH (but in case of INH resistance, are killed by RIF, streptomycin, or inhibited by EMB) (b) those that have spurts of metabolism, which are killed by RIF (c) those that are of low metabolic activity and reside in acid pH environment, which are killed by PZA and (d) those that are "dormant," which are not killed by any current TB drug. There is currently considerable interest in the study of mycobacterial persistence and dormancy (Flynn and Chan, 2001; Gomez and McKinney, 2003; Zhang, 2004), with the aim to better understand the basis of this phenomenon and devise therapeutic strategies that target the persistent or dormant organisms for improved treatment of TB. Even after lot of efforts to identify drugs against persistent dormant population, there is no effective drug to lower the burden of dormant *M. tuberculosis* (Zhang, 2004; Zhang, 2005).

1.3.3 Novel drug targets in *M. tuberculosis*

In today's post-genomic era, new molecular biology and genetics tools are complemented with whole genome sequences of *M. tuberculosis* (Cole et al., 1998), which has allowed high-throughput studies to identify possible drug targets against TB. Forward genetic approaches that assess if a gene is essential provide a rudimentary evaluation of a gene product's worthiness as a potential drug target (Lamichhane, 2011). Sassetti and coworkers develop a high-throughput technique called Transposon Site Hybridization (TraSH) to identify the *M. tuberculosis* genes required for the growth both *in vitro* and *in vivo* (Sassetti et al., 2003; Rengarajan et al., 2005). Based on this list of essential genes in

M. tuberculosis, high-throughput structural genomics studies have been carried out, including comparative proteomics studies, to prioritize functionally important targets essential for growth, persistence and virulence of *M. tuberculosis* (Ioerger and Sacchettini, 2009). These approaches along with other advanced genetic and biochemical tools have produced a long list of probable drug targets in *M. tuberculosis* targeting either actively growing bug or the dormant populations. A summary of potent novel drug targets sought out for future drug discovery in *M. tuberculosis* is schematically represented in **Fig 1.3** (Lamichhane, 2011). They can be classified as targets for active TB and targets for dormant TB.

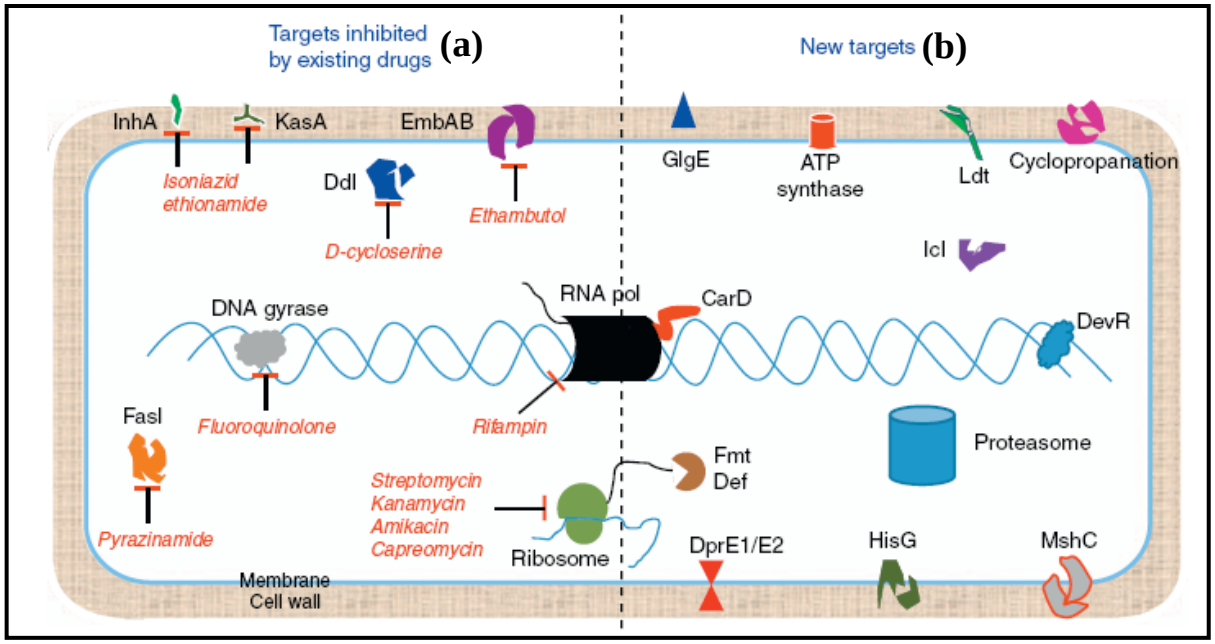

Fig 1.3: Drug targets in *M. tuberculosis*; (a) Inhibited by existing drugs; Fatty acid synthase (FasI); enoyl-acyl-carrier protein-reductase (InhA); β-ketoacyl ACP synthase (KasA); arabinosyltransferase (EmbAB); D-alanyl-D-alanine ligase (Ddl); DNA dependent RNA polymerase (RNA pol); DNA gyrase and ribosome. **(b) Novel drug targets**; maltosyltransferase (GlgE); ATP synthase; L,D-transpeptidase (Ldt); decaprenylphosphoryl-b-D-ribose20-epimerase (DprE1/E2); ATP phosphoribosyl transferase (HisG); mycothiol ligase (MshC); mycolic acid cyclopropanation, DosR (DevR) CarD; methionine aminopeptidase (Fmt); deformylase (Def); the proteasome complex and isocitrate lyase (Icl).

1.3.3.1 Drug targets against active TB

Some of the very recently identified novel drug targets in *M. tuberculosis* against active TB are as follows.

1.3.3.1.1 Maltosyltransferase

GlgE utilizes maltose-1-phosphate to elongate 1, 4-glucan chains. The accumulation of high levels of maltose-1-phosphate is toxic to *M. tuberculosis*, and that GlgE is required to metabolize the free maltose-1-phosphate .Using a conditional knockout strain of *M. tuberculosis*, the accumulation of maltose-1-phosphate in the absence of functional GlgE adversely affected the respiratory electron transport chain (Kalscheuer et al., 2010). Commensal gut flora and mammals lack proteins homologous to GlgE, making this a suitable drug target. An inhibitor of GlgE might be effective against existing drug-resistant strains of *M. tuberculosis* because this pathway is not targeted by any antibiotics in current clinical use (Lamichhane, 2011).

1.3.3.1.2 Mycolic acid cyclopropanation

The major constituents of the outer layer of the *M. tuberculosis* cell wall are mycolic acids of varying chain lengths and modifications. Cyclopropanation is a physiologically relevant modification carried out by multiple enzymes that might have specificity to unique mycolic acid molecules. Broad inhibition of cyclopropanation by dioctylamine is bacteriostatic at 6 μM (Barkan et al., 2009). Although the activity of the mycolic acid methyltransferase *Cma*2 was inhibited in an *in vitro* assay, data from this experiment suggested that dioctylamine targeted multiple pathways of cyclopropanation and the methylation of mycolic acids (Lamichhane, 2011).

1.3.3.1.3 ATP synthase

M. tuberculosis uses the proton motive force across the plasma membrane to synthesize ATP. Andries and coworkers identified the diarylquinoline compound R207910 with activity against *M. smegmatis* in a whole cell assay. The resistant *M. tuberculosis* cells to R207910 revealed that the *atp*E gene was mutated in all strains. Subsequent studies demonstrated that R207910 inhibited the synthesis of ATP in a dose-dependent manner (Koul et al., 2007). Researchers immobilized an analog of the compound onto a resin and passed *M. smegmatis* membrane protein extracts through it, and discovered that 'a' and 'b' subunits of ATP synthase is co-purified with the R207910 analog. These studies provide direct evidence that the ATP synthase complex can be effectively inhibited to prevent the growth of *M. tuberculosis*. A separate study showed that human mitochondrial ATP synthase was 20,000 fold less sensitive to R207910 compared with its homolog in *M. tuberculosis*. R207910 (now known as TMC207) is currently being evaluated in clinical trials for its effectiveness to treat infection with drug resistant strains of *M. tuberculosis* (Diacon et al., 2009).

The list includes enzymes like Decaprenylphosphoryl-β-D-ribose 2$^{'}$-epimerase in the cell wall synthesis, Mycothiol ligase from mycothiol biosynthesis, ATP phosphoribosyl transferase from histidine biosynthesis and enzymes in peptide processing like deformylase and methionine aminopeptidases (Lamichhane, 2011).

1.3.3.2 Drug targets against dormant TB

Extensive studies on dormancy have brought out a list of possible drug targets to combat dormant TB. This list includes some of the vital enzymes in metabolic pathways essential for the bug during dormancy.

1.3.3.2.1 Isocitrate lyase

M. tuberculosis encodes for two redundant enzymes, Icl1 and Icl2, with isocitrate lyase activity in its glyoxylate shunt pathway. Although it was initially shown that loss of *icl*1 compromised the ability of *M. tuberculosis* to persist during the chronic phase of infection (McKinney et al., 2000), the loss of both *icl*1 and *icl*2 results in a more severe phenotype (Munoz-Elias and McKinney, 2005) that includes loss in the ability to grow in fatty acids, loss of virulence and growth defects during the acute and chronic phases of infection. It was also demonstrated in the same study that the chemical inhibition of isocitrate lyase activity with 3-nitropropionate recapitulated the genetic loss of *icl*1 and *icl*2. Thus, isocitrate lyase is proposed as a bona-fide target that can be inhibited to slow or prevent mycobacterial growth, in addition to inhibiting persisters.

1.3.3.2.2 L, D-transpeptidase

A recent study identified a non-classical transpeptidase whose loss attenuates the ability of *M. tuberculosis* to persist. This transpeptidase generates 3-3 cross-linkages in the peptide chains of the peptidoglycan layer, which are different from the classical 4-3 linkages generated by D, D-transpeptidases whose activities are inhibited by β-lactam antibiotics. It was recently demonstrated that 80% of peptide chains are cross-linked with 3-3 bonds as *M. tuberculosis* transitions into the stationary phase of growth (Lavollay et

al., 2008). Soon thereafter, another study identified the L,D-transpeptidase and reported that the loss of the transpeptidase attenuated the growth, virulence and ability of *M. tuberculosis* to persist (Gupta et al., 2010). The loss of the transpeptidase activity also sensitized *M. tuberculosis* to amoxicillin-clavulanate *in vitro* and *in vivo*. These observations suggest that the inhibition of L, D-transpeptidase might prevent adaptation into the stationary phase and the ability of *M. tuberculosis* to persist.

1.3.3.2.3 CarD

A whole genome microarray screen to study changes in gene expression in response to DNA damaging agents identified *car*D in *M. smegmatis* whose expression increased in the presence of these stresses (Stallings et al., 2009). CarD interacts with the β-subunit of RNA polymerase and regulates stringent response, which includes the repression genes encoding ribosomal RNAs. *M. tuberculosis* possesses at least one additional stringent response regulator, namely RelA, which controls RNA polymerase activity by directly regulating the production of guanosine 3'-diphosphate 5-' diphosphate (ppGpp) and is required for maintaining chronic infection (Dahl et al., 2003). Although an *M. tuberculosis* mutant lacking a functional copy of *rel*A is viable, *car*D is essential for viability. The depletion of CarD one day following infection arrested the proliferation of *M. tuberculosis* in the lungs of mice. Similarly, a slight reduction in bacterial burden was observed during the chronic phase of infection when CarD was depleted, suggesting a potential role for CarD in maintaining persistent infection (Stallings et al., 2009). Therefore, CarD seems to be a novel class of target, and inhibiting CarD might limit the ability of *M. tuberculosis* to initiate stringent response and enter into dormancy.

Other potent targets suggested against dormant TB includes the proteasome complex, DevR/S transcription factors, *cyp*51, (cytochrome P450) etc. (Lamichhane, 2011; Hasan et al., 2006).

1.3.4 Protein N-terminal Methionine Excision (NME)

The translation of messenger RNAs (mRNAs) to generate proteins generally starts at an AUG codon. The translation machinery interprets AUG codons as methionine (Met). Only the specialized transfer RNA (tRNA) for translation initiation – $tRNA^{fMet}$ in Eubacteria and $tRNA^{iMet}$ in other organisms – can be used to start translation (Kozak et al., 1983; Meinne et al., 1993; Mechulam et al., 1995). The first residue incorporated in all nascent polypeptides should be Methionine (Met), with some exceptions as seen in case of viral mRNA translation (Sasaki and Nakashima, 2000). Although Met is the first amino acid of newly synthesized proteins, it is usually removed from the mature proteins following translation (Sherman et al., 1985). The process by which Met is removed from proteins is called N-terminal Met excision or NME. 60-70% of proteins in a proteome undergo NME, depending on the organism (Giglione et al., 2004). The simple rule governing NME is presence of non-bulky amino acid like Ala, Cys, Gly, Pro, Ser, Thr or Val at the penultimate position of the polypeptide. NME is an essential process and the role of this process is not so well characterized. Various hypotheses on crucial role of NME suggest its importance in further post-translational modifications and protein folding (Giglione et al., 2003; Giglione., 2004). It is also suggested that NME determines the protein half-life according to the N-end rule (Arfin and Bradshaw, 1988).

NME appears to be conserved from bacteria to eukaryotes, and the rules governing NME are thought to be similar in all organisms. Eubacterial and organellar protein biosynthesis begin with N-formylated Met compared to the eukaryotic counterparts where it begins with Met (**Fig 1.4**). This small modification of Met-tRNA^{fMet} seems to increase the rate of protein synthesis, as it plays an important role in the recognition of major translation factors such as IF2 and EFTu. This distinction separates bacterial and organellar NME from eukaryotic NME (**Fig 1.5**). Thus NME in bacteria and organelles require an additional step to remove the formyl group prior to removal of Met. Peptide deformylase (PDF) carries out the deformylation step in bacteria and organelles, which is followed by the action of methionine aminopeptidases (MAP) to cleave the initiator Met (Solbiati et al., 1999; Flinta et al., 1986). The deformylation step is mandatory for the subsequent action of MAP.

NME is an irreversible co-translational mechanism, completed before the nascent polypeptide chains are fully synthesized (Arfin and Bradshaw, 1988). It starts early in translation, as soon as the first residues emerge from the ribosomal exit tunnel, before the initiation of protein folding. This early start of NME has resulted in tri or tetra peptides as substrates for both PDF and MAP (Ball and Kaesberg, 1973).

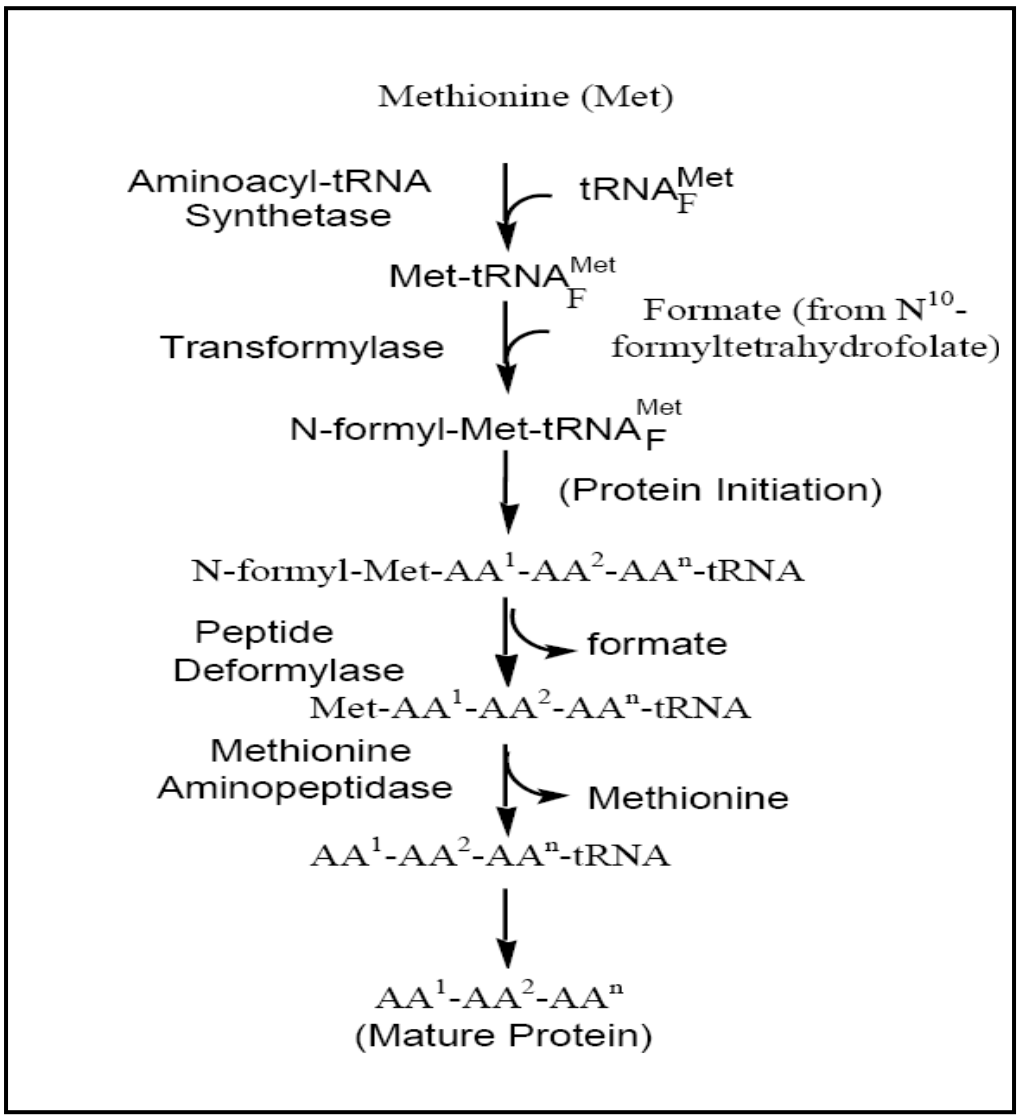

Fig 1.4: Peptide synthesis and NME pathway in bacteria and organells (Adopted from Nguyen, 2005).

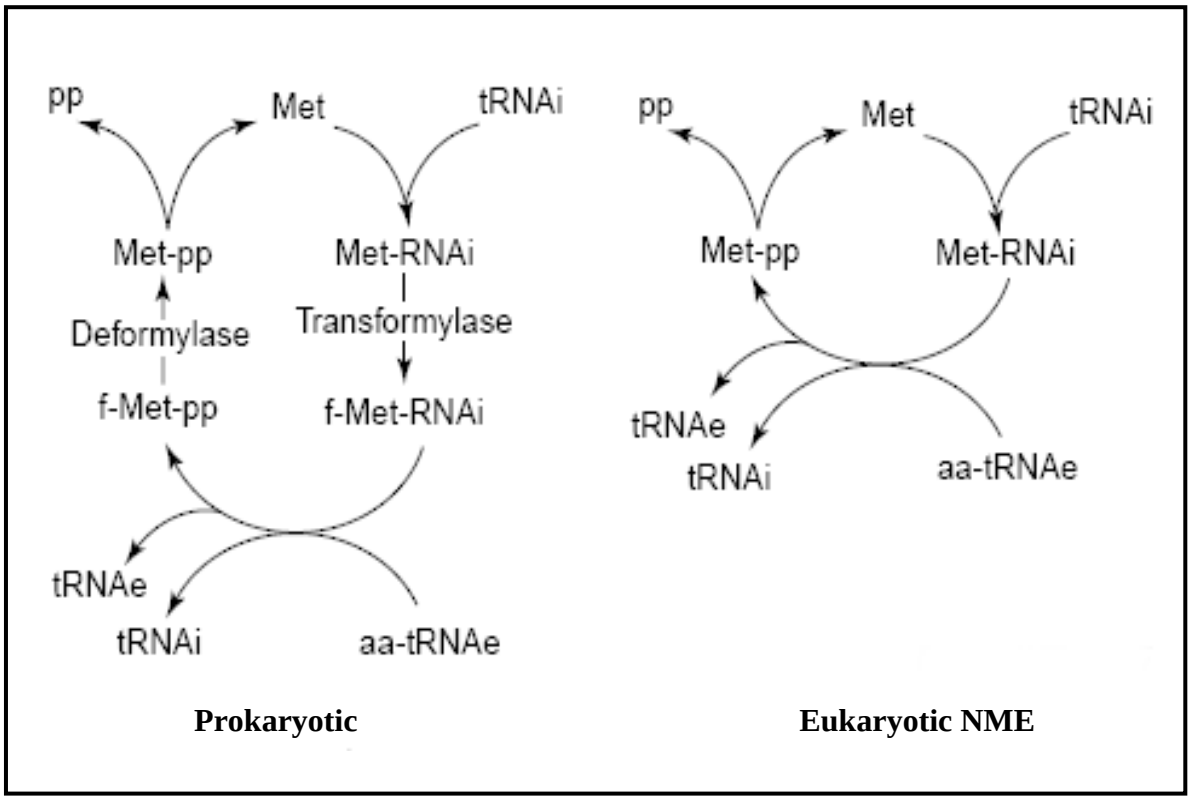

Fig 1.5: Comparison of prokaryotic and eukaryotic NME (Adopted from Yuan et al., 2001)

The pioneering studies on NME began as early as the 1960s (Waller, 1963; Adams, 1968; Vogt, 1970), but has increased in late 1980s and in 1990s mainly because NME was recognized to be an excellent therapeutic target (Giglione et al., 2000a; Pei, 2001). This suggestion mainly resulted from the studies on *Saccharomyces cerevisiae* and *Cenorhabditis elegans* where no PDF homologs were identified (Giglione et al., 2000b). But, soon it was realized that there is organelle NME involving PDF in eukaryotes, which led to characterization of eukaryotic NME processes from mitochondria and plastids (Giglione and Meinnel, 2001). The nuclear genome-encoded organelle-targeted PDFs were

identified in the genome of many eukaryotes (Meinnel, 2000; Giglione et al., 2000b). In general, plant genomes have two PDFs (PDF1A and PDF1B) where as only PDF1A was found in animals including humans. PDF1A is targeted to mitochondria and PDF1B is targeted to both plastids and mitochondria (Giglione and Meinnel, 2001; Giglione et al., 2000b). All these eukaryotic PDFs have cleavable N-terminal extensions having target sequences to organelles (Serero et al., 2001).

NME was initially thought to be unregulated constitutive process, but some proteomics and transcriptomics studies have revealed decreased *def* gene expression in case of fluoride stress and iron starvation in *Streptococcus pyogenes* and *Pseudomonas aeruginosa*, respectively (Thongboonkerd et al., 2002; Palma et al., 2003). Similar regulations of PDF and MAPs have been reported in higher eukaryotes like plants and in *Drosophila* during the embryo development and under several stress responses (Giglione et al., 2004).

Essentiality of NME has led to characterizing this pathway with therapeutic implications as the major goal. NME is essential process for the reason that both PDF and MAP genes are part of minimal genome required for viability of bacteria (Hutchison et al., 1999; Kobayashi et al., 2003) and that NME occurs even in organelles where there are fewer than 100 protein substrates (Giglione et al., 2000b). Another important reason for considering NME as potent therapeutic target is because of the availability of natural inhibitors against the components of this pathway. The distinction between the components of bacterial and organellar NME is required to carry forward the efforts on antibacterial drug discovery process based on NME.

1.3.5 Enzymes involved in protein NME

There are five enzymes responsible for integrating and removing amino acid methionine into and from a nascent polypeptide during polypeptide biosynthesis and subsequent peptide processing steps. They are (1) *methionyltRNA synthetase (MetRs):* involved in activation of methionine and its charging onto both initiator and elongater $tRNA_{Met}$ (2) *Met-tRNA transformylase* (FMT) which formylates methionine on initiator $tRNA_{Met}$ (3) *peptide deformylase* (PDF), which removes the formyl group from nascent polypeptides (4) *methionine aminopeptidase* (MAP), which remove the N-terminal methionine and (5) *peptide methionine sulfoxide reductae* (PMSR), which reduce methionine sulfoxide in a polypeptide back to its native sulfide form (Vaugan et al., 2002). All these enzymes have essential role to play in the protein biosynthesis. Among these five enzymes PDF and MAP are involved in the NME process. The present study concentrates on these two enzymes from the NME pathway.

1.3.5.1 Peptide deformylase

1.3.5.1.1 Bacterial peptide deformylase

Newly synthesized bacterial and organellar proteins are tagged with a one-carbon unit called a formyl group. However, the vast majority of the N-formyl moiety is removed from the mature proteins. The removal of the N-formyl moiety is catalyzed by peptide deformylase (PDF; EC 3.5.1.31) (**Fig 1.6**) (Adams, 1968). This step is mandatory for the subsequent removal of initiator methionine by methionine aminopeptidases and, thus PDF plays a critical role in mediating the maturation process in nascent polypeptides (Hirel et al., 1989).

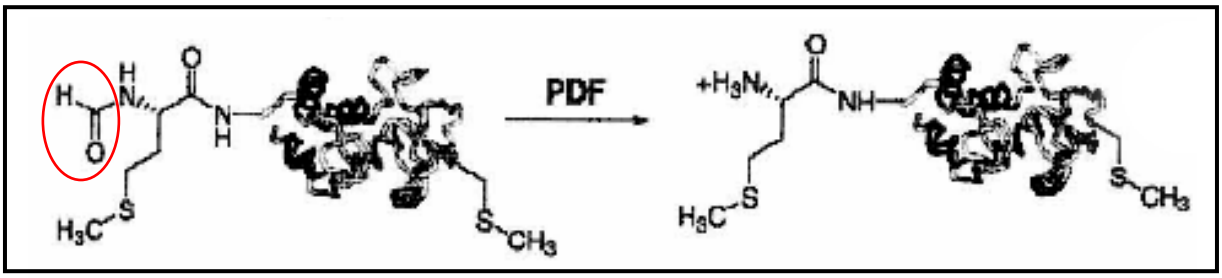

Fig 1.6: Deformylation of nascent polypeptide by peptide deformylase (PDF) (Adopted from Vaugan et al., 2002).

PDF activity was originally described in the late 1960s from *E. coli* and *Bacillus subtilis* (Adams, 1968; Takeda and Webster, 1968; Livingston and Leder, 1969) but its unusually high level of instability rendered further studies impossible for 25 years. Thus, major studies on the biology and structure of PDF were reported in 1990s (Giglione et al., 2000a; Giglione and Meinnel, 2001).

Analysis of bacterial sequences revealed the presence of deformylase (*def*) gene through out the eubacterial lineage (Mazel et al., 1997). The gene encoding PDF in *E. coli* and *Thermus thermophilus* were shown to belong to the same operon as of Formyl-methionine transferase (FMT) (Meinnel and Blanquet., 1993; Meinnel and Blanquet., 1994). Essentiality of *fmt* and *def* genes was first demonstrated in *E. coli* by targeted gene knock-out studies (Guillon et al., 1992; Mazel et al., 1994). It was shown that, *def* gene could be knocked out only when *fmt* gene was also knocked out. Such double mutants had serious growth impairment (Mazel et al., 1994). From that point onwards there was an increased interest in PDF as potential target for antibacterial drug discovery. .

Initial studies on prokaryotic PDFs were mainly from prototype *E. coli.* The effect of 1, 10, phenanthroline on PDF activity first suggested it to be a metallo-enzyme (Meinnel

and Blanquet, 1995; Rajagopalan *et al*., 1997). Further studies reported PDF to be a Zn^{2+} containing metallo-protease (Miennel et al., 1995). This suggestion was later challenged by the studies by Rajagopalan et al., (1997a) which proved PDF to be a Fe^{2+} containing enzyme. The instability of PDF was attributed to the oxidation of Fe^{2+} to Fe^{3+} by atmospheric oxygen and removing oxygen during purification by addition of anti-oxidant enzymes like catalase was suggested to improve stability (Rajagopalan et al., 1997a; Rajagopalan and Pei, 1998). It was later proved that Fe^{2+} in PDF could be replaced by Co^{2+} or Ni^{2+} during purification, in order to retain its full *in vitro* activity with high stability (Ragusa et al., 1998). These findings led to production of surrogate enzymes with Ni^{2+} or Co^{2+} which had identical structural features and enhanced stability due to the presence of inert metal ions (Groche et al., 1998; Han et al. 2004., Huang et al., 2006). With advancements in genome sequencing and recombinant DNA techniques, the *def* genes from various microorganisms including several pathogens have now been cloned and characterized (Rajagopalan et al., 1997a; Margolis et al., 2000; Li et al., 2002; Han et al. 2004., Huang et al., 2006). Over expression of PDFs from T_7 promoter (Rajagopalan et al., 1997a) has been reported as better method compared to expression under *lac* promoter (Meinnel and Blanquet, 1993).

Analysis of eubacterial PDF amino acid sequences revealed the presence of three highly conserved motifs (I: GXGXAAXQ, II: EGCLS and III: QHEXXH, where X is any hydrophobic residue), forming the architecture of peptide binding and metal binding pockets (Meinnel et al., 1997). The motif III has been characterized as typical signature sequence of Zn-metallo-protease (Hooper, 1994; Meinnel et al., 1996a). The metal ion in

the metal-binding pocket has a tetrahedral co-ordination with histidines from motif III and cystein from motif II along with one water molecule as ligands. Mutations of these residues affect the enzyme activity (Miennel et al., 1995b; Miennel et al., 1997). Deletion analysis revealed that amino acids from the extended C-terminal of *E. coli* PDF are disordered and dispensable for enzyme activity *in vitro* (Miennel et al., 1996b). Following the studies on *E .coli* PDF, structural and biochemical characterizations of various other bacterial PDFs were reported in past decade. The important findings from these studies are summarized in **Table 1.2**. All these studies highlighted the importance of bacterial PDFs as suitable targets for screening novel antibacterials.

Table 1.2 Summary of reports on bacterial peptide deformylases

Organism	Significant features	Reference
Leptospira interrogans	One *def* gene; active as Zn- PDF, LiPDF is a dimer, Structure revealed unique C-terminus and insertion sequences between motif I and II.	Li et al., (2002) Zhou et al., (2004)
Psedomona aeruginosa	Crystal structure elucidated.	Kim et al., (2002)
Haemophillus influenzae	Crystal structure elucidated.	Smith et al., (2003)
Helicobacter pylori	One *def* gene, Co-PDF; Thermo-stable enzyme at 50 ^{o}C.	Han et al., (2004)
Legionella pneumophila	Three *def* genes (*def* A,B,C), PDF A close to other bacterial PDFs, other two divergent, All three active as Ni-PDFs.	Huang et al., (2006)
Staphylococcus aureus	Two *def* genes (*def*A and *def*B), PDF B alone active. Crystallized with actinonin.	Margolis et al., (2000) Yoon et al., (2004)
Bacillus cereus	Two *def* genes (*def*1 and 2). PDF 2 is a dimer and highly active than PDF 1.	Park et al., 2007
Borrelia burgdorferi, Lactobacillus plantarum	Iron deficient organism with native PDF enzyme having Zn^{2+}.	Nguyen et al., 2007
Mycobacterium tuberculosis, Mycobacterium bovis	One *def* gene; Fe-PDF with indispensable C-terminal extension. *def* essential in *M. bovis*, Crystallized with PDF inhibitors.	Saxena and Chakraborti (2005a,b); Teo et al., (2006); Pichota et al., (2008)
Enterococcus faecaelis	Crystallized with Met-Ala-Ser	Nam et al., (2009)
Staphylococcus epidermidis	Two *def* genes (*def* 1 and 2), SePDF 1catalytically active as Co-enzyme, SePDF 2 inactive.	Lin et al., (2010)

1.3.5.1. 2 Eukaryotic / Organellar peptide deformylase

Protein synthesis in the cytoplasm of eukaryotes does not begin with N-formyl methionine, and undoubtedly the need for deformylation in the cytoplasmic process is apparently absent. Compared to prokaryotes, no PDF counterpart has been reported in yeast *S. cerevisiae* or nematode *C. elegans* (Giglione et al., 2000b; Meinnel, 2000). It was observed that protein synthesized in mammalian mitochondria retain their N-formyl group (Walker et al., 1991; Takeuchi et al., 1998). Deformylation was apparently found absent from mitochondrial protein translation in yeast, *Neurospora*, honey bee and bovine (Nguyen, 2005). These led to the common belief that PDF homologues are absent in eukaryotes. However, genome sequencing data from the completed eukaryotes revealed the presence of PDF like homologues in eukaryotes (Giglione et al., 2000b; Nguyen et al., 2003). All these have been shown to be targeted only to eukaryotic organelles such as apicoplast, plastids, chloroplast and mitochondria (Dirk et al., 2001; Seraro et al., 2003).

1.3.5.1.2a Peptide deformylase from yeast, plants and parasites

PDF-like sequences were reported very early in some higher plants such as *Arabidopsis thaliana*, tomato, corn, and rice (Schmidt et al., 1992). Two cDNAs of *Arabidopsis thaliana* PDFs (AtPDF1 and AtPDF2) has been cloned and over expressed in *E. coli* to find that their catalytically activities and properties were similar to bacterial PDF (Giglione et al., 2000b; Dirk et al., 2001). The two homologues were shown to be sub-cellular localized in the chloroplast and mitochondrion (Giglione et al., 2000b). Their essential role in protein processing in plant plastids were confirmed by inhibition of seedling growth and germination in *A. thaliana* in presence of actinonin (Dirk et al., 2001).

In addition to plants, several eukaryotic-plastid containing parasites like *Plasmodium falciparum* have nuclear encoded PDF– gene homolog (Meinnel, 2000). PDF from *P. falciparum* (PfPDF) shows a 33% identity to the bacterial PDF, plus a ~60-amino acid extension at the N-terminus. This extra-N-terminus sequence consists of a signal peptide for entry into the secretory pathway and a plant-like transit peptide for subsequent import into apicoplast of *P. falciparum*. Recombinant PfPDF showed catalytic behavior similar to bacterial PDFs and was inhibited by PDF inhibitors. *P. falciparum* was inhibited by a potent bacterial PDF-inhibitor in the intra-erythrocytic culture (Bracchi-Ricard et al., 2001). More importantly, PDF-like sequences have been identified in the genomes of *Drosophila Melangogaster*, as well as in the partial expressed sequence tags (ESTs) of mouse and human (Giglione et al., 2000b).

While plants have two PDFs (PDF1A and PDF1B), animals including human have only one PDF, PDF1A (Giglione et al., 2004). PDF1As are targeted to mitochondria, where as in plants PDF1Bs are targeted to both mitochondria and plastids (Serero et al., 2001). PDF1B was reported in case of apicomplexan parasites, *P. falciparum* (Bracchi-Ricard et al., 2001). Like in case PfPDF, all of these eukaryotic PDF sequences contain an extra ~60 amino acid N-terminal extension (Giglione et al., 2000b).

1.3.5.1.2b Human mitochondrial peptide deformylase

Since the time eukaryotic PDFs were reported and characterized, efforts were put into characterizing the human mitochondrial PDF with the goal of revealing its non-essentiality for safer use of PDF-inhibitors as therapeutics against infectious diseases. The cDNA encoding *Homo sapiens* PDF (HsPDF) was cloned as a truncated form that lacks the N-

terminal 58-aminoacid targeting sequence and was over expressed in *E. coli*. The recombinant, Co^{2+} substituted HsPDF was found catalytically active, but much lesser compared to its bacterial counter parts. Enzyme activities of HsPDF were 20-30 fold lower compared to *E. coli*. Potent inhibitors of bacterial PDFs were equipotent in inhibiting HsPDF activity *in vitro*. Expression of HsPDF fused to the enhanced green fluorescence protein in human embryonic kidney cells revealed its location in the mitochondrion. The lower catalytic activities were attributed to mutation of highly conserved Leucine in motif II of bacterial PDFs to a glutamate residue in HsPDF. None of the tested PDF inhibitors had any detectable effect on two different human cell lines (Nguyen et al., 2003). In yet another work, HsPDF was characterized both *in vivo* and *in vitro* and compared the properties of this PDF1A enzyme with PDF1A enzymes from *A. thaliana.* The N-terminal extension in HsPDF was reported to have role in mitochondrial targeting and enzyme stability. The N-terminal truncated HsPDF could complement the *def* (Ts) phenotype of PAL421Tr strain of *E. coli* (Meinnel and Blanquet, 1994). The study concluded that evolutionary substitutions at position 43 with cystein and at 91 with glutamate in animal PDFs are responsible for the reduction in its enzyme activity and iron-binding ability (Seraro et al., 2003).

Actinonin inhibited HsPDF activity with an IC_{50} of 43 nM and kills Daudi and HL60 human cancer cell lines with an LC_{50} of 5.3 and 8.8 μM, respectively (Lee et al., 2003). Actinonin and its 33 analogues showed anti-proliferative effects on 16 human cancer cells. Small interfering RNA inhibition of HsPDF expression in tumor cells was also proved to be anti-proliferative. Actinonin treatment of cells led to a tumor-specific mitochondrial

membrane depolarization and ATP depletion in a time- and dose-dependent manner. Based on these studies HsPDF was suggested as a novel target for anti-cancer therapy based on actinonin (Lee et al., 2004). This report on HsPDF as drug target for cancer led to development of high-throughput screening strategies to identify novel natural products that have inhibitory effects on HsPDF activities (Antczak et al., 2007). The first crystal structure of HsPDF was elucidated in by Escobar-Avarez et al., (2009) and it reaffirmed the conservation of PDF-actinonin interaction across PDFs. Very recently, the cellular function of HsPDF in mitochondrial translation and oxidative phosphorylation complex biogenesis was elucidated by studying the consequences of HsPDF inhibition by a series of structurally different inhibitor molecules (Escobar-Alvarez et al., 2010). Functional HsPDF appears to be necessary for the accumulation of mitochondrial DNA-encoded proteins and assembly of new respiratory complexes containing these proteins. Consequently, inhibition of HsPDF reduces respiratory function and cellular ATP levels, causing dependence on aerobic glycolysis for cell survival. This revelation actually complicates the antibacterial and anticancer drug discovery process based on PDF and demands screening of structurally different inhibitors with strict specificity for bacterial PDFs for reducing the toxicity towards normal human cells.

1.3.5.1.3 Structure and catalytic mechanism of peptide deformylase

PDF is widely accepted as a novel class of Fe or Zn metalloenzyme that is related in structure to the metalloproteinase super family. While other regions of its sequence may vary, all PDFs share three highly conserved motifs GXGXAAXQ, EGCLS, and QHEXDH

(where X encodes any hydrophobic amino acid) (**Fig 1.7a and 1.7b**). These motifs form the three sides of the active site pocket, a common architecture evidently conserved among all PDFs (Meinnel et al., 1997). Several X-ray crystal and NMR solution structures of both bacterial and eukaryotic PDFs have been determined as Fe-PDF, Zn-PDF, and Ni-PDF forms (Becker et al., 1998a; Chan et al., 1997; Dardel et al., 1998; Fieulaine et al., 2005; Escobar-Avarez et al., 2009). More than 70 crystal structures of different PDFs are available in the public domain, with or without any ligand / inhibitor bound to them. In every case the metal ion is tetrahedral co-ordinated by histidine residues of the conserved HEXDH motif, one cysteine residue from EGCLS motif, and a water molecule (Miennel et al., 1995b).

The co-crystallization of *E. coli* PDF with a reaction product (Met-Ala-Ser) revealed that the P1' site having appropriate volume to support a hydrophobic interaction with the methionine side chain (Becker et al., 1998*)*. More importantly, key interactions of the P1' and P2' are predominantly formed from hydrogen bonding between the carbonyl and amide protons of the peptide backbone. Further, the co-crystallization of *E. coli* Zn-PDF (Hao et al., 1999) with a transition state analog, (*S*)-2-*O*-(H-phosphonoxy)-L-caproyl-L-leucyl-*p*-nitroanilide(PCLNA), additionally revealed crucial interactions with the H-phosphonate moiety. The crystal complex showed one of the phosphonate oxygen is liganded to the metal, replacing the water molecule, as well as interacting with the side chain of the E133. The other phosphonate oxygen, which mimics the carbonyl oxygen of the formyl moiety, is within hydrogen bonding distance with the polypeptide amide of L91 and the side chain NH_2 of Q50. The (L)-caproyl group in the S1' position, which mimics

the methionine amino acid, sits in a pocket generated by residues Gly43, Ile44, Gly45, Glu88, Cys129, His132, and Glu133. In the S2' position, the (L)-leucine side chain makes van der Waals contact with Leu91 and the main chain carbonyl groups of residues Glu42 and Gly43 on one side, while the other side is exposed to solvent.

Crystal structure of *E. faecium* PDF (EfPDF) with a malonate group bound to it , revealed a 'U' shaped peptide binding cavity and a flexible 'CD' loop region (Nam et al., 2009). The residues form motifs II and III contribute residues critical for deformylase function. Based on the structure, motif II appears to contribute to the architecture of the catalytic pocket in the EfPDF structure., the side chains of conflict residues in motif I, Val59, Leu61 and Pro64, were found to form the outside of the substrate binding pocket (Fig 1.7c). Similarly, the side chains of Gly58, Gly60, Ala62, Ala63 and Gln65 contributed to the architecture of the substrate binding pocket by forming a chamber in the binding pocket. The structure also suggested that eight amino acids, Pro80–Pro87, between strands β2 and β3 make up the CD-loop region which forms a flexible lid over the substrate binding site. This lid has to be opened for the substrates to access the catalytic sites for catalysis. The size and flexibility of the CD-loop region has been found variable in different bacterial and eukaryotic PDFs, defining the opening and closing of the substrate binding sites (Fig 1.7a) (Zhou et al., 2004; Fieulaine et al., 2005).

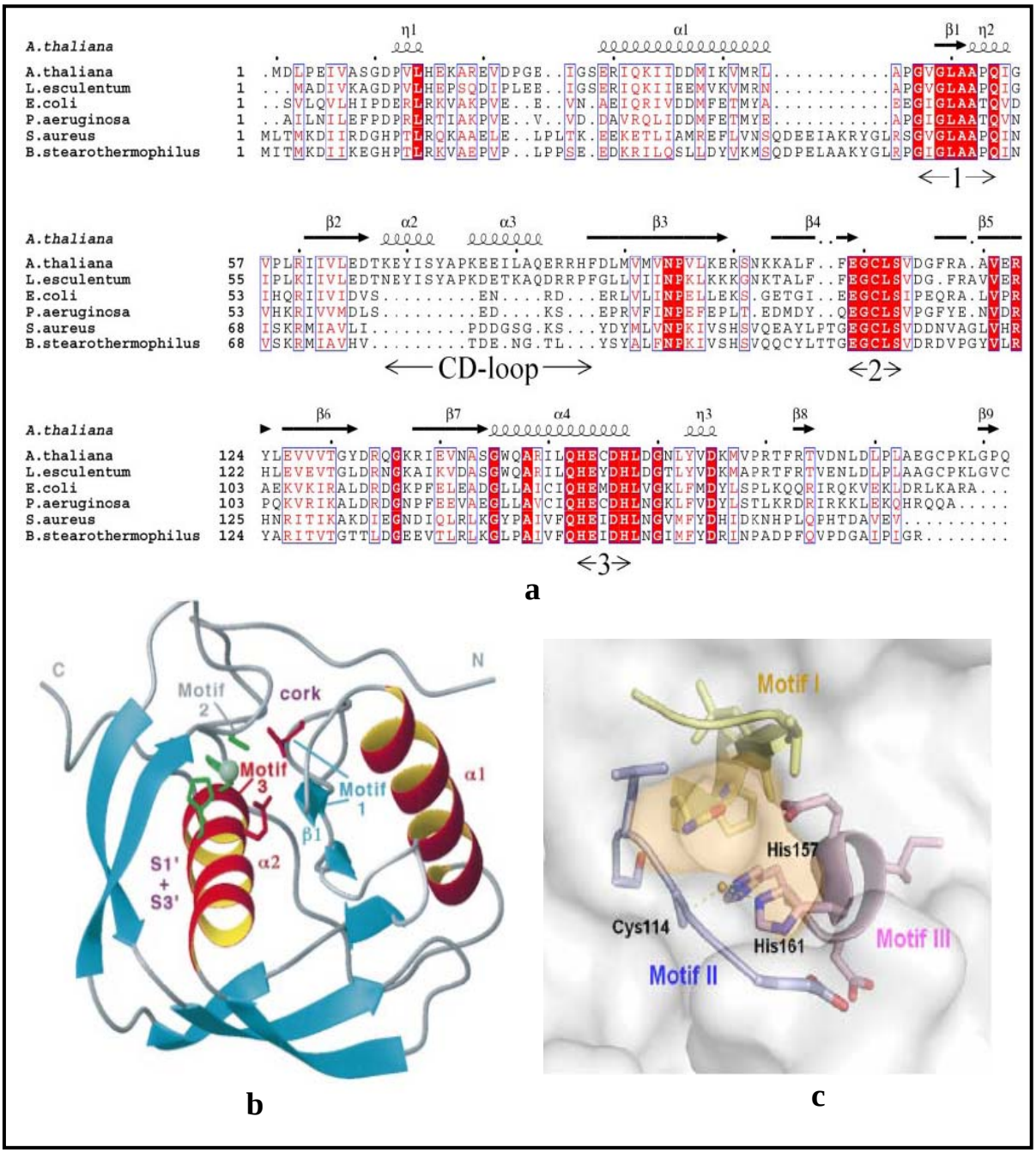

Fig 1.7: Structure of PDF: (a) Conserved residues from the three motifs in PDFs; **(b)** Crystal structure of Zn-*E. coli* PDF (Side chains metal binding residues in green and catalytic residues in red, metal-ion in grey sphere); **(c)** Architecture of substrate binding cleft in *E. faecium* PDF, lined by residues in the three motifs. (Adopted from Giglione et al., 2000a and Nam et al., 2009).

The crystal structure of HsPDF revealed similar architecture of the substrate binding pocket. The substrate binding pocket in HsPDF is relatively shallow with a well defined S1' binding pocket, and with out a defined S2' and S3' binding pockets. The HsPDF-actinonin complex suggested that the P2' and P3' sites are combined to form a wider opening at the substrate binding sites during substrate binding and enzyme turnover (Escobar-Avarez et al., 2009).

Based on structural and sequence variations, bacterial PDFs have been classified as type I (gram negative type) and type II (gram positive type) (**Fig 1.8**). Type I PDFs show a long C-terminal a-helix, which is parallel to β strand-F whereas type II PDFs has two insertion sequences around α-helix 1 and highly hydrophobic C-terminal domain forming a long loop which turns back to form mixed β-sheets with β strand-E and β strand-F (Guilloteau et al., 2002). The C-terminal region of *L. interrogens* PDF show variations in having a short β-strand (β-J) and an a-helix (α-K) which heads to the direction between type I and type II PDFs. β-J joins the antiparallel β-sheet, interacting with β-F, instead of β-E as in type II PDFs. Identification of eukaryotic PDFs and their structural characterizations have led to yet another classification of PDFs. Since both mitochondrial and plastid PDFs have no insertion sequences specific to the type II PDFs, they are classified as type I PDFs. Mitochondrial PDFs differs from the plastid type and type I bacterial types in having long insertion between β-strands$_2$ and β-strands$_3$ (CD loop region) and in having systematic amino acid changes in the vicinity of the active site (Serero et al., 2001). Thus mitochondrial PDFs were classified as PDF IA and plasmid PDFs as IB (Fieulaine et al., 2005).

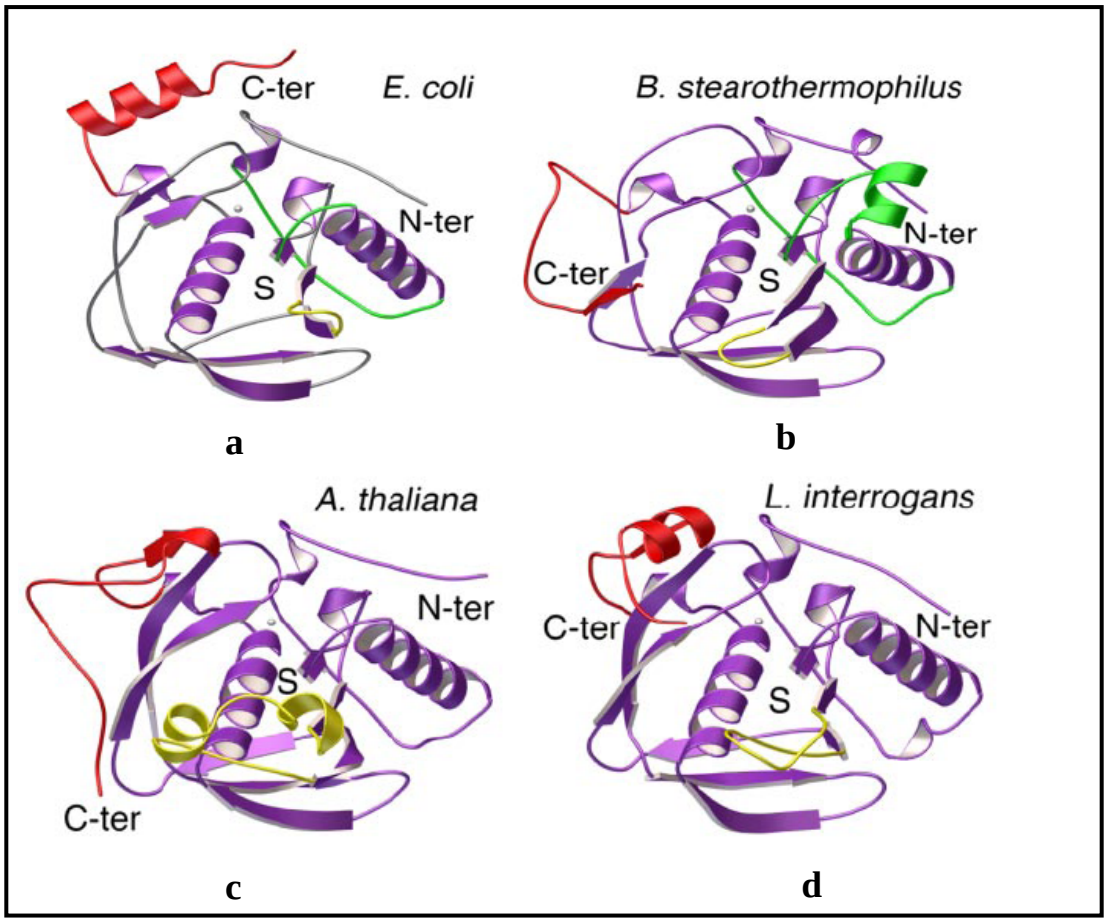

Fig 1.8: Comparison of folding patterns of the different PDF types. PDFs from **(a)** *E. coli* (PDF type 1a); **(b)** *B. stearothermophilus* (PDF type IIa); **(c)** *A. thaliana* (PDF type Ia); **(d)** *L. interrogans* (PDF type IIb) are shown in purple. The CD-loops are shown in yellow, and the C-terminal region is shown in red, to show the different conformations observed. The insertions 1 and 2 distinguishing bacterial PDFs of types 1 and 2 are shown in green in the *E. coli* and *B. stearothermophilus* PDFs. Metal ions and are shown in grey spheres. 'S' is the substrate binding site. (Adopted from Fieulaine et al., 2005).

Site-directed mutagenesis of the key catalytic residue E133 (in the HEXDH motif) to Ala and Asp provides additional insights into PDF's catalytic mechanism (Rajagopalan et al., 2000). Under the absorption spectra of various pH conditions, the metal-bound water of the cobalt-substituted mutants E133A and E133D was shown to have pK_a values of 6.5 and 5.6, respectively. Together, it was suggested that the role of the metal ion is to ionize the bound water molecule to generate a metal-bound hydroxide, which nucleophilically attacks the formyl moiety. In addition, the pK_a, 6.5, of the metal-bound water in E133A suggested that the most important role of E133 side chain involvement in catalysis is to serve as a H^+ shuttle as well as general acid mechanism, donating a proton to the leaving amide ion of the peptide (Rajagopalan et al., 2000).

Most widely accepted mechanism of catalysis of PDF as proposed by Becker et al., (1998) is depicted in **Fig 1.9**. In the free enzyme, the metal-bound water molecule is hydrogen bonded to the side chain of E133. Catalysis occurs when the N-formyl moiety of the peptide substrate enters the active site, making an E.S complex, to position next to the metal-bound water. Since the pK_a values of the metal-bound water (6.5) and the carboxyl group of E133 (~5) are similar, the shared proton may be transferred from the water to the carboxylate group. The reaction presumes to occur instantaneously due to the readily formed hydroxyl species, coordinated to the metal, via by performing nucleophilic attack on the formyl group. The resulting transition state tetrahedral intermediate, producing an oxyanion derived from the formyl group, is stabilized by a hydrogen bonding network between the NH backbone of L91 and the side chain NH_2 of Q50. The breakdown of the tetrahedral intermediate is facilitated by reforming the original C=O bond. During the

second transition state, the leaving NHR is likely hydrogen bonded to the side chain of E133. A proton transfer process from E133 to the leaving –HNR group and subsequently is followed by a water-formate exchange to complete the catalytic cycle.

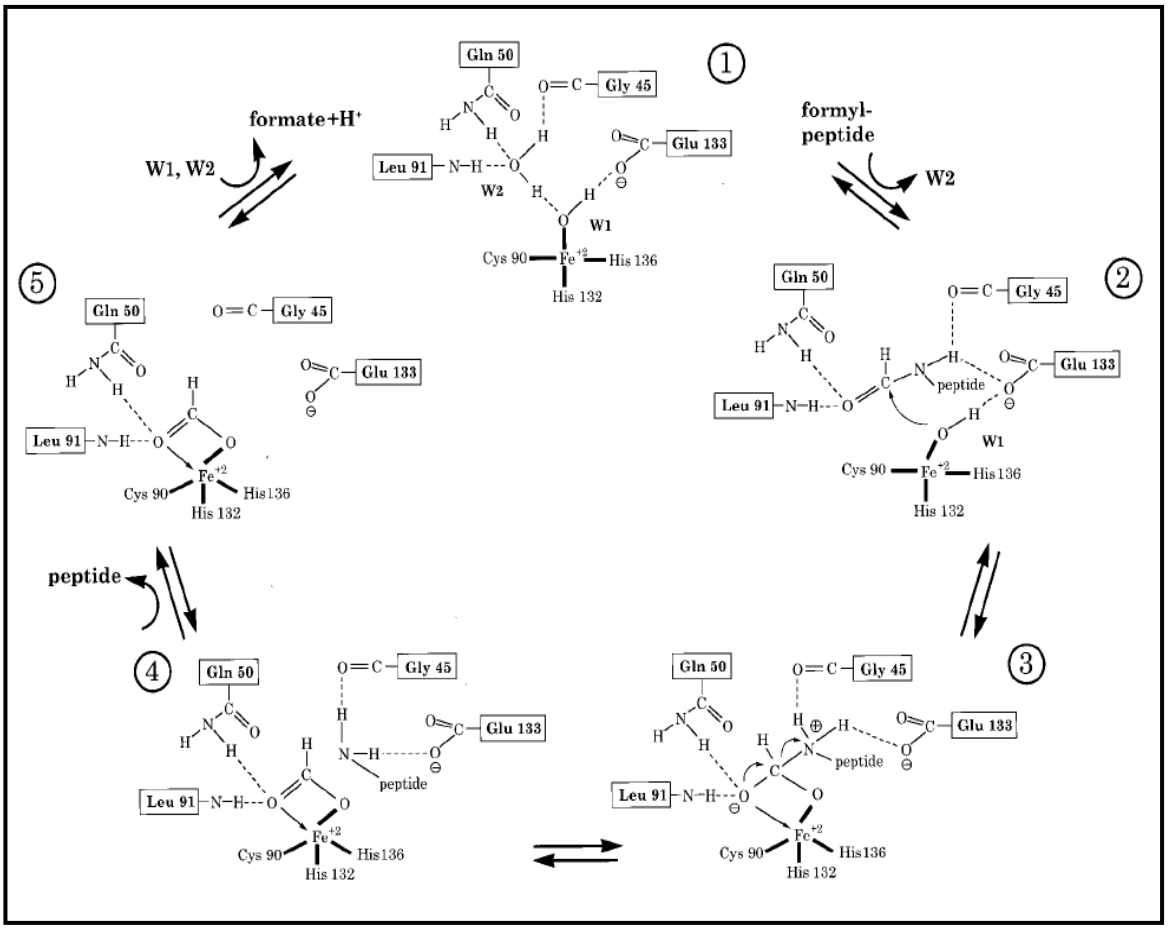

Fig 1. 9: Proposed catalytic mechanism of PDF

1.3.5.1.4 Peptide defomylase inhibitors

Arise in the proven ability of bacteria to adapt and to develop resistance to multiple classes of existing antibiotics is a problem that poses an urgent challenge to find new avenues to combat these antibiotic resistant bacteria. Therefore, the development of new

antibiotics is essential, i.e. by blocking or circumventing the resistance mechanisms or identifying novel targets. One novel target has recently received tremendous recognition and success, peptide deformylase (Nguyen, 2005). Since PDF is required for bacterial survival but apparently unnecessary in animal cells, it provides an attractive target for a novel antibacterial strategy. With the numerous three-dimensional structures of various bacterial PDFs solved (Baldwin et al., 2002; Bracchi-Ricard et al., 2001; Park et al., 2007) both with and without enzyme-bound inhibitor complexes, it appeared that the active site of PDF is conserved (Chan et al., 1997; Dardel et al., 1998). Consequently, PDF appears to be a broad spectrum novel antibiotic drug target.

The real interest of PDF as a drug target aroused from random screening work on PDF inhibitors. (Chen et al., 2000; Apfel et al., 2000). The work led to the identification of actinonin, a naturally occurring hydroxamic acid derivative known to have potent antibacterial activity and it has PDF as its target. Actinonin was previously isolated from *Streptomyces* as an antibacterial compound with unknown mechanism of action (Gordon et al., 1962). The chelating group present in actinonin is a hydroxamate (**Fig 1.10**). Using several lines of evidences like target over-expression, proteome analysis etc., PDF was proved to be the target for actinonin (Apfel et al., 2001). X-ray structure analysis of PDF with bound actinonin revealed direct interactions between backbone amide bonds of the ligand and the enzyme (**Fig 1.10**) (Guilloteau et al., 2002). Moreover, it suggested that the hydroxamate functionality is a valuable option as metal binding group. A range of different chelators have been attempted by British Biotech group in the quest to synthesize PDF inhibitors including hydroxamates, reverse hydroxamates, carboxylates and

sulfhydryls (Johnson et al., 2005). Among all these, the most potent and selective leads reported contain reverse hydroxamates (Smith et al., 2002).

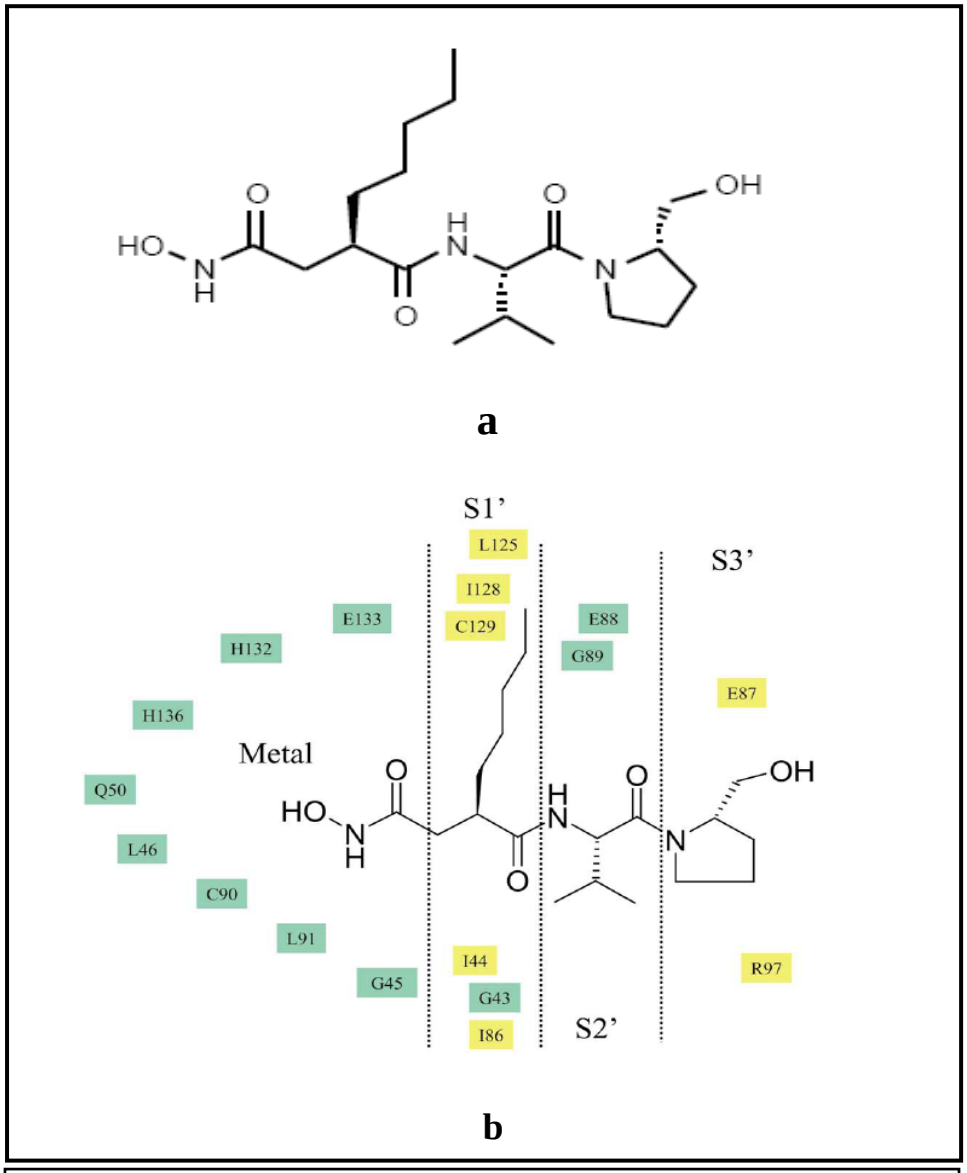

Fig 1.10: Structure and binding of actinonin; (a) Molecular structure of actinonin **(b)** Delineation of the sub-sites of the binding pocket of actinonin in PDFs. Residues highlighted in green correspond to conserved residues and in yellow to variable residues. (Adopted from Guilloteau et al., 2002).

BB-3497, a reverse-hydroxamate analogue of actinonin was most widely studied to optimize and fine tune the side chains of PDF inhibitors. The effects of shortening and lengthening side chains at various positions of PDF inhibitors were tried with BB-3497 and n-butyl, and cyclopentymethyl side chains at P1' were found to produce optimum inhibitory and antibacterial activities (Johnson et al., 2005). At P2' position there was little effect for substitution of side chains and *t*-butyl group was found to be best, owing to its effects on providing peptide analogues with increased stability and oral bioavailability. P3' served as ideal terminal group to fine-tune inhibitors for balanced properties including pharmacokinetic profile. Limited studies with analogs of BB-3497 indicated small secondary amines and cyclic 5- or 6-membered aliphatic amines such as pyrrolidine, morpholine or substituted piperazines to be optimal for PDF inhibition and antibacterial activity (Johnson et al., 2005).

Several studies have described the *in vitro* activity of PDF inhibitors against respiratory tract pathogens. Many compounds are active against *Streptococcus pneumoniae* and *Moraxella catarrhalis* with an MIC less than 1 μg/ml. *In vitro* activities against the gram-positive pathogens like *Staphylococcus aureus*, *Staphylococcus epidermidis*, and *Enterococcus spp*. were better compared to gram-negative pathogens such as *Escherichia coli*, *Klebsiella, pneumoniae*, *Enterobacter cloacae* and *Pseudomonas aeruginosa* (Johnson et al., 2005). After a lot of optimizations BB-83698 entered the Phase I clinical trials for respiratory tract infection (Ramanathan-Girish et al., 2004). The study proved no significant adverse effects at any dose studied.

Apart from actinonin, there are some other classes of PDF inhibitors reported from nature having non-hydroxamate side chains (**Fig 1.11**). Two pseudopeptides, Sch 382582 and Sch 382583 were isolated from the fermentated broth of *Streptomyces* sp having potent PDF inhibition and antibacterial activities with their MIC in the range of 32-50 μg/ ml (Chu et al., 2001). A new 24-membered ring lactone, macrolactin N, isolated from culture broth of *Bacillus subtilis* inhibited *Staphylococcus aureus* peptide deformylase with an IC_{50} value of 7.5 μM and showed antibacterial activity against *E. coli* and *S. aureus* (Yoo et al., 2006). Fumimycin, an unusual metabolite incorporating an unusual alanine unit linked to a phenyl group at the α-carbon with both lactone and amide moieties, was reported cultures of *Aspergillus fumisynnematus*. It inhibited *S. aureus* peptide deformylase with an IC_{50} value of 4.1 μM and also showed antibacterial activity against *S. aureus* with MIC of 100 μg/ml (Kwon et al., 2007). Hydroxylated 1, 3 di-hydroisobenzofurans were isolated from *Aspergillus flavipes* and it showed PDF inhibition with IC_{50} values of 2.5 μM and MIC of 25 μg/ml against *S. aureus*.

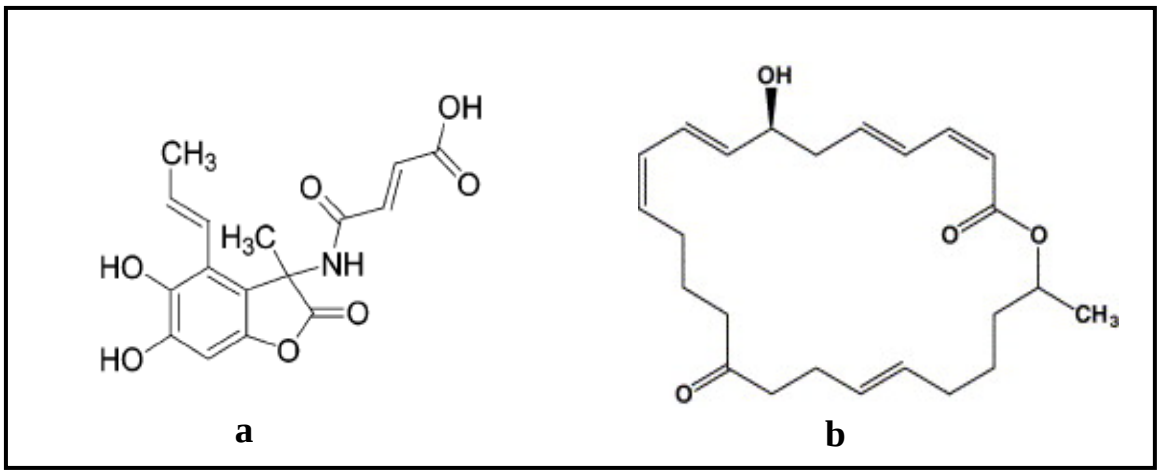

Fig 1.11: Non-hydroxamic acid based natural PDF inhibitors (a) Fumimycin**; (b)** Macrolactin**.**

Many reports regarding chemical synthesis and activity testing of PDF inhibitors have been reported in the previous decade since the identification of actinonin. Macrocyclic, peptidomimetic inhibitor and 2-(5-bromo-1*H*-indol-3-yl)-*N*-hydroxyacetamide based inhibitors are some of these which showed potent antibacterial activities (Hu et al., 2003; Boularot et al., 2007). But the most potent PDF inhibitors till date are derivatives of actinonin having hydroxamate or reverse-hydroxamate side chains.

Resistance against PDF inhibitors were also reported, mainly from the inhibition studies using actinonin and BB-84887. Resistance to PDF inhibitors in *S. aureus* and *E. coli* were mainly reported by mutation in the *fmt* gene and no mutations in the *def* gene (Clements et al., 2001). Hackbarth *et al.* reported resistance in a *Haemophilus influenza* mutant against PDF inhibitor VRC4332, due to a base pair deletion in the *fmt* gene (Hackbarth et al., 2002). In yet another study, reduced susceptibility of *H. influenzae* to PDF Inhibitor LBM415 was identified due to target protein over expression by amplified chromosomal *def* gene (Dean et al., 2007). Resistance in *Bacillus subtilis* to PDF inhibitor was mediated by mutations in *fmt*, *fol*D (5, 10-methylenetetrahydrofolate dehydrogenase) and *glyA* (serine hydroxymethyltransferase) (Duroc et al., 2009). Role of efflux pumps (ArcA and ArcB) in resistance to PDF inhibitors have been suggested in *E. coli* and *H. influenza*. The *arc*A and *arc*B mutants were shown to be more susceptible to PDF inhibitors (Clements et al., 2001; Hackbarth et al., 2002). A recent study suggests that improving membrane permeability of PDF inhibitors greatly enhance their inhibitory activities along with efflux pump inhibitors (Duroc et al., 2009).

1.3.5.2 Methionine aminopeptidases

1.3.5.2.1 Bacterial methionine aminopeptidase

Protein synthesis begins with methionine in eukaryotes or *N*-formyl methionine in prokaryotes, mitochondria, and chloroplasts. The N-formyl group is removed from proteins in prokaryotes and eukaryotic organelles by a deformylase, leaving a methionine residue at the amino terminus (Meinnel et al., 1993a). However, the majority of mature proteins do not retain the initiator residue. In the cytosolic extract of *E. coli* only 40% of the polypeptide chains retain the N-terminal methionine, whereas about 50% display Ala, Ser, or Thr at their N-termini (Waller, 1963). Methionine aminopeptidases (MAP E.C. 3.4.11.18) is a ubiquitous enzyme that serve to remove the N-terminal methionine residue of proteins and peptides of at least three residues in length (**Fig 1.12**), provided that the penultimate amino acid is small and uncharged (Ben-Bassat et al., 1987; Li and Chang, 1995). Typical penultimate residues have radii of gyration of 1.29 Å or less (Chiu et al., 1999) and include glycine, alanine, valine, cysteine, serine, threonine, and proline. These amino acids control the specificity of the enzyme and determine whether or not the initiator methionine is cleaved. The removal of the N-terminal methionine residue is a prominent step in the maturation of proteins for proper function, targeting and degradation (Giglione et al., 2003).

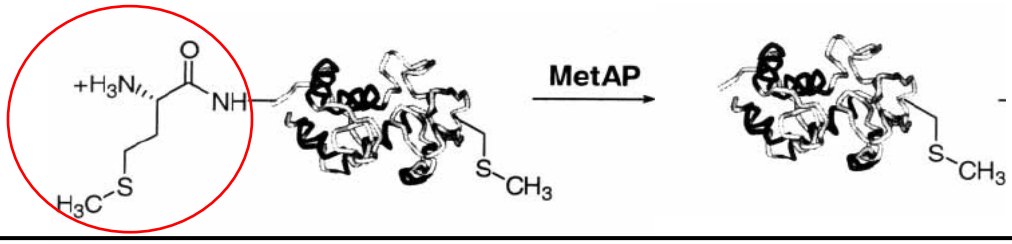

Fig 1.12: N-terminal methionine cleavage from nascent polypeptide by methionine aminopeptidase (MAP) (Adopted from Vaughan et al., 2002).

The pioneer works on MAP were reported in 1960s, mainly from *E. coli* (Waller, 1963; Fry and Lamborg, 1967; Vogt, 1970). But major studies on MAP were reported in late 1980s (Miller 1987; Arfin and Bradshaw, 1988). MAP has been proven essential for survival of gram negative bacteria such as *E. coli* and *S. typhimurium* (Chang et al., 1989; Miller et al., 1989). Its essentiality was later proved in gram positive bacteria also such as *Staphylococcus aureus* and *Bacillus subtiis* (Wong et al., 2005; You et al., 2005). Its physiological relevance has given rise to considerable interest among researchers to design antimicrobial inhibitors that specifically target this enzyme.

In general, bacteria and archaea have been shown to possess single gene encoding MAP, unlike the case of eukaryotic cytoplasm where there are at least two types of MAPs (Tsunasawa et al., 1997; Bradshaw et al., 1998). But advent of genome sequencing has revealed multiple *map* genes in many bacteria like *B. subtilis*, *Synechocystis* and *M. tuberculosis* (You et al., 2005; Atanassova et al., 2003; Addlagatta et al., 2005b) with all the homologues coding for functional enzymes. However, among these multiple *map*

genes, some of these *map* genes, like *ylf*G in *B. subtilis,* were proven to be dispensable for viability of the cell (You et al., 2005).

MAP enzymes have been proven to be metallo-enzymes from the time it was first characterized (Ben-Bassat et al., 1987; Wingfield et al., 1989). The purified MAP enzyme activity was affected by the presence of metal-ion chelators like EDTA and 1, 10, phenanthroline. Early studies on *S. typhimurium* MAP has proved the enzymes to be activated by Co^{2+} and not by Mg^{2+} or Zn^{2+}. However, the purified native MAP proteins revealed no significant amount of Co^{2+}, which led to the conclusions that the enzymatically important Co^{2+} is loosely associated (Wingfield et al., 1989). The identity of metal co-factor in MAP proteins *in vivo* has not been established and is still under debate. The x-ray crystal structure of MAP from *E. coli* revealed the presence of two Co^{2+}, suggesting it to be a di-nuclear metal binding enzyme (Roderick and Matthews, 1993). But, the later studies suggested the same enzyme to be mono-metelated and that the di-nuclear metal binding is due to the high concentrations of metal ions used during crystallization (Cosper et al., 2001; Ye et al., 2006). Characterizations of *E. coli* MAP in anaerobic conditions suggested Fe^{2+} as the physiologically relevant metal ion (D'souza and Holz, 1999). In addition, their analysis of the metal content of bacterial extracts without and with the plasmid- based over expression of *E. coli* MAP showed that the level of Fe^{2+} increased significantly in the latter case. Many of the recent studies support this view that Fe^{2+} is the physiologically relevant metal cofactor of *E. coli* MAP and Co^{2+} is only an *in vitro* activator of the enzyme (Chai et al., 2008; Wang et al., 2008). In contrast, an analysis of the metal content of endogenous and recombinant *Pyrococcus furiosus* prolidase,

another "pita-bread" enzyme, suggested Co^{2+} to be the relevant cation (Ghosh et al., 1998). Meng et al. (2002) found Fe^{2+}-loaded *P. furiosus* MAP II to be a much better catalyst at the optimum growth temperature of *P. furiosus* (85 ^{o}C). It has been demonstrated that different bacterial MAPs purified as apo-enzymes were activated *in vitro* by Co^{2+}, Mn^{2+}, Fe^{2+} or Zn^{2+} (Li et al., 2003). It remains unclear to what degree the metal ions used *in vivo* are intrinsic to the individual enzymes or are determined by the ambient levels of ions within the organism (Kobayashi and Shimizu, 1999). To date, nearly 50 different prokaryotic MAP proteins have been biochemically characterized from various bacteria and archeaebacteria, mainly bringing out their catalytic activities, metal ion activation profiles, inhibition and structure. **Table 1.3** summarizes studies on some bacterial and archaebacterial MAPs.

Table 1.3 Summary of reports on bacterial methionine aminopeptidases

Organism	Significant features	Reference
Escherichia coli	Single *map* gene; Type Ia bacterial MAP, Crystal structure show 'pita-bread' fold, Crystallized as mono and di-metalated, with either Co^{2+} or Fe^{2+}, Fe^{2+} as native metal ion.	Ben-Bassat et al., (1987) D'souza et al., (2002) Chai et al., (2008) Wang et al., (2008)
Salmonella typhimurium	*pep* M is essential; 34 kDa protein. MAP performs NME, Activated by Co^{2+}.	Wingfield et al., (1989) Miller et al., (1987) Miller et al., (1989)
Bacillus subtillis	Two MAP genes (*map* and *ylf*G), *ylf*G highly active *in vitro*, but dispensable *in vivo*.	You et al., (2005)
Bacillus stearothermophilus	Native MAP enzyme a dimer; optimum activity at 80 ^{o}C,Activated by Co^{2+}.	Chung et al., (2002)
Synechocystis sp. (Cyanobacteria)	Three MAPs encoded by slr0786 (*map-1*), slr0918 (*map-2*) and sll0555 (*map-3*); MAP 1 and MAP 3 highly active, MAP 1 deletion leads to impairment in Photosystem II.	Atanassova et al., (2003) Drath et al., (2009)
Pyrococcus furiosus (Archaea)	Single MAP, Bacterial type II MAP;Thermostable at 100 ^{o}C, insertion domain in crystal structure.	Tsunasawa et al., (1997) Tahirov et al., (1998)
Mycobacterium tuberculosis	Two MAP genes; MAP B crystallized show SH3 binding domain (type IIb), MAP A and MAP B expressed differentially in log and stationary phase.	Addlagatta et al., (2005b) Zang et al., (2009) Olaleye et al., (2010)
Mycobacterium smegmatis	Purified native MAP, activated by Mg^{2+}, inhibited by actinonin.	Narayanan et al., (2008)
Acinetobacter baumannii	Two putative MAP, Both activated best by Fe^{2+}	Yuan et al., (2011)

1.3.5.2.2 Eukaryotic methionine aminopeptidases

NME is a universal process and thus, MAP is an ubiquitous enzyme present in all compartments where protein biosynthesis takes place. Two types of MAP proteins have been suggested till date, MAP type 1 and MAP type 2. Bacteria have type 1 MAP; archea have type 2 MAP and eukaryotes have both type 1 and type 2 MAPs involved in their NME process in cytoplasm (Bradshaw et al., 1998). Additionally, organelle MAPs have been identified from plastids and mitochondria of all eukaryotes, except in case of fungus and nematodes (Giglione et al., 2004).

All eukaryotic MAPs have 50–100 residue long N-terminal extensions, which are absent from prototypic prokaryotic MAPs. Organellar MAPs are thought to have a cleavable N- terminal pre-sequence, targeting the catalytic domain to the correct cell compartment (Serero et al., 2003). Cytoplasmic MAP 1s also have an N-terminal extension, including a conserved zinc finger motif. Although not involved in catalytic activity, this additional domain is not removed from the mature form and is essential for the cellular function of MAP 1s. It has been suggested that this N-terminal extension may facilitate interaction with ribosomes (Zuo et al., 1995; Vetro and Chang, 2002). The N-terminal extensions of eukaryotic MAP 2s are not required for aminopeptidase activity (Yang et al., 2001), and this domain was found to be disorganized in the crystal structures of MAP 2 (Liu et al., 1998). This extensions have an N-terminal lysine rich domain (acidic domain) and is thought to be responsible the protection of animal eIF2α from stress-induced phosphorylation. This protective activity is mediated by both an N-terminal lysine- rich domain I and an O-glycosylation site in animal MAP 2s (Datta et al., 2001).

As at least one of these two domains is absent from the MAP 2s of plants and fungi, these enzymes are unlikely to display this protection of eIF2α (Giglione et al., 2004). Although both eukaryotic MAP 1s and MAP 2s have similar polypeptide length (380 aa vs 450 aa) and monomeric behavior, the former shows a molecular mass of 38 kDa and later shows 65 kDa on SDS-PAGE (Kendall and Bradshaw, 1992; Li and Chang, 1996).

1.3.5.2.2a Methionine aminopeptidases from plants, parasites and yeast

The genome of *A. thaliana* showed four MAP 1 genes (MAP 1A, MAP 1B, MAP 1C and MAP 1D) and one MAP 2 gene (MAP 2A). Among these, MAP 1A and MAP 2A are cytoplasmic, MAP 1B is targeted to plastids, MAP 1C to both plastids and mitochondria and MAP 1D to mitochondria (Giglione et al., 2000b). The homologs of these MAP genes were also found in other higher plants like rice and tomato by screening their genomes and expressed sequence tags (EST), suggesting the similarity in overall NME process in plants. Very recently, a new DNA binding MAP was reported from barley plants which got expressed during cold-treatment and changes its location from nucleus to cytoplasm. It was suggested to have an additional role in cold-tolerance in plants (Jeong et al., 2011).

One cytoplasmic MAP 1A and one organelle MAP 1B was found in the genome of protists *Dictyeostelium discoideum.* The genome of *Drosphilla* and *C. elegans* showed same number of MAP genes as in the case of *A. thaliana* (Giglione et al., 2000b).

The genome sequence of parasite *P. falciparum* revealed total of four MAP genes, MAP 1a, MAP 1b, MAP 1c and MAP 2 (Chen et al., 2006). Among the four, MAP 1b was found to be most similar to human and yeast MAP 1 and possessed the zinc-finger domain in the N-terminal extension. MAP 1b was demonstrated as potent target for anti malarial

drug targeting. Chen et al., (2006) identified pyridinyl-pyrimidine based inhibitors of *P. falciparum* MAP 1b as potent anti-malarial compounds. *P. falciparum* MAP 2 was later demonstrated to be a target for the inhibitor fumagillin and fumarranol, which non-covalently interacted with the enzymes. The anti-malarial activities using these drugs against *P. falciparum* MAP 2 were demonstrated both *in vitro* and in mouse models (Chen et al., 2009).

Saccharomyces cerevisiae (yeast) possess two MAP genes, MAP 1 and MAP 2, both having the characteristic N-terminal extensions with the zinc-finger domain and acidic-base domains, respectively. Deletions of either MAP 1 or MAP 2 in yeast lead to a slow growing phenotype, while deletion of both was lethal (Chang et al., 1992; Li and Chang, 1995). Both these genes have only 22% similarity between themselves, but MAP 2 has 55% similarity to initiation factor (IF P^{67}). The N-terminal extension with zinc-finger domain of MAP I was indispensable for ribosomal association and its normal functioning *in vivo* (Vetro and Chang, 2002). Studies on metal activation of yeast apo-MAP 1 enzyme in the reducing environment in presence of reduced-glutathione showed Zn^{2+} as better activator than Co^{2+}, which suggested the former to be the physiologically relevant metal ion in yeast MAP 1 (Walker and Bradshaw, 1998). Using site-directed mutagenesis, the substrate specificity of recombinant yeast MAP 1 was altered to utilize substrates with bulkier substrates at the penultimate positions (Walker and Bradshaw, 1999). Based on high-throughput screening using *map-2* deletion mutant of yeast, pyridine-2-carboxylic acid derivative was identified as an inhibitor of MAP 1 enzyme, suggesting this enzyme as a potent anti-fungal drug target (Chen et al., 2004). Studies showed that MAP 2, but not

MAP 1, is inhibited at excess concentrations of methionine, which makes MAP 1 essential for methionine salvage pathway in yeast (Dummit et al., 2003). Yeast MAPs serve as surrogates for screening drugs, such as antineoplastic agents, against human MAPs and other eukaryotic MAPs, due to the similarity in structure between the two (Cardenas et al., 1999).

1.3.5.2.2b Human methionine aminopeptidases

Similar to higher eukaryotes, human cells also posses two MAPs, MAP 1 and MAP 2, in cytoplasm and a mitochondrial MAP, MAP 1D (Serero et al., 2003). MAP 1 has typical zinc-finger domain and MAP 2 has acidic domain in their N-terminal extensions (Addlagatta et al, 2005a). Among the two, MAP 2 is known to play important role in translation initiation by its role in protecting eukaryotic initiation factor 2α, apart from its role in NME (Datta et al., 2001). Although many different metal ions like Co^{2+} Zn^{2+} and Fe^{2+} show *in vitro* activation of both human MAPs, the physiologically relevant metal ion for MAP 2 is suggested to be Mn^{2+} (Wang et al., 2003). For MAP 1, the metal preferences *in vivo* are unknown. Human MAP 2 has been reported to play important roles in many physiological processes like endothelial cell proliferation and angiogenesis (Griffith et al., 1997). Inhibition of MAP 2 in human endothelial cell lines arrested the cell cycle at G1 phase (Zhang et al., 2000). The physiological roles of MAP 1 in human cell were largely unknown until recent times.

Recently, inhibiting human MAP 1 with pyridine-2-carboxylic, inhibitor of yeast MAP 1 and by silencing its expression using gene-specific siRNA, led to arrest in the cell cycle at G2/M transition phase. So at present the role of MAP 1 is suggested in the

transition between G2 and M phase of cell cycle, in addition to NME (Hu et al., 2006). Recently the mitochondrial MAP enzyme, MAP 1D in human has been characterized as recombinant enzyme to be an active MAP enzyme with *in vitro* catalytic activity close to MAP 2 (Leszczyniecka et al., 2006). MAP 1D was found over expressed in colon cancer cell lines and their down regulation by siRNA reduced the anchorage-independent growth of colon carcinoma.

MAP 2 has long been recognized as a potent target for anti-angiogenesis, anti-cancerous and anti-rheumatoid drug designing (Selvakumar et al., 2006). Natural product fumagillin and its derivatives were known to inhibit MAP 2 and were also shown to be potent anti-angiogenic agents that prevent vascularization and metastasis of many forms of tumors (Griffith et al., 1998). The structure of fumagillin-MAP 2 complexes revealed that the inhibitor forms covalent bond to His231 (Liu et al., 1998). The conserved residue H212 in MAP 1 shows similar orientation of H231 in MAP 2. But, fumagillin and its derivatives face steric clashes in MAP 1, which are absent in MAP 2, that prevent them from modifying H212 (Addlagatta et al., 2005a). Along with MAP 2, the other two MAPs are also emerging as potent drug targets for various forms of cancer (Leszczyniecka et al., 2006; Hu et al., 2006).

1.3.5.1.3 Structure and catalytic mechanisms of methionine aminopeptidase

The crystallographic analysis of the prototypical MAP from *E. coli* revealed the pita- bread' fold (Roderick & Matthews, 1993). The pseudo two-fold-related N and C-terminal domains each contain two α-helices and two antiparallel β-strands. Both

domains contribute conserved residues to form the dinuclear metal center. Two metal ions are bound by monodentate (His171, Glu204 in *E.coli* MAP) and bidentate (Asp97, Asp108, Glu235) ligands (**Fig 1.13**). A metal bridging water or hydroxide ion is thought to act as the nucleophile during catalysis. Despite the apparent overall symmetry of the molecule, the active site is asymmetrically located with the methionine binding pocket generated by residues primarily from the N-terminal domain (Roderick & Matthews, 1993). Sequence alignments and structure determinations confirm that enzymes with different activities and substrate specificities also contain the pita-bread fold including aminopeptidase P, creatinase and prolidase (Lowther and Matthews, 2000).

The MAP family was initially divided into two classes based upon sequence alignments (Bazan et al, 1994; Arfin et al, 1995) (**Fig 1.14**). The X-ray structures of the *P. furiosis* and human MAPs have confirmed this distinction (Tahirov et al., 1998; Liu et al., 1998). The type II enzymes are distinguished from type I by a helical subdomain of approximately 60 residues in length inserted within the C-terminal domain. This inserted sub-domain shares no sequence or structural homology with any other known protein. The absence or presence of N-terminal domain extensions for both prokaryotic and eukaryotic MAPs further differentiates these enzymes (Bradshaw et al., 1998). *E. coli* MAP represents type Ia enzyme, yeast MAP represents type Ib, *M. tuberculosis* MAP B represents type Ic and human MAP 2 represents the type II MAP enzymes (Fig 1.13). Eukaryotic MAPs are differentiated from their prokaryotic counterparts by an additional N-terminal extension. The eukaryotic MAP1 has two putative zinc finger motifs in this 12-kDa region (Zuo et al., 1995), and the eukaryotic MAP2 has a highly charged N-terminus

with alternating polyacidic and polybasic stretches in a similarly sized segment (Chang et al., 1992).

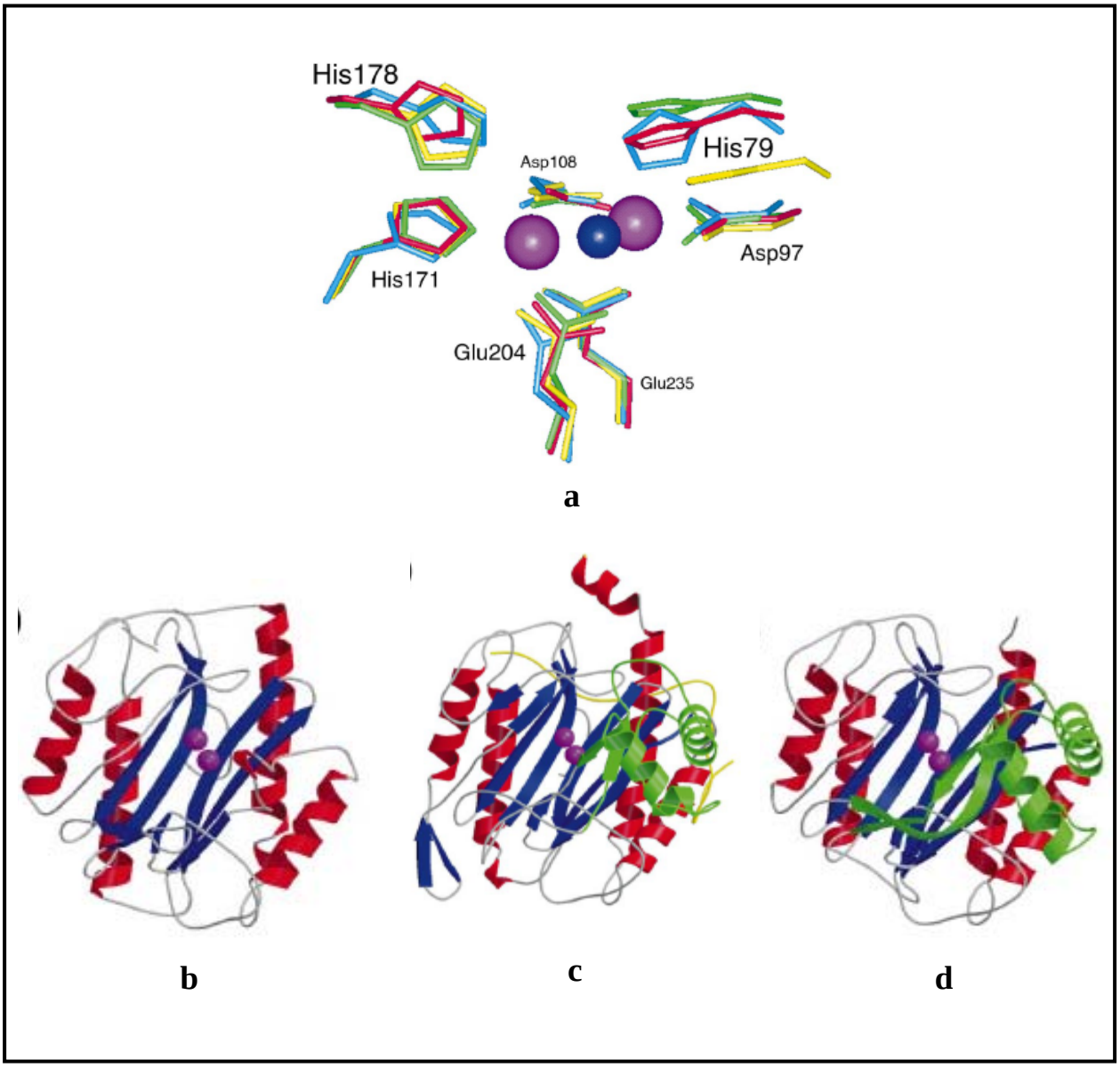

Fig 1.13: Structure of MAP; (a) Conserved di-nuclear metal-binding site of different MAPs overlapped; The numbering corresponds to *E. coli* MAP; **(b)** Crystal structure of *E. coli* MAP (PDB: 2MAT) **(c)** *P. furiosis* MAP (PDB:1XGS) **(d)** Human MAP II (PDB: 1BN5). The C-terminal insertions are shown in green helices and Co^{2+} in magenta spheres. (Adopted from Lowther and Mathews, 2000)

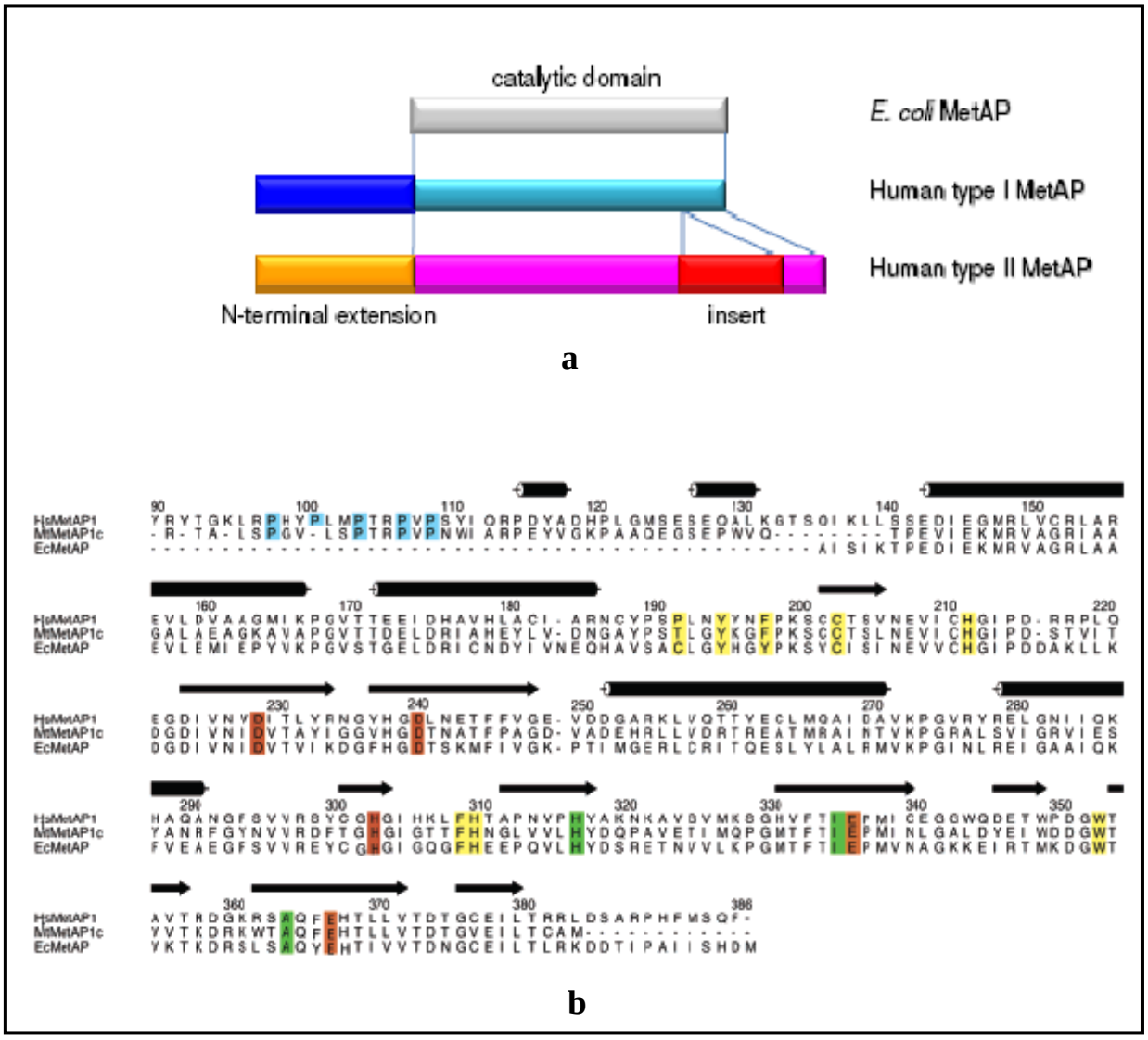

Fig 1.14:Domain organization and sequence conservation in MAP (a) Domain organization in type I and type II MAPs; **(b)** Multiple sequence alignment of subclasses of type I MAPs showing conservation of residues involved in formation of metal binding pocket (red), S1 (yellow) and S1'(green) substrate-binding sites (Adopted from Ma et al., 2007 and Addlagatta et al., 2005a).

MAP belongs to the dinuclear metallohydrolases. Many MAP structures have been reported with two metal ions at the active site (Lowther and Mathews, 2000), and the two metal ions are coordinated by five conserved amino acid residues (D97, D108, H171, E204 and E235 in *E. coli* MAP). The affinities of the two metal ions are quite different in solution. Based on electronic absorption spectra titration, isothermal titration calorimetry, and kinetics, D'souza et al., (2002) showed that dissociation constants for the tighter site were at or below micromolar (*K*D1 0.3 μM, 0.2 μM and 6 μM for Co^{2+}, Fe^{2+} and Mn^{2+}, respectively), but the affinity for the second metal ion was much weaker with a millmolar dissociation constant (*K*D2 2.5 mM for Co^{2+}).

The residues that contribute to the recognition of the substrates in different types of MAPs were located in approximately the same three-dimensional space. The S1 subsite of *E. coli* MAP is created by surface loops including residues 59-68 and 214-224 (Lowther et al., 1999b). These loops are shorter in other type I and type II MAPs. The type II enzymes also have a unique loop in this subsite that contributes a conserved tyrosine which corresponds in space to Trp221 of *E. coli* MAP (Tahirov et al., 1998; Liu et al., 1998). In S1' subsite of type II MAPs, this loop contributes an additional leucine (Leu447 in human MAP 2). Tyr168 and Met206 of *E coli* MAPs are also replaced by Leu and Phe in the type II enzymes. The importance of these residues is supported by the changes in substrate specificity for the Met329 and Gln356 mutants of yeast MAP 1b (Met206 and Gln233 in *E. coli* MAP) (Walker and Bradshaw, 1999). The substitution of smaller amino acids at these positions enabled the cleavage of substrates with larger penultimate residues. The mutant enzymes, however, were still not able to accommodate charged amino acids. The

human MAP 2 appears to be different from *E. coli* MAP in that it is able to cleave dipeptides and small chromogenic and fluorogenic substrates, though with significantly lower cleavage rates than the conventional tripeptides and larger substrates (Yang et al., 2001).

Based on the comparisons of the inhibited and native forms of *E. coli* MAP, the binding mode of the bestatin-based inhibitor, the kinetic analysis of His79 and His178 mutants, and the spectral analysis of the metal center in response to the addition of product, a possible reaction mechanism has been proposed for *E. coli* MAP (**Fig. 1.15**) (Lowther et al., 1999a; Lowther et al., 1999b). This mechanism assumes: (1) that the N-terminus of the substrate coordinates 2nd Co at the expense of a terminal solvent molecule; (2) the formation of a non-covalent tetrahedral intermediate; (3) that the carbonyl oxygen atom of the scissile bond (OC) interacts with 1st Co and His178; (4) that the nitrogen of the scissile bond interacts with Glu204 and His79; and (5) that the nucleophile of the reaction (ON) is an activated solvent molecule bridging between the metal ions.

The catalytic functions assigned to key residues in *E. coli* MAP have similarities to residues in other enzymes containing mononuclear and dinuclear metal centers. The role of Glu204 is to function as a proton shuttle. The significant residual activity of the His178Ala mutant of *E. coli* MAP and the His339Asn mutant of human MAP 1 suggests that the function of this histidine to help stabilize the transition state is not essential, but does promote catalysis. However, in a manner similar to that proposed for His141 and His64 in arginase and carbonic anhydrase II, His178 may expedite the formation of the nucleophile by providing a pathway for the release of a proton to solvent. The proposed role of His79

and the equivalent residues in creatinase is to facilitate the binding of substrates in a productive manner for catalysis via a hydrogen bond to the nitrogen atom of the scissile bond (Lowther and Matthews, 2000; Lowther and Matthews, 2002).

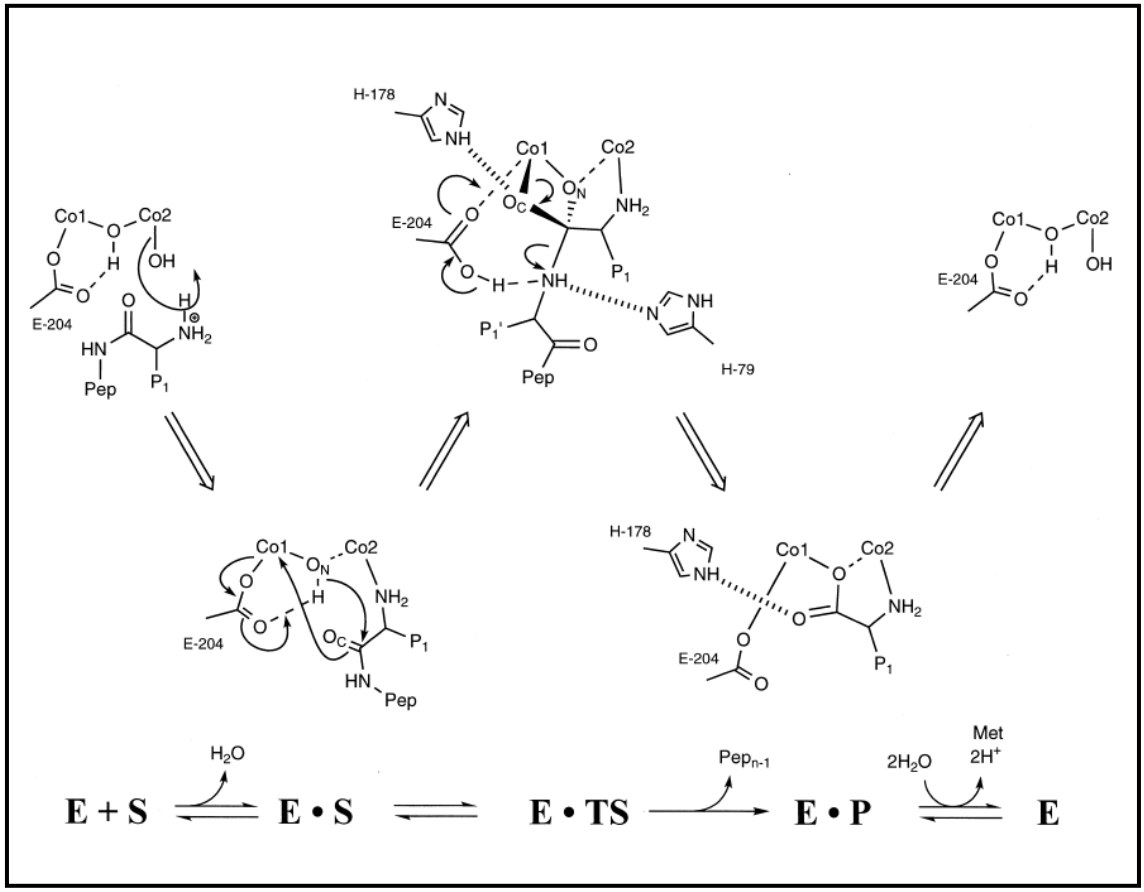

Fig 1.15: Proposed catalytic mechanism of di-nuclear MAP (Adopted from Lowther and Matthews, 2000).

Recent conception of MAP as mono-metalated enzyme *in vivo* has led to proposal of yet another catalytic mechanism of MAP as mono-metalated enzyme (Ye et al., 2006) (**Fig 1.16**). Based on norleucine phosphonate, transition-state analog and a single Mn^{2+} ion bound to the metal biding site 1 (M1), *E. coli* MAP structure was solved as mono-metalated enzyme. The study suggests that due to very weak binding constant for a second

metal binding at M2, mono-metalated catalysis is significant *in vivo*. Instead of unprotonated amino terminus of the substrate coordinating to M2, charge-charge interactions involving Asp97 and Asp108 with protonated (pH 7.0) amino terminus binds the substrate. The side chains of Asp97 and Asp108 shift towards the amino group of the substrate. The carboxyl group of Glu204 is positioned to act as a general base to deprotonate water molecule coordinated to M1, allowing it to act as a nucleophile. His79 participates in catalysis by donating a proton to departing amino group through a charge relay involving the imidazole ring of His79.

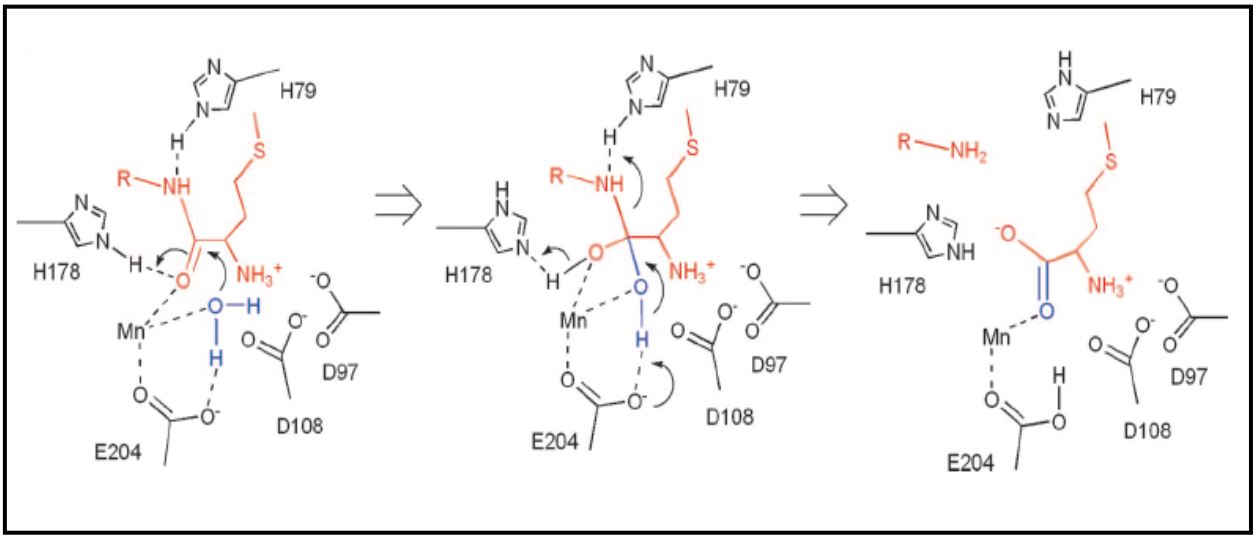

Fig 1.16: Proposed catalytic mechanism of mono-metalated MAP (Adopted from (Ye et al., 2006).

1.3.5.2.4 Methionine aminopeptidase inhibitors

As a result of its essentiality in microorganisms, as well as its role in angiogenesis in tumor growth, various inhibitors of MAPs have been studied. Although there are intensive

efforts in searching for MAP inhibitors, very few potent MAP inhibitors have been described so far. These are grouped as covalent and non-covalent inhibitors.

MAPs are inhibited by the natural product fumagillin and its derivatives such as TNP-470 and ovalicin (**Fig 1.17**). Fumagillin, the best-characterized inhibitor, was first identified as covalently modifying bovine brain and human umbilical vein endothelial cell MAP 2.These compounds have been shown to be potent anti-angiogenic agents that prevent the vascularization and metastasis of tumors (Sin et al., 1997). The core of this class of inhibitors is a cyclohexane ring substituted with an epoxide at C2-C3, an epoxide-containing hydrophobic side-chain at C4, and a methoxy group at C5. The specific, covalent modification by fumagillin did not block one function of MAP 2, namely, the prevention of the phosphorylation of the translation initiation factor eIF-2 (Griffith et al., 1997). Griffith and colleagues (1998) found that the ring epoxide was involved in the covalent modification of MAP 2 while the side chain epoxide groups were dispensible. The site of covalent attachment was first reported for *E. coli* MAP as the conserved His79 residue in the active site, although biochemically fumagillin has a preference for MAP 2s (Lowther et al., 1998).

There are few identified effective non-covalent inhibitors of both MAP 1 and MAP 2. The natural product bestatin, a potent inhibitor of leucine aminopeptidase, was used as a framework for the design of *E. coli* MAP inhibitors (Burley et al., 1992). The N-terminal side-chain of bestatin was replaced with that of norleucine, a Met analogue with the sulfur atom of the side chain replaced with carbon, while an alanine was placed at the P1' position (**Fig 1.17d**). The resulting compound, SL648, or AHHpA-Ala-Leu-Val-Phe-Ome,

bound to the metal center in *E. coli* MAP and inhibited the enzyme with a modest IC_{50} of 5 μM (Lowther and Matthews, 2000). Transition-state analogues have also been designed as inhibitors for *E. coli* MAP and have been shown to bind to the metal center in a manner similar to SL648 (Lowther et al., 1999).

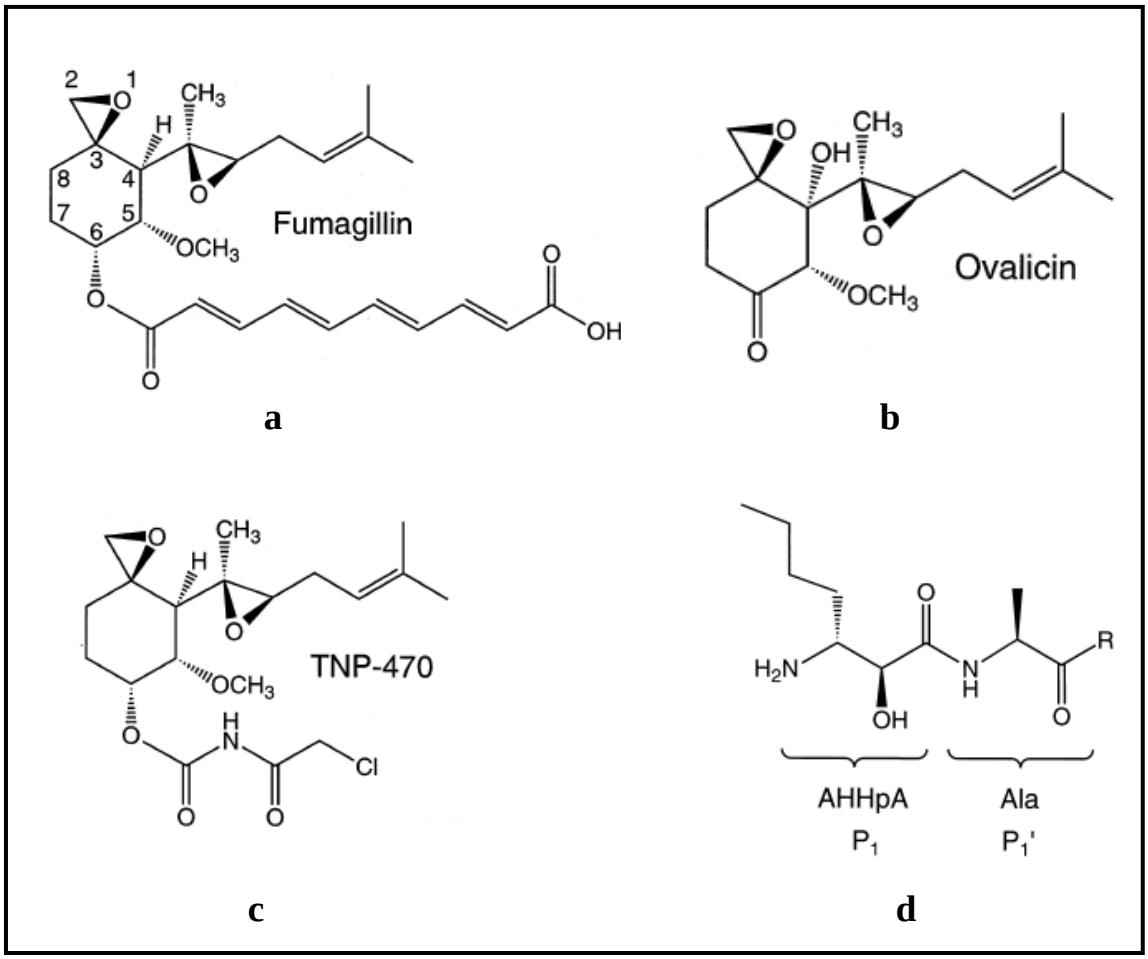

Fig 1.17: Chemical structures of covalent (a,b, c) and non-covalent inhibitors (d) of MAP; (a) Fumagillin **(b)** Ovalicin **(c)** TNP-470 **(d)** Bestatin-based analog (3R)-amino-(2S) hydroxyheptanoic acid (AHHpA). (Adopted from Lowther and Matthews, 2000).

Many works have utilized high-throughput screening of a diverse small chemical library followed by structural modifications of screening leads to identify potent inhibitors

of *E. coli* MAP and yeast MAP 1 (Luo et al., 2003; Chen et al., 2004). Some of these turned to be potent small molecule inhibitors of MAPs in *in vitro* assays. But these compounds generally showed low to moderate antibacterial activity when tested against various organisms. All these inhibitors were screened against Co^{2+} substituted MAP in the *in vitro* assay. One explanation for the lack of antibacterial activities may be a disparity between the metalloform tested using a purified enzyme and the one that exists in cells. It is apparent that MAP inhibitors have to effectively inhibit the cellular MAP to be therapeutically useful. Many recent works have concentrated on designing and screening metalloform-selective inhibitors against different metallo-forms of MAPs and several sets of these inhibitors have been described in recent past (Ye et al., 2004; Wang et al., 2008). Using this approach it was confirmed that only Fe^{2+} selective inhibitors show antibacterial activity on several *E. coli* and Bacillus strains (Wang et al., 2008). Thus it was concluded that Fe^{2+} is likely to be the metal cofactor *in vivo* for *E. coli* and other bacterial cells. These studies also highlight the importance of studying the metal ion preferences of MAPs from different bacteria, prior to screening inhibitors against them.

1.3.5 Contemporary studies on NME enzymes of *M. tuberculosis*

The importance of NME enzymes as potential drug targets in bacteria for identification of next generation antimicrobials has been conceived and established in 1990s. The complete genome information of *M. tuberculosis* was available in the public domain since 1998. But, relevant studies on the NME enzymes of *M. tuberculosis* started to appear in literature only by 2005. When the present study was initiated, there were only limited reports available on these enzymes from *M. tuberculosis.* The following portion

summarizes the contemporary efforts of different groups in characterizing the structural, functional and biochemical aspects of peptide deformylase and methionine aminopeptidases of *M. tuberculosis*.

1.3.6.1 Studies on Mycobacterium peptide deformylase (MtbPDF)

As part of screening the activity spectrum of peptide deformylase inhibitor BB-3497, a derivative of actinonin, its *in vitro* activity against *M. tuberculosis* was tested (Cynamon et al., 2004). This study demonstrated that BB-3497 is a potent inhibitor of *M. tuberculosis* in culture. Biochemical studies on recombinant MtbPDF were reported by Saxena and Chakraborti (2005a; 2005b). They reported MtbPDF to be a Fe^{2+} containing enzyme showing stability towards oxidizing agents with moderate thermo-stability. The C-terminal extension in MtbPDF was identified as indispensable for the activity of the enzyme. Similarly, an insertion region between motif I and motif II of MtbPDF was identified as the region determining stability of the enzyme. Based on biophysical studies, they suggested MtbPDF to be functional as dimer in solution. Later the same group reported the importance of three consecutive arginines in insertion sequences of MtbPDF in providing stability to the enzyme towards oxidizing agents (Saxena et al., 2008). They identified this insertion region as unique for MtbPDF and demonstrated its essentiality *in vivo* for cell viability of *M. smegmatis* by targeting them with anti-sense oligo nucleotides. In a parallel study by Teo et al., (2006), the essentiality of *def* gene for cell viability was demonstrated by creating targeted gene knock-outs in *M. bovis* BCG. Their studies also reported the evaluation of antimycobacterial effects of a novel class of PDF inhibitors, the *N*-alkyl urea hydroxamic acids, against both *M. bovis* and some MDR strains of *M. tuberculosis*.

These inhibitors were highly effective in arresting the growth of both the tested cultures. This study also demonstrated that spontaneous resistance development in Mycobacterium towards PDF inhibitors, mediated by mutations in the formyl metheionine transferase gene (*fmt*). The same group elucidated the crystal structure of MtbPDF along with inhibitor molecule LBK-611 bound to the peptide binding pocket (Pichota et al., 2008). The structure had Ni^{2+} as the metal-cofactor and revealed that tertiary structure of MtbPDF is made up of three α-helices, seven β-sheets and three 3_{10} helices, forming three motifs and a structurally conserved active site. This is the only crystal structure of MtbPDF available till date in the public domain (PDB ID: 3E3U) (**Fig 1.18**). Recently the *in vitro* and *ex vivo* activities of various PDF inhibitors were tested on *M. tuberculosis* H37Rv and the results demonstrated that while BB-3497 and 1,10-phenanthroline were potent antimycobacterials *in vitro*, BB-3497 and actinonin were showed significant antimycobacterial activities *ex vivo* with efficacy comparable to isoniazid (Sharma et al., 2009).

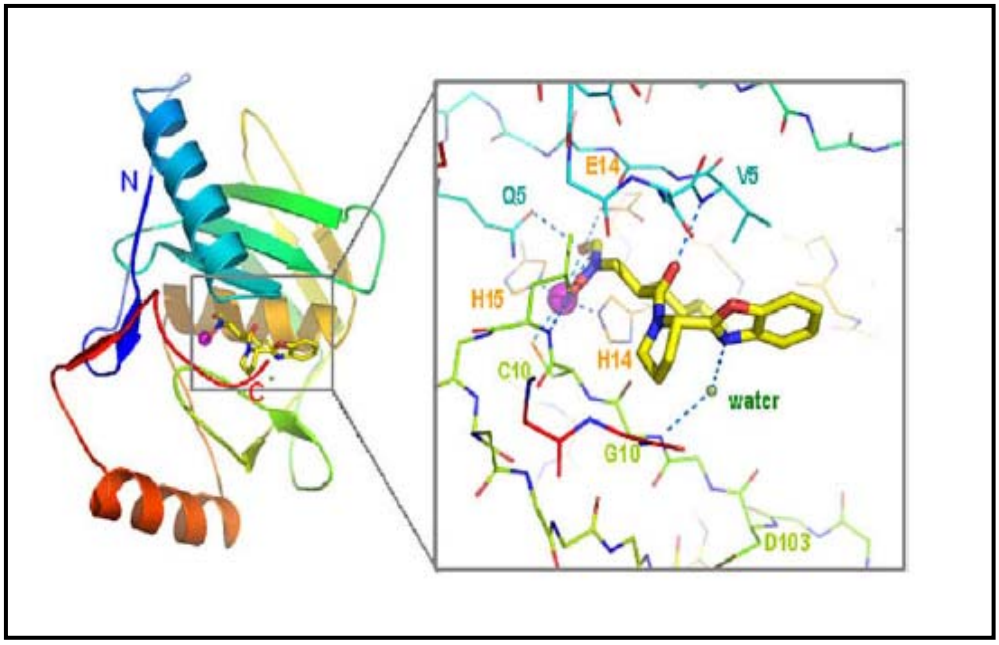

Fig 1.18: Crystal structure of MtbPDF with inhibitor bound to it (PDB ID: 3E3U). (Pichota et al., 2008). Inset shows the mode of inhibitor binding in the active site

1.3.6.2 Studies on Mycobacterium methionine aminopeptidases (MtbMAPs)

The X-ray crystal structure of MAP B from *M. tuberculosis* H37Rv (MtbMAP B) as Co^{2+} enzyme was elucidated to provide structural evidences for the mode of interaction of this enzyme with the ribosome (Addlagatta et al., 2005b). The extended N-terminal of MtbMAP B was reported to possess a Pro-Thr-Arg-Pro (PXXP) segment which can interact with the SH3 protein motif on ribosomes. Based on the variations in the N-terminal extensions in MtbMAP B, they have suggested classifying this enzyme as type Ib MAP (**Fig 1.19**). From then, for long time there were no reports on either structural or biochemical properties of MtbMAPs. During this period, in our lab, we could purify a putative MAP protein from the cell lysates of *M. smegmatis* mc^2 155 and characterize its properties (Narayanan et al., 2008). This protein could hydrolyse the tested substrate L-

Met-*p*-Nitro anilide with high efficiencies and showed activation by both Co^{2+} and Mg^{2+}. The MAP activity of this enzyme was inhibited by actinonin and based on these properties we proposed it to be a bonafied MAP enzyme from *M. smegmatis*.

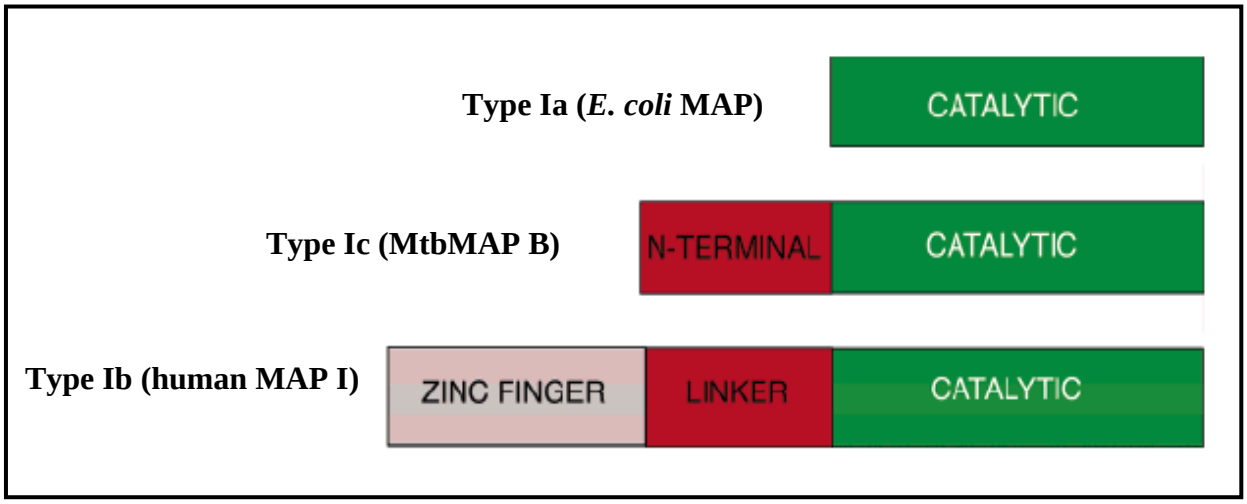

Fig 1.19: Classification of MtbMAP B as type Ic MAP (Adopted from Addlagatta et al., 2005b).

Zhang and colleagues expressed both MtbMAP A and MtbMAP B as recombinant proteins in *E. coli* and characterized the biochemical properties of these enzymes (Zhang et al., 2009). They compared the properties of both these enzymes with MAP from *M. smegmatis* and suggested MtbMAP A to have similar properties. In their studies, both the MtbMAP enzymes had similar catalytic activities. The transcript levels of both *map*A and *map*B were determined using real-time quantitative PCR in both log-phase and stationary phase cultures of *M. tuberculosis* H37Rv and *M. tuberculosis* H37Ra to reveal the increased expression of MtbMAP A in log-phase cultures and MtbMAP B in stationary phase cultures. Simultaneously, another group characterized the recombinant MtbMAPs and reported MtbMAP B to have better *in vitro* activity compared to MtbMAP A (Olaleye

et al., 2010). Importantly, the knock-down of MtbMAP A, but not MtbMAP B, was reported to cause decrease in growth of *M. tuberculosis*. Their results supported the findings from Zhang et al., (2009) that MtbMAP A is expressed in the active phase of growth in *M. tuberculosis*. Olaleye et al., (2010) also described 2, 3-dichloro-1, 4-naphthoquinone class of compounds as inhibitors of both MtbMAPs. The above two studies were performed using MtbMAPs as holo-enzymes purified from *E. coli* and activated in presence of Co^{2+} thus, didn't give priorities in determining the effects metal ion co-factors in these enzymes. Studies on MtbMAPs as apo-enzymes and their activation by metal-ion cofactors were described by Prof. Qi-Zhuang Ye's group (Lu et al., 2010; Lu and Ye, 2010). They reported Ni^{2+} as the best co-factor in activating the *in vitro* enzyme activities of both MtbMAP A and MtbMAP B. They determined the metal-affinities of divalent cations to the active sites of MtbMAPs using a multiple independent binding sites (MIBS) model proposed by them (Chai et al., 2009) and revealed that the metal affinity for the first metal ion is much higher than the second metal ion at the di-nuclear metal center of MtbMAPs. Their results suggest that at optimum metal ion concentrations MtbMAP A shows catalytic efficiencies folds higher than MtbMAP B. Metallo-form selective inhibitors of both MtbMAPs were reported by Lu et al., (2010) and Lu and Ye (2010) based on derivatives of cathecols and trizoles, showing potent inhibition of *in vitro* activities of both the enzymes. X-ray crystal structures of MtbMAP B with some of these inhibitors were solved at high resolution (PDB ID 3IU7 to 3IU9) to reveal the mode of binding of these inhibitors in the active sites (Lu et al., 2010). Very recently, derivatives of bengamides, a natural product derived from marine sponges having inhibitory activities on

human MAPs, were reported to show inhibition of different metallo-forms of MtbMAPs (Lu et al., 2011). Moreover, some of these inhibitors showed modest growth inhibition of *M. tuberculosis* in culture. X-ray crystal structures of these inhibitors with different metallo-form MtbMAP B (PDB ID 3PKA to 3PKC) were also elucidated to suggest their mechanism of action. Even though biochemical characterizations and inhibition of MtbMAP A has been reported in past two years, there have not been any reports on elucidating the crystal structure of this enzyme. Structural data on MtbMAP A is the need of the hour to determine the mode of binding of inhibitors to the enzyme and for further refinement of existing MtbMAP A inhibitors for developing them as antimycobacterials.

The literature review based on various studies conducted by independent research groups showed that NME is an important step in the peptide processing of most of the eubacteria and the enzymes involved in it, PDF and MAP, have immense potential to be developed as drug targets. It is only recently (since 2005), these enzymes from *M. tuberculosis* started to gain much interest. Since these enzymes are not fully characterized based on their biochemical and structure-function relationships, we decided to produce the recombinant enzymes for a detailed investigation.

CHAPTER 2

Materials and General Methods

CHAPTER 2

Materials and General Methods

2.1 Materials

2.1.1 Microorganisms

E. coli DH5α [(F- mcrA Δ (mrr-hsdRMS-mcrBC) φ80lacZΔM15 ΔlacX74 nupG recA1 araD139 Δ (ara-leu) 7697 galE15 galK16 rpsL (Str^R) endA1 λ^-) (Invitrogen, CA, USA)] was used for all transformation related to recombinant DNA work and for the expression of recombinant proteins of *M. tuberculosis*, *E. coli* BL21 (DE3) [(F^- ompT gal dcm lon $hsdS_B$ (r_B^- m_B^-) λ (DE3 [lacI lacUV5-T7 gene 1 ind1 sam7 nin5)] (Novagen Inc., CA, USA) was used.

2.1.2 Genomic DNA, Plasmid DNA and Primers

Genomic DNA of *M. tuberculosis* H37Rv was obtained from Colorado State University, USA, on material transfer agreement. The T_7 expression vector pET28a was from Novagen Inc., CA, USA and the chaperonin expressing plasmid, pGrO7, was from Takara Bio Inc., Japan **(**Nishihara et al., 1998). All the oligos used for Polymerase Chain Reactions (PCR) and Site-directed mutagenesis were custom-synthesized from Integrated DNA Technologies (IDT), USA.

2.1.3 Chemicals, Culture media and Reagent Kits

Luria-Bertani (LB) broth or LB agar dehydrated culture medium for growing *E. coli* cells were procured from Hi-Media, India. Plasmid isolation kits, PCR clean up kits and Gel extraction kits were obtained from Qiagen, Germany. Quickchange™ Site-directed mutagenesis kit was obtained from Stratagene, USA. Pro-Matrix™ protein refolding kit

for refolding the insoluble recombinant proteins was procured from Pierce Biotechnology, USA. Ni-NTA spin kit for His-tag assisted Ni-affinity chromatography was purchased from Qiagen, Germany.

Restriction enzymes (*EcoR*I, *Nde*I, *Xho*I, *EcoR*V and *Dpn*I), *Pfu* DNA polymerase, T_4 DNA Ligase, dNTPs, Alkaline Phosphatase, Polynucleotide kinase and Adenosine tri-phosphate (ATP) were purchased from Fermentas, USA. *Taq* DNA polymerase for PCR, Isopropyl β-D-1-thiogalactopyranoside (IPTG), Lysozyme, 2,4,6-Trinitrobenzenesulfonic acid (TNBSA), Substrates for deformylase assay; i.e. *N*-formyl-Met-Ala-Ser, *N*-formyl-Met-Leu-Phe, *N*-formyl-Met; Substrate for methionine aminopeptidase assay, i.e. L-Methionine-*p*-Nitro anilide (L-Met-*p*NA); *p*-Nitro aniline (*p*NA), L- Methionine, Bovine Serum Albumin (BSA); Inhibitors like Actinonin, Bestatin, Amastatin, Fumagillin etc. were procured from Sigma-Aldrich, India. Antibiotics like kanamycin and chloramphenicol were purchased from Hi-Media, India. All other molecular biology grade chemicals like Calcium chloride ($CaCl_2.6H_2O$), Magnesium chloride ($MgCl_2$), Dithiothreitol (DTT), 1, 10, phenanthroline, Ethylene diamine tetra acetic acid (EDTA) etc. were procured from Sigma-Aldrich, India.

2.2 Softwares and Bioinformatics tools

Genolist-tuberclist (*http://genolist.pasteur.fr/TubercuList/*): The server is provided by Institute Pasteur, France. This database was used to search the annotated genes of *M. tuberculosis* H37Rv and to retrieve the nucleotide and amino acid sequences of *def* and *map* genes and gene products.

Graphpad Prism. V 5.0 (*http://www.graphpad.com*): Software is provided by Graphpad software, San Diego CA. This software was used for all non-linear curve

fittings, mainly for calculating the enzyme kinetic parameters of the enzymes in the study. V_{max}, K_m and K_{cat} values of each of these enzymes were calculated with the help of this software.

Netprimer (*http://www.premierbiosoft.com/netprimer/index.html*): Online version of Netprimer was used to analyse the specific PCR primers for their T_m values and secondary structures, prior to getting them custom synthesized.

Quick-Change® Primer Design (*http://www.genomics.agilent.com/*): This program supports mutagenic primer design for site-directed mutagenesis experiments by calculating and designing appropriate primer sequences with optimal melting temperature. The primer pairs picked by the software were synthesized to perform site-directed mutagenesis on *def* and *map* genes.

Modeller Version 9.6 (*http://salilab.org/modeller/*): Modeller is a web-based program used for homology or comparative modeling of protein three-dimensional structures from their amino acid sequences based on the closest template structure available against it (Fiser and Sali, 2003). Windows based program was used in the present study to model the mutated structures of MtbPDF.

Protein Data Bank (PDB) (http://*www.pdb.org/*): PDB contains information about experimentally determined structures of proteins or nucleic acids and complex assemblies. The high resolution structure of MtbPDF and MtbMAP B was retrieve from PDB in order to study the structural details in relation to its activity and stability.

PyMOL Version 0.99 (*http://www.pymol.org*): PyMOL is an open-source, user-sponsored, molecular visualization system created by Warren Lyford DeLano and commercialized by DeLano Scientific LLC. It produces high quality 3D images of

small molecules and biological macromolecules, such as proteins. PyMOL is one of the few open source visualization tools available for use in structural biology. In present study, all the PDB structures of MtbPDF and their mutant proteins retrieved or modeled were visualized using PyMOL. All the figure drawings of either crystal structures or homology models of MtbPDF were generated using PyMOL. The inter-molecular and intra-molecular hydrogen-bondings and their distances were calculated using the in-built features in the software.

Clustal W (*www.ebi.ac.uk/clustalW/index.html*) (Thompson et al., 1997): This is a free online program provided by the European Bioinformatics Institute (EBI) and European Molecular Biology Laboratory (EMBL) for alignment of multiple nucleotide or amino acid sequences of genes or proteins. In present study, ClustalW has been used extensively to align different bacterial and eukaryotic PDF or MAP protein sequences with MtbPDF or MtbMAPs, in order to identify the subtle amino acid variations between *M. tuberculosis* enzyme sequences with that of human and other bacterial enzymes.

Genedoc (*http://www.nrbsc.org/gfx/genedoc/*) (Nicholas et al., 1997): Gendoc is a full featured multiple sequence alignment editor with tools for visualizing, editing, and analyzing multiple sequence alignments of protein and nucleic acid sequences. It can open the alignment files (*.ALN or *.MSF), edit or shade the aligned amino acids according to their different properties. Editing can incorporate structural or biochemical information about which residues should be aligned.

VMD / NAMD **(***http://www.ks.uiuc.edu/Research/namd/*) (Humphrey *et al.*, 1996; Phillips *et al.*, 2005): NAMD is a parallel molecular dynamics code designed for high-performance simulation of large biomolecular systems like proteins.

Based on Charm++parallel objects, NAMD scales to hundreds of processors on high-end parallel platforms and tens of processors on commodity clusters using gigabit ethernet. NAMD uses the popular molecular graphics program *Visual Molecular Dynamics* (VMD) for simulation setup and trajectory analysis. VMD is designed for modeling, visualization, and analysis of biological systems such as proteins, nucleic acids, lipid bilayer assemblies, etc. It may be used to view more general molecules, as VMD can read standard Protein Data Bank (PDB) files and display the contained structure. VMD can also be used to animate and analyze the trajectory of a molecular dynamics (MD) simulation.

AutoDock (*http://autodock.scripps.edu/*) (Morris *et al.*, 1998): AutoDock is a molecular modeling simulation software. Since 2009, it has been open source and is free for non-commercial usage. It is especially effective for Protein-ligand docking. AutoDock is a suite of automated docking tools. It is designed to predict how small molecules, such as substrates or drug candidates, bind to a receptor of known 3D structure.

2.3 General Methodology

All the molecular biology methods were performed as per standard protocol described by Sambrook et al., (1989) and the specific cases were discussed in individual chapters.

2.3.1 Plasmid isolation

Plasmid isolation was done by alkaline lysis method of Birnboim and Doly (1979) using the QIAprep plasmid Mini Preparation Kit following the manufacture's protocol.

2.3.1.1 Principle

Bacteria are lysed under alkaline conditions in NaOH/SDS buffer in the presence of RNaseA. SDS solubilizes the phospholipid and protein components of the cell membrane,

leading to lysis and release of the cell contents while the alkaline conditions denature the chromosomal and plasmid DNAs, as well as proteins. However, the optimized lysis time allows maximum release of plasmid DNA without release of chromosomal DNA, while minimizing the exposure of the plasmid to denaturing conditions. The lysate is neutralized and adjusted to high-salt binding conditions in one step by the addition of 3 M potassium acetate pH 5.5. The high salt concentration causes denatured proteins, chromosomal DNA, cellular debris, and SDS to precipitate, while the smaller plasmid DNA renatures correctly and stays in solution. This released plasmid is adsorbed on to silica in presence of high salt using unique silica membrane used in QIAprep plasmid columns. They are washed in presence of medium salt concentrations, where chromosomal DNA and other protein contaminants get precipitated. The column gets desalted in presence of ethanol in wash buffer. Finally the plasmid is eluted out from the column at low-salt concentrations in the 10 mM Tris-Cl, pH 8.0.

2.3.1.2 Materials

Buffer I (Resuspension buffer): 50 mM Tris-Cl, pH 8.0, 10 mM EDTA, 100 µg/ml RNase A; Buffer II (Lysis buffer): 200 mM NaOH and 1% SDS (w/v); Buffer III (Neutralization buffer): 3.0 M potassium acetate, pH 5.5; Wash buffer :1.0 M NaCl, 50 mM Tris-Cl, pH 7.0, 15% ethanol (v/v); Elution buffer: 10 mM Tris-Cl, pH 8.0.

2.3.1.3 Procedure

a) 1.5 ml overnight culture was placed in a microcenrifuge tube and pelleted the cells
b) The supernatant was poured off and the pelleted bacterial cells were resusuepnded in 250 µl Buffer I
c) 250 µl Buffer II was added and gently inverted the tube 4–6 times

d) 350 µl Buffer III was added and invert the tube immediately 4–6 times

e) The resulting precipitate was centrifuged for 10 min at 13,000 rpm on a table-top microcentrifuge

f) The supernatant from the previous step was applied to QIAprep spin column by decanting or pipetting

g) This was centrifuge for 30–60 s and the flow-through was discarded

h) The column was washed with 750 µl of wash buffer by centrifuging for 30-60 min

i) The flow-through was discarded and column was centrifuged for an additional 1 min to remove residual wash buffer

j) The column was placed in a clean 1.5 ml microcentrifuge tube and DNA was eluted by adding 50 µl elution buffer and centrifuging for 1 min

k) The purified plasmid was visualized on an agarose gel and quantified at A_{260} using a spectrophotometer

2.3.2 Competent cell preparations and transformation

Competent cells of *E. coli* DH5α and BL21 (DE3) were prepared according to the modified protocol of Inoue et al., (1990).

2.3.2.1 Principle

Competent cells are those that possess more easily altered cell walls so that DNA can be passed through easily. These cells readily incorporate foreign DNA. But, DNA is a very hydrophilic molecule; it will not normally pass through a bacterial cell's membrane. In order to make bacteria take in the plasmid, they must first be made "competent" to take up DNA. This is done by creating small holes in the bacterial cells by suspending them in a solution with a high concentration of calcium. DNA can then be forced into the cells by

giving heat shock. The transformation efficiency is calculated as per the formula given,

$$\text{Transformation efficiency} = \frac{\text{No. of Transformants (colonies) X Final volume at recovery}}{\mu\text{g of plasmid DNA X Volume plated (ml)}}$$

A good preparation of competent cells normally will give ~ 10^8 colonies per µg DNA

2.3.2.2 Materials

E. coli cells, pET28a plasmid / pET28a + insert (ligation mixture), LB broth, sterile-ice cold 0.1 M $CaCl_2$, sterile-ice cold 0.1 M $MgCl_2$, sterile-ice cold 0.1 M $CaCl_2$ + 15% glycerol, LB-Kanamycin plates, 42 °C incubator, 1.5 ml sterile eppendorffs, laminar air flow chamber, centrifuge.

2.3.2.3 Procedure

a) One colony from LB plate was inoculated into 5 ml LB broth and left for overnight incubation at 37 °C and 200 rpm
b) 1 ml of overnight cell culture was inoculated into 100 ml LB medium (in a 250 ml flask)
c) This was incubated at 200 rpm at 37 °C to OD_{600} ~ 0.5-0.6
d) The culture was chilled on ice for 15 min. All solutions such as 0.1 M $MgCl_2$, 0.1 M $CaCl_2$ and 0.1 M $CaCl_2$ + 15% glycerol were also chilled on ice
e) Centrifuged the cells for 10 min at 3,000 rpm on a refrigerated centrifuge (Kubota, Japan) at 4 °C
f) The medium was discarded aseptically and the cell pellet was resuspended in 25 ml ice cold 0.1 M $MgCl_2$
g) Cells were centrifuged as in step ‘e’ and again resuspended in 25 ml 0.1 M $CaCl_2$

h) Kept the cells on ice for 30 min. Centrifuged the cells as above

i) The supernatant was removed aseptically and the cell pellet was resuspended in 2 ml 0.1 M $CaCl_2$ solution in 15% glycerol

j) 0.1 - 0.2 ml of the cell suspension was aliquoted into sterile 1.5 ml micro-centrifuge tubes and was frozen on dry ice and transferred to -80 ^oC freezer

For transformation with DNA such as pET28a plasmid, a vial of competent cells was thawed in ice and incubated with 10-30 ng of plasmid along with the competent cells on ice by gentle tapping and left on ice for another 40 min and then the vial was shifted to 42 ^oC without shaking for 90 min and immediately immersed into ice. After 2 min, 800 µl of LB broth was added and left at 37 ^oC at 200 rpm for 45 min. 100 µl of these cells were plated on to LB agar-Kan petriplates (30 µg/ ml Kanamycin) and left in an incubator at 37 ^oC for over night. The colonies appeared on the plates were counted to find out the competency of the prepared cells.

2.3.3 Ni-Affinity chromatography

Ni-affinity purification of the polyhistidine-tagged proteins were performed using the Qiagen Ni-NTA spin column kit according to the modified protocol of Hengen et al., (1995) as provided by the manufacturers.

2.3.3.1 Principle

A polyhistidine-tag is an amino acid motif in proteins that consists of at least five histidine (His) residues, often at the N- or C-terminus of the recombinant proteins. It is also known as hexa histidine-tag, 6xHis-tag, and by the trademarked name His-tag. pET28a vector used in present study has provision for N-terminal His-tag (**Fig 2.1a**). This His-tag is followed by a suitable amino acid sequence that facilitates a removal of the

polyhistidine-tag from the purified proteins using endopeptidases such as thrombin in case of pET28a vector.

Immobilized metal ion affinity chromatography (IMAC) is based on the specific coordinate covalent bond of amino acids, particularly histidine, to metals. This technique works by allowing proteins with an affinity for metal ions to be retained in a column containing immobilized metal ions, such as cobalt, nickel or copper for the purification of histidine containing proteins or peptides. Qiagen kit utilizes Ni-Nitrilotriacetic acid (Ni-NTA)-silica as the resin in the spin columns (**Fig 2.1b**). NTA has a tetradentate chelating group that occupies four of six sites in the nickel coordination sphere. The metal is bound much more tightly than to a tridentate chelator such as IDA (imidodiacetic acid). This allows more stringent washing conditions, better separation, higher purity, and higher capacity without nickel leaching. Silica material in the resin has been modified to provide a hydrophilic surface to avoid non-specific hydrophobic interactions. Polyhistidine-tagging is the option of choice for purifying recombinant proteins in denaturing conditions because its mode of action is dependent only on the primary structure of proteins. Methods used to elute the His-tagged protein include changing the pH to acidic range (in case of denaturing conditions) or adding a competitive molecule, such as imidazole (in case of native conditions).

2.3.3.2 Materials

Lysozyme (10 mg /ml), Triton-X 100, Ni-NTA spin columns (e.g. Qiagen), Table-top microcentrifuge

2.3.3.2a Buffers for native purification

a) Lysis Buffer: 20 mM Phosphate buffer, pH 7.4; 500 mM NaCl; 10 mM imidazole.

b) Wash Buffer: 20 mM Phosphate buffer, pH 7.4; 500 mM NaCl; 20 mM imidazole.

c) Elution Buffer: 20 mM Phosphate buffer, pH 7.4; 500 mM NaCl; 250 mM imidazole.

2.3.3.2b Buffers for denaturing purification

a) Lysis buffer: 20 mM Phosphate buffer, pH 7.4; 3 M urea

b) Wash buffer I: 20 mM Phosphate buffer, pH 6.3; 3 M urea

c) Wash buffer II: 20 mM Phosphate buffer, pH 5.9; 3 M urea

d) Elution buffer: 20 mM Phosphate buffer , pH 4.5; 3 M urea

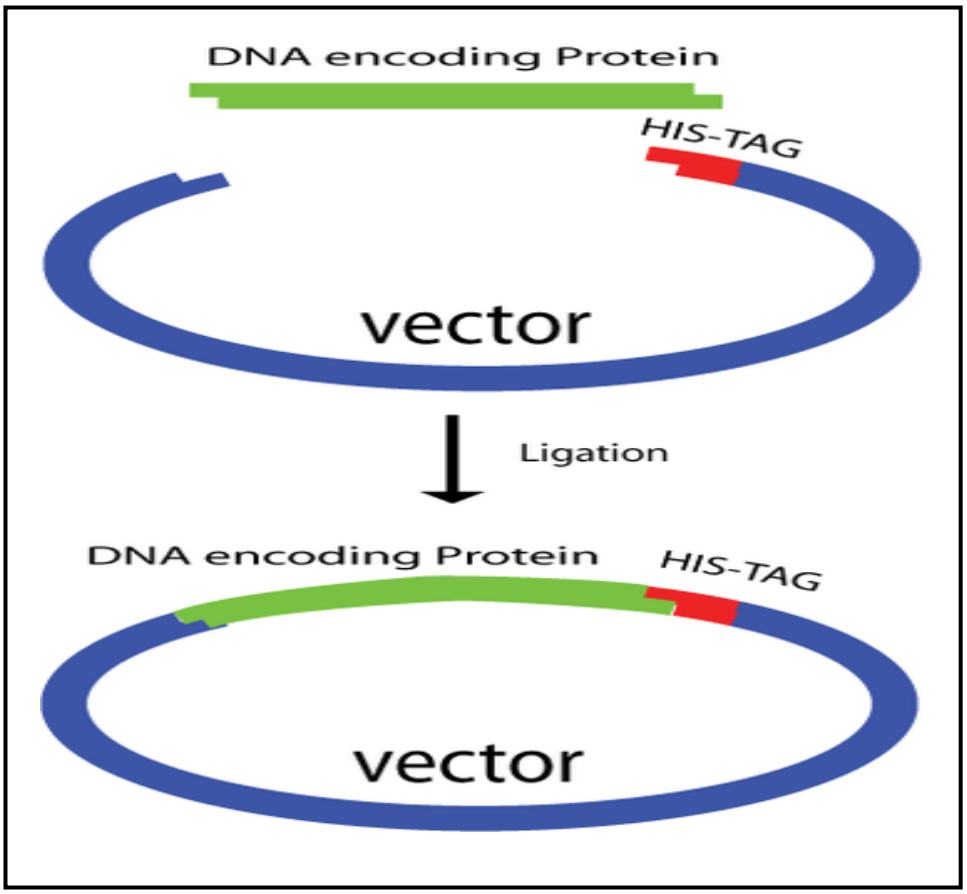

Fig 2.1a: Schematic representation of recombinant construction for expression with polyhistidine tag fusion for Ni-affinity purification.

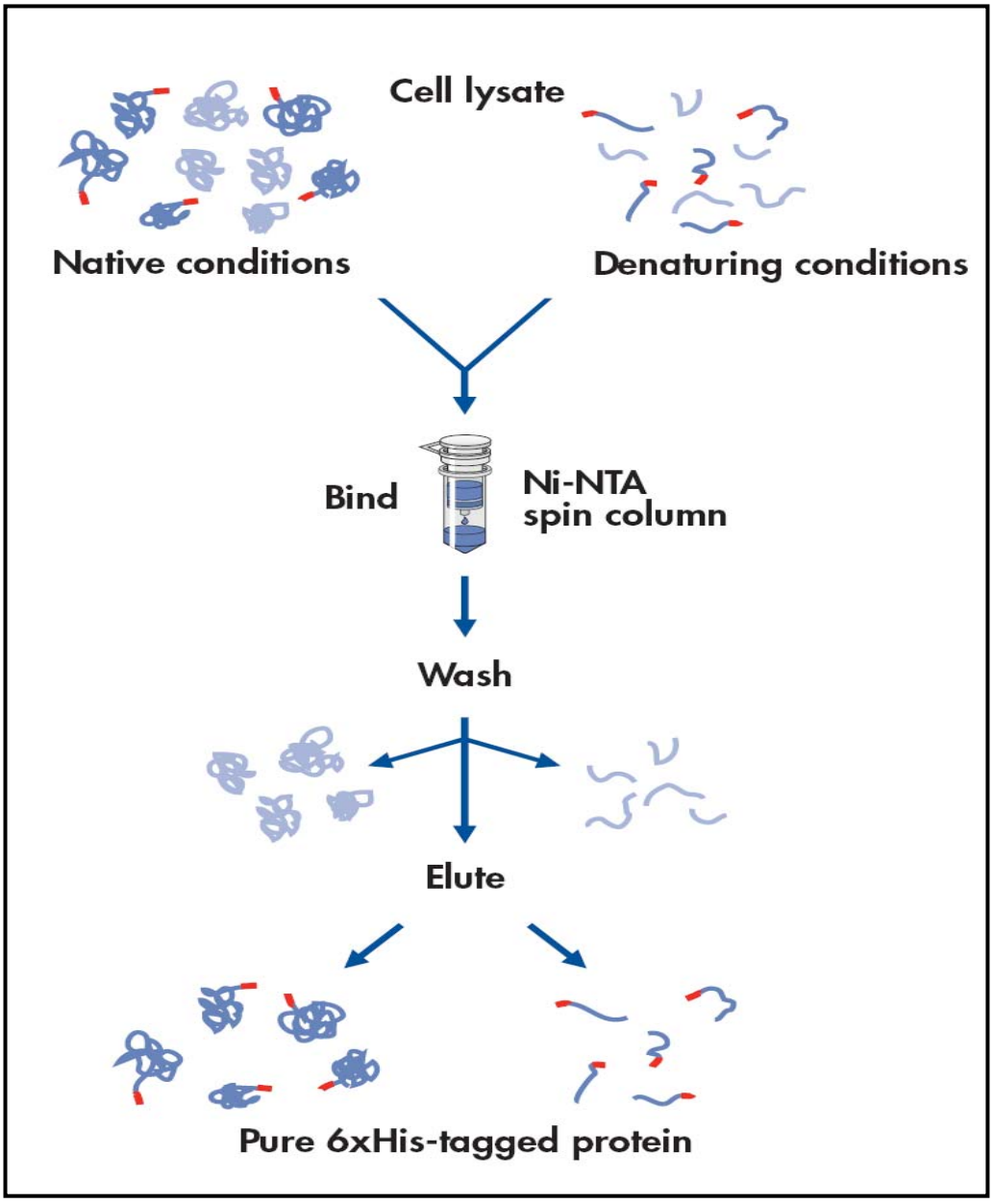

Fig 2.1b: Schematic representation of the different strategies and steps involved in purification of His-tagged recombinant proteins using Ni-affinity chromatography (Qiagen protocols).

2.3.3.3 Procedure

2.3.3.3a Preparation of cell-lysate

a) The induced *E. coli* BL21 (DE3) cells expressing His-tagged recombinant proteins were centrifuged down to recover the cell pellet.
b) The cell pellet was resuspended in 5 ml lysis buffer (for cell pellet from 100 ml culture) and left over-night at -20 ^{o}C.
c) The resuspended cell pellet was then thawed in ice and lysozyme was added to a final concentration of 0.5 mg/ ml and was left on ice for 30 min.
d) The cells were completely disrupted by sonication using a sonicator at 42% amplitude and 30 s ON: 30 s OFF cycle for 5 cycles.
e) The cell lysate was clarified by high speed centrifugation at 13,000 rpm on a refrigerated centrifuge at 4 ^{o}C for 30 min.
f) The supernatant containing soluble proteins were stored for purification under native conditions.
g) The cell pellet was washed twice with lysis buffer containing 2% Triton-X 100.
h) The insoluble pellet was then extracted with lysis buffer containing 3 M urea for 30 min with constant stirring.
i) The solublised inclusion bodies were separated by centrifugation at 13,000 rpm for 30 min. This was further used for purification under denaturing conditions.

2.3.3.3b Purification of His-tagged proteins

a) Ni-NTA silica column was equilibrated with 600 µl of lysis buffer (3 M urea buffer for denaturing conditions) by spinning the column at 2000 rpm for 2.5 min at room temperature with open lid.

b) 600 µl of soluble proteins or solublized inclusion bodies were added to the pre-equilibrated column and was centrifuged as above with closed lid to slow down the flow rate. This step was repeated thrice. The flow through was collected and stored to check the binding efficiency.

c) The column with bound protein was washed twice with 600 µl of wash buffer and the wash fraction was collected and stored for analysis.

d) In case of denaturing purification, 600 µl wash buffer II was added and centrifuged

e) The bound recombinant proteins were eluted in 250 µl of elution buffer to fresh eppendorff tubes. In denaturing condition, elution at lower pH buffer is preferred over imidazole gradient.

f) Step 5 was repeated again. Protein content in different fractions was quantified using Bradford's method of protein quantification (2.4.2.1) or A_{280} method on a Nanodrop spectrophotometer (2.4.2.2).

g) The purity of the eluted proteins was confirmed by SDS-PAGE (2.4.1.1) and Western blotting (2.4.1.2).

2.3.4 Site-directed mutagenesis

In vitro site-directed mutagenesis is an invaluable technique for studying protein structure-function relationships and for identifying intra-molecular regions or amino acids, both of which may mediate gene expression and vector modification. Stratagene's Quick-change site directed mutagenesis kit protocol (Stratagene, USA) was used for creating specific substitutions, deletions or insertions of nucleotides from different constructs.

2.3.4.1 Principle

The Quick-change site-directed mutagenesis method is performed using *Pfu*Turbo™ DNA polymerase II and a thermal temperature cycler. *Pfu*Turbo DNA polymerase replicates both plasmid strands with high fidelity and without displacing the mutant oligonucleotide primers. The basic procedure utilizes a supercoiled double-stranded DNA vector with an insert of interest and two synthetic oligonucleotide primers containing the desired mutation. The oligonucleotide primers, each complementary to opposite strands of the vector, are extended during temperature cycling by using *Pfu*Turbo DNA polymerase. Incorporation of the oligonucleotide primers generates a mutated plasmid containing staggered nicks. Following temperature cycling, the product is treated with *Dpn*I. The *Dpn*I endonuclease (target sequence: 5′-Gm6ATC-3′) is specific for methylated and hemimethylated DNA and is used to digest the parental DNA template and to select for mutation-containing synthesized DNA. DNA isolated from almost all *E. coli* strains routinely used in routine cloning and expression is methylated and therefore susceptible to *Dpn*I digestion. The nicked vector DNA incorporating the desired mutations is then transformed into competent *E. coli* DH5α cells. The small amount of starting DNA template required for performing this method, the high fidelity of the *Pfu*Turbo DNA polymerase, and the low number of PCR cycles all contributes to the high mutation efficiency and decreased potential for random mutations during the reaction. The entire steps are shown in **Fig 2.2**.

2.3.4.2 Materials

*Pfu*Turbo™ DNA polymerase (2.5 U / µl), 10 X reaction buffer, *Dpn*I restriction enzyme (10U/ µl), Oligonucleotide forward primer (25 nmol), Oligonucleotide reverse

primer (25 nmol), dNTP mix (10 mM), Thermo-cycler, Competent *E.coli* DH5α cells and pET28a constructs (template DNA).

2.3.4.3 Procedure

2.3.4.3a Mutagenic primer designing

The mutagenic oligonucleotide primers used were designed individually according to the desired mutation. Both the mutagenic primers contain the desired mutation inorder to anneal to the same sequence on opposite strands of the plasmid. Primers length was kept between 25 and 45 bases in length and the melting temperature (*T*m) of the primers was greater than or equal to 78 °C. The desired mutation (deletion or insertion) was incorporated in the middle of the primer with ~10–15 bases of correct sequence on both sides. The primers were designed with a minimum GC content of 40% and were terminated in one or more C or G bases. All primers were designed based on Quick Change® Primer design software.

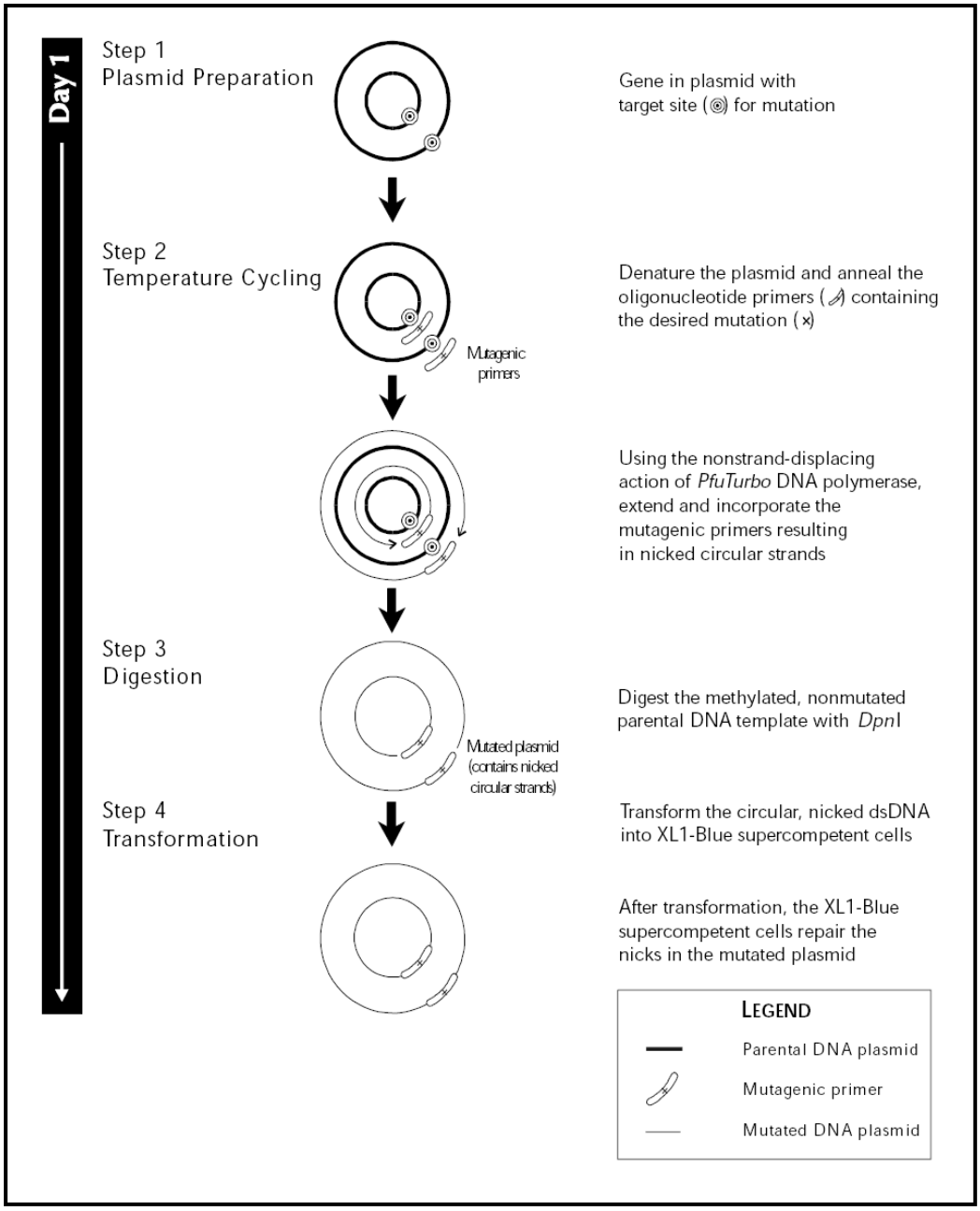

Fig 2.2: Schematic representations of the steps involved in introducing site-directed mutations into intact plasmids by PCR based strategy (Stratagene protocols).

2.3.4.3b PCR reaction and conditions for mutagenesis

The composition of PCR reaction mixture was as shown in **Table 2.1** and the program used for PCR was as shown in **Table 2.2**.

Table 2.1 PCR reaction mixture for mutagenesis

Reagents	Quantity (μl)
10X reaction buffer	5
Template DNA (5-50 ng)	1
Forward primer (100 ng/ μl)	1.25
Reverse primer ((100 ng/ μl)	1.25
dNTP mix	1
Pfu Turbo DNA polymerase	1
MilliQ water	39.5

Table 2.2 PCR program for mutagenesis

Cycles	Temperature (^{o}C)	Time (s)
1	95	30
12-18*	95	30
	55	60
	68	120 /kb plasmid length

***** Point mutations-12; Single amino acid changes-16; Multiple amino acid deletions or insertions -18.

2.3.4.3c DpnI digestion

After PCR cycling, an aliquot from the reaction was loaded on to agarose gel to confirm amplification of the plasmid. Once amplification was confirmed, 1 µl of *DpnI* (10 U/ µl) enzyme was added to each of the reaction and incubated at 37 ^{o}C for 90 min. The restriction reaction was arrested by incubating at 65 ^{o}C.

2.3.4.3d Transformation into E. coli DH5α cells

10 µl of the reaction mixture was transformed in to *E.coli* DH5α chemical competent cells according to the standard protocol mentioned in 2.3.2. The transformed cells were plated on LB-kanamycin plates and left overnight for incubation at 37 ^{o}C. The colonies formed were inoculated in to fresh 5 ml LB broth for plasmid isolation.

2.3.4.3e Plasmid isolation

Plasmids from the selected colonies were isolated according to standard protocol (2.3.1). The isolated plasmids were sent for DNA sequencing (Scigenome Pvt. Ltd, India) using T_7 forward and reverse primers to confirm the mutation in the plasmids.

2.3.4.3f Transformation into E. coli BL21 (DE3) cells.

The plasmids bearing the intended mutations were transformed into *E. coli* BL21 (DE3) chemical competent cells (2.3.2) for expression and purification according to the standard protocol (2.3.3).

2.4 Analytical methods

2.4.1 Electrophoretic analysis

Electrophoresis is the migration of charged molecules in solution in response to an electric field. Their rate of migration depends on the strength of the field; on the net

charge, size and shape of the molecules and also on the ionic strength, viscosity and temperature of the medium in which the molecules are moving. It is used analytically to study the properties of a single charged species, and as a separation technique.

2.4.1.1 SDS-PAGE

The homogeneity of enzymes and molecular weight of proteins were determined using 12% SDS-PAGE using the method of Laemmli (1970). Proteins are amphoteric compounds; their net charge therefore is determined by the pH of the medium in which they are suspended. In a solution with a pH above its isoelectric point, a protein has a net negative charge and migrates towards the anode in an electrical field. Below its isoelectric point, the protein is positively charged and migrates towards the cathode. The net charge carried by a protein is in addition independent of its size - *i.e*. the charge carried per unit mass of molecule differs from protein to protein. At a given pH therefore, and under non-denaturing conditions, the electrophoretic separation of proteins is determined by both size and charge of the molecules. Sodium dodecyl sulphate (SDS) is an anionic detergent which binds to proteins fairly specifically in a mass ratio of 1.4:1 thus SDS confers a negative charge to the polypeptide in proportion to its length. It is usually necessary to reduce disulphide bridges in proteins before they adopt the random-coil configuration necessary for separation by size: this is done with 2-mercaptoethanol or dithiothreitol. In denaturing SDS-PAGE separations therefore, migration is determined not by intrinsic electrical charge of the polypeptide, but by molecular weight.

The separating gel in the SDS-PAGE analysis was comprised of 30% acrylamide /

bis-acrylamide (30:1), 1.5 M Tris-Cl pH-8.8, 0.1% SDS, 0.15% Ammonium per sulphate (APS), 0.004% Tetramethylethylenediamine (TEMED). The stacking gel was composed of 30% acrylamide- bis acrylamide (30:1), 0.5 M Tris pH 6.8, 0.1% SDS, 0.15% APS, 0.01% TEMED. The protein samples were loaded with a loading buffer composed of 0.5 M Tris (pH 6.8), 10% glycerol, 0.1% β-mercaptoethanol, 0.1% SDS and 0.1% bromophenol blue. Tris-glycine buffer (pH 8.3) with 0.1% SDS was used as tank buffer. The proteins separated in the gel were detected by staining with Coomasie brilliant blue R-250.

2.4.1.2 Western Blotting for His- tagged Proteins

The Western blotting (alternatively, protein immune-blotting), developed by Towbin et al., (1979) is a widely used analytical technique used to detect specific proteins in the given sample of tissue homogenate or extract. It uses SDS-PAGE to separate denatured proteins which are then transferred to a membrane (typically nitrocellulose or PVDF), where they are probed (detected) using antibodies specific to the target protein. In case of recombinant proteins with His-tag, anti-his antibodies provides a convenient way for their detection on a Western blot.

The recombinant proteins were subjected to SDS-polyacrylamide gel electrophoresis along with pre-stained protein molecular weight ladder (Fermentas) as reference marker. After this the gel was placed over a sheet of nitrocellulose membrane (Immobilon P, Millipore), which was previously soaked in the tank blotting buffer (25 mM Tris-base, 150 mM Glycine and 20% methanol in distilled water). These two were sandwiched between a stalk of filter papers and cushion pads and were placed between the electrode cassettes of Western blotting apparatus with polyacrylamide gel towards the anode. The

proteins in the gel were electrophoretically transferred to the nitrocellulose at 8 mA current for 2.5 h. After transfer the nitrocellulose was soaked in blocking buffer (3% BSA in TBS buffer (10 mM Tris-Cl, pH 7.5 and 150 mM NaCl) overnight to block the nonspecific binding of proteins. After several washings in TBS/Tween/Triton buffer (20 mM Tris-Cl, pH 7.5, 500 mM NaCl, 0.05% v/v Tween-20 and 0.2% v/v Triton-X-100), the membrane was incubated with the primary antibody (Anti-his antibodies, Qiagen) at 1:1000 dilution in blocking buffer for 1 h at room temperature. After extensive washing in TBS/Tween/Triton buffer followed by TBS buffer, the blot was incubated with secondary antibody solution (Anti-mouse IgG developed in goat, conjugated with alkaline phosphatase (Sigma) at 1: 5000 dilution in blocking buffer for 1 h. Extensive washing was done with TBS/Tween/Triton buffer and the blot was immersed into 5-Bromo-4-Chloro-3'-Indolyl Phosphate *p*-Toluidine/Nitro-Blue Tetrazolium Chloride solution (BCIP/NBT) (Sigma) until dark brownish-red colour developed at corresponding size of his-tagged recombinant proteins, as compared by the pre-stained protein ladder. The membrane was dried and photographed.

2.4.1.3 Agarose gel electrophoresis

As DNA has a net negative charge in solution, it moves towards the positive pole in an electric field. The yield and purity of genomic and plasmid DNA, progression of restriction digestion and fractionation of DNA were done by agarose gel electrophoresis. DNA was separated in agarose gel by electrophoresis in Tris-acetic acid-EDTA (TAE) buffer, pH 8.0 at 1X concentrations. 1% agarose gels were used and ethidium bromide (10 μg / ml) was included in the gels to enable fluorescent visualization of DNA fragments under UV light.

2.4.2 Analysis of protein concentrations

A large number of assays of protein concentration have been developed and in our studies we have used Bradford's method to quantify protein concentrations in different samples.

2.4.2.1 Bradford protein assay

The Bradford protein assay, developed by Bradford, (1976) is a spectroscopic analytical procedure used to measure the concentration of protein in a solution. This assay is dependent on amino acid composition of the measured protein.

Bradford's assay is a colorimetric protein assay based on an absorbance shift of the dye Coomassie Brilliant Blue G-250 (CBB-G250) in which under acidic conditions the red form of the dye is converted into its bluer form to bind to the protein being assayed. During the formation of this complex, two types of bond interaction take place: the red form of Coomassie dye first donates its free electron to the ionizable groups on the protein, which causes a disruption of the protein's native state, consequently exposing its hydrophobic pockets. These pockets on the protein's tertiary structure bind non-covalently to the non-polar region of the dye via van der Waals forces, positioning the positive amine groups in proximity with the negative charge of the dye. The bond is further strengthened by the ionic interaction between the two. The binding of the protein stabilizes the blue form of the Coomassie dye; thus the amount of the complex present in solution is a measure for the protein concentration, and can be estimated by use of an absorbance reading. The blue form absorbs maximum at 595 nm. The increase of absorbance at 595 nm is proportional to the amount of bound dye, and thus to the amount (concentration) of protein present in the sample.

The assay was performed with CBB-G250 (Genei, Bangalore) in a total volume of 2.5 ml. A standard graph was prepared with 0-80 µg / ml of BSA. 2 ml of CBB- G250 was added to each reaction. The protein samples were diluted accordingly to fit into this concentration range and the protein concentrations were calculated from the OD_{595} values by incorporating the slope values from the standard graph (**Fig 2.3**) and the dilution factors.

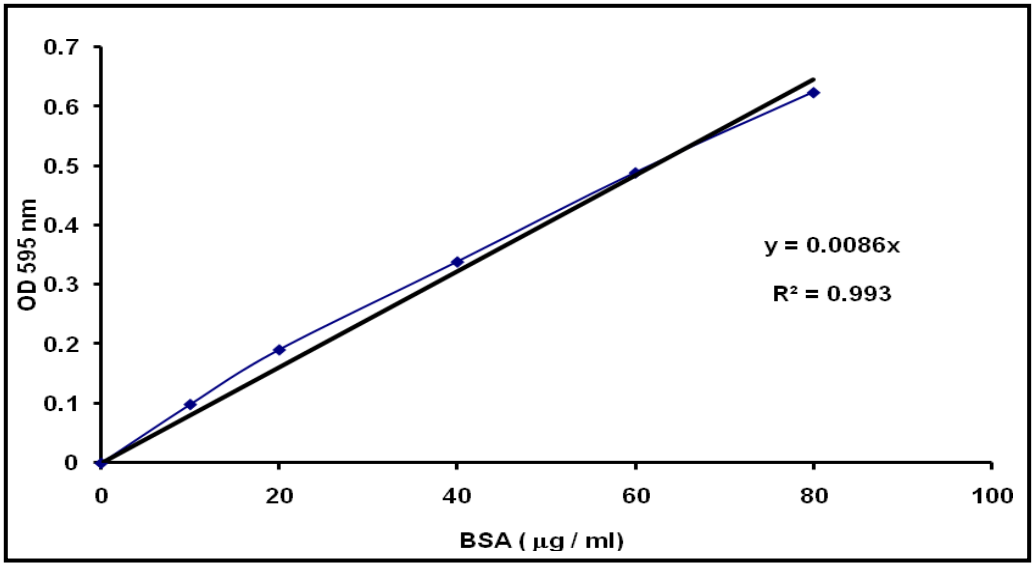

Fig 2.3: Standardization of protein concentration of BSA with CBB-G250.

2.4.2.2 Protein quantification by Nanodrop method

Proteins that contain tryptophan, tyrosine residues or cys-cys disulphide bonds will absorb in the UV range (i.e. 280 nm) making absorbance spectroscopy a fast, convenient method for the quantification of purified protein preparations. NanoDrop 1000 Spectrophotometer (Thermo Scientific) was used to quantify the purified proteins. Purified sample (2 µl) was used in quantification of the proteins using NanoDrop. This

method uses the internal standard curve in the instrument and provides results in mg /ml. Using NanoDrop methods utilizes minimum sample compared to Bradford's assay, but cannot be used for accurate quantification of proteins in crude samples as many other compounds like nucleic acids absorbs at 280 nm.

2.4.3 Assay for N-terminal methionine excision (NME) enzymes

NME step involves sequential action of two enzymes, peptide deformylase (PDF) and methionine aminopeptidases (MAP). The former cleaves formyl group from N-terminal methionine and later cleaves the N-terminal methionine from the polypeptide. Short N-terminal formylated di, tri or tetra peptides serve as substrates for PDF in *in vitro* assay. Similarly, short di, tri or tetra peptides with N-terminal methionine serve as substrate for MAP in *in vitro* assay. The activities of the two enzymes are measured separately using two different *in vitro* assays.

a) Peptide deformylase assay (Saxena and Chakraborti, 2005a)

b) Methionine Aminopeptidase assay (Mitra et al., 2006)

2.4.3.1. ***Peptide deformylase assay***

2.4.3.1a Principle

2,4,6,Trinitrobenzene sulfonic acid (TNBSA) reacts readily with the free primary amino a group of amino acids in aqueous solution at pH 8-9 to form yellow adducts. The colored derivatives are monitored at 335 to 345 nm and have extinction coefficients in the range of 10,000-15,000. In deformylase assay, peptide deformylase removes the formyl group from the N-terminal methionine of the substrate leaving the free amino group, which can be detected by TNBSA assay. The amount of free amines released corresponds to the deformylase activity.

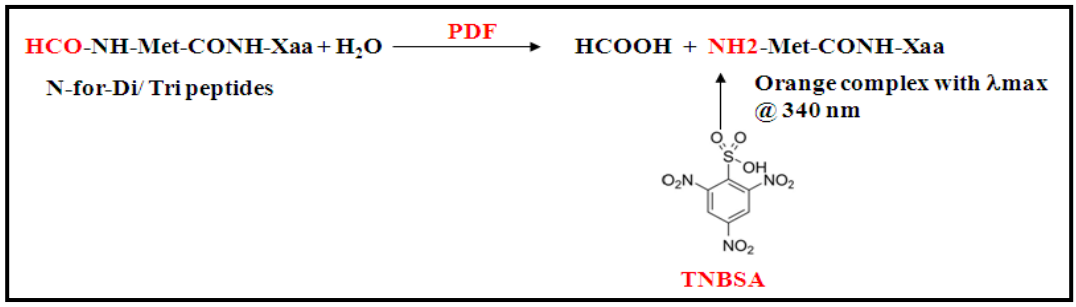

2.4.3.1b Reagents

a) 100 mM Phosphate buffer, pH 7.4

b) PDF enzyme sample

c) Substrates (*N*-formyl-Met-Ala-Ser, *N*-formyl-Met-Leu-Phe, *N*-formyl-Met)

d) Bicarbonate buffer (0.1 M $NaHCO_3$, pH 8.5)

e) TNBSA (0.01% in 0.1 M $NaHCO_3$, pH 8.5)

f) 4% Perchloric acid ($HClO_4$).

g) 10% SDS

h) 1 N HCl

i) BSA

j) Catalase

2.4.3.1c Procedure

The peptide deformylase activity assay for MtbPDF was done using spectrophotometric method according to Saxena and Chakraborti, (2005a), with slight modification, using (TNBSA) (Snyder and Sobocinski, 1975) as the reagent to determine the free amine concentration. Substrates used for the assay were N-formylated di or tri-peptides like *N*-formyl-Met-Ala-Ser, *N*-formyl-Met-Leu-Phe and *N*-formyl-Met at a concentration of 5 mM.

The assay was carried out in 96 well microtiter plates (Axygen, India), in 100 mM phosphate buffer, pH 7.4 containing 10 µg/ml of catalase, 0.2 mg/ml BSA and 5 mM substrates in a total reaction volume of 50 µl. The deformylase reaction was initiated by addition of purified MtbPDF or its mutants and was incubated for 30 minutes at 30 ^{o}C. The reaction was quenched by addition of 50 µl 4% $HClO_4$. To this 50 µl of 0.01% TNBSA in 0.1 M bicarbonate buffer, pH 8.5 was added and left for incubation at 37 ^{o}C for 1 h. The TNBSA reaction was stopped by addition of 100 µl 10% SDS and 50 µl 1N HCl. The highly chromogenic derivative formed was read at 340 nm in a microtiter plate reader (Biorad-680XR, USA). The final values were corrected by subtracting values from blank reaction (all ingredients except MtbPDF). A standard curve was done similarly with 0-100 µM L-Methionine (**Fig 2.4**). The deformylase activities were expressed as µM free amines produced / min/ mg proteins.

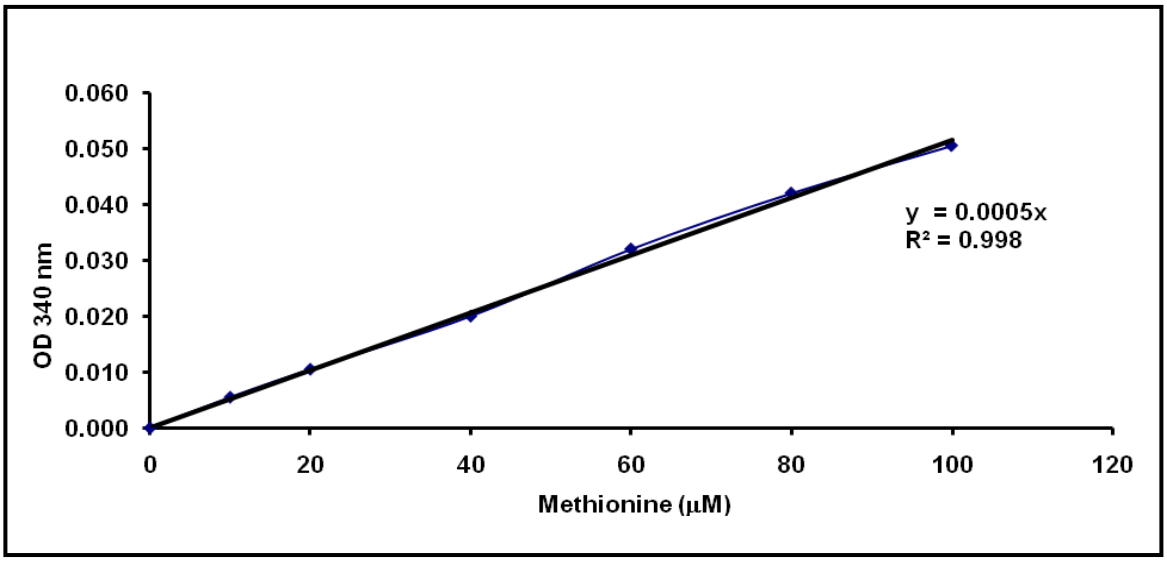

Fig 2.4: Standard graph of L-Methionine with TNBSA

2.4.3.2 Methionine aminopeptidase assay

2.4.3.2a Principle

Methionine aminopeptidase (MAP) cleaves the first methionine from nascent polypeptide *in vivo*, following translation. *p*- Nitro aniline derivatives of L-methionine offer an easy method to detect MAP activity using spectrophotometry. Up on action of MAP enzyme on the peptide bond in L-Met-*p*-Nitro anilide, the chromogenic *p*- Nitro aniline is released, which can be monitored at 405 nm.

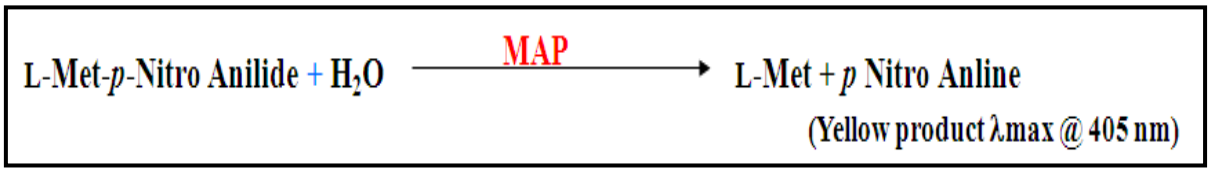

2.4.3.2b Reagents

a) 50 mM Tris-Cl (pH 8.0) + 0.1 M KCl

b) MAP enzyme sample

c) Substrate (L-Met-*p*-Nitro anilide)

d) Divalent cations.

e) 30% glacial acetic acid.

f) *p*-nitro aniline

2.4.3.2c Procedure

The enzyme assay was adopted from Mitra *et al*., (2006) using the L-Met-*p*-Nitro anilide (L-Met-*p*NA) as substrate, with slight modifications. Assay was carried out in a microtiter plates (Axygen, India) in total volume of 250 µl, in 50 mM Tris-Cl (pH 8.0) containing 0.1 M KCl with 1 mM of substrate L-Met-*p*NA. The reaction was initiated by

addition of purified MAP enzyme. In case of assay with apo-enzymes, 1 μM –1 mM divalent cations were also included in the assay. The reaction was carried out at 37 ^{o}C for 30 min. At the end of 30 min, the reaction was stopped by addition of 100 μl of 30% glacial acetic acid and the absorbance was measured at 405 nm in a microtiter plate reader (Biorad-680XR, USA). The final absorbance values were corrected by subtracting appropriate blanks values. The *p*-nitro aniline released was analyzed according to the standard graph plotted with 0-100 μM *p*-nitro aniline (**Fig. 2.5**). The MAP activity was expressed as μM *p*-nitro aniline released / min /mg protein.

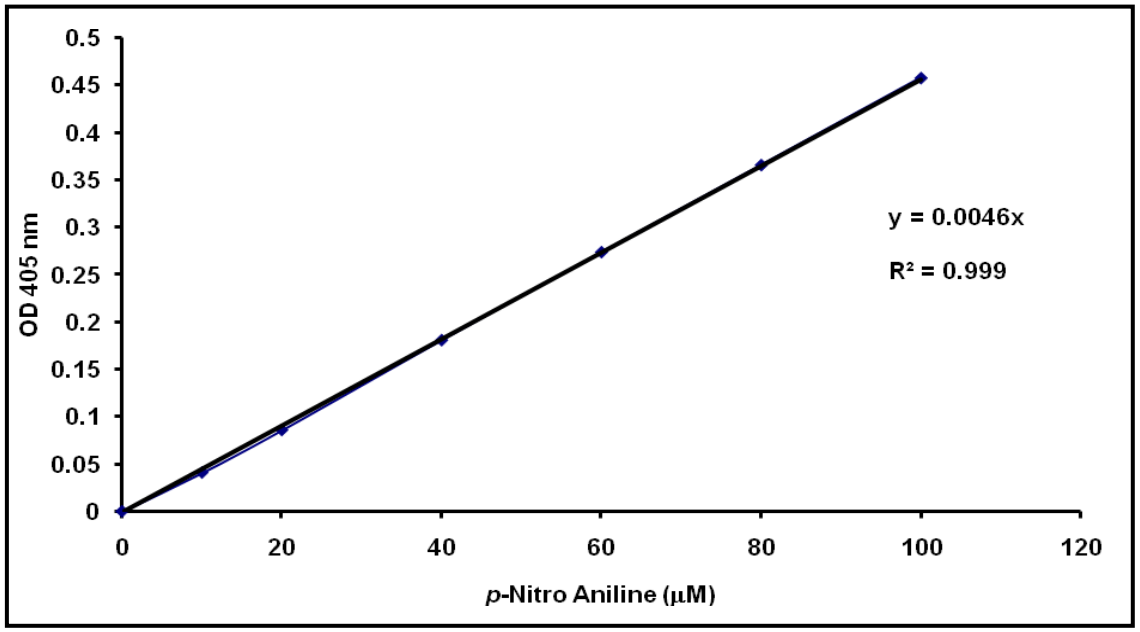

Fig 2.5: Standard graph of *p*-Nitro Aniline

The major instruments used throughout the studies were listed in annexure I.

CHAPTER 3

Molecular Cloning, Expression, Purification and Biochemical Characterization of Peptide deformylase of *M. tuberculosis* H37Rv

CHAPTER 3

Molecular Cloning, Expression, Purification and Biochemical Characterization of Peptide deformylase of *M. tuberculosis* H37Rv

3.1 Introduction

The process by which initiator methionine is removed from nascent polypeptide is called N-terminal Methionine Excision (NME). In eubacteria and organelle protein biosynthesis, the initiator methionine is always formylated by the action of enzyme Met-tRNA formyl methionine transformylase (FMT) (Ball and Kaesberg, 1973). So there is an additional step involved in the NME of eubacteria and organelles where in the formyl group is cleaved off from the initiator methionine.This step is carried out by dedicated enzyme peptide deformylase (PDF: EC: 3.5.1.27), encoded by *def* gene in all eubacteria and organelles. Action of PDF is a mandatory step to unmask initiator methionine by the subsequent action of methionine aminopeptidase (MAP: EC 3.4.11.18) (Solbiati et al., 1999).

Adams (1968) was the first to demonstrate the presence of PDF (EC 3.5.1.27) activity in a bacterial extracts of *E. coli* and noticed the enzyme to be highly instable. Subsequently, it was realized that the formylation/deformylation event of methionine was specific to prokaryotes and has no role to play in eukaryotic cytoplasmic NME. But due to the instability of PDFs, there was no proof to support this hypothesis by experimental evidence and it took nearly 20 years to solve this issue of instability. In 1993, the gene

encoding PDF in *E. coli* was shown to belong to the same operon as of FMT (Meinnel and Blanquet., 1993). Essentiality of *def* gene was first demonstrated in *E. coli* by targeted gene knock-out studies by Mazel et al., (1994). From that point onwards there was an increased interest in PDF as potential target for antibacterial drug discovery.

E. coli PDF was reported to be zinc containing metallo-protease by Miennel et al., (1995), but the Zn-enzyme had very low specific activity. The problem of instability was finally solved in 1997 by determining the metal ion in highly active *E. coli* PDF as ferrous ion. The instability was attributed to the oxidation of Fe^{2+} to Fe^{3+} and was solved by excluding oxygen during purification procedure (Rajagopalan et al., 1997a) or by replacing Fe^{2+} ion with Ni^{2+} or Co^{2+} during purification (Ragusa et al., 1998). The first crystal structure of PDF was reported using *E. coli* enzyme and from the structural information, PDF was suggested to belong to a new subfamily of metallo-proteases (Chan et al., 1997) with its substrate binding and metal binding sites highly similar to that of thermolysin family (Holmes and Matthews, 1982). Based on systematic site-directed mutagenesis studies on *Thermus thermophilus* and *E. coli* PDFs, three conserved motifs (**GXGXAAXQ, EGCLS** and **HEXDH**) were defined in PDF family, forming the architecture of peptide binding and metal binding pockets (Meinnel et al., 1997). Catalytic mechanism of PDF was postulated based on thermolysin, in which the metal-bound water / glutamate network was proposed to be responsible for the hydrolysis of formyl group (Becker et al., 1998).

Increased interest in biochemistry of PDF had prompted researchers to develop novel enzyme assays for PDF activity. Traditional PDF assay using ninhydrin was replaced with formate dehydrogenase coupled assay (Lazennec and Meinnel, 1997); aminopeptidase

coupled assay using formyl-Met-Leu-*p*-nitroanilide (Wei and Pei, 1997) and TNBSA reagent based assay (Groche et al., 1998), with the first one being the most popular.

Advances in the number of microbial genomes sequenced in the post-genomic era had paved way to identification and characterization of PDFs across a wide variety of bacteria. Genomic data confirmed the presence of PDF in all eubacteria, and in some instance two PDFs were found as in case of *Streptococcus penumoiniae* (Margolis et al., 2001) and *Bacillus subtilis* (Haas et al., 2001). The presence of PDF in most of the pathogenic bacteria sequenced till then had evoked the interest in screening PDF specific inhibitors as antibacterial agents. Simultaneously, the increase in the structural data on bacterial PDFs led to proposal of two subfamilies of PDFs based on their amino acid sequences and structures, PDF class I (Gram negative bacterial PDFs) & PDF class II (Gram positive bacterial PDFs). In search of potent PDF inhibitors, researchers form Vicuron Pharmaceuticals recognized actinonin, a natural antimicrobial product identified in 1962 (Gordon et al., 1962), as potent inhibitor of *E. coli* PDF (Chen et al., 2000). Actinonin has hydroxymate side chains as metal ion chelating group. Later on many derivatives of actinonin having hydroxamates, reverse hydroxamates, carboxylates or sulfhydryls side chains have been synthesised and tested for the inhibition of bacterial PDFs both *in vitro* and in culture (Jain et al., 2005). There were reports on excellent antibacterial activities of PDF inhibitors on different respiratory pathogens like *Haemophilus influenza*, *Mycoplasma pneumoniae* and *Chlamydophila pneumonia* (Yuan and White, 2006).

It is interesting that PDF-like genes were also reported in genomes of *Homo sapiens*, eukaryotic parasites, and plants (Giglione et al., 2000). Most of the eukaryotic PDFs are

chromosome encoded organelle-targeted proteins with N-terminal, organelle-specific, cleavable target sequences. PDFs from many eukaryotic parasites like *Plasmodium falciparum* were characterized as active enzymes and were proved as potent targets for anti-parasite drugs (Meinnel, 2000). But on the other hand, the human mitochondrial PDF was found to be feebly active resulting in *N*-formylated proteins in mitochondria. The essentiality of deformylation in human mitochondria was an unanswered question (Nguyen et al., 2003), and still remains so. However, PDF is still considered as an important target for next generation antibiotics.

The limited number of reports and the ongoing interest on MtbPDF have prompted us to initiate the work on PDF enzyme of *M. tuberculosis* in order to characterize them at molecular and biochemical levels. Detailed characterization of the recombinant enzyme was carried out in order to bring out their salient features which would be helpful in screening novel and specific inhibitors of PDF from *M. tuberculosis*.

3.2 Materials and Methods

3.2.1 Genome search

A complete search of the genome of *M. tuberculosis* H37Rv was done using the list of annotated genes (Cole et al., 1998) available from the Tuberculist website (*http://genolist.pasteur.fr/TubercuList*) for genes coding for peptide deformylase (*def* gene).

3.2.2 Primer designing

The nucleotide sequence of an open reading frame (ORF) coding putative *def* gene of *M. tuberculosis* H37Rv was retrieved from the Tuberculist website. Based on the nucleotide sequences, specific primers were designed for amplification of *def* gene from the genomic

DNA of *M. tuberculosis* H37Rv by polymerase chain reaction (PCR). The primers were designed with 5' linker sequences incorporating base sequences for restriction enzymes to facilitate cloning of the *def* amplicons into pET28a expression vector. The qualities of the designed primers were tested using online version of Net primer software. Primers were custom synthesized from Integrated DNA Technologies (IDT, USA).

3.2.3 PCR amplification of *def* gene

The *def* gene was amplified from chromosomal DNA of *M. tuberculosis* H37Rv by standard PCR strategies using *Taq* DNA polymerases according to Sambrook et al., (1989). The primers used were, *def*–sense, 5' FP: 5' CAT AAG CCG AAT CCT **CAT ATG** GCA GTC G 3' (containing a *Nde I* restriction site, underlined); and *def* – antisense 5' ACC CTC GAG **GAA TTC** TAA TTA GTG ACC GAC C 3' (containing a *EcoR I* restriction site, underlined). PCR conditions standardized for the amplification of *def* gene were standardized and *def* gene was amplified. The 594 bp PCR amplicons was resolved on 1% agarose gel and was purified from the excised gel fragment using gel extraction kit (Qiagen, Germany).

3.2.4 Cloning of *def* gene into pET28a expression vector

For recombinant expression of *def* gene of *M. tuberculosis* H37Rv in *E. coli, def* gene was ligated into pET28a expression vector using standard ligation protocol (Sambrook et al., 1989). pET28a is an *E. coli* expression vector, having T_7 promoter under the control of IPTG inducible lacI' operator, with provision for N-terminal His-tag fusion (Fig 3.1). The purified PCR amplicons of *def* gene was double- digested with restriction enzymes *Nde*I and *EcoR*I and was ligated using T_4 DNA ligase, into pET28a vector previously digested ,

at 22 ^{o}C, to construct pET 28a: *def* recombinant plasmid. The ligation mix was transformed into *E. coli* DH5α chemical competent cells (2.3.2) and recombinants were screened from the mobility shifts of plasmids isolated (2.3.1) on agarose gel. From the isolated plasmid, 594 bp insert was further confirmed by releasing the insert by double digestion with *Nde I* and *EcoR I* and the orientation and position of the insert in-frame with N-terminus 6x His-tag was further verified by DNA sequencing (Scigenomics, India) of both the strands. The confirmed recombinant constructs were further transformed into *E. coli* BL21 (DE3) chemical competent cells for expression studies.

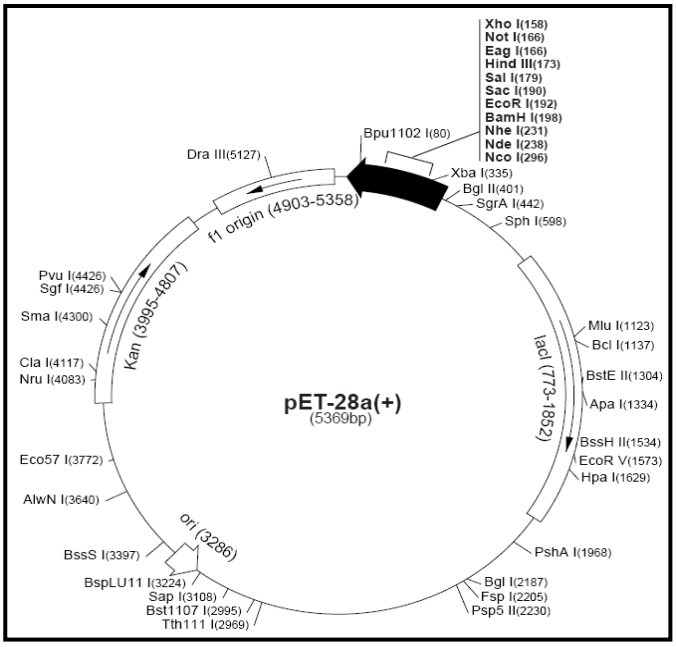

Fig 3.1: Restriction map of pET28a (+) vector

3.2.5 Over-expression of recombinant *M. tuberculosis* Peptide Deformylase (MtbPDF)

An overnight culture of *E. coli* BL21 (DE3) carrying pET28a: *def* was inoculated into 100 ml of LB broth supplemented with 30 μg/ml kanamycin and was incubated at 37 °C

under shaking at 200 rpm until the $OD_{600\ nm}$ reached 0.6 - 0.7. The culture was then induced with 0.5 mM IPTG. Growth was continued for another 4 h at 37 °C, 200 rpm and the cells were harvested by centrifugation at 8000 rpm, 4 ^{o}C for 15 min. The cell pellets were stored at -80 ^{o}C until use. The pellets were resuspended in 5 ml of ice-cold lysis buffer (20 mM phosphate buffer, pH 7.4, 300 mM NaCl, 5 mM imidazole, 10 µg/ml catalase, 1 mM PMSF, 10 µl protease inhibitor cocktail for his-tagged proteins and 0.5 mg/ml lysozyme) and left on ice for 30 min. The cells were then disrupted by sonication (5 cycles of 30 s ON 30 s OFF at 42% amplitude) and the resulting lysate was centrifuged at 13,000 rpm for 30 min at 4 °C to recover the soluble proteins in the supernatant. The insoluble pellet fraction was washed twice with ice-cold lysis buffer containing 2% Triton X-100. The washed pellet was solublised in 3 ml of urea buffer (20 mM phosphate buffer, pH 7.4, 300 mM NaCl, 5 mM imidazole, 10 µg/ml catalase, 5 mM DTT and 3 M urea) for 30 min by continuous stirring with a magnetic bead at 4 ^{o}C. The solubilised proteins in urea fraction were recovered by centrifugation at 13,000 rpm for 30 min. Extraction in urea buffer was repeated again to recover complete proteins. The proteins in different fractions were analyzed by running them on 12% SDS-PAGE (2.4.1.1) to check for the over-expression of protein bands. The recombinant proteins in each of the fractions were confirmed by performing Western blotting using anti-His antibodies (2.4.1.2). Total protein contents in each of the fractions were quantified using Bradford's assay (2.4.2.1).

3.2.6 Optimization of expression conditions for solubilisation of recombinant MtbPDF

It was observed that recombinant MtbPDF was expressed almost completely in the insoluble fractions. Hence, attempts were made to bring more of the over expressed MtbPDF proteins to the soluble fraction by varying the IPTG concentrations, incubation temperatures and by co-expressing with molecular *E.coli* chaperonins.

3.2.6.1 Effect of different IPTG concentrations

Different IPTG concentrations were screened for induction as suggested from the results of various recombinant expression studies (Winograd et al., 1993; Yildir et al., 1998). Expression was performed essentially as described in previous section, but induction was done with 5 different concentrations of IPTG like 0.1, 0.25, 0.5, 0.75 and 1 mM at 37 ^{o}C for 4 h. Soluble expression at 0.5 mM IPTG was taken as control.

3.2.6.2 Effect of different induction temperature

The idea of using a lower temperature for solubilising recombinant proteins was reported previously for many recombinant proteins (Schein, 1989; Vasina and Baneyx, 1997; Sørensen and Mortensen, 2005). In the expression protocol mentioned in 3.2.5, after the OD_{600} reached 0.6, the cells were induced with 0.5 mM IPTG and left for incubation at various temperatures (16 ^{o}C, 30 ^{o}C and 37 ^{o}C) for a period of 12 h. Soluble expression at 37 ^{o}C was taken as control.

3.2.6.3 Effect of co-expression of chaperonin GroEL/ GroES

A possible strategy reported for the prevention of inclusion body formation during recombinant expression is the co-overexpression of molecular chaperones (Schwarz et al.,

1996; Mogk et al., 2002). GroEL/ES chaperone (Hsp60 chaperone family) operates the protein transit between soluble and insoluble protein fractions and participates positively in disaggregation and inclusion body formation (Schlieker et al., 2002). Chaperones GroEL/ES were over expressed in *E. coli* BL21 (DE3) cells from plasmid pGro7 (Takara, Japan) (Fig 3.2), carrying chloramphenicol resistance marker and an *ara* promoter. Briefly, pET28a: *def* plasmid was transformed into BL21 (DE3) containing pGro7 plasmid and was grown in 5 ml LB broth containing 20 μg/ml chloramphenicol and 30 μg/ml kanamycin for over night and 1% of this culture was inoculated to 100 ml LB broth with 20 μg/ml chloramphenicol and 30 μg/ml kanamycin containing 0.5 mg/ml arabinose and was allowed to grow until OD_{600} reached 0.7. The culture was induced with 0.5 mM IPTG for 12 h at 30 ^{o}C before retrieving the cell pellet and processing as described in 3.2.5.

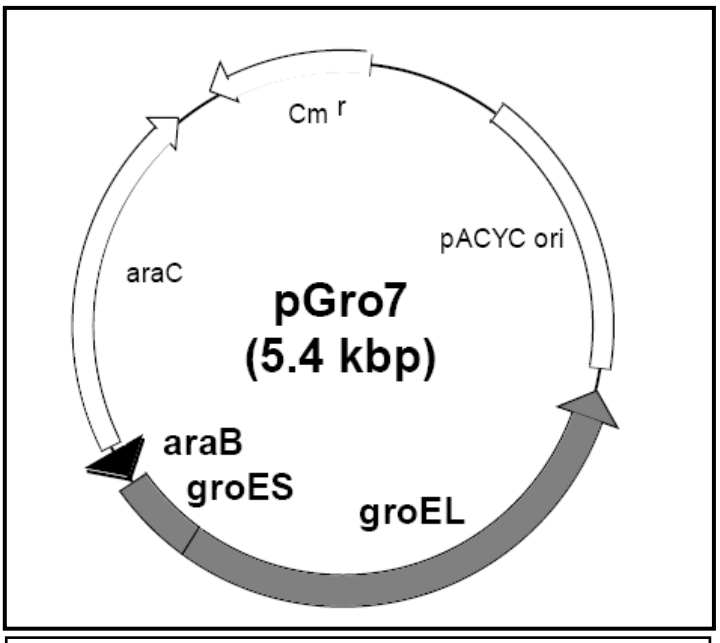

Fig 3.2: Map of pGro7 chaperone plasmid

3.2.7 Refolding and purification of MtbPDF from inclusion bodies

Refolding of MtbPDF, extracted in 3 M urea lysis buffer from insoluble fraction, was done according to Saxena and Chakraborti (2005a), with necessary modifications. Briefly, the extracted inclusion bodies containing over expressed MtbPDF were first diluted in 20 mM phosphate buffer, pH 7.4 to a total protein concentration of 0.3 mg/ml along with 0.2 mg/ml BSA and 10 μg/ml catalase. This was subjected to extensive dialysis, in an 8 kDa dialysis bag, against cold dialysis buffer (20 mM phosphate buffer, pH 7.4, 300 mM NaCl and 5 mM imidazole) at 4 ^{o}C for 14 h with two buffer changes. This is to facilitate slow removal of urea from the proteins and to renature MtbPDF to its native state.

The refolded proteins and proteins co-expressed with chaperone were passed through Ni-affinity column (Qiagen, Germany) under native conditions, washed with wash buffer and eluted in elution buffer containing 250 mM imidazole as described in 2.3.3. The refolded enzyme was concentrated using 10 kDa Amicon centri-concentrators (Millipore, India) to 1 mg/ ml and was stored at -20 ^{o}C. For all assay purpose, enzyme was diluted in dilution buffer (20 mM phosphate buffer, pH 7.4 containing 0.2 mg/ml BSA and 10 μg/ml catalase) to a protein concentration of 10 μg /ml.

3.2.8 Peptide deformylase Assay

Deformylase activity assay of MtbPDF was performed according to the standard PDF assay as described in 2.4.3.1 using 83 ng (73.3 nM) of refolded-purified MtbPDF in a total volume of 50 μl. Deformylase activities were expressed as μM free amines produced / min/ mg protein based on L-methionine standard curve.

3.2.9 Biochemical and Biophysical characterization of purified MtbPDF

3.2.9.1 Substrate specificity of MtbPDF

Substrate specificities of purified MtbPDF was studied by checking its ability to deformylate the *N*-formylated di or tri peptide substrates in standard PDF assay. The substrates screened were *N*-formyl-Met-Ala-Ser (*N*-f-MAS), *N*-formyl-Met-Leu-Phe (*N*-f-MLF) and *N*-formyl-Met (*N*-f-M) at concentration of 5 mM. Assay was performed with 73.3 nM MtbPDF at 30 ^{o}C and pH 7.4. The best substrate for MtbPDF was used for all further assays.

3.2.9.2 Temperature and pH optimum for MtbPDF activity

The temperature and pH optimum for deformylase activity of MtbPDF was studied with 5 mM of substrate *N*-f-MAS. Deformylase activity of MtbPDF (73.3 nM) at different temperatures ranging from 10 – 65 ^{o}C were studied using the standard PDF assay at pH 7.4. Similarly, the effect of pH on deformylase activity of MtbPDF was studied using different pH buffer set of 20 mM concentrations at 30 ^{o}C with the above mentioned substrate. The buffers used to set different pH were sodium acetate buffer (pH 3.5-5.0), phosphate buffer (pH 5.5- 7.5), sodium-glycine buffer (pH 8.0-10.5). Blanks were performed in each buffer system so as to cancel out the back ground values produced by the reaction of primary amines in buffers with TNBSA.

3.2.9.3 Effect of catalase and BSA on MtbPDF activity

PDF enzyme is known for its oxidative instability (Rajagopalan et al., 1997b; Rajagopalan and Pei, 1998). The effect of catalase as oxygen-scavenging enzyme and BSA as a carrier protein was assessed during dilution of MtbPDF. During dilution of MtbPDF

from stock, 10 μg/ml catalase and 0.2 mg/ml BSA was added either individually or together and their effect was studied by performing standard PDF assay with 5 mM *N*-f-MAS at pH 7.4 and 30 ^{o}C using 73.3 nM MtbPDF. An experiment where both these proteins were omitted during dilution of MtbPDF was taken as negative control.

3.2.9.4 Effect of metal ions on MtbPDF activity

The effect of different metal ions on MtbPDF activity was studied by including chloride salts of seven different divalent cations (Co^{2+},Ca^{2+}, Cu^{2+}, Mg^{2+}, Mn^{2+}, Zn^{2+}, $Ni^{2+}$and Fe^{2+}), two monovalent cations (Na^{+} and K^{+}) and one trivalent cation (Fe^{3+}) at a concentration of 1 mM in the standard PDF assay. The assay was performed using 5 mM *N*-f-MAS at pH 7.4 and 30 ^{o}C with 73.3 nM MtbPDF in presence of 10 μg/ ml catalase and 0.2 mg/ ml BSA. Reaction where no metal ion was added was taken as control.

3.2.9.5 Enzyme Kinetics of MtbPDF

In order to understand the basic enzyme kinetics of purified MtbPDF, continuous PDF assay with TNBSA was set up to monitor the increase in OD_{340} with time. Various concentrations of substrate *N*-f-MAS (0-20 mM) was used with 73.3 nM of MtbPDF in continuous PDF assay to determine the initial velocity. K_m and V_{max} values were determined from the slopes of various concentrations of substrate by applying nonlinear curve fit of Michaelis-Menten (Menten and Michaelis, 1913). Kinetic analysis was performed using Graph Pad Prism version 5.0 (Graphpad software). The turnover number, K_{cat} value was determined directly from the software by applying the formula $K_{cat} = V_{max} / [E_T]$, where V_{max} is the maximum velocity and E_T is the total enzyme concentration.

3.2.9.6 Thermo-stability of MtbPDF

Temperature stability of the purified MtbPDF was studied by incubating 1 μg of purified enzyme along with 10 μg/ ml catalase and 0.2 mg/ ml BSA at different temperatures (30 ^{o}C, 40 ^{o}C and 50 ^{o}C) and withdrawing aliquots of 100 ng to perform standard PDF assay at 30 ^{o}C, every 1 h for a period of 6 h. PDF activity at time 0 was taken as control to assess the relative activity of MtbPDF with respect to time at each temperature and the results are expressed as percentage relative activity of the activity at time 0.

3.2.9.7 Determination of metal content by Atomic Absorption Spectroscopy

Atomic absorption spectroscopy (AAS) is a spectroanalytical procedure for the qualitative and quantitative determination of chemical elements employing the absorption of optical radiation (light) by free atoms in the gaseous state. AAS can be used to determine over 70 different elements in solution or directly in solid samples (L'vov, 2005). Metal content in MtbPDF was determined by using Varian AA775 spectrophotometer equipped with an air-acetylene burner.

3.2.9.7a. Principle

The technique makes use of absorption spectrometry to assess the concentration of an analyte in a sample. It requires standards with known analyte content to establish the relation between the measured absorbance and the analyte concentration. So it relies on Beer-Lambert Law. In short, the electrons of the atoms in the atomizer can be promoted to higher orbitals (excited state) for a short period of time (nanoseconds) by absorbing a defined quantity of energy (a given wavelength). This amount of energy, i.e., wavelength, is specific to a particular electron transition in a particular element.

In general, each wavelength corresponds to only one element, and the width of an absorption line is only of the order of a few picometers (pm), which gives the technique its elemental selectivity. The radiation flux without a sample and with a sample in the atomizer is measured using a detector, and the ratio between the two values (the absorbance) is converted to analyte concentration or mass using Beer-Lambert Law.

3.2.9.7b Determination of Fe-content in MtbPDF by AAS

PDFs are generally considered as metallo-proteases having either Fe^{2+} (Rajagopalan et al., 1997b) or Zn^{2+} (Meinnel et al., 1995) as their metal ion co-factors. The Fe content of purified MtbPDF protein samples were determined by atomic absorption spectroscopy as described by Meinnel et al., (1997). 400 µl of purified-refolded proteins at a concentration of 2 mg / ml was dialysed overnight against 20 mM phosphate buffer (pH 7.4) and 0.1 M KCl to remove any unbound metal ion in the solution. Dialysed samples were mixed with concentrated nitric acid in a ratio of 1:1 v/v and were serially diluted in a volumetric flask to get different concentrations of proteins. Using a Varian AA775 spectrophotometer equipped with an air-acetylene burner and in "peak height" mode, atomic absorbances were measured at 248 nm during five seconds after the injection of 0.1 ml sample. Metal ion concentrations in serial dilutions of the enzyme samples were calculated by comparison to serial dilutions of standard $FeCl_2$ (Merck). The results are expressed as g-Fe atoms/ g of protein.

3.2.9.8 Stability of MtbPDF towards oxidizing agents

Fe^{2+} containing PDFs have been reported to be highly prone to oxidative inactivation in presence of oxidizing agents like hydrogen peroxide (H_2O_2) (Rajagopalan and Pei, 1998). In order to study the H_2O_2 stability of MtbPDF, 100 ng of diluted enzyme in the absence of

catalase was incubated with 0-500 mM H_2O_2 in 100 mM phosphate buffer pH, 7.4 at 30 ^oC for 30 min. Standard PDF assay was initiated by addition of 5 mM *N*-f-MAS to the reaction. Appropriate blank reactions were performed using H_2O_2 and other components except MtbPDF and were subtracted to correct the final values. The results are represented as percentage relative activities of the uninhibited reactions.

3.2.9.9 Effect of divalent metal ion chelators on MtbPDF activity

The importance of divalent metal ions for the activity of metallo-proteases can be studied by chelating the metal ions by strong metal chelators (Auld, 1988). Effects of divalent metal chelators like EDTA and 1, 10 phenanthroline on MtbPDF activity were studied by including varying concentration (0-10 mM) of these chelators in standard PDF assay. Appropriate blanks were performed to cancel out any background values. The uninhibited reactions were taken as control to calculate the percentage relative activities at different concentrations.

3.2.9.10 Effect of metallo-protease inhibitors on MtbPDF activity

The effects of PDF specific metallo-protease inhibitor, actinonin (Chen et al., 2000) and two other strong metallo-protease inhibitors bestatin and amastatin (Rich et al., 1984) were studied on MtbPDF. All the three inhibitors were dissolved in 100% dimethyl sulfoxide (DMSO). 100 ng of purified enzyme was incubated with varying concentrations (0.001 μM-10 μM) of these inhibitors for 15 min before initiating the assay by addition of 5 mM *N*-f-MAS. Corresponding inhibitor blanks were also performed. The uninhibited reaction in each case was taken as control and the results were expressed as percentage relative activity of the control.

3.2.9.11 Determination of MIC of actinonin on E. coli cells over-expressing MtbPDF

In order to study the antimicrobial activities of actinonin, for which the mode of action reported was by inhibition of PDF, *in vitro* microbiological assay was performed on *E. coli* cells over-expressing MtbPDF. The minimal inhibitory concentrations (MIC) of actinonin on *E.coli* cells expressing MtbPDF were determined by micro-titre broth dilution method as reported by Clements et al., (2001) and Nampoothiri et al., (2008). Briefly, *E.coli* BL21 (DE3) cells, *E.coli* BL21 (DE3) cells harboring pET28a plasmid and *E. coli* BL21 (DE3) cells harboring pET28a: *def* plasmids were grown up to an inoculums size of 5 x 10^5 CFU / ml. A 1 mg/ml stock of actinonin was prepared in DMSO and was serially diluted in LB broth in sterile 96 well plates (Nunc, India) to get 11 serial dilutions ranging from 0- 500 μg / ml. Similar dilutions were made with ampicillin, which is a distinct class of antibiotics with different mechanism of action, to serve as a control experiment. Kanamycin (30 μg /ml) was added to set of wells with cultures harboring pET28a or pET28a: *def* plasmids. These two cultures were allotted two rows for studying the IPTG- induced and uninduced conditions. 10 μl of overnight grown respective cultures were added to each of these 11 wells with the 12^{th} well left as uninoculated control. The cells were incubated for a period of 3 h at 37 ^oC with orbital shaking. At the end of 3 h, 0.1 mM IPTG was added to one set of wells each in case of *E.coli* BL21 (DE3) – pET28a and *E. coli* BL21 (DE3)-pET28a: *def* and was left overnight at 37 ^oC with orbital shaking. The growth inhibition was recorded by measuring the OD_{600}, with the uninoculated control as the blank, on a micro-titer plate reader (Bio-Rad, 680XR). MIC_{90} was defined as the concentration of actinonin above which there was 90% decrease in OD_{600} compared to the uninhibited wells.

The same experiment was demonstrated by well diffusion method on LB-Kan agar plates. LB-Kan agar plates with or without 0.1 mM IPTG was used in the study to set induced and uninduced conditions. 100 µl of overnight grown cultures of *E. coli* BL21 (DE3) (pET28a) or *E. coli* BL21 (DE3) (pET28a: *def)* were spread plated on to LB-Kan agar plates with or with out IPTG. Wells were made on the agar plates with well borer and 50 µl of two concentrations of actinonin (100 µg/ ml and 500 µg/ ml in 100% DMSO) was added to these wells.

This *in vitro* antibacterial assay was tested for screening PDF inhibitors from natural sources, in order to validate their target. Bioactive fractions were prepared from soil microbes isolated from Western ghats region of Kerala. Briefly, the cell free broth of bacterial cultures, 29 (b), A11 and A12 were collected after 48 h of growth. The metabolites in this cell free broth were isolated by passing the cell free broth through Diaion HP-20 resin and eluting the bound metabolites in 100% methanol. These methanol fractions were concentrated by vacuum concentrator and the resulting fractions were dissolved in 100% DMSO. 50 µl of these microbial bioactive preparations (29(b), A11 and A12), which showed antibacterial activities and *in vitro* MtbPDF enzyme inhibition, were tested for their inhibitory effects on *E. coli* cultures over expressing MtbPDF, on LB-Kan plates.

3.2.9.12 Circular Dichroism spectroscopy

Circular dichroism (CD) refers to the differential absorption of left and right circularly polarized light. It is exhibited in the absorption bands of optically active chiral molecules. CD spectroscopy has a wide range of applications in many different

fields. Most notably, UV CD is used to investigate the secondary structure of proteins (Greenfield, 2006).

3.2.9.12a Principle

Electromagnetic radiation consists of an electric and magnetic field that oscillate perpendicular to one another and to the propagating direction. Circularly polarized light occurs when the electric field vector rotates about its propagation direction and retains constant magnitude and thus, it forms a helix in space while propagating. When circularly polarized light passes through an absorbing optically active medium, the speeds between right and left polarizations differ ($c_L \neq c_R$) as well as their wavelength ($\lambda_L \neq \lambda_R$) and the extent to which they are absorbed ($\varepsilon_L \neq \varepsilon_R$). Circular dichroism is this absorbance difference, $\Delta\varepsilon = \varepsilon_L - \varepsilon_R$. In a CD spectropolarimeter, molar circular dichroism is usually determined from the formula

$$\mathbf{dA = (\varepsilon_L - \varepsilon_R)\, Cl}$$

Where, ε_L and ε_R are the molar extinction coefficients for left circularly polarized light and right circularly polarized light, *C* is the molar concentration and *l* is the path length in centimeters (cm). Usually the CD measurements are reported in degrees of ellipticity (θ), which is related to $\Delta\varepsilon$ as $(\theta) = 3298.2\Delta\varepsilon$. Mean residue ellipticity is normally used to represent the molar ellipticity value of polypeptides, where in the molar ellipticty value is divided by the number of residues in the polypeptides. CD is exhibited by biological molecules, because of their dextrorotary and levorotary components. Even more important is that a secondary structure like helix, β-sheets and random coils in a protein structure will also impart a distinct CD (**Fig 3.3**) to its respective molecules (Whitmore and Wallace,

2008). The capacity of CD to give a representative structural signature makes it a powerful tool in modern biochemistry with applications that can be found in virtually every field of study.

3.2.9.12b Estimation of secondary structures in MtbPDF by CD spectroscopy

In order to determine the secondary structures in purified MtbPDF, the CD spectrum of purified MtbPDF was recorded in a Jasco J-810 (Jasco, Japan) spectropolarimeter in the far-UV region (190–300 nm). CD spectroscopy was performed using 0.1 mg / ml of purified MtbPDF in 20 mM phosphate buffer, pH 7.4, at 25 ^{o}C using a cell with path length of 1 cm (Saxena et al., 2008). Each spectrum represented is the average of three separate scans. The percentage of secondary structures in MtbPDF was predicted using K2D2 software (*http://www.ogic.ca/projects/k2d2/*) for secondary structure estimation from CD data.

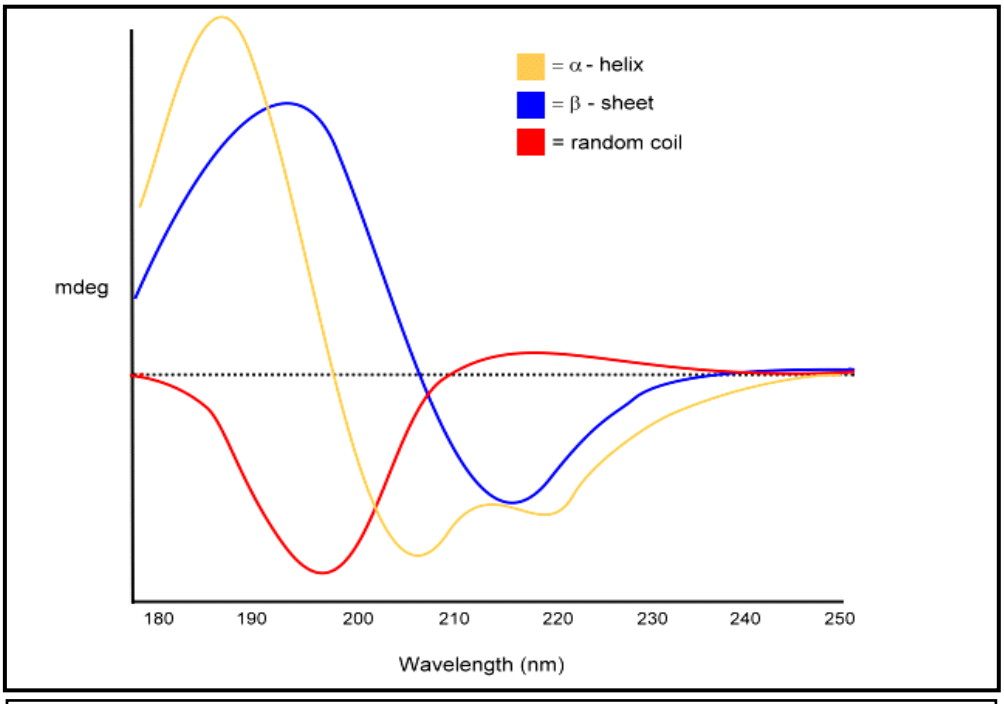

Fig 3.3: Typical CD spectra of the secondary structure of a pure protein

3.3 Results and Discussion

3.3.1 Genome search for *def* gene in *M. tuberculosis* H37Rv

Genome search for *def* gene in *M. tuberculosis* H37Rv genome returned one putative *def* gene (Rv0429c) coding for peptide deformylase. The translated nucleotide sequences were also retrieved from the same website (**Table 3.1**) and it was found to be a 197aa polypeptide, expected to have approximate molecular mass of 21 kDa

Table 3.1 Nucleotide and amino acid sequences of *def* gene of *M. tuberculosis* H37Rv

- ***M. tuberculosis* H37Rv|Rv0429c|*def*: 594 bp - PROBABLE POLYPEPTIDE DEFORMYLASE DEF (PDF) (FORMYLMETHIONINE DEFORMYLASE)**

```
atggcagtcgtacccatccgcatcgtgggcgatcccgtcttacacactgcgaccacaccg
gtgacggtcgccgccgacggttcactcccggcggatctcgcccagttgatcgccaccatg
tacgacaccatggacgccgccaacggagtcggcctggctgccaaccagatcggctgcagc
ctgcggctcttcgtctacgattgcgccgcggaccgcgcaatgaccgcccgccgacgcggt
gtggtcatcaatccggtgcttgagacctccgaaatacctgagaccatgcccgacccggac
accgacgacgaaggctgtctgtcggttcccggcgagtcatttcctaccggacgcgcgaag
tgggcacgagtcaccggactcgacgccgatggcagtccggtcagtatcgagggcaccggc
ctgttcgcgcggatgctgcagcacgaaaccgggcaccttgatggattcctgtacctggac
cgcctcatcggccggtacgcccgcaacgccaaacgggccgtcaagtcacatggctggggc
gttcccggactgtcgtggctgcccggcgaggaccccgacccgttcggtcactaa
```

- ***M. tuberculosis* H37Rv|Rv0429c|Def: 197 aa - PROBABLE POLYPEPTIDE DEFORMYLASE DEF (PDF) (FORMYLMETHIONINE DEFORMYLASE)**

MAVVPIRIVGDPVLHTATTPVTVAADGSLPADLAQLIATMYDTMDAANGVGLAANQIGCSLRLFVYD
CAADRAMTARRRGVVINPVLETSEIPETMPDPDTDDEGCLSVPGESFPTGRAKWARVTGLDADGSPV
SIEGTGLFARMLQHETGHLDGFLYLDRLIGRYARNAKRAVKSHGWGVPGLSWLPGEDPDPFGH

3.3.2 PCR amplification and cloning of *def* gene

def gene was amplified from the genomic DNA of *M. tuberculosis* using gene specific primers and *Taq* DNA polymerase at annealing temperature of 48 ^{o}C. The optimized PCR conditions of the *def* gene were as shown in **Table 3.2**. The amplicons showed an

expected size of 594 bp on 1% agarose gel (**Fig 3.4**). The amplified *def* gene was digested with *Nde I* / *EcoR I* and ligated into pET28a which was previously digested with the same restriction sites (**Fig 3.5**). The recombinant pET28a: *def* plasmid was confirmed by double digestion of the plasmid with *Nde I* and *EcoR I* (**Fig 3.6**). The recombinant plasmid DNA sequenced with T_7 forward primer confirmed the in-frame insertion of *def* gene without ant PCR artifacts (**Fig 3.7**).

Table 3.2 PCR conditions standardized for the amplification of *def* gene (Rv0429c) of *M. tuberculosis*

Cycles	Temperature (^oC)	Time
1	**94**	**3 min**
30	**94**	**30 sec**
	48	**2 min**
	72	**1 min**
1	**72**	**10 min**

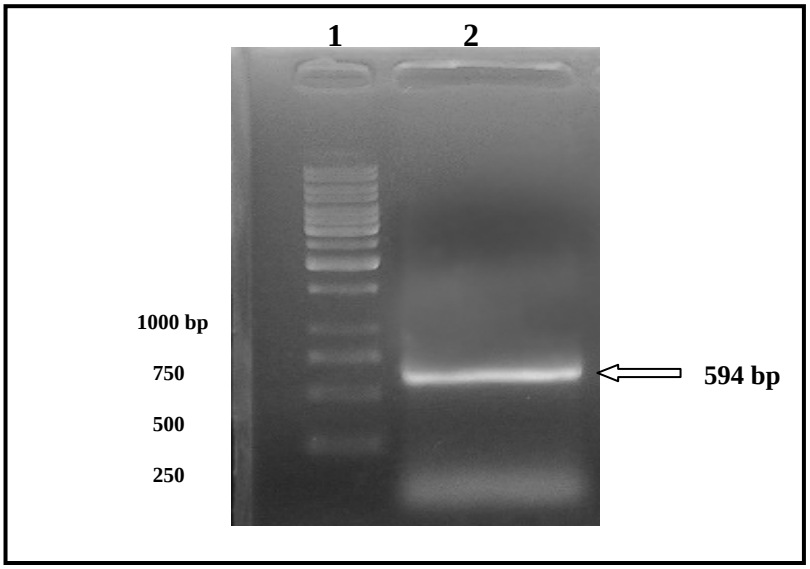

Fig 3.4: PCR amplification of *def* gene. Lane 1: 1 kb DNA ladder; Lane 2: *def* PCR amplicons.

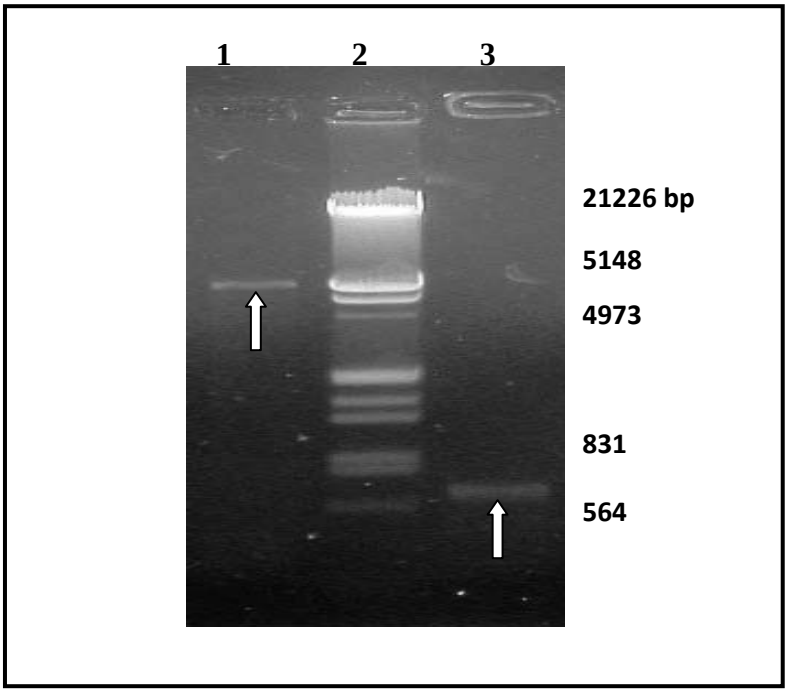

Fig 3.5: Digested pET 28a vector and *def* insert for ligation. Lane 1: pET 28a double digested with *Nde I* / *EcoR I*; Lane 2: l DNA *EcoR I*/ Hind III double digest DNA ladder; Lane 3: *def* PCR amplicons double digested with *Nde I* / *EcoR I*.

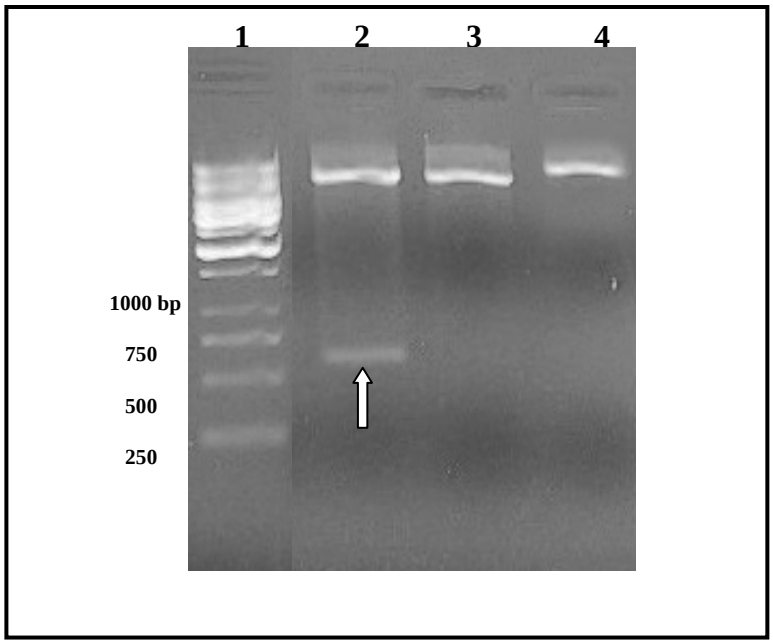

Fig 3.6: pET28a: *def* recombinant confirmation by double digestion. Lane 1: 1 kb DNA ladder**;**Lane 2: pET28a: *def Nde I / EcoR I* double digest showing insert release.**;**Lane 3: pET28a *Nde I / EcoR I* double digest.**;**Lane 4: pET28a: *def Nde I* single digest.

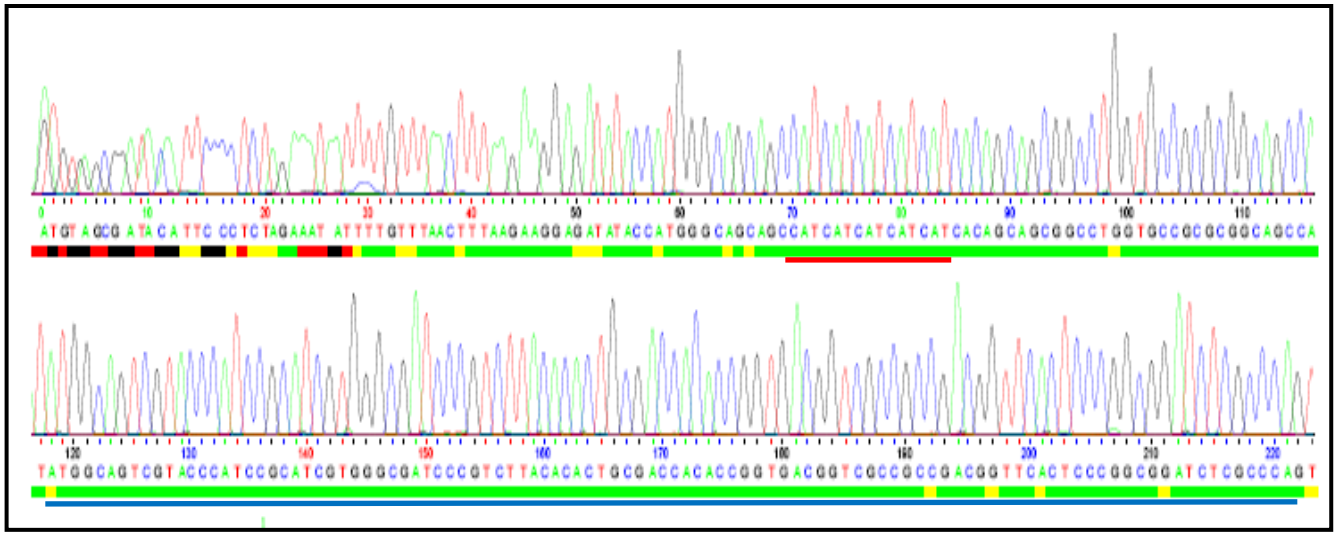

Fig 3.7: DNA sequencing chromatogram of pET28a: *def* plasmid using T_7 primer. The in-frame insertion of *def* gene (underlined with blue line) at *Nde* I site is confirmed. Sequences coding for N-terminal penta-His tag is underlined in red.

3.3.3 Over-expression, refolding and purification of recombinant MtbPDF

Upon expression, MtbPDF was seen as an overexpressed band at 29 ±1 kDa on SDS-PAGE (**Fig 3.8**), against the calculated molecular weight of 22.5 kDa (including the His-tag). These anomalous migrations have been reported previously for many bacterial PDFs and have been correlated with high proline contents in PDF sequences (Rajagopalan and Pei, 1998; Han et al., 2004; Saxena and Chakraboti, 2005a).

During IPTG induction, most of the over expressed recombinant proteins were transferred to insoluble pellet fraction (**Fig 3.8**). Immuno-dot blotting confirmed the absence of recombinant MtbPDF in the soluble protein fraction (data not included). Nearly 70 % of the *M. tuberculosis* proteins expressed in *E. coli* was reported to be found in the insoluble fractions as inclusion bodies (Bashiri et al., 2007; Goldstone et al., 2008). Attempts to vary the expression conditions like IPTG concentrations and induction temperature too did not prove effective in bringing recombinant MtbPDF to the soluble fraction (**Fig 3.9a & 3.9b**). No his-tagged recombinant proteins could be purified from the soluble fractions of any of these experiments.

Co-expression of chaperone GroEL/S along with MtbPDF resulted in expression of later in the soluble fraction to a small extent. MtbPDF (~29 kDa) was purified from soluble fractions along with GroEL protein (~60 kDa) by Ni-affinity chromatography. However, the chaperone was found to be very strongly associated with MtbPDF and could only be separated by precipitating at 80% saturation of ammonium sulfate (**Fig 3.10**). This kind of association of GroEL with recombinant PDF was reported in case of *Borrelia burgdorferi* PDF (Bb-PDF), where the association had no effect on the deformylase activity of Bb-PDF

(Nguyen et al., 2007). Soluble expression of MtbPDF from pQE30 vector with C-terminal His-tag was reported to get a final yield of 1.2 mg / L (Teo et al., 2006). But in present case and in case of previous workers (Saxena and Chakraboti, 2005a) who expressed MtbPDF with N-terminal His-tag, soluble expression was possible only in presence of chaperone co-expression.

Refolding of MtbPDF from the inclusion bodies solublised by 3 M urea was possible by simple dilution and dialysis. This proves that MtbPDF resides in the inclusion bodies in their near-native structure and needed only the dilution, which prevented them from aggregation and dialysis, which removed the denaturant, for restoring its activity. Refolding and further purification resulted in a final yield of 18-22 mg of purified refolded MtbPDF per liter of culture. The purified protein too showed a molecular weight of 29 ±1 kDa on SDS-PAGE and its recombinant nature was further confirmed by its detection at the corresponding size on a Western blot (**Fig 3.11**).

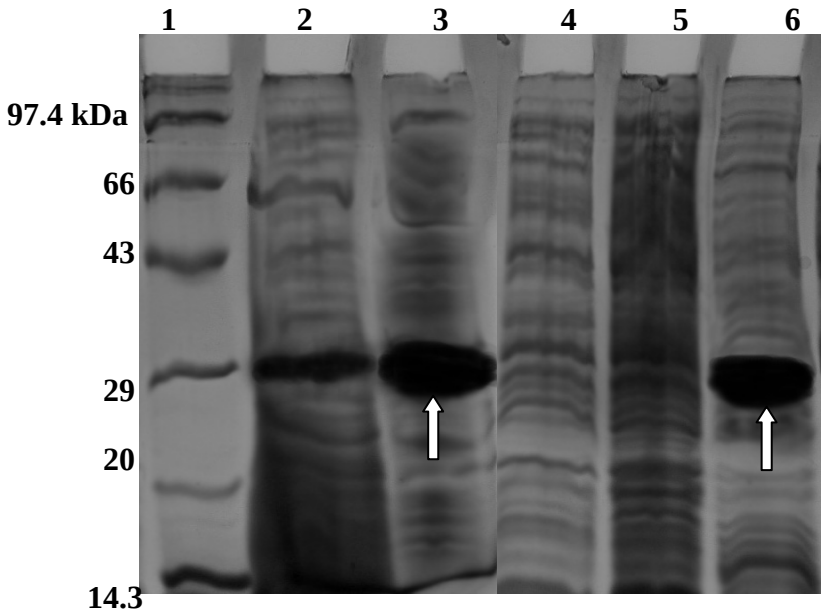

Fig 3.8: Expression of MtbPDF in different fractions from *E. coli*. Lane 1: Protein molecular weight ladder; Lane 2: Un-induced total cell lystae; Lane 3: Induced total cell lysate***;*** Lane 4: Induced soluble fraction***;*** Lane 5: Induced Triton X-100 fraction***;*** Lane 6: Induced 3 M urea solublised inclusion bodies.

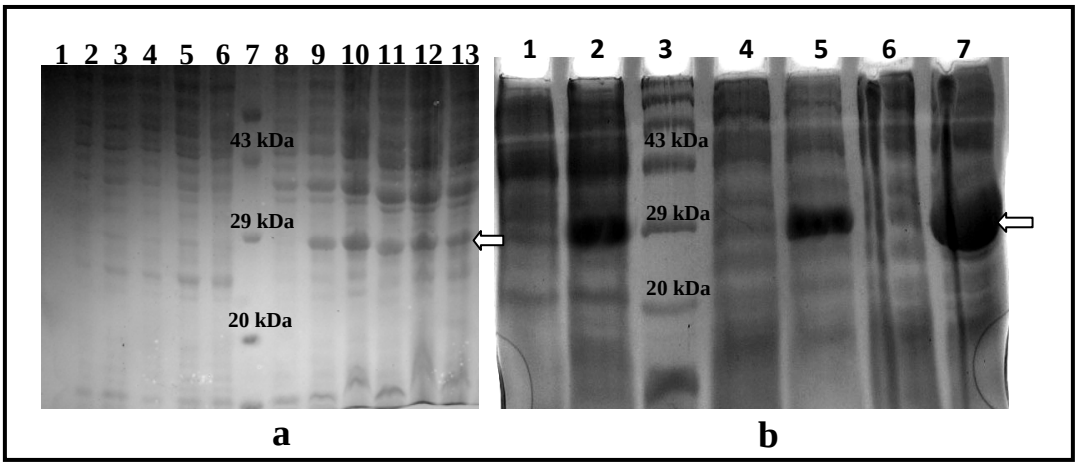

Fig 3.9: Optimization of conditions for soluble expression of MtbPDF. (a) IPTG concentration **(b)** Temperature**;** (a) Lane 1-6: Soluble fractions from 0, 0.1, 0.25, 0.5, 0.75 and 1mM of IPTG induction; Lane 7: Protein ladder; Lane 8-13 insoluble fractions from respective IPTG induction; (b) Lane 1-2: soluble and insoluble fraction from induction at 18 ^{o}C; Lane 3: Protein ladder; Lane 4-5: soluble and insoluble fractions from induction at 30 ^{o}C; Lane 6-7: soluble and insoluble fractions from induction at 37 ^{o}C.

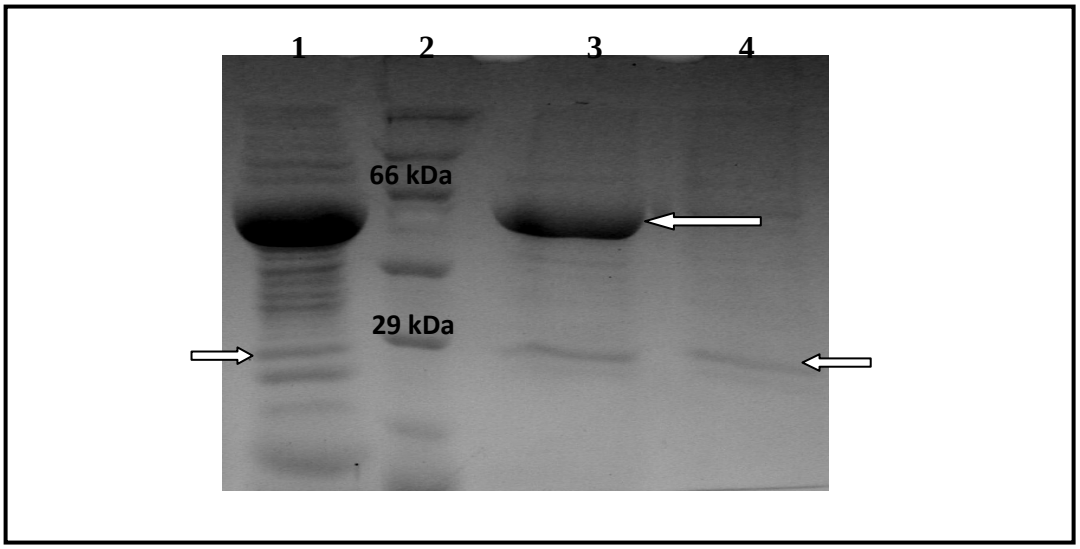

Fig 3.10: Co-expression of chaperone GroEL/S with MtbPDF. Lane 1: Soluble fractions from GroEL/S co-expression showing over expressed GroE (60 kDa) and expression on MtbPDF (29kDa); Lane 2: Protein ladder; Lane 3: Ni-affinity purified MtbPDF complexed with GroEL; Lane 4: 80 % ammonium sulfate precipitated fraction of purified MtbPDF.

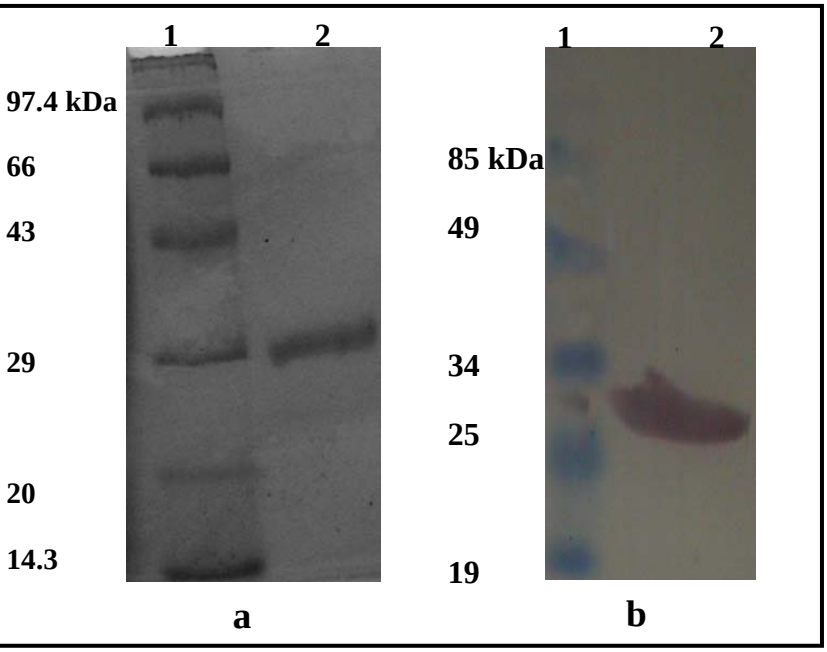

Fig 3.11: Purification of refolded MtbPDF and Western Blotting. (a) Purified MtbPDF; Lane 1: Protein ladder; Lane 2: Refolded and purified MtbPDF; **(b)** Western blotting; Lane 1: Pre-stained protein marker; Lane 2: MtbPDF detected on Western blot.

3.3.4 Biochemical characterization of purified MtbPDF

Deformylase activity of both the refolded-purified MtbPDF and MtbPDF purified from soluble fraction were compared using *N*-f-MAS as the substrate and the former was found to be highly active (Specific activity: 1500 ± 189) compared to the later (Specific activity: 300 ± 47) (**Fig 3.12**). The ammonium sulfate precipitation step was found to reduce the deformylase activity of the soluble MtbPDF, which might be due to oxidation of Fe^{2+} in presence of atmospheric oxygen (Rajagopalan and Pei, 1998). This association between MtbPDF and GroEL could not be separated through size exclusion chromatography (Nguyen et al., 2007). So for all further biochemical studies the refolded-purified MtbPDF was used.

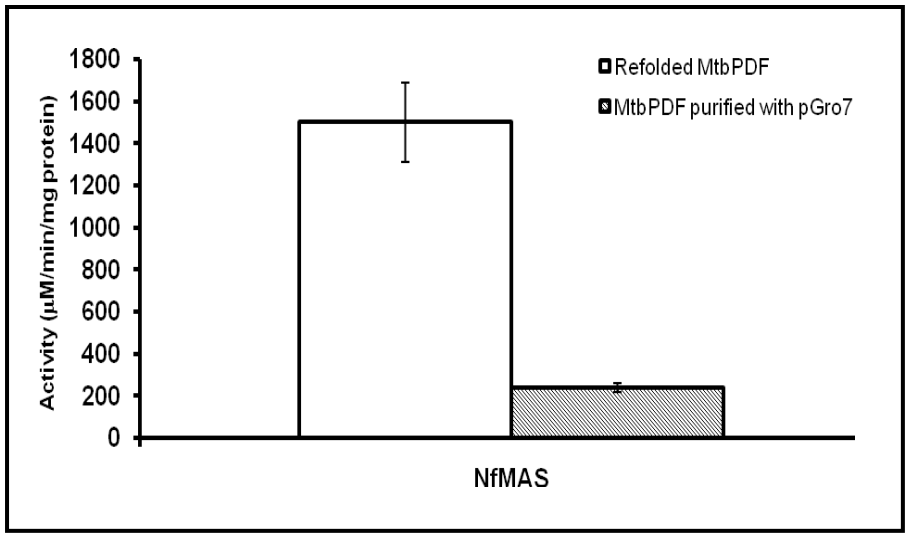

Fig 3.12: Comparison of deformylase activity of refolded MtbPDF and MtbPDF purified with GroEL from soluble fraction

3.3.4.1 Substrate specificity

Substrate specificity of purified MtbPDF with the tested substrates was in the order *N*-f -MAS > *N*-f- MLP > *N*-f-M (**Fig 3.13**). *N*-f -MAS was deformylated almost four and six times faster than the later two respectively. Studies on PDF from *E. coli*, *Helicobacter pylori* and *Leptospira interrogans* and previous studies on MtbPDF reported *N*-f-MAS as the best substrate for PDF activity (Rajagopalan et al., 1997; Han et al., 2004; Li et al., 2002; Saxena and Chakraborti 2005a). This shows that the peptide binding pocket of bacterial PDFs have limited space in the substrate binding pockets at S2' and S3' positions to accommodate residues with small side chains like alanine and serine. All further deformylase assays were carried out using *N*-f-MAS as the substrate, unless mentioned otherwise.

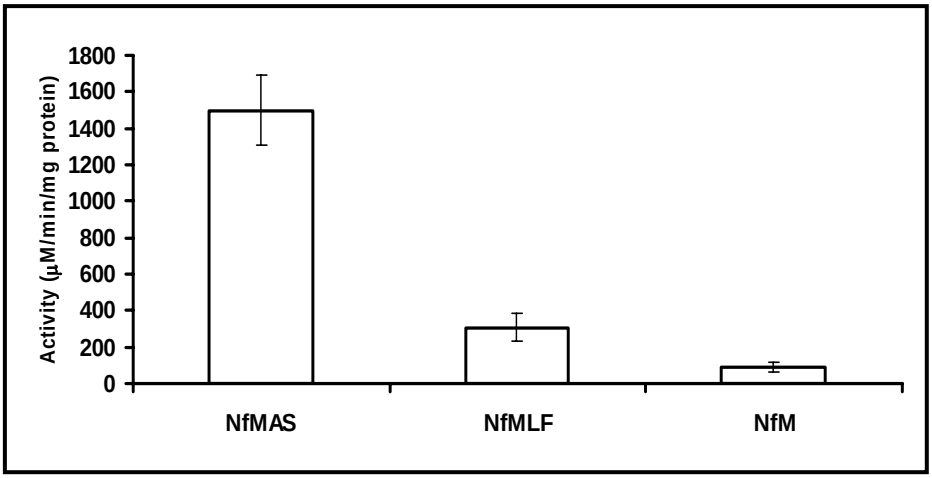

Fig 3.13: Substrate specificity of MtbPDF. NfMA: *N*-for-Met-Ala-Ser; NfMLP: *N*-for-Met-Leu-Phe; NfM: N-for-Met. Substrates were used at 5 mM concentration.

3.3.4.2 Temperature and pH optimum

The optimum temperature and pH for deformylase activity of MtbPDF was 20–30 ^{o}C and pH 7.4 (**Fig 3.14a** and **3.14b**). There was no detectable deformylase activity beyond 65 ^{o}C. There was also very low enzyme activities detected at acidic and basic range of pH. The temperature optimum for MtbPDF activity was very low compared to all the previous PDFs studied to date, which had the optimum temperature for deformylase activity between 37-60 ^{o}C (Rajagopalan et al., 1997; Li et al., 2002; Han et al., 2004; Bracchi-Ricard et al., 2001). Similar results were reported on MtbPDF by Saxena and Chakraborti (2005a). The reported ranges of pH optima for deformylase activity of *E. coli* and *Plasmodium falciparum* PDFs were 5.5–7.0, with only a slight decrease in activity in the basic range up to pH 9.0 (Rajagopalan et al., 1997a; Bracchi-Ricard et al., 2001; Meinnel and Blanquet, 1995; Li et al., 2002). Only a single ionization event (pKa~5.2) has been assigned to the deprotonation of the metal-bound water/glutamate network in these PDFs (Bracchi-Ricard et al., 2001), which led to a flat pH profile in the basic range (Rajagopalan et al., 1997a; Bracchi-Ricard et

al, 2001). For all further deformylase assays with MtbPDF these conditions were maintained.

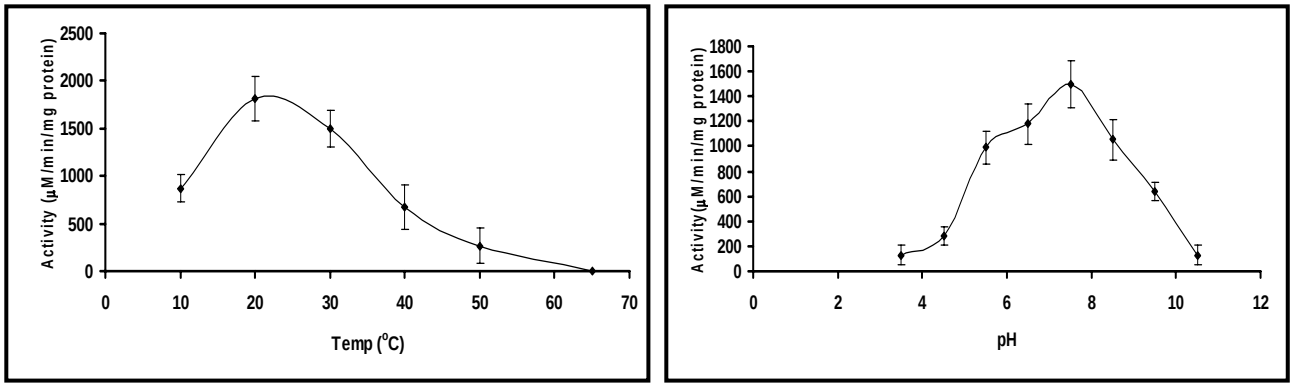

a **b**

Fig 3.14: Optimization of Temperature (a) and pH (b) for MtbPDF activity performed against 5 mM *N*-for-MAS

3.3.4.3 Importance of BSA and catalase in dilution buffer

Atmospheric oxidation of Fe^{2+} to Fe^{3+} in the metal core and /or oxidation of the S^{γ} in metal-coordinating cystein are the reasons reported for the high *in vitro* instability of PDF enzyme (Rajagopalan and Pei, 1998; Kreusch et al., 2003). Inclusion of oxygen scavenging enzymes (e.g. catalase) and some carrier proteins (e.g. BSA) have been reported to prevent atmospheric oxidation of PDFs (Rajagopalan and Pei, 1998; Groche et al., 1998). The absence of BSA in the dilution buffer affected the deformylase activity of MtbPDF more profoundly than the absence of catalase (**Fig 3.15**). In absence of both BSA and catalase, there was nearly 40% activity compared to the activity in their presence. These points to the fact that MtbPDF is not so highly sensitive to the atmospheric oxidation when compared to the PDF from *E. coli*, which requires the presence of catalase to be active *in vitro* (Rajagopalan and Pei, 1998). Absence of catalase was found not to affect the deformylase

activity of PDF II of *Staphylococcus aureus* (Baldwin et al., 2002). Unlike *E. coli* PDF, where BSA did not have an effect as a carrier protein, MtbPDF requires the presence of BSA during dilution to be fully active. From these results it could be concluded that MtbPDF is sensitive to atmospheric oxidation, even though far less extent compared to *E. coli* PDF. It indicate that Fe^{2+} as the possible co-factor since the Zn^{2+} containing PDFs are not sensitive to atmospheric oxidation, even though less active than Fe^{2+} forms (Rajagopalan and Pei, 1998). Similar kinds of results were reported by studies of Saxena and Chakraborti (2005a) on MtbPDF, even though there are variations in degree of effects. To restore complete activity, MtbPDF was always diluted in presence of 0.2 mg/ml BSA and 10 µg / ml catalase for all further studies unless mentioned other wise.

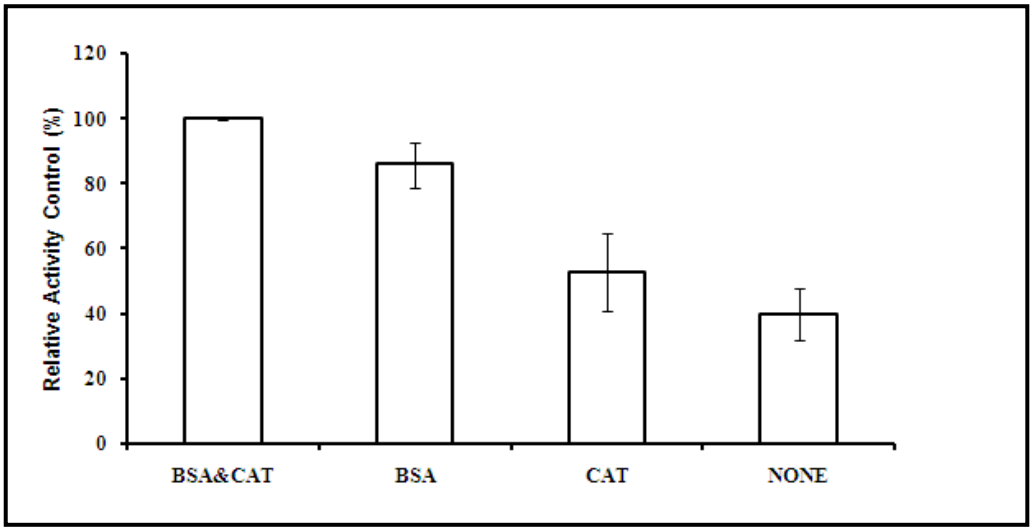

Fig 3.15: Effect of inclusion of BSA (0.2 mg/ml) and catalase (10 µg /ml) during dilution of MtbPDF. The results are represented as % relative activity of assay with MtbPDF having BSA and catalase.

3.3.4.4 Effect of metal ions on MtbPDF activity

Out of the metal ions studied, Cu^{2+} completely abrogated MtbPDF activity, Fe^{3+} strongly reduced the activity and Ni^{2+} was slightly inhibitory. Ca^{2+}, Mg^{2+} and Zn^{2+} had very slight positive effects at 1 mM concentration. Both the monovalent cations tested showed slight enhancement of MtbPDF activity (**Fig 3.16**). Cu^{2+} was reported to be inhibitory in contemporary studies on MtbPDF by Teo et al., (2006). But the same study reports Zn^{2+} and Ni^{2+} to be partially inhibitory. Both the previous studies on MtbPDF reported inhibitory effects of K^+ and Na^+ on deformylase activity of MtbPDF at concentrations beyond the one in present study (Saxena and Chakraborti, 2005a; Teo et al., 2006). But, K^+ has been reported to enhance the deformylase activity of *E. coli* PDF up to 1.5 M concentrations (Meinnel and Blanquet, 1995). Inhibitory effect of Fe^{3+} was very interesting to note and this could be due to oxidation of S^{γ} in the metal binding cystein in a fraction of enzyme by oxidized form of Fe, as postulated by Kreusch et al (2003). There are many reports on substitutions of metal cofactors in PDFs by addition of different divalent metal ions during expression and purification. Metal substituted forms of PDFs like Ni^{2+} and Co^{2+} forms have been reported with higher stability and comparable activities with the native Fe^{2+} forms. Zn^{2+} forms have been generally reported to be less active, but stable (Ragusa et al., 1998). There are also eubacteria which generally grow in iron deficient situations, like *Borrelia burgdorferi* and *Lactobacillus plantarum*, which has PDFs with native metal ion co-factors as Zn^{2+} (Nguyen et al., 2007). The metal co-factor in native MtbPDF is still unknown and is difficult to work with. Considering all the above results, there were no significant enhancing effects on the recombinant holo-MtbPDF enzyme by any of the tested cations at the studied

concentration. Thus no additional metal ions were used in any further assays and no attempts were made to exchange the native metal ion in recombinant MtbPDF.

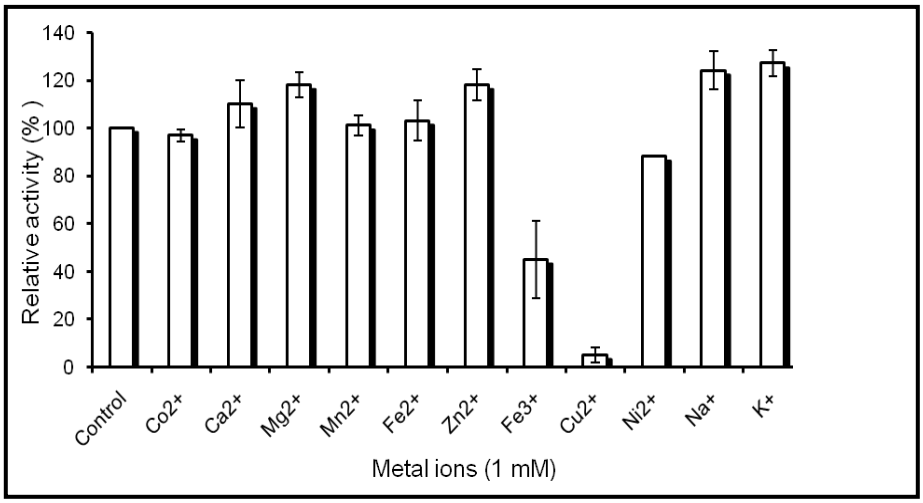

Fig 3.16: Effect of metal ions on the deformylase activities of MtbPDF. Results are represented as % relative activities of reaction with no metal addition (control).

3.3.4.5 Kinetic properties of MtbPDF

MtbPDF followed typical Michealis Menten kinetics for catalysis against *N*-f-MAS (**Fig 3.17**). The V_{max} and K_m values as derived from the MM plot were 15.8 ± 1.2 μM / min and 4.3 ± 0.9 mM. The K_{cat} value, as calculated from software from the V_{max} value and total enzyme concentration (MtbPDF molecular weight of 22.5 kDa), was 3.6 ± 0.6 s^{-1}. The catalytic efficiency value (K_{cat}/K_m) was 842 ± 9 M^{-1} s^{-1}. The K_m value and K_{cat} value in previous studies on MtbPDF were 4.1 ± 0.2 mM and 5.0 ± 0.3 s^{-1} (Saxena and Chakraborti, 2005a). The K_{cat}/K_m was reported as 1220 ± 6.0 M^{-1} s^{-1}. Thus, our catalytic efficiency value was comparatively lower to the previous report which might be due to variations in the refolding protocols and concentrations of carrier proteins in the assay buffer. The catalytic

efficiency of MtbPDF was very low compared to Ni^{2+} or Fe^{2+} form of *E. coli* PDF (Ragusa et al., 1998; Rajagopalan et al., 1997a), but falls close to the range of Zn-PDF of *L. ineterrogans* (Li et al., 2002) or Co-PDF of *H. pylori* (Han et al., 2004).

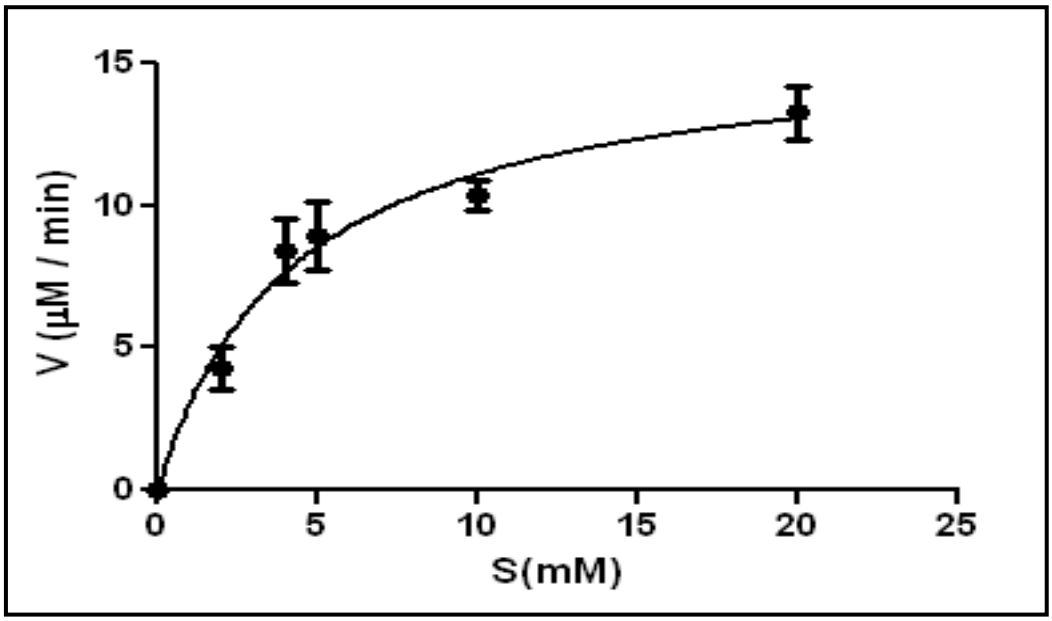

Fig 3.17: Michealis -Menten plot for enzyme kinetics of MtbPDF against substrate *N*-f-MAS. 73.3 nM purified MtbPDF was used. MM Plot was made with Graph pad prism software.

3.3.4.6 Thermo-stability of MtbPDF

MtbPDF was stable at 30 ^{o}C with a half-life ($t_{1/2}$) close to 4.5 h. At 40 ^{o}C $t_{1/2}$ was reduced to 90 min and at 50 ^{o}C to 40 min (**Fig 3.18**). The temperature stability of MtbPDF at 30 ^{o}C in our studies was very similar to that reported by Saxena and Chakraborti (2005a), indicating the consistency in enzyme preparations. *E. coli* Fe-PDF showed a half-life close to 15 min in absence of catalase at 23 ^{o}C, when kept at high enzyme concentration (Rajagopalan and Pei, 1998). But in case of Zn-PDF of *L. ineterrogans*, there was high

thermo-stability ranging up to a half-life of 17 h (Li et al., 2002). In our case purified MtbPDF had a shelf-life of 2 weeks, when stored at 4 ^{o}C as 1 mg / ml proteins (data not shown). Thus, we consider MtbPDF to be a moderately thermo-stable protein.

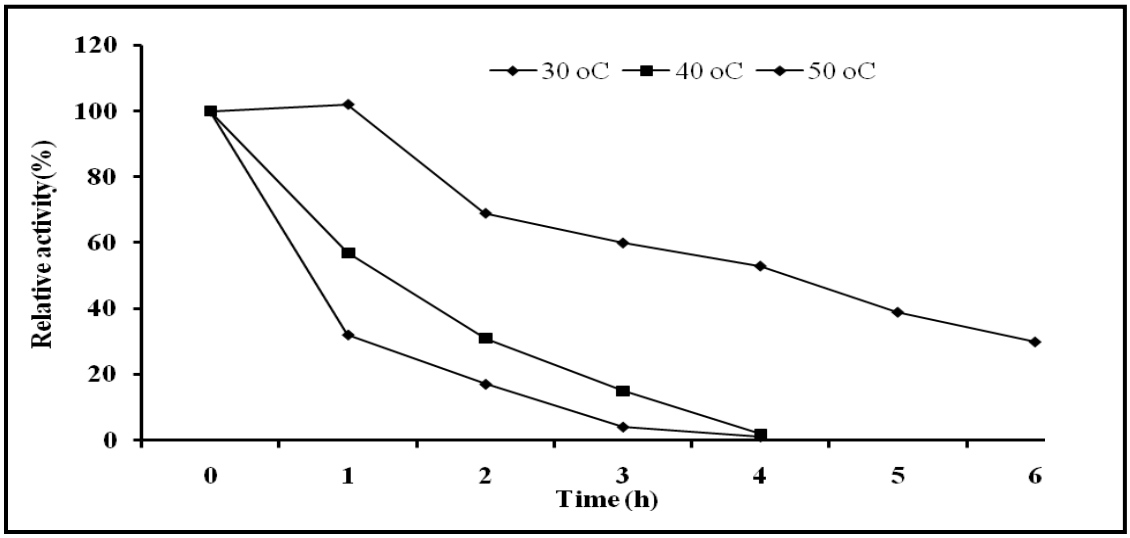

Fig 3.18: Thermo-stability of MtbPDF. 1μg /ml of MtbPDF was incubated at the respective temperatures and activity assay was performed at 30 ^{o}C. The activity at time zero at each indicated temperature was taken as control to calculate the percentage relative activities.

3.3.4.7 Quantification of Fe content in MtbPDF

Based on the loss of activity in absence of catalase, it was presumed that the metal co-factor in MtbPDF is Fe. The Fe content quantified by AAS was 0.72 ± 0.21 g-atoms of Fe/g of MtbPDF. From this value, it was assumed a 1:1 ratio of Fe to polypeptide in MtbPDF (considering MtbPDF to be a monomeric protein). The slight variation in Fe content could be that while refolding, all the polypeptides might not have refolded to accomodate a metal ion or that there were traces of Zn present in rest of the form as reported in case of recombinant *E. coli* PDF (Rajagopalan et al., 1997b). Fe was detected as the major metal ion cofactor in MtbPDF by previous workers too (Saxena and Chakraborti, 2005a).

Metal ion determination from different bacterial PDFs and crystal structure determinations of many PDFs have confirmed the presence of a mononuclear metal centre having a single metal ion bound in the metal binding pocket (Chan et al., 1997; Ragusa et al., 1998; Nguyen et al., 2007).

3.3.4.8 Stability of MtbPDF towards H_2O_2

Confirming MtbPDF to be a Fe-containing metallo-protease when expressed in *E. coli*, its stability towards oxidizing agents like H_2O_2 was checked to verify the extent to which it can prevent oxidation of Fe^{2+} co-factor to Fe^{3+} and maintain its activity. MtbPDF was found to retain 30% of its activity at 500 mM H_2O_2 after 30 min incubation (**Fig 3.19**). The absence of catalase has caused a slight decrease of activity in the control experiment where there was no H_2O_2. The present results vary with the previous work on H_2O_2 stability of MtbPDF where incubation with 500 mM H_2O_2 for 2 h resulted in only 40% decrease in activity (Saxena and Chakraborti, 2005a; 2005b). Since the results on thermo-stability and Fe content of MtbPDF were highly similar to the previous study, we consider the obtained results on H_2O_2 stability as valid. *E. coli* Fe-PDF was reported to be highly sensitive to H_2O_2 as concentrations less than 100 μM was enough to completely abrogate its activity (Rajagopalan et al., 1997b). H_2O_2 stability has been reported to all other metallic forms of PDFs except for Fe-PDF (Nguyen et al., 2007). Thus our results are good enough to place MtbPDF as Fe containing PDF showing considerable resistance to oxidative stress. Presuming that MtbPDF uses Fe^{2+} as its metal cofactor in native form *in vivo*, this resistance towards oxidative stress could be considered as an intrinsic structural property of the enzyme which would help *M. tuberculosis* to survive under the oxidative environment in

macrophages. Saxena and Chakraborti (2005b) have identified regions in MtbPDF structure, having three consecutive arginine residues in it, as possible structural basis for the observed resistance to H_2O_2.

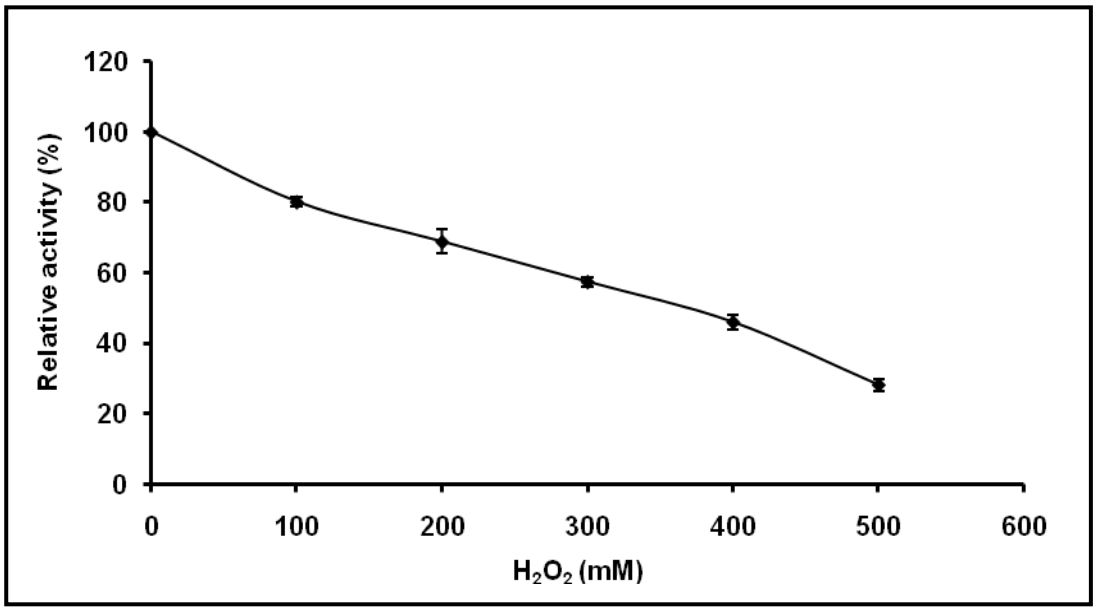

Fig 3.19: Stability of MtbPDF towards H_2O_2. 100 ng MtbPDF in absence of catalase was used for 30 min incubation with indicated H_2O_2 concentrations. The residual activities are reported as % relative activities of control reaction in absence of H_2O_2.

3.3.4.9 Metal chelators on MtbPDF activity

Among the two metal ion chelators tested, 1, 10 phenathroline inhibited the activity of MtbPDF, in a concentration dependent manner, almost completely at 10 mM concentration. But EDTA at the same concentration produced only 30% inhibition of MtbPDF (**Fig 3.20**). In case of *E. coli* PDF, incubating with 250 mM EDTA did not affect the activity but, incubation with 5 mM 1, 10, phenathroline completely inactivated the enzyme. 1, 10, phenanthroline was assumed to form complexes with the metal ion and the catalytic residues close to it with in the peptide binding pocket of PDFs. EDTA may not be

structurally fit enough to reach the metal ion deeply situated in the peptide binding pocket (Meinnel and Blanquet, 1995). In the above stated study metal ion was not removed out from PDF metal binding pocket by 1, 10, phenanthroline, proving that it is in a very tightly bound form. In case of MtbPDF too it is assumed that similar mechanism would have taken place during inactivation in presence of 1, 10, phenathroline, even though the metal contents after treatments were not quantified.

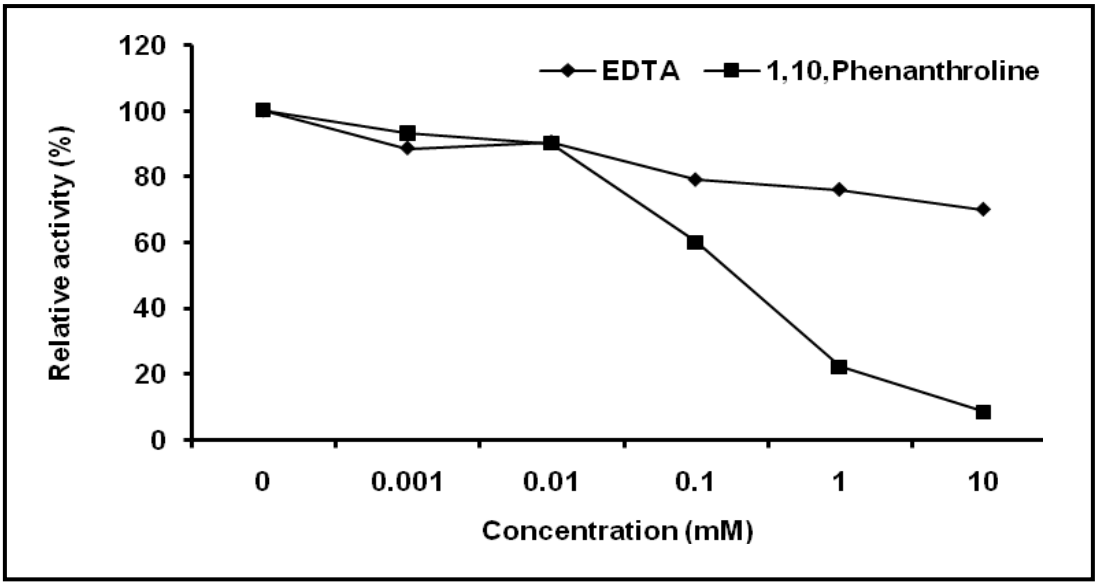

Fig 3.20: Effect of metal chelators on MtbPDF activity. The indicated concentrations of chelators were added in the assay mixture containing 100 ng MtbPDF and resulting activities are represented as % relative activity to the control reaction without chelators in it.

3.3.4.10 Metallo-protease inhibitors on MtbPDF

Among the three metallo-protease inhibitors studied on MtbPDF, only the competitive inhibitor of PDF, actinonin, showed remarkable inhibition of MtbPDF activity with an IC_{50} value of 120 nM. The other two inhibitors showed no significant inhibition at the concentrations studied (**Fig 3.21**). Actinonin, a hydroxamic acid pseudo-peptide, is a

competitive, irreversible inhibitor of PDF with its hydroxamic acid metal chelating side chains binding to the water bound catalytic metal ion in the peptide binding pockets of all PDFs (Van Aller et al., 2005). Actinonin was found to bind into all the different kinds of eukaryotic and prokaryotic PDFs, proving the conserved nature of PDF binding pocket across the living world (Guilloteau et al, 2002). Similar inhibition of MtbPDF was reported by the previous workers where in they calculated the *Ki* value of actinonin for MtbPDF as 19.7 nM (Saxena and Chakraborti, 2005a). Even with repeated trials we were unsuccessful in determining the kinetics of actinonin inhibition.

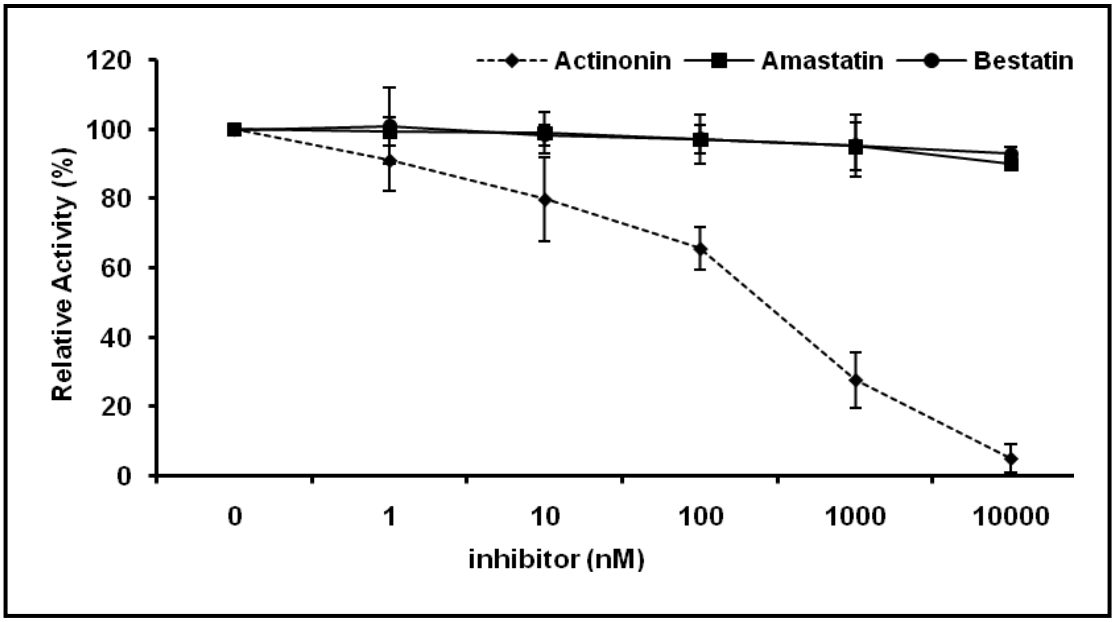

Fig 3.21: Inhibition of MtbPDF by metallo-protease inhibitors. Inhibition was studied on 100ng MtbPDF in presence of 5 mM *N*-f-MAS incubated with the indicated concentration. Uninhibited reaction control was used to calculate the % relative activity at different concentrations of inhibitors.

Bestatin, amastatin and actinonin were found to inhibit a putative methionine aminopeptidases purified from cell lysate of *Mycobacterium smegmatis* (Narayanan et al.,

2008). The site of action of both peptide deformylase and methionine aminopeptidases is proved to be near to the large subunit of ribosomes close to the exit tunnel (Addlagatta et al., 2005; Bingel-Erlenmeyer et al., 2008).Thus, we looked into the inhibition profile of bestatin and amastatin also with MtbPDF, but found them ineffective in inhibiting MtbPDF.

3.3.4.11 MIC of actinonin on E. coli cells over-expressing MtbPDF

Actinonin was proved to inhibit recombinant MtbPDF by *in vitro* enzyme assay. Antibacterial effects of actinonin was tested *in vitro* on *E. coli* BL21 (DE3) cells expressing MtbPDF, in order to see whether target over expression affects the antibacterial effects of actinonin. The MIC_{90} values of actinonin were found to increase more than 10 folds up on over expression of MtbPDF in BL21 (DE3) cells harboring pET28a: *def* plasmid (**Table 3.3**). The *E. coli* host strain was inhibited beyond 32 μg /ml actinonin, presumably due to inhibition of all active PDFs required for vital deformylation in the cell. This concentration of actinonin was not enough to inhibit the strain of *E. coli* over expressing MtbPDF, which proves that MtbPDF could very well deformylate the vital proteins of *E. coli* in cytoplasm. Moreover, there was no such increase in MIC_{90} in strains harboring pET28a alone, which confirms PDF as the target for actinonin. In control experiments in presence of ampicillin, there was a decrease in the survival rate of *E. coli* cells upon over expression of MtbPDF protein, presumably due to weakened cell wall in presence of over expressed foreign proteins or IPTG. MIC for actinonin and its derivative BB-3497 was determined in similar way by over expressing *E. coli* PDF and was reported to be beyond >800 (Clements et al., 2001). Recently, Sharma et al., (2009) have reported the MIC value of actinonin against the *in vitro* culture of *M. tuberculosis* H37Rv to be 56 μg /ml.

The results from our studies prove this method of determining MIC of PDF inhibitors to be reliable and thus, it could be useful in confirming the target specificity of novel PDF inhibitors. The effect of target over expression on MIC of actinonin against MtbPDF was further confirmed from the results obtained from the well diffusion assay on LB agar plates. There was a clear reduction in the zone of inhibition of actinonin on *E. coli* BL21 (DE3) (pET28a: *def)* cells grown on LB-Kan-IPTG plates compared to the *E. coli* BL21 (DE3) (pET28a) cells (**Fig 3.22**). This clearly confirmed PDF as the target for the action of actinonin. Three of the bioactive fractions (29b, A11 and A12) showing antibacterial effects on *E. coli* and moderate *in vitro* enzyme inhibition of MtbPDF were also included in the study to confirm their site of action. The results confirmed that the antibacterial activity shown by bioactive fractions 29b, A11 and A12, may not be due to PDF inhibition since they showed no significant variations in the zone of inhibition of the above stated strains over expressing MtbPDF compared to the control strains.

Table 3.3 MIC_{90} of actinonin on *E.coli* strains over expressing MtbPDF

***E.coli* Strain & Conditions**	**MIC_{90} of Actinonin (μg /ml)**	**MIC_{90} of Ampicillin (μg /ml)**
BL21(DE3) (Host strain)	**>31.25**	**> 8**
BL21 (DE3) (pET28a)	**>31.25**	**> 4**
BL21 (DE3) (pET28a) + IPTG	**>31.25**	**>2**
BL21 (DE3) (pET28a:*def*)	**>125**	**> 2**
BL21 (DE3) (pET28a:*def*)+ IPTG	**> 500**	**> 1**

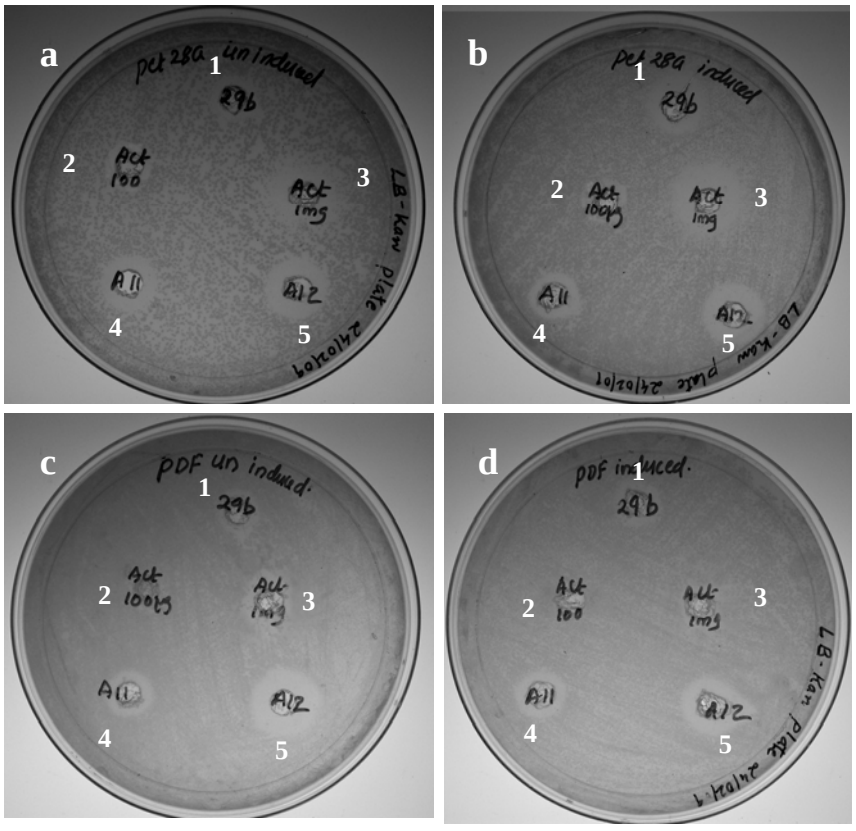

Fig 3.22: Demonstration of the effect of MtbPDF over expression on antibacterial activity of actinonin. (a) BL21 (DE3) cells with pET28a plasmid on LB-Kan plate; **(b)** BL21 (DE3) cells with pET28a plasmid on LB-Kan-IPTG plate; **(c)** BL21 (DE3) cells with pET28a: *def* plasmid on LB-Kan plate; **(d)** BL21 (DE3) cells with pET28a: *def* plasmid on LB-Kan-IPTG plate. IPTG was added at 0.1 mM concentration. Inhibitors were added at the indicated concentrations into respective wells and cells were grown over night at 37 ^{o}C. **(1)** 50 µl of crude 29b; **(2)** 50 µl of 100 µg / ml actinonin **(3)** 50 µl of 500 µg / ml actinonin; **(4)** 50 µl of crude A11; **(5)** 50 µl of crude A12.

3.3.4.12 CD spectrum of MtbPDF

The far-UV-CD spectrum of purified MtbPDF had two typical negative minima at 208 nm and 222 nm with a crossover point at 198 nm (**Fig 3.23**). This indicates predominant helical structures. But the comparatively low mean residue ellipticity (θ) value at 222 nm (~ -7) indicates the presence of sheets and coils along with these helical structures. The CD spectrum of MtbPDF matches very well with the previously reported CD data on MtbPDF (Saxena et al., 2008), which confirms the proper renaturation of refolded MtbPDF from the inclusion bodies. From this CD data, K2D2 secondary structure prediction software predicted 30% of helical structures, 14% of beta sheets and rest 56% of 3_{10} helix and random coils in MtbPDF structure. The recently published X-ray crystal structure of MtbPDF indicated three α-helices, seven β-sheets, and three 3_{10} helices in the 3D protein structure (Pichota et al., 2008). The over all core structure of MtbPDF was very similar to *E. coli*, except for subtle variation introduced by the amino acid sequence variations between the two.

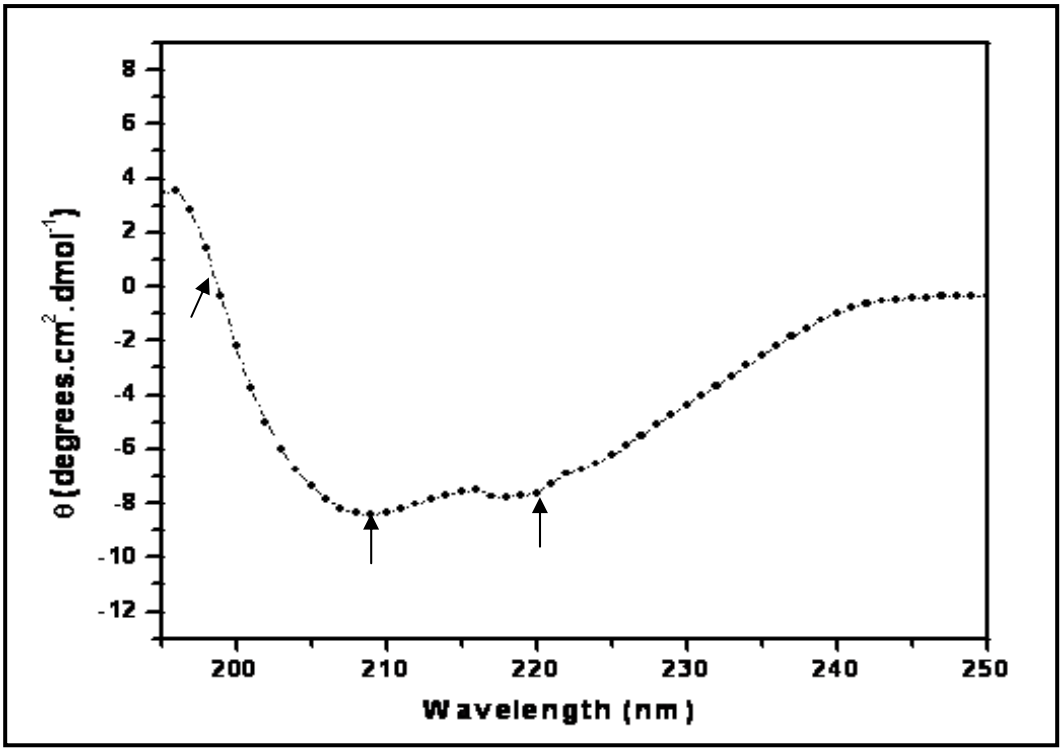

Fig 3.23: CD spectrum of purified MtbPDF at 0.1 mg / ml of protein concentration. The negative minima at 222 nm, 208 nm and 198 nm are indicated by arrow heads.

3.4 CONCLUSIONS

Studies on recombinant MtbPDF showed that irrespective of the varying expression conditions, majority of the protein was over expressed as inclusion bodies. It proved the essentiality to refold the recombinant proteins expressed in inclusion bodies for making it as active proteins. Successful refolding of MtbPDF by simple dilution and dialyses, indicated that the proteins are in their near- native structure in the inclusion bodies. The experimental detection of metal ion, Fe in the refolded-purified protein very well supported the strategy used for refolding to obtain active MtbPDF. Interestingly, the catalytic efficiency of MtbPDF was below to other bacterial PDFs and the physical properties of the enzyme such

as temperature and pH optimum showed significant variations from all the reported PDFs. From the biochemical characterizations of MtbPDF, it could be classified as a Fe-containing PDF having moderate thermo-stability with significant stability towards oxidative-stress. Inhibition studies on *E. coli* culture expressing MtbPDF proved its ability to moderately compensate the *E. coli* enzyme. Finally, the inhibitors such as actinonin and 1, 10, phenanthroline can be utilized as possible starting points for designing mechanism-based MtbPDF inhibitors.

CHAPTER 4

Design, Construction and Characterization of Relevant Site-Directed Mutants of Peptide deformylase of *M. tuberculosis* H37Rv

CHAPTER 4

Design, Construction and Characterization of Relevant Site-Directed Mutants of Peptide deformylase of *M. tuberculosis* H37Rv

4.1 Introduction

Amino acid sequences in proteins determine their structure and function with high redundancy. Proteins evolve by rare mutations that provide functional innovations without affecting the pre-existing global structure and activity (Bowie *et al.*, 1990). As beneficial mutations are rare, the ability of an enzyme to accumulate sequence changes and maintain the required activity for better survival of the host organism is an important aspect of its evolvability (Woycechowsky et al., 2008). The best way to understand the effects of mutations on protein structure and function is to perform site-directed mutagenesis. Site-directed mutagenesis is a molecular biology technique in which a mutation is created at a defined site in a DNA molecule (Hutschison et al., 1978). This technique has proved to be extremely useful in mapping the active sites of proteins that are not yet amenable to direct biophysical characterization. The construction of modified enzymes with engineered amino acid substitutions allows an assessment of the role of any particular amino acid in the catalytic activity or stability and an understanding of the relationships between the protein structure and its function or stability (Fersht and Serrano, 1993; Gerlt., 1994).

PDF is widely accepted as a novel class of iron metalloenzyme that is related in structure to the metallo-proteinase superfamily. While other regions of its sequence may vary, all PDFs share three highly conserved motifs GΦGΦAAxQ, EGCLS, and HEΦDH (where Φ encodes any hydrophobic amino acid and x is any amino acid). These motifs form

the three sides of the active site pocket and metal-binding pocket, a common architecture evidently conserved among all PDFs (Chan et al., 1997; Becker et al., 1998a; Becker et al., 1998b). In each case, structural conservation was apparent through its metal ion tetrahedrally coordinated by two histidine residues of the conserved HEΦDH motif, one cysteine residue from EGCΦS motif, and a water molecule.

The first report on structure-function relationship of PDF was from Meinnel et al., (1996), wherein using deletion analysis they reported the N-terminal regions of *E. coli* PDFs to be indispensable and C-terminal domain as disordered and dispensable for enzyme activity *in vitro*. Recently, the *in vivo* role of C-terminal domain extension, which form a helix in case of type I PDFs, in aligning PDFs on to ribosome have been elucidated by its deletion and ribosome-binding studies (Bingel-Erlenmeyer et al., 2008).

Based on the multiple sequence alignment of nine PDF sequences identified then with *E. coli* PDF, Meinnel et al., (1997) performed extensive site-substitution mutagenesis on *E.coli* PDF sequence to define the crucial role of each of the residues in the three signature sequences in deformylase activity and metal ion binding. Apart from the residues in the signature sequences, the conservation of hydrophobic characters of many residues forming the hydrophobic core next to the catalytic crevice of PDFs were also confirmed in the study by site-substitution mutagenesis of these residues (Meinnel et al., 1997). Site-substitution mutations of metal binding cystein residue in case of *L. inetrrogans* PDF proved the essentiality of these residues for enzyme activity (Li et al., 2002).

X-ray crystal structure analyses of PDF structures, in presence or absence of ligands bound to them, have led to the classifications of different PDFs into two structural classes. Based on structural and sequence variations, bacterial PDFs have been classified as type I

(gram negative type) and type II (gram positive type), where in the later type have two insertion sequences around helix α1 and highly hydrophobic C-terminal domain forming a long loop and a short β-strand (Guilloteau et al., 2002). Identification of eukaryotic PDFs and their structural characterizations have led to yet another classification of PDFs (Giglione et al., 2000b; Giglione and Meinnel, 2001). Since these two kinds of PDFs have no insertion sequences specific to the type II PDFs, they are classified as type I PDFs (Serero et al., 2001; Fieulaine et al., 2005). The human mitochondrial PDF, which is a type IA PDF, has been extensively studied to reveal its activity and stability (Serero et al., 2003; Nguyen et al., 2003). Owing to the conserved architecture of core regions in PDFs, actinonin was found to be an inhibitor of human mitochondrial PDF too (Lee et al., 2004) which caused a lot of concerns regarding toxicity of PDF inhibitors on human cells. But mitochondrial PDFs were found to be far less active compared to the bacterial counter parts (Serero et al., 2003; Nguyen et al., 2003).

Systematic comparison of amino acid sequences of human mitochondrial PDF and other PDFs revealed 3 important substitutions in key residues involved in catalytic mechanisms: (1) the first Gly of motif I is replaced by a Cys; (2) the first Ala of motif I is replaced by a Ser; (3) the conserved Leu of motif II is replaced by a Glu. Site-substitution mutagenesis of these residues in human mitochondrial PDF to the corresponding conserved ones in bacterial PDFs have increased activity of former by many folds (Nguyen et al., 2003). The physiological role of human mitochondrial PDF, other than deformylaion, is still not clear (Nguyen et al., 2003; Lee et al., 2004). The crystal structure of human mitochondrial PDF bound to actinonin suggested a conservation of PDF-actinonin interactions across all PDFs (Escobar-Alvarez et al., 2009). Very recently, systematic studies

on human mitochondrial PDFs concluded that inhibition of mitochondrial PDF with structurally unrelated PDF inhibitors disrupts mitochondrial function (Escobar-Alvarez et al., 2010). These new findings have complicated the antibacterial drug discovery process based on PDF. Due to these reasons, it is important to explore variations in sequences and structure in bacterial and parasitic PDFs compared to human mitochondrial PDF.

Apart from the conserved metal binding ligands, the C-terminal extension of MtbPDF was reported to be indispensable for *in vitro* activity and stability of the enzyme (Saxena and Chakraborti, 2005a). In their following publication (Saxena and Chakraborti, 2005b), the essentiality of an insertion sequence between motif I and II signature sequences of MtbPDF in *in vitro* enzyme activity and stability was reported by its deletion mutagenesis. The role of three consecutive arginine residues in the above mentioned insertion sequences in conferring resistance of MtbPDF towards H_2O_2 stress was also reported (Saxena et al., 2008) based on substitution/deletion mutagenesis and molecular dynamic simulations.

In this chapter, apart from characterizing substitution mutants of conserved residues which were not previously characterized in MtbPDF, efforts have been made to characterize residues in the conserved regions which are different from human PDFs. Special importance has been given in characterizing the role of a specific glycine in motif III of MtbPDF by substitution mutagenesis and molecular dynamic simulations.

4.2 Materials and Methods

4.2.1 Multiple sequence alignment of MtbPDF sequences

In order to compare the protein sequences of MtbPDF with other type I and type II PDFs and human PDF, multiple sequence alignments of MtbPDF sequences with these PDF

sequences were performed using Clustal W program (Thompson et al., 1997). *E.coli* PDF represents type I and *Bacillus stearothermophilus* PDF represent type II PDF. Human mitochondrial PDF represents the type IA eukaryotic PDF. Similarly PDF sequences from pathogenic (*M. bovis*, *M. leprae* and *M. avium*) and non-pathogenic (*M. smegmatis*, *M. vanbaalenii* and *M .gilvum*) Mycobacterium species were aligned with *E. coli* in order to study any sequence variations in PDFs associated with pathogenesis. Apart from that, orthologus PDF sequences of species belonging to different families (Nocardiaceae, Tsukamurellacea, Gordoniacea and Mycobacteriaceae) under suborder Corynebacterianeae were also aligned to study the evolution of specific sequence variations of MtbPDF. Amino acid sequences of PDFs were retrieved from the annotated genome data base Kyoto Encyclopedia for Genes and Genomes (KEGG) (*www.genome.jp/kegg*). The alignment file generated was visualized and edited using the Genedoc software (Nicholas et al., 1997).

4.2.2 Design and construction of site-directed mutants

Based on multiple sequence alignment of MtbPDFs with other bacterial and human PDF and based on the structural data available from different bacterial and eukaryotic PDFs, five sites were identified from the three conserved motifs of MtbPDFs to construct seven site-substitution mutants (G49C, G49P, E104A, G105P, L107E, G151D and G151A). Mutagenic primers were designed by incorporating the corresponding mutations in them and by using the primer designing program from Stratagene (QuickChange® Primer design software) (**Table 4.1**). The primers were custom synthesised from IDT, USA and substitution mutagenesis was performed on pET28a::*def* plasmid according to the manufacturer's protocol (2.3.4). Individual mutations were confirmed by DNA sequencing of both the strands of mutated plasmids using T_7 primers (Scigenomics, India). The

confirmed mutated plasmids were transformed into *E. coli* BL21 (DE3) cells for expression of mutant recombinant proteins of MtbPDF.

Table 4.1 List of mutagenic primers used to construct MtbPDF mutants

Mutagenic Primer	Sequence (5' to 3')
G151A FP	GCAGCACGAAACCG**CGC**ACCTTGATGGAT
G151A RP	ATCCATCAAGGT**GCG**CGGTTTCGTGCTGC
G151DFP	GCTGCAGCACGAAACC**GAT**CACCTTGATGGATTCCT
G151D RP	AGGAATCCATCAAGGTG**ATC**GGTTTCGTGCTGCAGC
G49C FP	GGACGCCGCCAAC**TGC**GTCGGCCTGGCTG
G49C RP	CAGCCAGGCCGAC**GCA**GTTGGCGGCGTCC
G49P FP	GACGCCGCCAAC**CCA**GTCGGCCTGGC
G49P RP	GCCAGGCCGAC**TGG**GTTGGCGGCGTC
L107E FP	CGACGAAGGCTGT**GAG**TCGGTTCCCGGC
L107E RP	GCCGGGAACCGA**CTC**ACAGCCTTCGTCG
E104A FP	GACACCGACGAC**GCA**GGCTGTCTGTCG
E104A RP	CGACAGACAGCC**TGC**GTCGTCGGTGTC
G105P FP	GACACCGACGACGAA**CCC**TGTCTGTCGGTTC
G105P RP	GAACCGACAGACA**GGG**TTCGTCGTCGGTGTC

4.2.3 Over expression and purification of site-directed mutants of MtbPDF

Mutant proteins of MtbPDF were overexpressed essentially in the same as the wild type as described in previous chapter (3.2.5). The mutants were extracted from the insoluble fraction in 3 M urea containing buffer and were refolded by direct dilution and dialysis method. The refolded mutant proteins were purified through Ni-NTA columns using the native purification protocol and were stored at 1mg /ml protein concentration in presence of 0.2 mg /ml BSA and 10 mg /ml catalase at -80 ^{o}C freezer until use. Soluble expressions and purification of mutant proteins in presence of chaperone GroE L / S were performed in the same way as described in 3.2.6.3.

4.2.4 Comparison of biochemical properties of mutant proteins with MtbPDF

Biochemical properties of mutants were compared with the wild type based on their ability to deformylate *N*-formylated di or tri peptides in standard PDF assay (2.3.3.3 and 3.2.8) at different conditions. 83 ng (73.3 nM) of purified proteins were used in all the assays. In all the studies, enzyme activity of wild type MtbPDF was taken as reference to calculate the percentage relative activities of mutant proteins.

4.2.4.1 Deformylase activity of mutant proteins

Deformylase activities of all the seven mutant proteins were compared with wild type enzyme in standard deformylase assay with 5 mM *N*-f-MAS as substrate using 73.3 nM proteins. The results were expressed as μM free amines released / min/ mg protein. The mutants which showed significant activities compared to that of MtbPDF are further studied for other properties.

4.2.4.2 Substrate specificity of G151D and G151A mutants

Substrate specificity of the G151D mutant which showed enhanced deformylase

activity with *N*-f-MAS compared to wild type was studied by performing deformylase assay with other formylated peptides like *N*-f-MLF and *N*-f-M as described in 3.2.9.1. G151A mutant was studied as control for G151D mutation.

4.2.4.3 Enzyme kinetics of active mutants of MtbPDF

The enzyme kinetics of those mutants of MtbPDF which showed significant deformylase activity with *N*-f-MAS (G151D, G151A and G49C) were determined by performing continuous PDF assay at 30 ^{o}C and pH 7.4 with various concentrations of substrate *N*-f-MAS (0-20 mM) and 73.3 nM of mutant proteins. The kinetic parameters of each of these active mutants were determined in the same way as described in 3.2.9.5.

4.2.4.4 Optimum temperature and pH for G151D activity

Temperature and pH optimum for deformylase activity of G151D mutant against *N*-f-MAS was studied by performing deformylase assay at different temperatures and in differ rent pH buffers as described in 3.2.9.2.

4.2.4.5 Effect of catalase and BSA on G151D activity

The effect of catalase as oxygen-scavenging enzyme and BSA as a carrier protein on G151D activity was assessed by including these two proteins in the dilution buffer during dilution of G151D protein from the stock as described earlier in 3.2.9.3.

4.2.4.6 Effect of metal ions on G151D activity

Effect of metal ions were studied by incorporating 1 mM concentrations of chloride salts of different mono, di or trivalent cations in the standard PDF assay using G151D as described in 3.2.9.4. The results are represented as percentage relative activities of the control activity of MtbPDF in absence of metal ions.

4.2.4.7 Thermo-stability of G151D

Thermo-stability of G151D mutant was determined at 30 ^{o}C, 40 ^{o}C and 50 ^{o}C similarly as in the case of wild type enzyme by incubating the enzymes at these temperatures and performing standard PDF assay at 30 ^{o}C. Thermo-stability of G151A mutant was also examined similarly. Details of this experiment were described in 3.2.9.6.

4.2.4.8 Determination of Fe-content in MtbPDF by AAS

In order to determine the Fe content in G151D mutant enzyme, it was processed similarly as the wild type protein as described in 3.2.9.7.3. Atomic absorbances of the serially diluted G151D mutant proteins were measured at 248 nm and the results were expressed as g-Fe atoms/ g of protein.

4.2.4.9 Stability of G151D mutant towards H_2O_2

In order to study the H_2O_2 stability of G151D mutant, 100 ng of diluted enzyme in absence of catalase was incubated with 0-500 mM H_2O_2 in 100 mM phosphate buffer pH, 7.4 at 30 ^{o}C for 30 min prior to initiation of standard PDF assay. This experiment was performed essentially the same way as described for wild type enzyme in 3.2.9.8.

4.2.4.10 Effect of actinonin on G151D activity

Actinonin, the metallo-protease inhibitor which showed inhibition of MtbPDF activity, was studied for its inhibition on G151D mutant. Actinonin was dissolved in 100% dimethyl sulfoxide (DMSO) and inhibition was studied by incubating 100 ng of G151D mutant enzyme with different inhibitor concentrations (0.001 μM-10 μM) for 15 min and performed the standard PDF assay with 5 mM *N*-f-MAS as described in 3.2.9.10.

4.2.4.11 CD spectroscopy of mutants of MtbPDF

In order to study any possible secondary structure alterations induced in the MtbPDF

structure, far-UV CD spectrum of all the seven mutant proteins were recorded using 0.1 mg / ml concentration of refolded purified proteins in 20 mM Phosphate buffer pH 7.4 at 25 ^{o}C, as described in 3.2.9.12b.

4.2.5 Computational biology approach to study the effect of G151D mutation

The high resolution crystal structure of MtbPDF was published very recently (Pichota et al., 2008) and it provided the opportunity to explore and visualize structural changes in MtbPDF associated with any mutations. Molecular modeling and molecular dynamics simulations studies have proved effective in studying the consequences of different mutations on crystal packing, substrate binding and stability of various proteins (Yan et al., 1999; Weng, 2009). In a previous study on MtbPDF, computational approaches have been used to confirm the effects of *in vitro* site-directed mutagenesis by performing homology modeling of MtbPDF structure and its mutants and performing dynamics simulations on them (Saxena et al., 2008). Similar approaches were taken in the present study to characterize G151D mutant, but based on high resolution crystal structure of MtbPDF.

4.2.5.1 Molecular modeling and Molecular Dynamics (MD) Simulation of G151D mutant

High resolution (1.56 Å) crystal structure of MtbPDF was retrieved from PDB (PDB ID: 3E3U) (Pichota et al., 2008). G151D mutant structure was generated by using Modeller9v6 program (Fiser & Sali, 2003).The atomic coordinates were obtained from the template structure, MtbPDF, to model G151D mutant structure. Care was taken to make the coordination geometry of side chain atoms most favorable. The Ni^{2+} present in the crystal structure (Pichota et al., 2008) was replaced with the native metal cofactor of MtbPDF, Fe^{2+}. For all the energy minimization and molecular dynamics (MD) routines, AMBER03 force

field in conjunction with VMD/NAMD was employed (Humphrey et al., 1996; Phillips et al., 2005). The protein (MtbPDF or G151D mutant) was solvated with at least 1.2 nm thickness of rectangular water box and counter ions were added to neutralize the system. Periodic boundary condition was employed to eliminate surface effects, while it was made sure that the protein atoms in the simulation box were well distanced from protein atoms in the periodic boxes to avoid any artifacts. The simulation system was energy minimized initially with positional restraints on protein atoms and followed by unrestrained energy minimization. Energy minimized system was equilibrated first with positional restrained MD simulation and followed by unrestrained MD simulation for 50 ps each, at 250 K to gently relax the system. The equilibrated systems were subjected to productive MD for 600 ps at 300 K with the time step of 2.0 fs and trajectory being saved at every 0.2 ps. NPT (constant number of atoms, pressure and temperature) ensemble was used for the simulation. Particle mesh ewald was used to calculate long-range electrostatics and 1.0 nm cutoff was used for short-range non-bonded interactions. MD trajectory was analyzed using customized Tcl/Tk scripts as implemented in VMD.

4.2.5.2 Molecular Docking of MtbPDF and G151D mutant with N-f-Met-Ala-Ser

Crystal structure of MtbPDF with Fe^{2+} in place of Ni^{2+} cofactor was energy minimized and used for docking studies. In the case of G151D mutant structure, a stable conformation was selected from the MD trajectory based on PROCHECK report and energy minimized prior to the docking studies. Substrate molecule (*N*-f-MAS) was prepared using arguslab and geometry optimized with AM1 semi-empirical method. Flexible small molecule-rigid protein docking experiments were performed by the use of Autodock 4.0 (Morris et al., 1998) with AutoDock tools. Default parameters were used for docking. Grid

size was set large enough to cover the active site and to allow unrestrained flexible movement of the small molecule. Genetic algorithm in combination with local search was employed for conformational search and empirical scoring function was used to estimate free energy of binding of the substrate with the protein.

4.3 Results and Discussion

4.3.1 Multiple sequence alignment of MtbPDF

Multiple sequence alignment of MtbPDF with other type I, type II bacterial PDFs and type IA human mitochondrial PDFs revealed high level of conservation among the residues in the three signature motifs of PDFs. Among the residues strictly conserved for activity of PDFs, some variations were found between bacterial and human PDFs (**Fig 4.1**). The conserved glycine residue in motif I of bacterial PDFs has been replaced with cystein in case of human PDF. Secondly, the conserved leucine in motif II of bacterial PDFs has been replaced with a glutamate residue in human PDF. An important substitution was observed in motif III of MtbPDF where a conserved aspartate residue present in bacterial and human PDFs has been substituted by a glycine residue. Hence, these three sites were selected for creating single mutants of MtbPDF, substituting MtbPDF residues with the corresponding ones in human PDF (i.e. G49C, L107E and G151D). Two control mutants were created for these two glycine-substitution mutations, G49P and G151A, in order to compare the properties of the former substitutions. Apart from these three sites, effect of mutation of two highly conserved residues in motif II of all PDFs were studied by substituting them in MtbPDF, i.e. E104A and G105P.

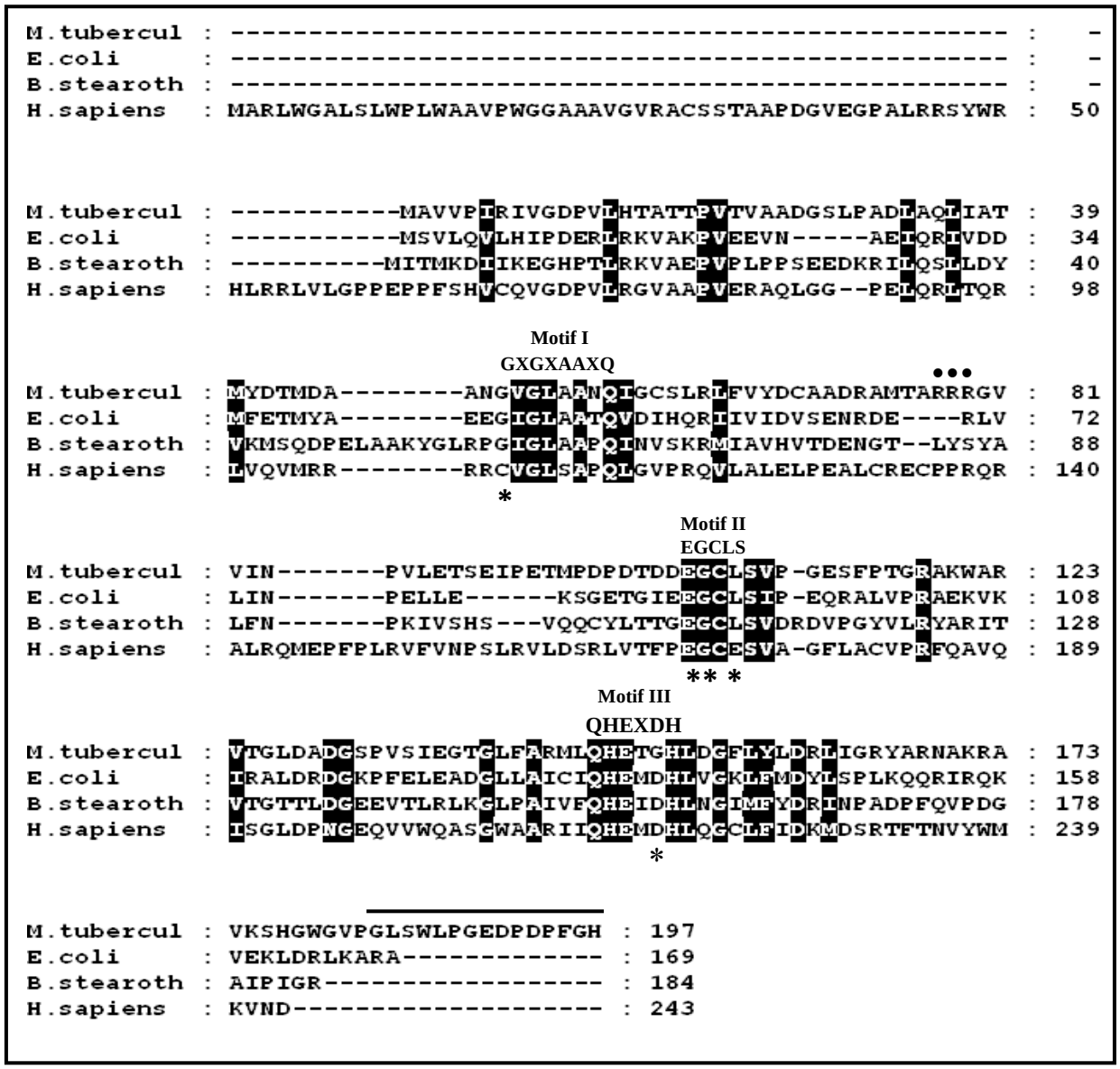

Fig 4.1: Multiple sequence alignment of different prokaryotic and human PDFs with MtbPDF. The three conserved motifs of deformylase are labeled above. The three arginines in the insertion region are shown above them with filled circle (•). The residues selected for mutagenesis are shown below them with an asterisk (*****).The extended C-terminal of MtbPDF is over lined.

The alignment highlighted the specific arginine rich insertion sequence between motif I and motif II and the extended C-terminal of MtbPDF in comparison to other bacterial and human PDFs. These two specialties in the MtbPDF sequences were studied and reported previously (Saxena and Chakraborti, 2005a; Saxena et al., 2008). Multiple sequence alignment of PDF sequences from family Mycobacteriacea with *E. coli* PDF revealed that there is high level conservation of sequences among the PDFs from different species within the family of Mycobacteriaceae, irrespective of their pathogenic or non-pathogenic mode of life (**Fig 4.2**).

One major variation observed between the sequences of Mycobacterium PDFs and that of other well characterized bacterial and eukaryotic PDFs is the presence of a glycine in the motif III of former instead of the conserved aspartate residue found in the later (**Fig 4.1 and 4.2**). This motif is known to form the core helix in the 3D structure of all the crystallized PDFs (Becker et al., 1998a; Serero et al., 2001; Escobar-Avarez et al., 2009). Glycine residues are potentially considered as helix-breakers due to the unfavorable entropy it has in the folded conformations (Javadpour et al., 1999; Cho et al., 2008). In the absence of structural information on MtbPDF, the structural and functional role of this residue without a side chain in place of a conserved acidic residue was studied by characterizing a G151D mutant of MtbPDF. G151A mutant was constructed to serve as a control for the charged side chains in the aspartate substitution mutant.

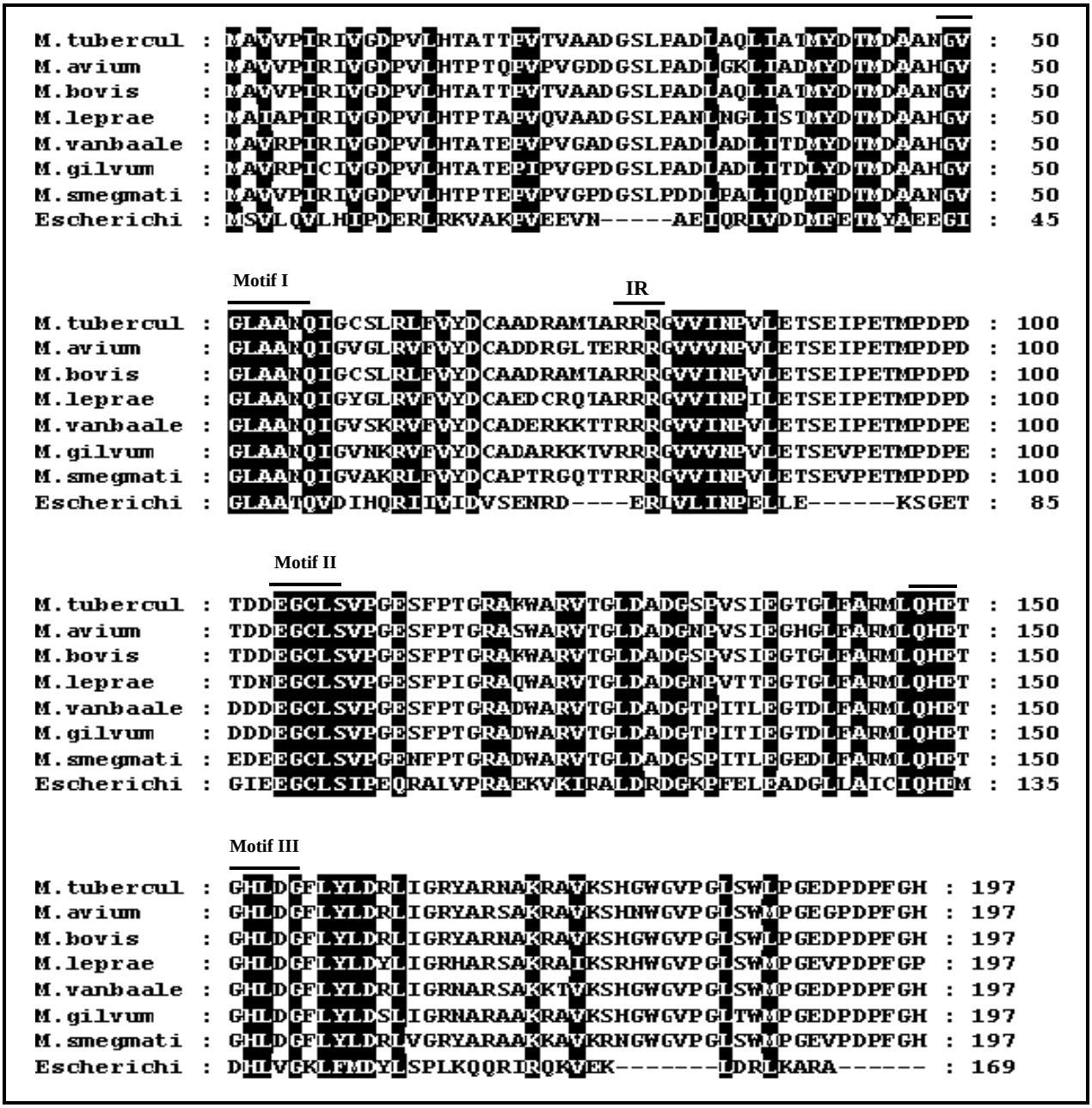

Fig 4.2: Multiple sequence alignment of PDFs from different pathogenic and non-pathogenic species of Mycobacterium with *E. coli* PDF. shows complete conservation of residues in the three conserved motifs and three arginines in the specific insertion region (IR) (Saxena et al., 2008) between motif I and II across the family Mycobacteriacea. In motif III, a glycine residue replaces the conserved aspartate (*) of *E. coli* PDF in all Mycobacterium PDFs.

4.3.2 Construction of site-directed mutants

The seven site-directed mutations of MtbPDF designed for the substitution of five selected residues was performed and the recombinant plasmids bearing these seven mutations were confirmed by DNA sequencing (**Fig 4.3**).

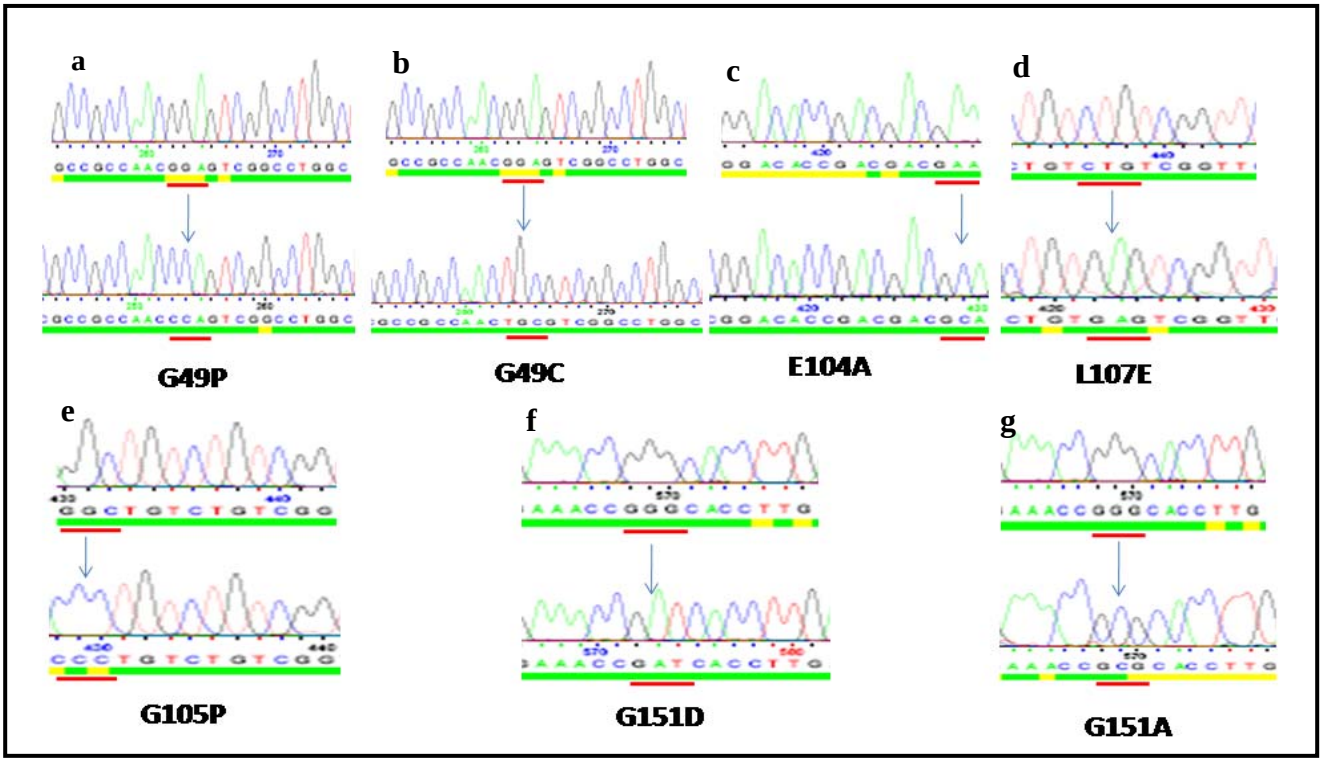

Fig 4.3 Confirmation of site-specific mutations on pET28a: *def* plasmid by DNA sequencing. The upper chromatogram in each figure shows the wild type sequence and the lower one shows the mutated sequence. The codons mutated are underlined in red in each case and the corresponding amino acids replaced at those sites are denoted at the bottom of each figure.

4.3.3 Over expression and purification of site-directed mutants of MtbPDF

During over expression in *E. coli* BL21 (DE3), all the mutant enzymes were expressed in the insoluble fraction as in the case of wild type. All the seven mutants were purified through Ni-NTA column and were detected as 29 ± 1 kDa proteins on 12% SDS-PAGE, similar to the wild type enzyme (**Fig 4.4a**). Soluble expression along with GroEL

chaperon in the soluble fractions was possible only with G151D, G151A and G49C and these were co-purified with GroEL through Ni-NTA column (**Fig 4.4 B**).

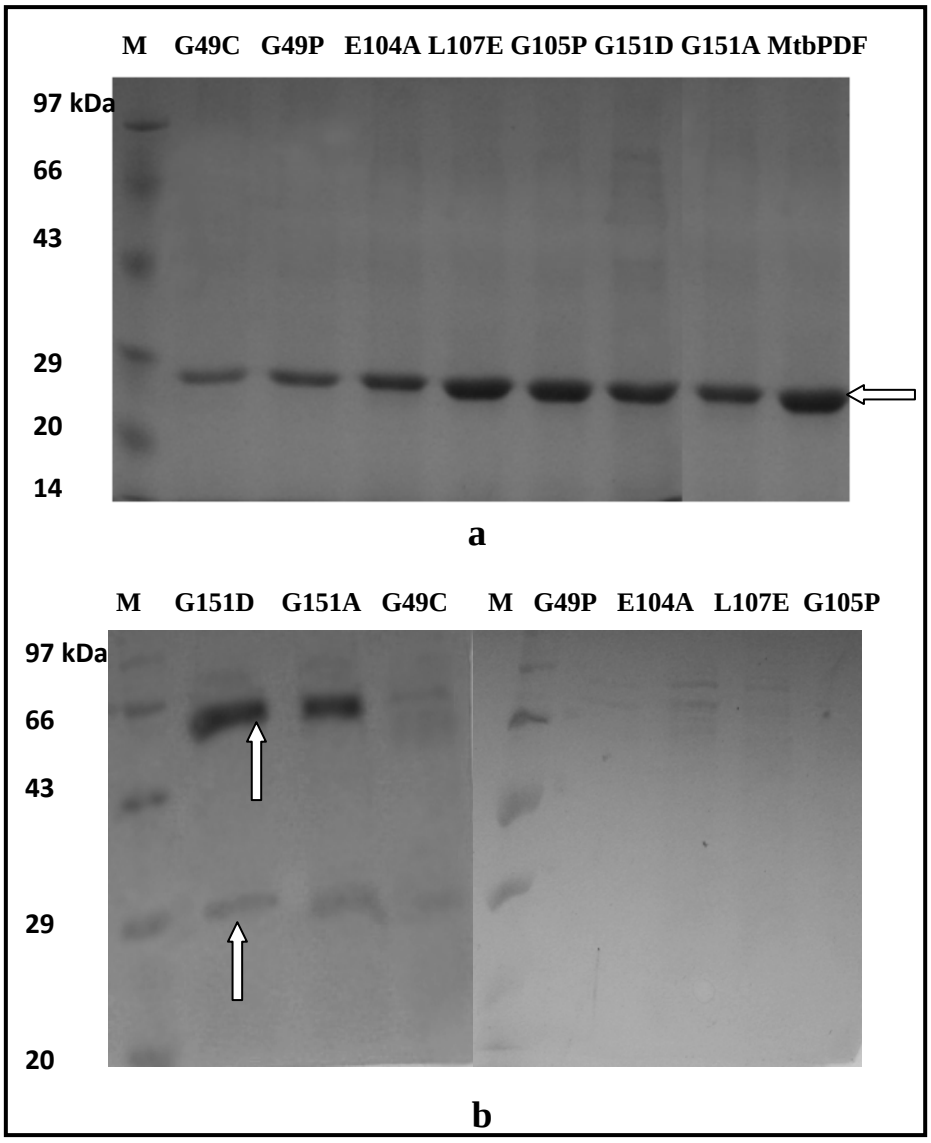

Fig 4.4: Purification of recombinant MtbPDF-mutant proteins (a) Refolded from urea fraction (b) Co-expressed with GroEL/S chaperon. All the mutants got purified to homogeneity as refolded proteins similar to the wild type. But only G151D, G151A and G49C could be expressed and purified from soluble fraction along with GroEL chaperon.

4.3.4 Comparison of biochemical properties of mutants with MtbPDF

4.3.4.1 Deformylase activity of mutant proteins

Deformylase activities of all the seven mutants of MtbPDF against 5 mM *N*-f-MAS in comparison with wild type enzyme are depicted in **Fig 4.5**.

Among the mutants corresponding to the human PDF, G49C retained nearly 36.1±9% activity relative to the wild type protein. A proline substitution at G49 (G49P) resulted in almost complete loss of activity. The second mutant, L107E, showed relative deformylase activity less than 10% of the wild type. Apart from human PDF, amino acid sequences of *Clostridium beijerinckii* PDF also have cystein in place of first glycine in motif I and this enzyme was shown to exhibit deformylase activity and complement the PDF activity of conditional *def* mutant of *E. coli* (Evans *et al.*, 1998). Similarly with cystein at position G49, MtbPDF was also seen retaining some of its activity compared to the proline mutant (Fig 4.5). Structural studies with *E. coli* PDF and *Enterococcus faecium* PDF showed that the residues without reactive side chains are essential at this region in order to form a turn in the structure, forming a chamber in the inner of the binding pocket (Meinnel *et al.*, 1997; Nam *et al.*, 2009). L107 forms part of a loop in the crystal structure of *E. faecium* PDF and play an important role in forming the hydrophobic S1' pocket to accommodate methionine side chain of substrate (Nam *et al.*, 2009). These two residues occupy similar structures in the published crystal structure of MtbPDF (Pichota *et al.*, 2008). It has been recently proved that mutating these two residues back to the corresponding bacterial residues in human PDF increases its deformylase activity by many folds (Escobar-Avarez *et al.*, 2009). By characterizing these two mutants in MtbPDF, it could be inferred that mutations at these two positions would have resulted in the decrease in deformylase activities of human

mitochondrial PDF. The mitochondrion is believed to have evolved from an endosymbiotic bacterium and shares many features in protein synthesis with bacterial protein synthesis. It could be possible that during the course of evolution, the essentiality of deformylation is lost in human mitochondria and thus the PDF in the mitochondria has under gone the above two mutations to form the feebly active human PDF (Nguyen, 2005).

Mutation E104A and G105P in motif II of MtbPDF resulted in drastic decrease in the deformylase activity of the mutant proteins (**Fig 4.5**). The corresponding mutations have been characterized in *E. coli* PDF to find similar trends in activity decrease (Meinnel et al., 1995; 1997). This first glutamate in motif II was reported to surround the metal binding cavity in *E. coli* PDF structure, with its side chains forming a lid above the metal binding cleft (Meinnel et al., 1996). But no changes were reported in the metal content up on alanine substitution of this glutamate. So it is believed that acidic side chains of E104 in PDFs plays and important role in stabilizing the metal binding and catalysis, even though not directly involved in it. The role of glycine in motif II of PDF is reported to be structural, by allowing a kink to position the side chain atoms of metal binding cystein towards the metal (Meinnel et al., 1997). It was also reported to aid in formation of S1' pocket in case of *E. faecium* PDF structure (Nam et al., 2009).

It was interesting to note that G151D mutation produced active protein with nearly 1.5 times the activity of MtbPDF with substrate *N*-f-MAS (**Fig 4.5**). This was an interesting observation as the presence of glycine at this position in motif III was specific for PDFs from Mycobacterium. This result indicated that glycine instead of aspartate in motif III could be one of the reasons for lower activity of MtbPDF compared to other reported bacterial PDFs. Moreover, the alanine substitution mutant, G151A, showed 99± 4% relative

activity of wild type enzyme (**Fig 4.5**), proving the specificity of charged side chain atoms at that position in improving the deformylase activity. In case of *E. coli* PDF, alanine and asparagine substitution for aspartate in motif III have resulted in 34% and 75% relative activity of wild type respectively (Meinnel *et al.*, 1995). No catalytic, metal-binding or structural role has been assigned to the residue at this position.

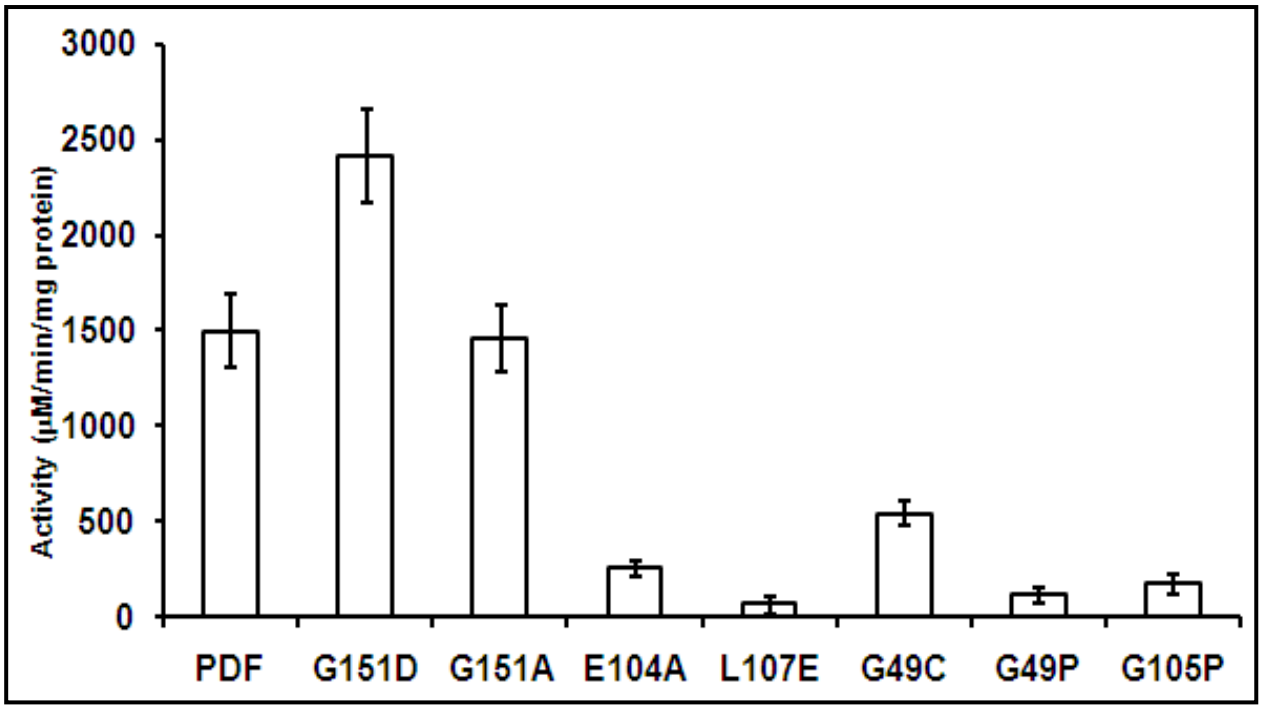

Fig 4.5: Deformylase activity of site-directed mutants of MtbPDF with 5 mM *N*-f-MAS.

4.3.4.2 Substrate specificity of G151D mutant

Owing to its higher activity than the wild type, G151D mutant was further characterized for its properties. The substrate specificity of G151D mutant against different *N*-formylated di and tri-peptides was in the same order as that of wild type (**Fig 4.6**). Among the three substrates tested, *N*-f-MAS was the best. G151D also deformylated *N*-f-MLF nearly five times better than MtbPDF (Fig 4.6), which suggests a possible increase in space

within the substrate binding site at S2' and S3' positions to accommodate the bulkier side chains on the substrates. The G151A mutant showed high similarity with wild type enzyme in deformylating different substrates. It is very well defined that substrate specificity of PDF depends on the first three N-terminal residues (P1'-P3') (Giglione et al., 2003) and only limited studies have defined the residues deciding the substrate specificities of PDFs (Hu et al., 1999; Dirk et al., 2008).

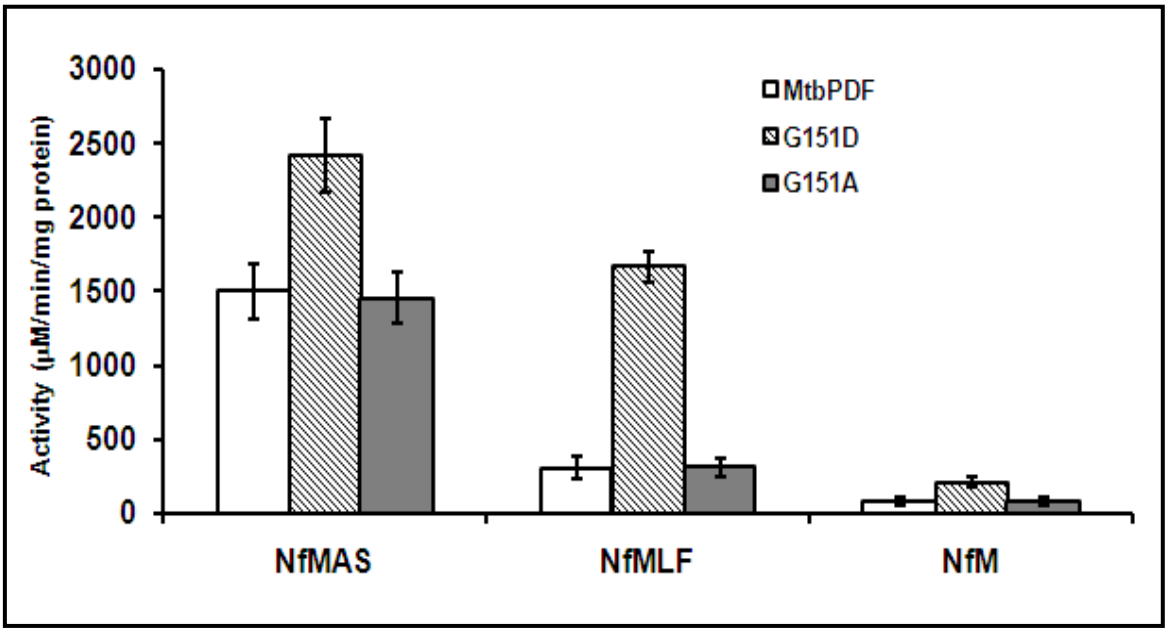

Fig 4.6: Comparison of substrate specificities of G151D and G151A mutant with MtbPDF. 5 mM of each of the substrates and 73.3 nM of each of the proteins were used in the assay. NfMAS: *N*-for-Met-Ala-Ser; NfMLF: *N*-for-Met-Leu-Phe; NfM: N-for-Met.

4.3.4.3 Kinetic properties of active mutants of MtbPDF

The Michealis-Menten plots for enzyme kinetics of MtbPDF and its active mutants against substrate *N*-f-MAS are shown in **Fig 4.7**. The kinetic parameters for the three mutants in comparison with the wild type values are provided in **Table 4.2**. The G49C mutant showed the least catalytic activity among the active mutants, proving this mutation to be one of the reasons behind the diminished deformylase activity of human PDF. There was an increase in K_m value for this mutant, suggesting reduced substrate affinity which might

have been caused by the structural variations in the binding pocket due to this mutation. Catalytic properties of G151D suggested an improved substrate affinity compared with MtbPDF, as evident from the decreased K_m values. There was also a significant increase in K_{cat} value for G151D. The catalytic efficiency value for this mutant is very close to the previously characterized *H. pylori* PDF and *L. interrogans* PDF (Han et al., 2004; Li et al, 2002). The G151A mutant showed similar catalytic properties as MtbPDF (**Table 4.2**).

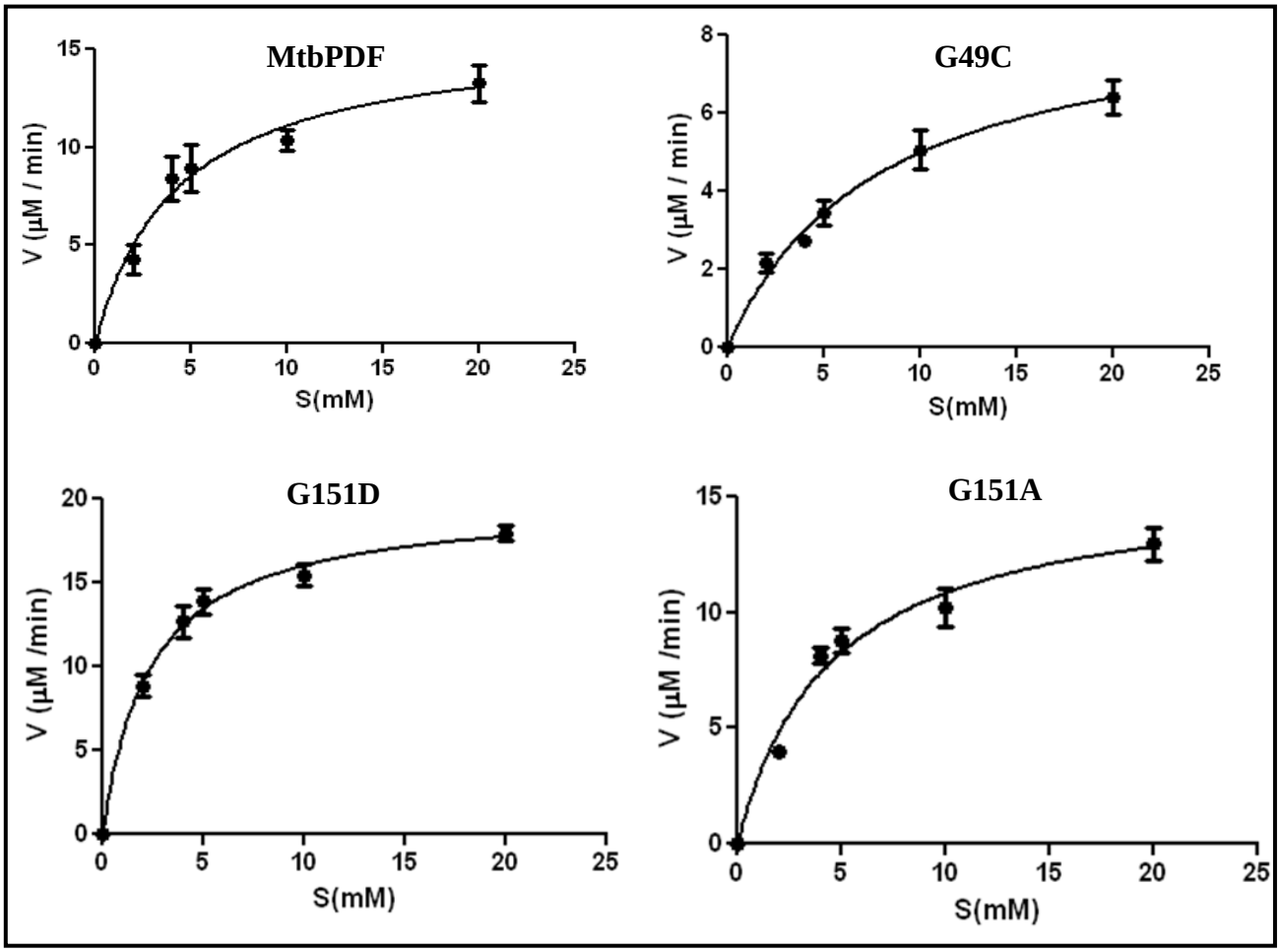

Fig 4.7: Michealis-Menten plot for enzyme kinetics of wild type and active mutants of MtbPDF against substrate *N*-f-MAS. 73.3 nM of each of the proteins were used in the assay. MM plot was made with Graph pad prism software.

Table 4.2. Kinetic parameters of MtbPDF and its active mutants

Kinetic Parameters				
Protein	**V_{max} ($\mu Mmin^{-1}$)**	**K_m (mM)**	**K_{cat} (s^{-1})**	**K_{cat}/K_m ($M^{-1}s^{-1}$)**
PDF	**15.8 ± 1.2**	**4.3 ± 0.9**	**3.6 ± 0.6**	**842 ± 9**
G151D	**19.8 ± 0.7**	**2.5 ± 1.1**	**4.5 ± 0.6**	**1786 ± 19**
G151A	**15.6 ± 0.4**	**4.4 ± 0.7**	**3.5 ± 0.7**	**795 ± 8**
G49C	**8.9 ± 1.0**	**7.8 ± 0.8**	**2.0 ± 0.3**	**260 ± 9**

4.3.4.4 Temperature and pH optimum for G151D mutant

G151D mutant exhibited highest activity at 50 ^{o}C with nearly 2 fold increase in efficiency compared to the wild type activity at 30 ^{o}C (**Fig 4.8a**). In present study and in the previous studies, temperature optimum for MtbPDF activity was lower compared to all reported PDFs (Saxena and Chakraborti, 2005a). In all the reports on bacterial and eukaryotic PDFs having aspartate at this position, the temperature optimum for activity ranges from 37-60 ^{o}C (Rajagopalan *et al.*, 1997; Bracchi-Ricard *et al.*, 2001; Li *et al.*, 2002; Han *et al.*, 2004). Introduction of aspartate restored the temperature optimum back to this range similar to other reported PDFs supporting the importance of aspartate residue in motif III of PDFs in modulating its thermo-stability. This is for the first time such a property is being associated with the conserved aspartate in motif III of PDFs.

Similarly, the pH optimum for G151D mutant activity was shifted towards 5.5 from the pH optimum of MtbPDF, 7.4 (**Fig 4.8b**). Only a single ionization event (pKa ~ 5.2) has been assigned to the deprotonation of metal-bound water/glutamate network in previously studied PDFs, which lead to a flat pH profile in the basic range (Rajagopalan *et al*, 1997, Bracchi-Ricard *et al*, 2001). In order to gain insight in to the effect of mutation on the protonation states of putative catalytic E149 in MtbPDF, computational predictions of pKa

value of E149 in the wild type (Pichota et al., 2008) and G151D mutant structures were done using the H++ web server (http://biophysics.cs.vt.edu/H++/) (Gordon *et al.*, 2005) under the default physical conditions by employing finite difference Poisson-Boltzmann equation for pH 7.5. The pKa values predicted by H++ server for catalytic residue E149 in the MtbPDF and G151D mutant structures were 6.48 and 4.88 respectively, which confirmed the experimental results. The shift in optimum pH for activity to acidic range in case of G151D can very well be explained by a drop in predicted pKa value of E149 by 1.6 units in mutant structure. These results proved that the presence of a side chain with negative charge adjacent to catalytic glutamate modulates its pKa value for optimum catalysis.

The catalytic efficiency of G151D at pH 5.5 and temperature 50 ^{o}C was found to be very close to the reported values of *L. interrogans* and *H. pylori* PDFs (Li *et al.*, 2002; Han *et al.*, 2004), even though 10 folds lower compared to Ni^{2+} containing *E.coli* PDF (Ragusa *et al.*, 1998). However, for the sake of comparison, the optimum temperature (30 ^{o}C) and pH (7.4) of the wild type enzyme was used in all further studies.

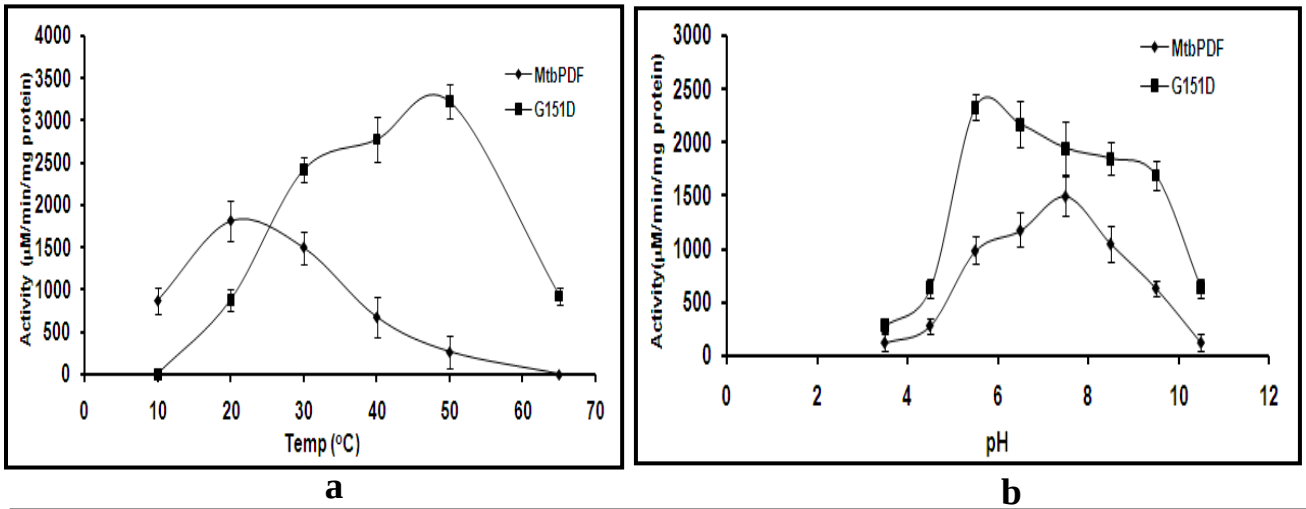

Fig 4.8: Comparison of temperature (a) and pH (b) optimum for deformylase activity of G151D mutant with wild type enzyme.

4.3.4.5 BSA and catalase on G151D activity

Effect of BSA and catalase during dilution of G151D mutant proteins is depicted in **Fig 4.9** in comparison with the wild type protein. As seen from the results, the exclusion of both BSA and catalase had significant effect on the G151D activity. More than 50% activity of mutant protein was lost upon exclusion of either of these carrier proteins and in absence of both there was only 30% of the original activity. The effect was more pronounced in case of G151D mutant when compared to the wild type protein. This shows that even though the mutant protein is more active than wild type protein, it is prone to atmospheric oxidation of Fe^{2+} much more than the wild type protein in absence of carrier proteins. The shelf-life of G151D mutant proteins stored at a concentration of 1 mg/ml at 4 ^{o}C was 4 days in absence of these carrier proteins (data not shown).

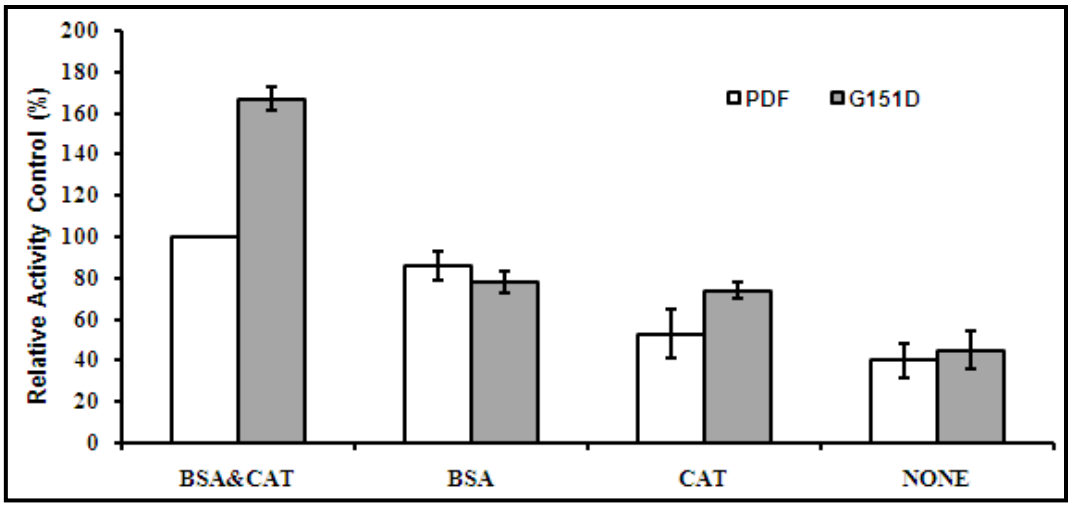

Fig 4.9: Effect of BSA and catalase on deformylase activity of G151D mutant protein and wild type protein. The results are represented as percentage relative activities of the wild type enzyme in presence of both BSA and catalase.

4.3.4.6 Thermo-stability of G151D mutant

G151D mutant was very stable at 30 ^{o}C with little loss of activity up to 6 h. Interestingly, the $t_{1/2}$ of G151D at 40 ^{o}C was > 6 h and at 50 ^{o}C was 2 h (**Fig 4.10**). Thus,

there was a clear improvement in the thermo-stability of G151D mutant protein compared to the wild type enzyme. The increase in temperature optimum for deformylase activity of G151D mutant was very well supported by the increase in thermo-stability. Thermo-stability of a mutant protein reflects the enhanced stability of the structure induced by the mutation (Bloom *et al.*, 2006). Thus, it was assumed that a stabilization of the MtbPDF structure had taken place by replacing a glycine on the core-helix with an aspartate residue. This increase in thermo-stability was specific for G151D and was absent in case of G151A (data not shown). Structural details determining the thermo-stability of PDFs have not been reported yet in detail. Saxena and Chakraborti (2005a; 2005b) have reported the extended C-terminal in MtbPDF to be important for its activity. Examining the crystal structure of MtbPDF (Pichota et al., 2008), it was clear that the extended C-terminal is surface exposed and resides close (with in 5 Å radius) to the core-helix in the substrate binding pocket of MtbPDF and it lead to the assumption that this extended C-terminal region to have a role to play in the stability of MtbPDF.

4.3.4.7 Metal ions on G151D activity

The effects of different metal ions under study on G151D mutant activity were highly similar to their effects on wild type enzyme (**Fig 4.11**). There were no major changes observed in the trends of metal ion effects between mutant and wild type enzyme. But, the effect of Fe^{3+} on G151D mutant was inhibitorier than its effect on wild type proteins. This observation goes in hand with the previously discussed increased instability of mutant proteins to atmospheric oxygen. Inhibitory effect of Fe^{3+} was very interesting to note and this could be due to oxidation of S^{γ} in the metal binding cystein in a fraction of enzyme by oxidized form of Fe, as postulated by Kreusch et al., (2003). These results clearly

demonstrated the increased susceptibility of G151D mutant to oxidative attacks compared to the wild type enzyme.

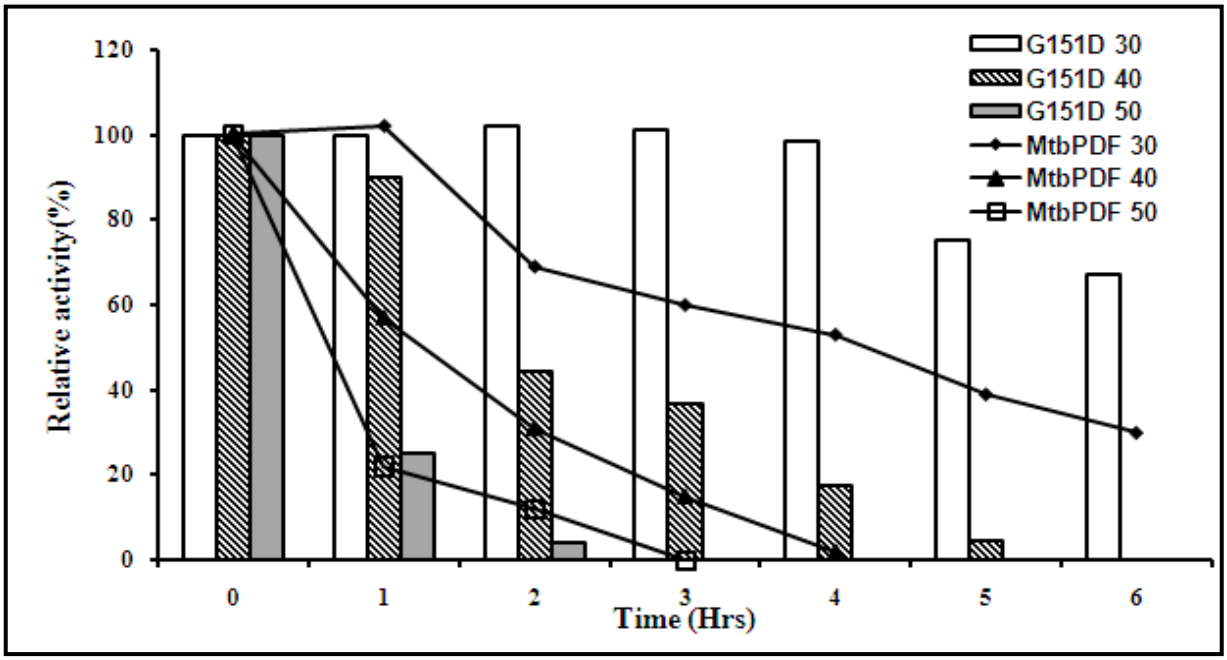

Fig 4.10: Comparison of thermo-stability of G151D mutant with wild type enzyme. 100 µg of purified proteins were incubated at the indicated temperatures in presence of BSA and catalase and aliquots of 100 ng were added in standard PDF assay. Results are represented as percentage relative activities of the enzyme activity at time 0.

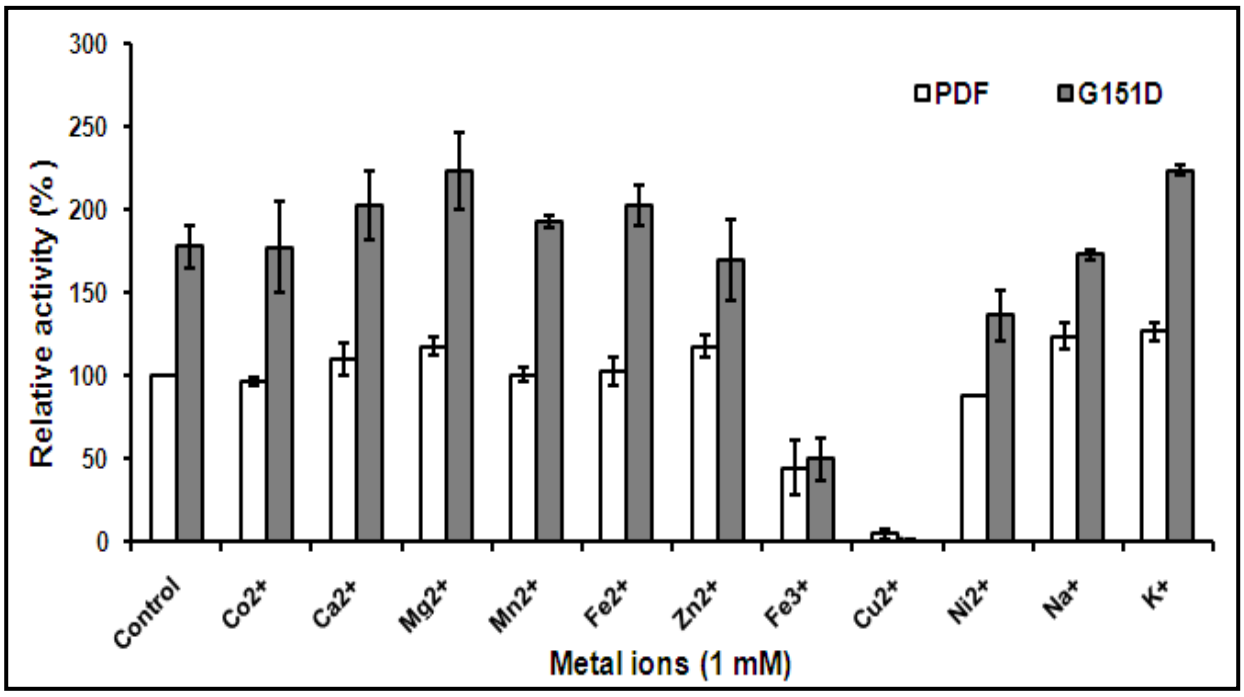

Fig 4.11: Comparison of the effects of metal ions on the enzyme activity of G151D mutant and wild type enzyme. Results are represented as percentage relative activities of the wild type enzyme in absence of any added metal ions.

4.3.4.8 Quantification of Fe-content in G151D mutant

Fe-content in G151D, as quantified using AAS, was 0.69 ± 0.23 g-atoms of Fe/g of protein. Thus G151D mutant was shown to contain essentially the same amount of Fe as in the case of wild type protein. This rule out the notion that the increased activities of G151D mutant protein could be due to replacement of the Fe-cofactor with Ni^{2+} during purification as observed by Pichota et al., (2008) during crystallization. It was clear that the enhanced activity and thermo-stability of G151D mutant was associated with structural changes induced by the mutation and not by replacement of metal ion cofactor during purification. This result was also supported by the susceptibility of G151D mutant to atmospheric oxidation in absence of catalase, which is a typical property of Fe- containing PDFs.

4.3.4.9 H_2O_2 stability of G151D mutant

G151D completely lost its activity upon incubating with 200 mM H_2O_2 (**Fig 4.12**) with an IC_{50} value of 89 mM. This proved the marked reduction in stability of G151D mutant towards H_2O_2 as compared to the wild type enzyme. Thus the increase in thermo-stability was accompanied by a decrease in stability towards H_2O_2 in case of G151D. Saxena et al., (2008) proved that the arginine-rich insertion sequence between motif I and motif II of MtbPDF is involved in its oxidative stress resistance. This insertion sequence forms a surface exposed loop in the MtbPDF crystal structure (Pichota et al., 2008). Using site-directed mutagenesis it was proved that three arginines in the insertion sequence responsible for this property. The mechanism predicted was an 'action-at-distance', where in the mutation at R77-79 present in a loop away from the active site affects resistance to H_2O_2. Side chains of arginines are reported to interact and scavenge oxygen (Lass et al., 2002). But the actual mechanism by which these residues prevent Fe^{2+} and / or metal co-ordinating cystein S^{γ} from getting oxidized is still not clear. Since we have confirmed the presence of equal amounts of Fe in both wild type and G151D mutant, the reason for higher susceptibility of the later towards oxidizing agents must lie in the structural variations that the mutation induced in overall structure other than the metal binding pocket. Analyzing the effects of mutation on the three arginines in the insertion region of G151D mutant may reveal some of the structural clues to this property.

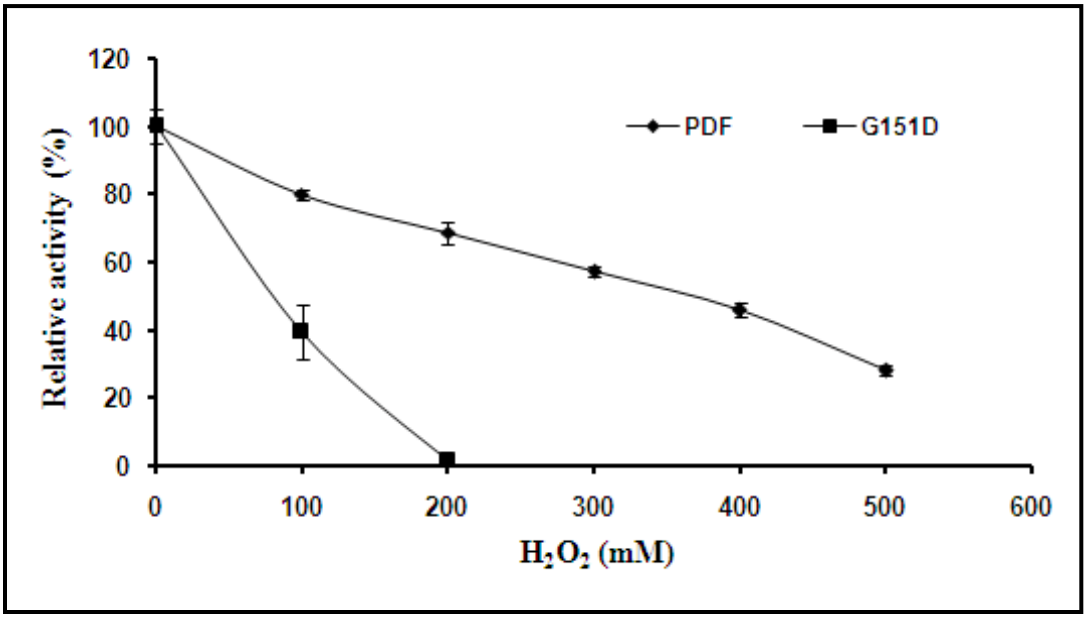

Fig 4.12: Comparison of the stability of G151D mutant and wild type enzymes towards H_2O_2. Results are represented as percentage relative activities at each H_2O_2 concentration compared to the uninhibited reaction without H_2O_2.

4.3.4.10 Inhibition of G151D by actinonin

G151D was inhibited completely at 10 μM of actinonin with an IC_{50} value of 800 nM compared to the complete inhibition of wild type enzyme at 5 μM with IC_{50} value of 120 nM (**Fig 4.13**). This increase in IC_{50} value of a competitive inhibitor points to the higher substrate affinity in case of G151D mutant. These results from inhibition go in hand with the observed decrease in K_m value of G151D mutant for *N*-f-MAS, denoting the improved substrate binding. This suggested a possible restructuring in substrate binding pocket of G151D mutant, induced by the substituted aspartate residue, leading to better substrate binding.

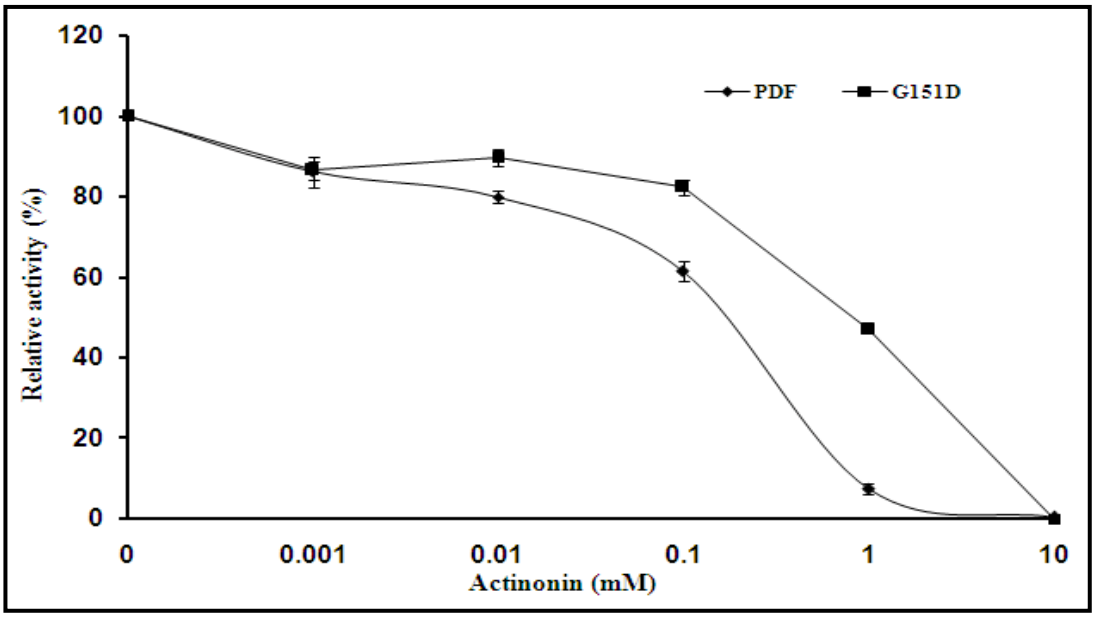

Fig 4.13: Inhibition of G151D and wild type enzyme by actinonin. Results are represented as percentage relative activities of uninhibited control reaction.

4.3.4.11 CD spectrum of mutants of MtbPDF

The far-UV CD spectra of mutants of MtbPDF along with the wild type enzyme are shown in **Fig 4.14**. CD spectra of mutants of MtbPDF corresponding to motif I and motif II residues (G49C, G49P, L107E, E104A, and G105P) were all nearly superimposable to wild type spectrum. These results indicated that only very little secondary structure variations were induced by each of these substitutions. One possible reason for insignificant variations in CD spectra of these mutants could be that all these residues form part of loop structures in MtbPDF structure (Pichota et al., 2008) and any of the slight changes in the less stable loop structure may not have had a global effect on the protein structure. Among these mutants, only G49C showed slight activity towards the tested substrate.

Unlike the other four variants, the CD spectra of G151D showed scatter to low mean residue ellipticity. However, there was no shift in the negative minima at 222 nm or 208 nm.

There was an increase in the mean residue ellipticity (θ) values at 222 nm and 208 nm to -9.3 and -11.6, respectively, which signifies only slight restructuring in the less stable scaffolds like turns and 3_{10} helices without affecting the alpha helical fold. It signifies that replacing glycine with aspartate in the core helix has not disturbed the helical fold in the structure, but instead has lead to slight restructuring in the overall protein structure to accommodate the charged side chain of aspartate. These kinds of scatter in CD spectra associated with restructuring in globular proteins up on glycine to aspartate mutation have been reported previously (Woycechowsky et al., 2008).

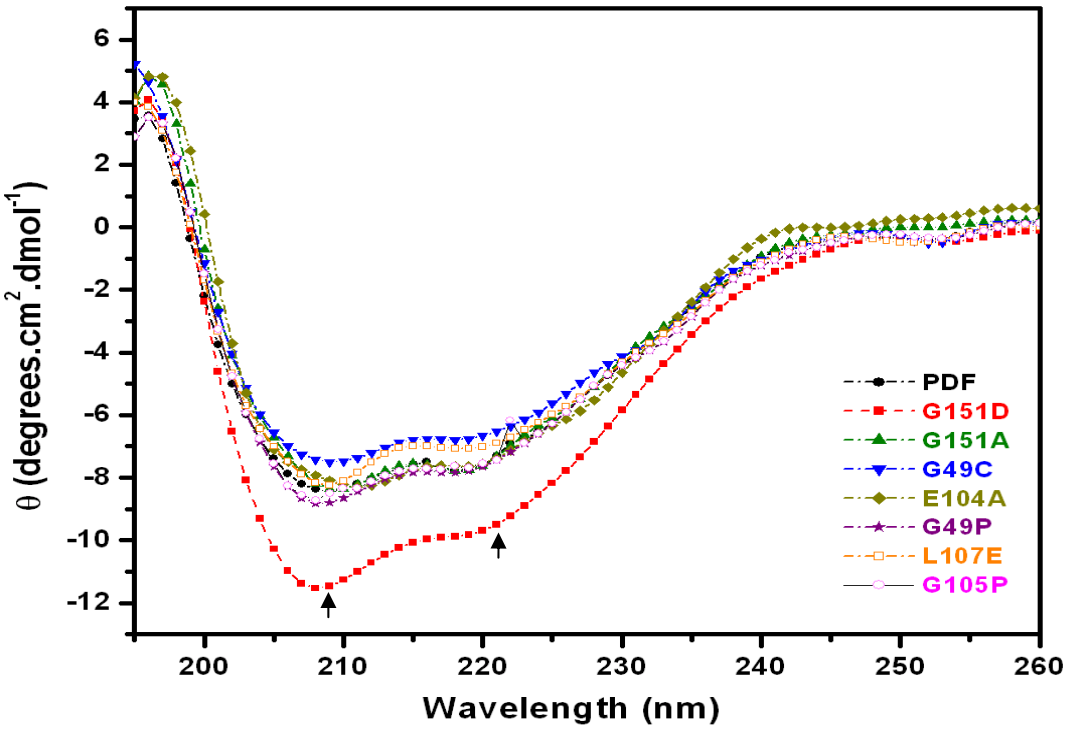

Fig 4.14: CD spectrum of MtbPDF and its mutants at 0.1 mg / ml of protein concentration. The negative minima at 222 nm, 208 nm and 198 nm are indicated by arrow heads.

Since the similar trends in CD spectra were missing in case of G151A mutant, the structural variation and improvement in deformylase activity was considered specific to aspartate substitution.

4.3.5 Computational approaches

Using the published crystal structure of MtbPDF and the modeled G151D mutant structure, an attempt was made to answer some of the observed variations in properties of MtbPDF associated with the G151D mutations. Using molecular dynamics simulations and molecular docking studies on these structures, the variations in thermo-stability, oxidative stress resistance and substrate binding were analysed and possible structural basis for these properties were postulated.

4.3.5.1 *Molecular Modeling and MD simulations*

The overall structure and stability of MtbPDF and G151D were examined by MD simulation. In the G151D model, the side chains of D151 was not a part of the catalytic site and was located more than 5 Å from the metal ion (**Fig 4.15a**). MD simulations of both structures were carried out for 600 ps (**Fig 4.15b**). The main chain root men square deviations (RMSD) plots for the trajectories of the two structures during MD simulation are given in **Fig 4.15c**. RMSD profile for the two structures (**Fig 4.15d**) showed that G151D reached a flat profile after ~100 ps while MtbPDF showed a variable profile during the entire simulation period. This demonstrated the higher stability of G151D over MtbPDF structure. The root mean square fluctuations (RMSF) plots of MtbPDF and G151D indicated that L1 loop (T22-D30), L5 loop-β-4-strand-L6 loop (I83-T101), and C-terminal loop (D191-H197) were found to be highly fluctuating regions (**Fig 4.15d**). However, the MtbPDF structure fluctuated higher than the mutant in L1 loop (0.4 Å) and C-terminal loop (0.7 Å), whereas G151D structure showed higher fluctuations in L6 loop (E91- T95). In spite of the observed differences, both structures showed similar fluctuation patterns. The similar patterns in RMSF for residues of MtbPDF and G151D during the dynamics indicated that there were only slight differences between the over all structure of the two. MtbPDF

structure contains 3 α-helices, seven β-sheets and three 3_{10} helices, forming three motifs and structurally conserved active site (Pichota *et al.*, 2008). Both MtbPDF and G151D had comparable secondary structures except that, in later the first two 3_{10} helices (^{12}PVL^{14} and ^{53}ANQI^{56}) were transformed into turns. Additionally, the helix H1 started from A31 in case G151D instead of D32 in MtbPDF (**Fig 4.15a**). The CD spectrum of G151D reflected these variations in the less stable scaffold.

The MtbPDF crystal structure revealed that the extended C-terminal forms a long loop containing a β-sheet which interacts with the N-terminal β- sheet, placing the side chains of F195 and H197 residues with in 5 Å radius of the substrate binding pocket (Pichota *et al.*, 2008). The residues in the extended C-terminal are all surface exposed in the structure. Closer examinations of the structure revealed that side chain atoms of W186 interact with side chain atoms of L107 and side chain atoms of D191 and H197 interact with those of N48. These interactions along with the interactions with N-terminal β- sheet stabilize the C-terminal loop. Both L107 and N48 form part of the loop lining the substrate binding cavity. Hence, the removal of C-terminal extension in MtbPDF might affect the architecture of substrate binding cavity leading to loss of enzyme activity (Saxena and Chakraborti, 2005a). During MD simulations of MtbPDF structure, residues in helix (R164-H175) preceding the C-terminal loop was found stabilized by formation of internal hydrogen bonding between side chain atoms of these residues. In G151D structure these hydrogen bondings were remarkably reduced, leading to higher RMSF values of these residues compared to wild type. But the fluctuations in the residues forming C-terminal extended loop is greatly reduced in the case of G151D structure (**Fig 4.15d**). This stability of the

surface exposed loop might have contributed to increase in the overall stability of the mutant.

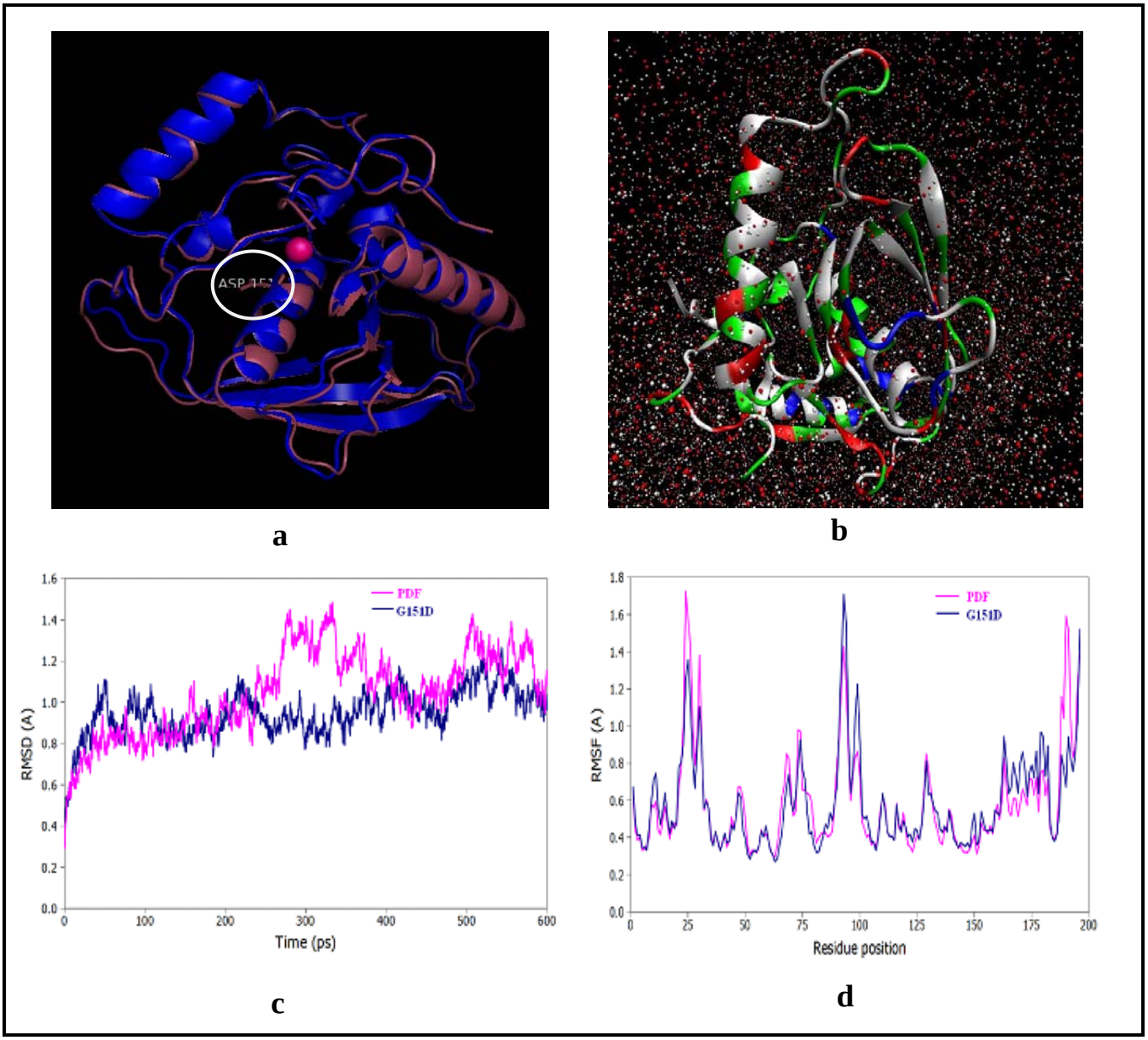

Fig 4.15: Molecular modeling and MD simulations of MtbPDF and G151D. (a) Superimposed cartoon structure (Pymol) of modeled G151D mutant (brown) over MtbPDF structure (blue) with the Asp 151 highlighted with in a circle. The metal ion is represented as hot pink sphere; **(b)** Snap-shots of MtbPDF structure during MD simulations; **(c)** The RMSD plot of MtbPDF and G151D during MD simulation; **(d)** The RMSF plot of MtbPDF and G151D during MD simulations.

The vital residues for metal binding and catalysis (C106, H148, H152 and E149) were all within 3 Å space around the metal ion. MD simulations of MtbPDF and G151D structures revealed no significant differences in the conformation of metal binding residues and their average distance from Fe^{2+} ion (**Fig 4.16**). Atomic absorption spectroscopy results revealed equal amount of Fe in both MtbPDF and G151D which asserted the results from molecular modeling.

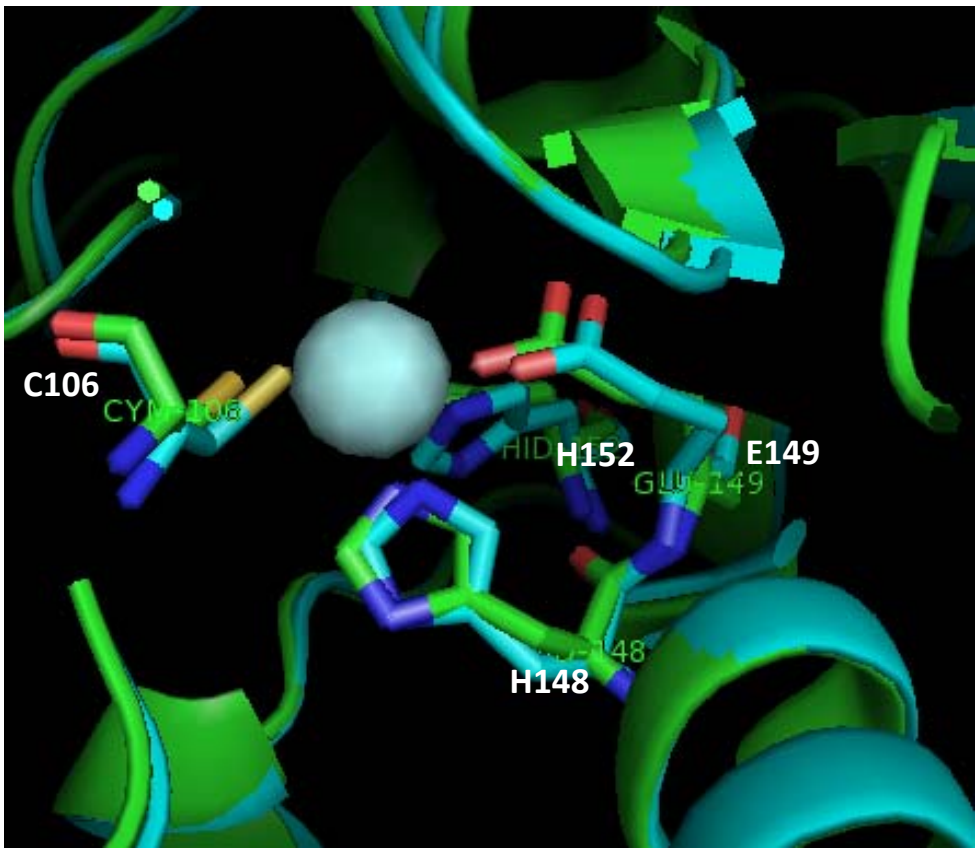

Fig 4.16: Superimposed cartoon models of MtbPDF (green) and G151D (cyan) structures showing metal-binding pocket (C106, H148, H152 and E149). All the metal-binding residues were spatially conserved around the metal ion (cyan sphere) in both the structures.

Analyzing the residues lining the substrate-binding cavity (G49, V50, G51, E104, G105, C106, L107, R144, and M145) from both the structures indicated slight fluctuations

in backbone atoms of these residues. Mass-weighted centre of side chain atoms were used for the calculation of distance distribution of side chains. From the analysis of the spatial

distribution of side chains, the average distance between the side chain atoms of M145 with L107 of the mutant was found to be higher than the wild type by 2 Å (**Fig 4.17 a & b**). The average distance between side chain atoms of the residues lining substrate binding pocket on either side were found increased in case of G151D than wild type. The distance between side chain atoms of G49, V50 and G51 with residues ^{104}EGCL^{107} was increased by nearly 1 Å, 0.5 Å and 1 Å respectively, in case of G151D (**Fig 4.18 a-f**). These differences might have lead to increase in space within the peptide binding pocket. These differences were reported to be decreased in case of R77-79K mutation in case of MtbPDF which lead to the reduction in size of substrate binding site (Saxena *et al.*, 2008). There has been a slight restructuring of the G151D mutant structure as seen from the CD spectrum. The side chain of the substituted aspartate was not pointing towards the substrate binding site, but has led to slight movements in the side chain atoms of residues lining the substrate binding pocket. These movements would have led to increase in size of the substrate binding pocket in G151D mutant compared to MtbPDF.

In our studies, G151D mutant was able to use substrates with bulkier side chains at P2' and P3' positions better than wild type which indirectly points out the overall increase in space within substrate binding site.

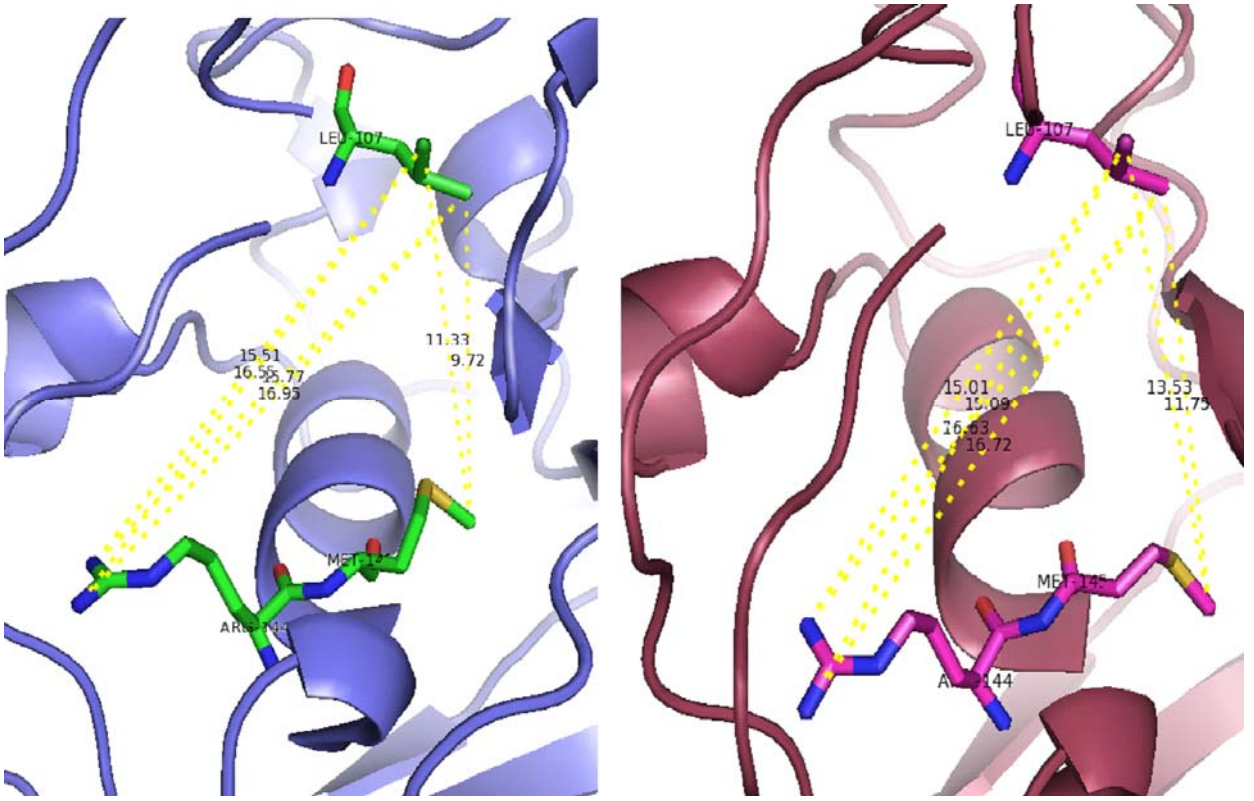

Fig 4.17: Distance between side chain atoms of L107 with side chain atoms of R144 and M145 delineating substrate binding site of MtbPDF (a) and G151D (b) structures. The distances are represented in Å

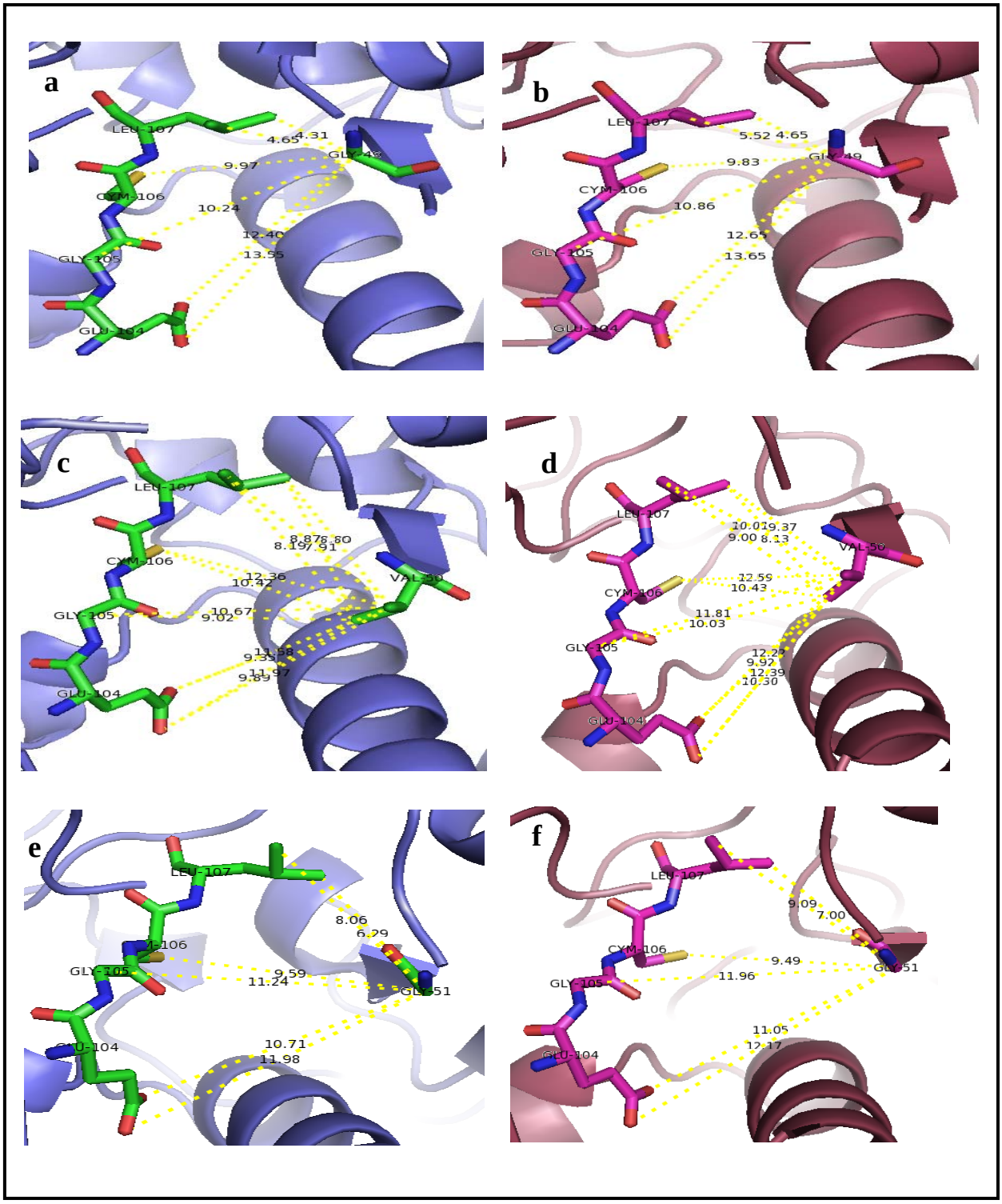

Fig 4.18: Distance between side chain atoms of G49, V50 and G51 with side chain atoms of ^{104}EGCL^{107} delineating substrate binding site of MtbPDF (a, c, e) and G151D (b, d, f) structures

Three arginines in the insertion sequence (^{77}RRR^{79}) (**Fig 4.1**) of MtbPDF were reported as responsible for the observed resistance to oxidative stress (Saxena *et al*., 2008). The higher sensitivity of G151D mutant to oxidizing agents made it interesting to look into the structural variations in the loop containing three arginines. During MD simulations, the distance between side chain of R78 and R79 and Fe^{2+} and did not show significant difference between MtbPDF and G151D structures, but the side chain of R77 in G151D was displaced by 3.5 Å from Fe^{2+}, loosing its stabilization from hydrogen bonding with side chain atoms of D128. This stabilization is present in case of MtbPDF structure (**Fig 4.19a** and **4.19b**). This destabilizes the loop containing three arginines, which was reported to interact with the core helix, in G151D mutant structure.

Mutation of R79, among the three arginines of MtbPDF, had more drastic effect on the stability and resistance to H_2O_2 of MtbPDF (Saxena *et al*., 2008). Results from the previous studies show that R79K and R79A mutations in MtbPDF did not affect its K_m value, infact the latter showed lower K_m value than wild type, but reduced the K_{cat} value drastically. This proves that mutating R79 do not affect substrate binding in the pocket, but affects the enzyme activity and stability due to global restructuring of the protein. So the reduction in size of substrate binding pocket in case of R77-79K, as predicted by molecular modeling and dynamics mutation in the previous study, would be attributed mainly to mutation of R77 and R78 than R79. R77K mutation did not affect the thermo-stability of the protein like the other two mutations, even though the CD spectrum of R77K showed highest blue-shift and scattering in mean residue ellipticty (θ) value compared to R78K or R79K (Saxena *et al*., 2008). It is interesting to note that in our case the higher scatter in mean residue ellipticty shown by CD spectra of G151D was accompanied by disturbances in the

side chain of R77, as seen from the modeling results. In the previous study, the decrease in resistance to H_2O_2 induced by different mutations was accompanied by an overall decrease in stability of the enzyme. But in these studies the increase in temperature stability of G151D mutant was accompanied by decrease in resistance to H_2O_2. The predicted mechanism of this interaction was an 'action-at-distance', where in the R77-79 present in the loop away from the active site, modulate the thermo-stability and resistance to H_2O_2 in case of MtbPDF (Saxena *et al.*, 2008). Even though, the side chains of arginines are reported to interact and scavenge oxygen (Lass *et al.*, 2002), the actual mechanism by which these residues prevent Fe^{2+} and / or metal coordinating cystein from getting oxidized is still not clear. In G151D, destabilization of the loop containing three arginines might have lead to increased oxidation of Fe^{2+} and / or metal coordinating cystein. More systematic studies on this property would unveil the underlying mechanism of action.

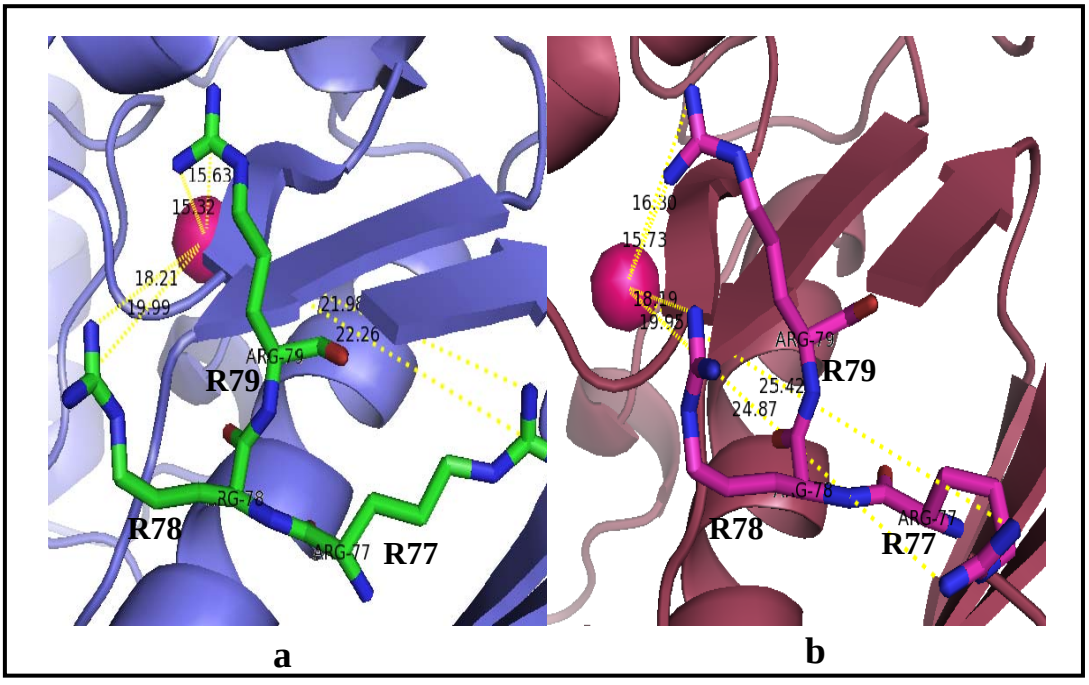

Fig 4.19: Movements of side chain atoms of R77-R79 residues in the insertion loop with reference to metal cofactor Fe^{2+} in MtbPDF (a, green sticks) and G151D (b, pink sticks) structures during dynamics.

4.3.5.2 Molecular Docking

The free energy of binding of substrate *N*-f-MAS into MtbPDF was -6.34 kcal/mol and for G151D was -7.25 kcal/mol. Superimposition of the two docked structures indicated that, the positioning of residues at P' and P_1' position of the substrate (formyl group and Met) were essentially the same in both cases (**Fig 4.20**). But residues at P_2' and P_3' positions of the substrate (Ala and Ser) were well aligned in case of G151D than MtbPDF. In MtbPDF, the lowest energy complex had substrate rotated almost 90^o between P_1' and P_2' in order to accommodate the side chains of residues at P_2' and P_3' positions in the pocket. In MtbPDF pocket, a single hydrogen bonding between CO of G105 and NH of substrate Met stabilized the substrate, where as in G151D pocket, substrate binding was stabilized by increased hydrogen bonding interactions such as the one between NH of substrate Ala and CO of G105, between NH of substrate Met and Nε2 of H148 and between OH of substrate Ser and NH of E104 (**Fig 4.21**). The low free energy for docking of *N*-f-MAS to G151D compared to the wild type structure clearly proves that there is higher affinity for substrate in case of G151D. This actually reflects our experimental results where there is a decrease in K_m value of G151D towards *N*-f-MAS leading to increase in catalytic efficiency of this mutant than wild type. The substrate is stabilized well in the peptide-binding site by additional H-bonding in case of G151D. The movement of the backbone and side chain atoms of the residues lining the peptide-binding site due to introduction of additional aspartate group produces slightly more space for substrate binding. Unlike MtbPDF, G151D was able to utilize substrates with bulkier groups at P1' and P2' positions like *N*-f-MLF to a better extent. This is an indirect evidence for the better space availability at P2' and P3' in case of G151D. The stability of substrate binding in case of G151D mutant was reflected

again by the increase in IC_{50} values of competitive inhibitor like actinonin. Docking results provided additional evidence for increased space in the peptide binding pocket of G151D, leading to stable substrate binding environment compared to MtbPDF.

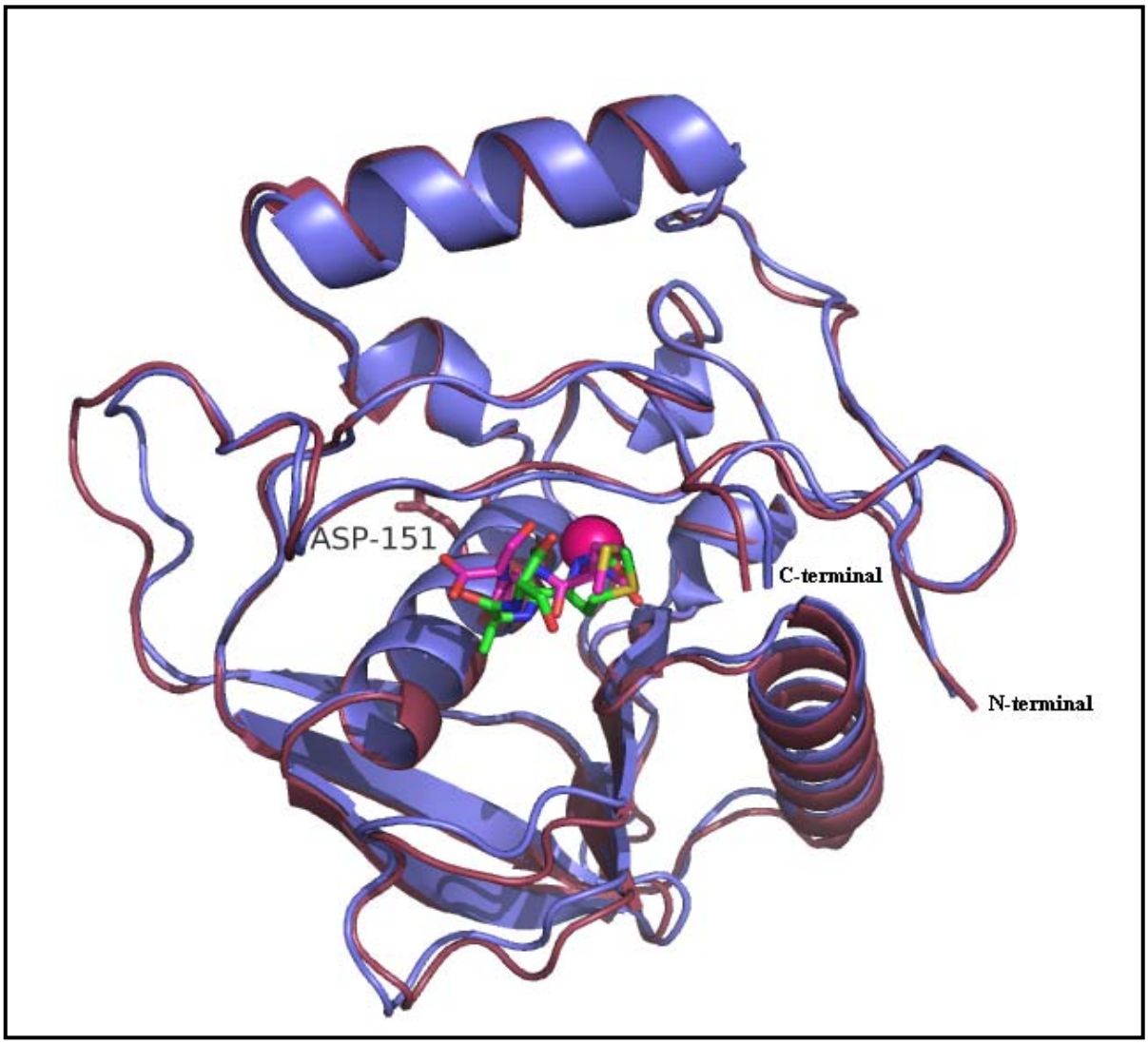

Fig 4.20: Superimposed cartoon models of MtbPDF (blue) G151D (brown) structures, in complex with substrate N-for-Met-Ala-Ser (shown as green & pink sticks in the substrate binding pockets of MtbPDF and G151D, respectively). Metal ion is shown as pink spear in the metal binding pocket. The side chain of substituted D151 is shown as brown stick protruding away from active site.

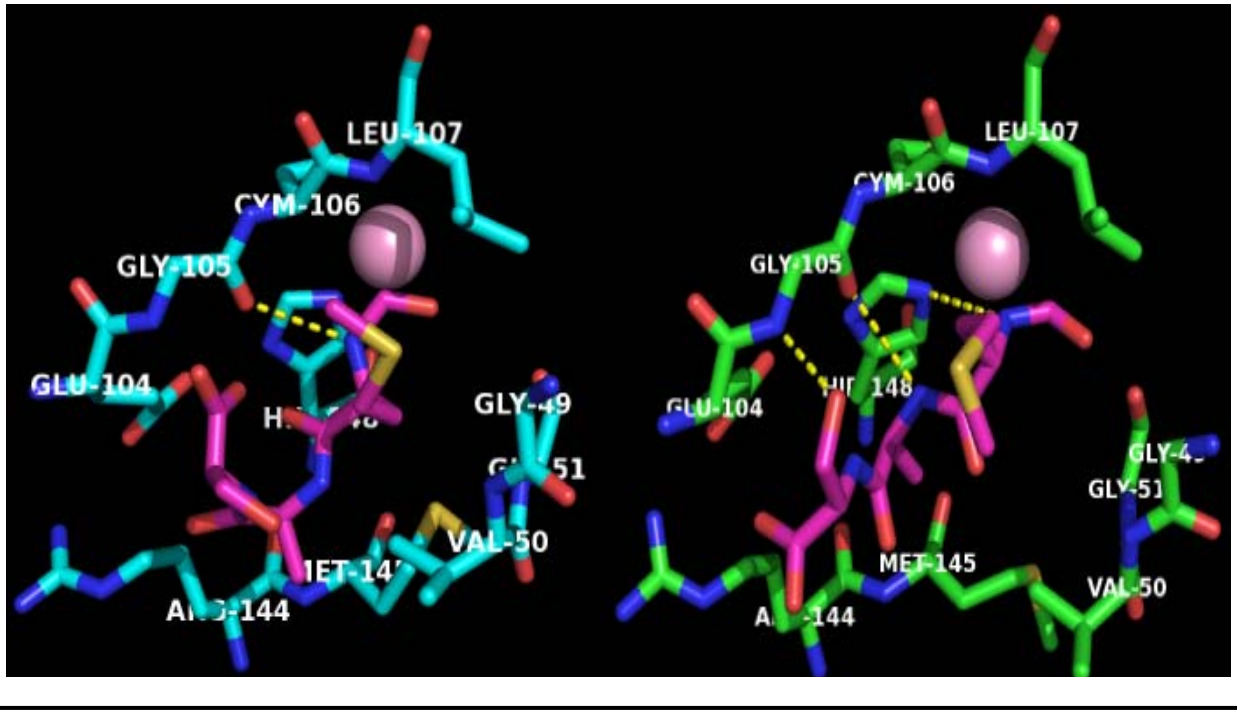

Fig 4.21: Closer look at the substrate binding site in MtbPDF and G151D structures with the *N*-f-MAS docked in it. Substrate binding sites of MtbPDF (Cyan) and G151D (Green) with substrate N-for-Met-Ala-Ser docked in (Pink sticks). The hydrogen bonds stabilizing the substrates in the cavity are shown as yellow dotted line.

4.3.6 MtbPDF: a sequence based evolutionary look

In order to see whether PDFs with glycine in motif III are present out side family Mycobacteriacea, a detailed examination of sequenced genomes (*www.genome.jp/kegg/*) (Until August 2010) of organisms belonging to different families in suborder Corynebacterineae (Nocardiaceae, Corynebacteriacea, Tsukamurellacea and Gordoniacea) was performed. The genome of *Nocardia farcinica, Corynebacterium diptheriae* and *Tsukamurella paurometabola* showed two genes and *Gordonia bronchialis* showed one gene coding for putative PDF. Of the two PDFs in these organisms, one had aspartate residue (D) and the other had glycine residue (G) before second metal binding histidine residue in motif III. *G. bronchialis* PDF had glycine in motif III like that of MtbPDF. For convenience, PDF

with aspartate is termed as PDF D and the one with glycine is termed as PDF G. Genome organizations of all PDF D showed association with methionyl-tRNA^{fMet} formyltransferase (*fmt*) in all these organisms, as in case of *E. coli* genome (Miennel *et al.*, 1995), where as PDF G was physically separated from *fmt* gene in the genome, as in case of *Mycobacterium* (Teo *et al.*, 2006). Extensive genome search outside suborder Corynebacterineae for orthologs of PDF G did not return any PDF sequence with glycine in motif III. Thus, due to the absence of a common ancestor with PDF G, it is understood that PDF G may be specific to suborder Corynebacterineae.

Multiple sequence alignments of PDF D and PDF G from these organisms with MtbPDF provided molecular distinction between the two at amino acid sequence level (**Fig 4.22**). Detailed examination of PDF G for reported molecular domains and signatures of MtbPDF (Saxena & Chakarborti, 2005a; 2005b) showed that all the PDF G had insertion region with three arginines (RRR) between motif I and motif II and C-terminal extension (CTE). Exception was seen in case of *Corynebacterium* PDF II, which lacked first two arginines in IR (**Table 4.3**). These observations were not in agreement with the previous claim that insertion region with three arginines are *Mycobacterium* specific (Saxena *et al*., 2008).

In an attempt to explore the evolution pattern of PDF with in suborder Corynebacterineae, anomalies were found with the linear course of evolution based on 16s rRNA (data not shown). Similar observations were previously reported in case for methionine aminopeptidases (MAP) and PDF in Firmicutes (You *et al*., 2005) and in case of many ribosomal proteins (Fang *et al*., 2005). PDF G was selected over PDF D in Mycobacteriacea as it evolved from its common ancestor. Rapid growing non-pathogenic

Mycobacterium evolved prior to slow growing pathogens (Gey van Pittius *et al.*, 2006). But PDF G was retained in pathogens with more than 90% homology and more than 80% identity in amino acid sequence with non-pathogens. Parallel divergences from the same common ancestor lead to evolution of other families in Corynebacterineae. PDF D and G were retained in all these families until evolution of family Gordoniaceae, the time corresponds to the evolution of pathogenesis and intracellular localizations in Mycobacterium. PDF D was lost and PDF G was retained in the genome of *G. bronchialis*. Recently sequenced genome of *Segniliparus rotundus* belonging to family Seginiliparacea under suborder Corynebacterineae, which evolved later to Gordoniaceae, showed only PDF G (Sikorski *et al.*, 2010). Thus during the course of evolution PDF G is selected and maintained over PDF D in families belonging to Corynebacterineae. Even though the PDFs with aspartate in motif III are proven to have better enzyme activity over PDFs with glycine in motif III, the later was selected in course of evolution. This suggests that PDF G might be advantageous over PDF D for the adaptive survival of the host organism to a particular niche. Analysis of the molecular signatures between PDF D and PDF G proved that the former could not accommodate the three arginines in the IR which are proved to be important in providing oxidative stress stability to PDF (**Fig 4.22** and **Table 4.3**). The results from G151D mutation in MtbPDF clearly demonstrated that the insertion region containing three arginines were destabilized during molecular dynamics. As a result, the oxidative stress stability of mutant protein was reduced. Thus, this glycine could be an adaptation for optimal arrangement of three arginines in the insertion sequences in order to impart oxidative stress stability to Fe^{2+} containing PDF G. Hence, this selection of glycine in motif III of PDF could be considered as an important step in evolution of intracellular pathogenesis, overcoming the oxidative stress with in macrophages, leading to successful

intracellular pathogens like *M. tuberculosis*. Studies on PDF from non-pathogenic mycobacterium like *M. smegmatis* may confirm whether the properties exhibited by MtbPDF are specific for pathogenic Mycobacterium. Similarly, results from the studies on both PDFs from organisms belonging to close families of Mycobacterium, like *N. farcinica*, will provide us good comparison for studying the evolution of properties exhibited by MtbPDF.

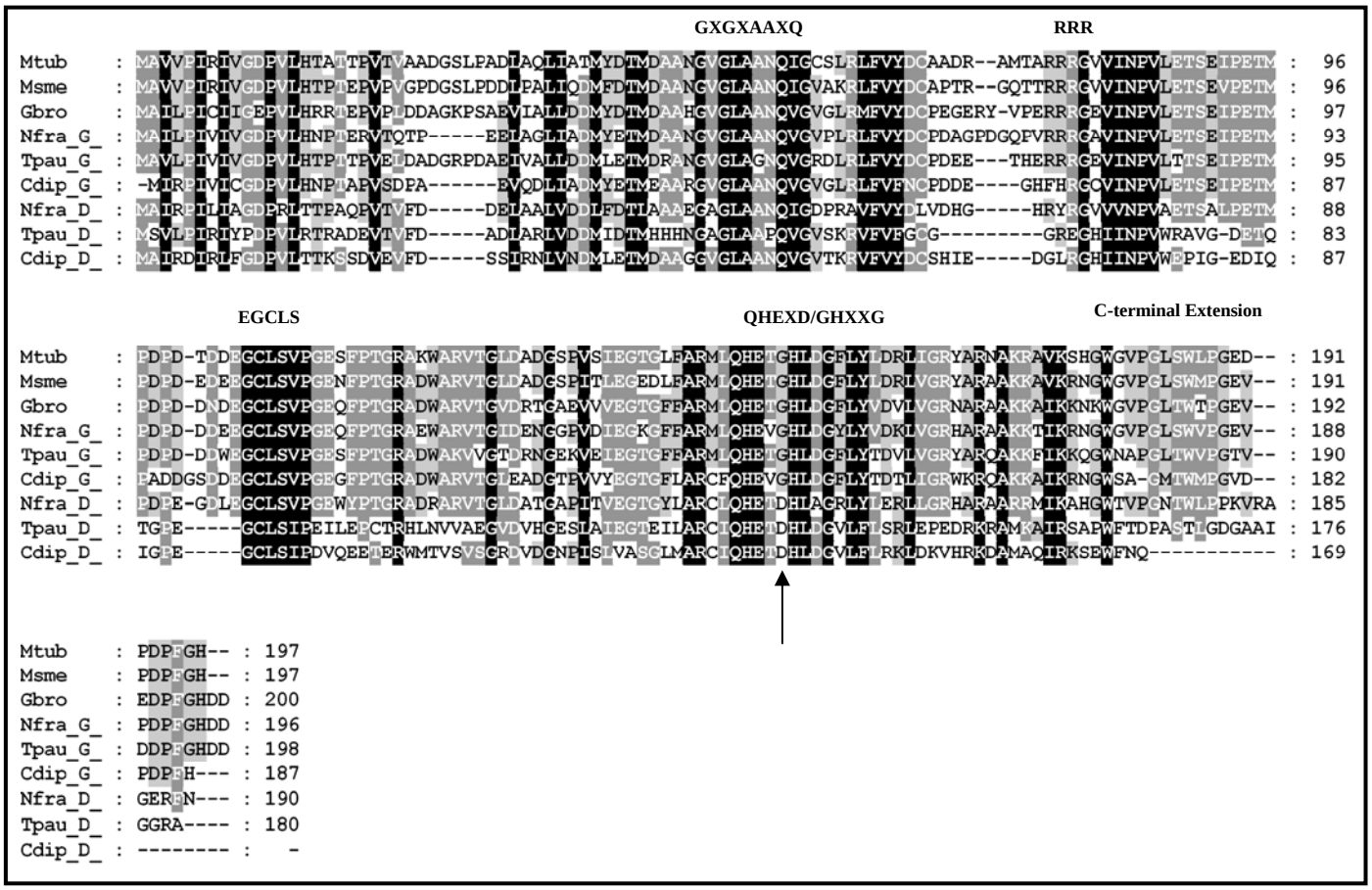

Fig 4.22: Multiple sequence alignment of PDFs from representative organisms from different families belonging to suborder Corynebacterineae showing the variations in molecular patterns between two types of PDFs in these families. The three conserved motifs, arginines in the insertion region and C-terminal extension are labeled above. *Mycobacterium tuberculosis* (Mtub), *Mycobacterium smegmatis* (Msme), *Nocardia farcinica* (Nfra), *Corynebacterium diptheriae (*Cdip*), Tsukamurella paurometabola (*Tpau*) and Gordonia bronchialis(*Gbro*).* Depending on glycine or aspartate in motif III of PDFs alphabet 'G' or 'D' is included following the names of organisms having two types of PDFs.

Table 4.3 Molecular patterns in PDFs from suborder Corynebacterineae

Organism –PDF (Protein - ID)	G/D[a]	RRR[b]	CTE[c]
Nocardia farcinica PDF D (Uniprot:Q5YWE2)	**D**	**R - R**	**+**
Nocardia farcinica PDF G (Q5YNT8)	**G**	**RRR**	**+**
Corynebacterium diptheriae PDF D (Q6NF56)	**D**	**- - R**	**+**
Corynebacterium diptheriae PDF G (Q6NH22)	**G**	**- - K**	**-**
Tsukamurella paurometabola PDF D (NCBI: 9157911)	**D**	**- R -**	**+**
Tsukamurella paurometabola PDF G (NCBI: 9156729)	**G**	**RRR**	**+**
Gordonia bronchialis PDF (D0L298)	**G**	**RRR**	**+**
Mycobacterium smegmatis PDF (A0QQP8)	**G**	**RRR**	**+**
Mycobacterium tuberculosis PDF (P96275)	**G**	**RRR**	**+**

***a*- Glycine or aspartate in motif III (This study). *b*- Three arginines in insertion sequences (Saxena & Chakraborti, 2005b; Saxena *et al,* 2008). *c*- Extended C-terminal region (Saxena & Chakraborti, 2005a).**

4. 4 Conclusions

The sequence variations and properties of bacterial enzymes compared to their human counter part will have to be explored further for the improvement of inhibitor screening process against peptide deformylase. The mutation G49C and L107E proved a major variation between the bacterial and human PDFs, in proving the reason behind the inactive state of human mitochondrial PDF. G151D mutation specifically differentiates MtbPDF from other bacterial and human enzymes at sequence level. Results from the present study bring out the molecular basis for one such property, i.e. oxidation stability, in MtbPDF. It is concluded from the study that aspartate residue in motif III of PDFs play

important role in providing stability to the enzyme and modulating the protonation of catalytic glutamate side chains. Presence of glycine instead of this aspartate in MtbPDF costs the thermo-stability of enzyme, instead, provides resistance to oxidative stress. Evolutionary selection of glycine over aspartate in motif III of PDF prior to *Mycobacterium* genera, leading to better survival of the organism in the oxidative environment, is a typical example of maintenance of beneficial mutations for better survival of the organism. Characterizing PDF from non-pathogenic Mycobacterium and from organisms belonging to related families will provide us a good comparison for studying the molecular basis for oxidative stress resistance in MtbPDF. The present study also describes the subtle variations in the peptide binding pocket of the enzyme associated with the above mentioned substitution, which could be further explored to design inhibitors with specificity towards MtbPDF. Cracking down the molecular basis of oxidative resistance of MtbPDF further will provide us with opportunities to design mechanistic-based inhibitors targeting MtbPDF, which prevents *M. tuberculosis* from survival within macrophages.

CHAPTER 5

Molecular Cloning, Expression, Purification and Characterization of Methionine Aminopeptidases (MAP) of *M. tuberculosis* H37Rv

CHAPTER 5

Molecular Cloning, Expression, Purification and Characterization of Methionine Aminopeptidases (MAP) of *M. tuberculosis* H37Rv

5.1 Introduction

Protein synthesis is always initiated with either methionine or N-formyl-methionine. Many newly translated proteins in both prokaryotic and eukaryotic cells are functional only after the initiator methionine is removed by the enzyme methionine aminopeptidase (MAP). This enzyme is ubiquitous in nature. Many putative MAP coding genes (*map*) have been found by sequence similarity and several of them have been shown to be functional in different organisms (Ben-Bassat et al., 1987; Chang et al., 1989; Wingfield et al., 1989; Li and Chang, 1995). MAPs have important physiological roles in cell, which makes them indispensable for growth and metabolism (Boxem et al., 2004; Bernier et al., 2005; Hu et al., 2006).The physiological importance of MAP enzymatic activity is underscored by the lethality of the deletion or inhibition of all MAP genes or gene products in *E. coli*, *Salmonella typhimurium* and *Saccharomyces cerevisiae* (Chang et al., 1989; Miller et al., 1989; Li and Chang, 1995). Due to its physiological importance in cells MAP has become an attractive drug target in recent years.

Based on amino acid sequence alignment, MAP is divided into two major classes (type I and type II) (Arfin et al., 1995; Bradshaw et al., 1998). Eubacteria possess only MAP1; archea have MAP2; while eukaryotes have both the classes (Lowther and Matthews,

2000). MAP2 are distinguished from MAP1 in having a 60-amino acid insertion within the catalytic domain. MAP1 enzymes are subdivided into type 1a and type 1b depending on the presence or absence of an N-terminal extension (Bradshaw et al., 1998). Type 1a enzymes have only the catalytic domain (e.g. *E. coli* MAP), where as type 1b enzymes have an N-terminal extension of about 120 amino acids including two zinc-finger domains with a linker to the catalytic domains (e.g. Yeast MAP1) (Lowther and Matthews, 2002). Crystallographic analysis of different MAP proteins have revealed a 'pita-bread' fold in its three dimensional structure with a pseudo two-fold-related N and C-terminal domains, each containing two α-helices and two antiparallel β-sheets (Roderick and Matthews, 1993; Tahirov et al., 1998). Both these domains contribute conserved residues to form the dinuclear metal-binding pocket. Two metal ions are bound by conserved monodentate (His-171, Glu-204 in *E. coli* MAP) and bidentate (Asp-97, Asp-108, Glu-235 in *E. coli* MAP) ligands. A metal-bridging water or hydroxide ion is thought to act as the nucleophile during catalysis (Lowther and Matthews, 2000).

MAPs are metallo-proteases requiring divalent metal ions for catalysis. Metal dependence studies have shown that MAPs can be activated by a number of divalent metal ions such as Co^{2+}, Zn^{2+}, Mn^{2+} and Fe^{2+}. However, the nature of the metal cation present in physiological situations remains unclear for MAP1s and MAP2s (Walker and Bradshaw, 1998; D'souza and Holz, 1999; D'souza et al., 2002). Early attempts to purify and crystallize MAPs involved Co^{2+} as the metal ion and most of the crystal structures published revealed two cobalt ions per polypeptide. But some bacterial MAP1s were later proved to be mononuclear Fe^{2+} containing metallo-enzymes based on structural and functional evidences (Cosper et al., 2001; Meng et al., 2002). In case of bacteria having multiple MAP enzymes,

there could be differences in the metal ion preferences. In contrast to this the human MAP2 enzyme is thought to be a manganese enzyme (Wang et al., 2003).

N-terminal methionine will be removed by MAPs only if the second residue is small and uncharged like Ala, Cys, Gly, Pro, Ser, Thr or Val (Lowther and Matthews, 2000). This substrate preference is opposite to the `N-end rule' for protein degradation (Varshavsky, 1997).

Previous drug discovery efforts for antibacterial therapies have focused primarily on PDF. However, emergence of resistant mutants might limit the utility of the PDF inhibitors, especially because the mutations in transformylase gene render deformylation nonessential. But, removal of initiating methionine is still crucial for protein maturity, posttranslational modifications, translocation and stability of a significant number of proteins (Olaleye et al., 2009). Thus, MAP has been considered as potent target for discovery of antibacterials, which would overcome the possible development of resistance against PDF inhibitors during treatment. Furthermore, several groups have reported potential roles of the eukaryotic MAP 2 inhibitors, like fumagillin and ovalicin, in targeting diseases such as cancer, rheumatoid arthritis, and fungal infections (Griffith et al., 1997; Griffith et al., 1998; Bradshaw and Yi, 2002; Chen et al., 2004). More recently, *Plasmodium falciparum* MAP 1b was reported as a potential anti-malarial target, and their inhibitors were identified with potent anti-malarial activity, both *in vitro* and *in vivo* (Chen et al., 2006).

Although there are some natural products like fumagillin and bengamide derivatives inhibiting MAP2, there are no natural MAP inhibitors discovered for bacterial MAPs. With lot of efforts from pharmaceutical chemists, some few chemical classes of *E. coli* MAP inhibitors were reported since 2003. Peptidic inhibitors and the methionine mimetic (3R)-

amino-(2S)-hydroxyheptanoic acid were the first reported MAP inhibitors for *E. coli* MAP with metallo-specificity (Li et al., 2003). Peptidyl hydroxamic acid derivatives were reported to have strong inhibitory activities towards *E. coli* MAP with low specificity (Hu et al., 2004). Later on pyrazole-diamine class of *E. coli* MAP inhibitors were also reported to show good MAP inhibition (Evdokimov et al., 2007).

The reports on MAPs as potential drug targets and the successful discoveries of bacterial MAP inhibitors have provoked researchers to characterize MAP proteins from various prokaryotic and eukaryotic organisms. With the alarming emergence of drug resistant TB, apart from the studies on PDF, it was decided to characterize MAP class of enzymes from *M. tuberculosis* to validate the extent to which it can be used as a drug target for the development of new antimycobacterials. There were not much biochemical studies on MAP enzymes from *M. tuberculosis* except like the one describing the structural relationships of MAP B protein of *M. tuberculosis* H37Rv with ribosomes (Addlagatta et al., 2005b). Earlier we were successful to purify and to characterize an enzyme from the cell lysates of *M. smegmatis* mc^2 155 showing MAP activity. The catalytic activities and inhibition of this MAP enzyme proved the relevance of Mg^{2+} as metal cofactor and actinonin as its inhibitor (Narayanan et al., 2008). This chapter summarizes the efforts to characterize the putative MAP proteins from *M. tuberculosis* H37Rv as recombinant proteins in order to bring out their salient biochemical and biophysical properties which could be useful in designing specific inhibitors against them.

5.2 Materials and Methods

5.2.1 Genome search

A complete genome search was done in the list of annotated genes of *M. tuberculosis* H37Rv genome (Cole et al., 1998) for genes coding for methionine aminopeptidase (*map* gene). *M. tuberculosis* H37Rv annotated genome was accessed from the Tuberculist website (*http://genolist.pasteur.fr/TubercuList*).

5.2.2 Primer designing

The nucleotide sequence of open reading frames (ORF) coding for putative *map* genes of *M. tuberculosis*H37Rv and the nucleotide based amino acid sequences were retrieved from the Tuberculist website. Based on the nucleotide sequences, specific primers were designed for amplification of *map* genes from the genomic DNA of *M. tuberculosis* H37Rv by polymerase chain reaction (PCR). The primers were designed according to the restriction map of the genes either with 5' linker sequences incorporating base sequences for restriction enzymes to facilitate directional cloning or by blunt end of the *map* amplicons into pET28a expression vector. The qualities of the designed primers were tested using online version of Net primer software. Primers were custom synthesized from Integrated DNA Technologies (IDT, USA).

5.2.3 PCR amplification and cloning of *map*A and *map*B genes

The two putative *map* genes annotated in the *M. tuberculosis* H37Rv genome, *map*A (Rv0734) and *map*B (Rv2861c) were amplified using chromosomal DNA of *M. tuberculosis* H37Rv as template by standard PCR strategies using *Pfu* DNA polymerases or *Taq* DNA polymerases according to Sambrook et al., (1989).

5.2.3.1 PCR amplification and cloning of Rv0734 (mapA)

The *map*A gene (Rv0734) was amplified using primers *map*A sense 5: 5'TGC GCC CAC TGG CAC GGC T 3' (designed for blunt end cloning) and *map*A antisense: 5'CCC CTC GAG CTA ACC GAG CGT CA (containing *Xho*I restriction site, underlined. The 801 base pair PCR product was purified from agarose gel, digested with *Xho*I and phosphorylated at the 5'end by T_4 polynucleotide kinase (Genei, India) reaction at 37 ^{o}C according to the manufacturer's protocol. On the other hand pET28a vector was digested with *Nde*I and was made blunt by filling the 5' overhang using DNA polymerase I (Klenow fragment) (Genei, India) at 37 ^{o}C according to the manufacturer's protocol. The end-filled vector was dephosphorylated using calf intestinal phosphatase (CIP) reaction (Genei, India) at 37 ^{o}C. Finally the blunt-dephosphorylated vector was digested with *Xho*I to produce a blunt/sticky pET28a vector. The *map*A insert with phosphorylated 5' end was ligated in-frame with N-terminus 6x His-tag of pET28a vector using T_4 DNA ligase at 22 ^{o}C. The ligation mix was transformed into *E. coli* DH5α chemical competent cells (2.3.2) and recombinants were screened from the mobility shifts of plasmids isolated (2.3.1) on agarose gel. Recombinant pET28a: *map*A plasmids were confirmed by releasing the insert by double digestion with *EcoR*V and *Xho*I and were further verified by DNA sequencing (Scigenomics, India) of both the strands. The confirmed recombinant constructs were transformed into *E. coli* BL21 (DE3) chemical competent cells.

5.2.3.2 PCR amplification and cloning of Rv2861c (mapB)

The *map*B gene (Rv2861c) was amplified using the primers, *mapB* sense 5'ACC ATA AAT GCT AGC CAT ATG CCT AGT C 3' (containing a *Nde*I restriction site, underlined) and *mapB* antisense 5'GCC CTC GAG GAA TTC TAA CTA CAG ACA GGT

3' (containing a *EcoR*I restriction site, underlined). The 858 base pair PCR product was purified, digested with *Nde*I and *EcoR*I, and ligated in-frame with N-terminus 6x His-tag of pET 28a vector digested with these enzymes, using T_4 DNA ligase at 22 ^{o}C. The ligation mix was transformed into *E. coli* DH5α chemical competent cells (2.3.2) and recombinants were screened from the mobility shifts of plasmids isolated (2.3.1) on agarose gel. Recombinant pET28a: *map*B plasmids were confirmed by releasing the insert by double digestion with *EcoR*I and *Nde*I and were further verified by DNA sequencing (Scigenomics, India) of both the strands. The confirmed recombinant constructs were transformed into *E. coli* BL21 (DE3) chemical competent cells.

5.2.4 Over-expression of recombinant MtbMAP proteins

Over-expression of recombinant MtbMAP proteins was done similarly to that of MtbPDF, with slight modifications in the post-induction phase according to D'souza and Holz (1999). Overnight culture of *E. coli* BL21 (DE3) carrying pET28a: *map*A or pET28a: *map*B was inoculated into 100 ml of LB broth supplemented with 30 μg/ml kanamycin and was incubated at 37 °C and 200 rpm until the $OD_{600\ nm}$ reached 0.6 - 0.7. The culture was then induced with 0.5 mM IPTG and allowed to grow for another 12 h at 30 °C, 200 rpm and the cells were harvested by centrifugation at 8000 rpm, 4 ^{o}C for 15 min. The cell pellets were stored at -80 ^{o}C until use. The pellets were resuspended in 5 ml of ice-cold lysis buffer (20 mM phosphate buffer, pH 7.4, 300 mM NaCl, 5 mM imidazole, 10 μg/ml catalase, 1 mM PMSF, 10 μl protease inhibitor cocktail for his-tagged proteins and 0.5 mg/ml lysozyme) and left on ice for 30 min. The cells were then disrupted by sonication (5 cycles of 30 s ON 30 s OFF at 42% amplitude) and the resulting lysate was centrifuged at 13,000 rpm for 30 min at 4 °C to recover the soluble proteins in the supernatant. The insoluble

pellet fractions were washed twice with ice-cold lysis buffer containing 2% Triton X-100. The washed pellet was solublised in 3 ml of urea buffer (20 mM phosphate buffer, pH 7.4, 300 mM NaCl, 5 mM imidazole, 10 μg/ml catalase, 5 mM DTT and 3 M urea) for 30 min by continuous stirring with a magnetic bead at 4 ^{o}C. The solublised proteins in urea fractions were recovered by centrifugation at 13,000 rpm for 30 min and this step was repeated to recover complete recombinant proteins. All the different fractions containing proteins were analyzed by running them on 12% SDS-PAGE (2.4.1.1). The recombinant proteins were further confirmed by Western blotting using anti-His antibodies (2.4.1.2). Total protein contents in samples were quantified using Bradford's assay (2.4.2.1).

5.2.5 Purification and preparation of apo-enzymes of MtbMAP A and MtbMAP B

Recombinant proteins in the soluble fractions were purified under native conditions by passing through Ni-affinity column (Qiagen, Germany) as described in 2.3.3. In order to remove the metal-cofactors in the MAP enzymes to produce apo-enzymes, the proteins were eluted from the column using an elution buffer containing 250 mM imidazole into EDTA (concentration), making its a final concentration of 100 mM EDTA. EDTA was later removed by extensive dialysis against the activity buffer (50 mM Tris-Cl, pH 8.0, 150 mM KCl) (Mitra et al., 2006) at 4 ^{o}C with two buffer exchanges. The purified apo-enzymes were concentrated using 10 kDa amicon centri-concentrators (Millipore, India) to 1 mg/ ml and were stored at -80 ^{o}C until use. For all assay purposes enzymes were diluted in the activity buffer to a final concentration of 10 μg/ ml.

5.2.6 MAP assay

The enzyme assay was adopted from Mitra *et al*., (2006) using L-Met-*p*-Nitro anilide (L-Met-*p*NA) as substrate, with slight modifications as described in 2.4.3.2. MAP activities

of apo-MtbMAP A and apo-MtbMAP B were assayed in presence of 0.2 mM $CoCl_2$ (Zhang et al., 2009) with 1 mM L-Met-*p*NA as substrate using 1.6 μg (0.22 μM) of purified apo-MtbMAP A (MW~ 29 kDa) and purified apo-MtbMAP B (0.2 μM) (MW~ 32 kDa) in assay buffer (50 mM Tris-Cl, pH 8.0, 100 mM KCl), pH 8.0 at 37 ^{o}C in a total reaction volume of 250 μl. The enzyme activities were expressed as μM *p*NA released/min/mg protein.

5.2.7 Biochemical and Biophysical characterization of purified MtbMAPs

5.2.7.1 Substrate specificity of MtbMAPs

Substrate specificity of MtbMAP A and MtbMAP B were analyzed using *p*-NA derivatives of different *N*-terminal amino acids like methionine, glycine, arginine, proline, leucine and valine in the standard MAP assay in presence of 0.2 mM $CoCl_2$ (Ramırez-Zavala et al., 2004). Their activities were represented as percentage relative activities of the enzymes with L-Met-*p*-NA.

5.2.7.2 Metal ion preferences of MtbMAP A and MtbMAP B

The necessity for divalent metal ions in catalysis of MAP enzyme is very well established fact from the studies on MAP enzymes from various prokaryotic, eukaryotic and archaebacterial sources (Bradshaw et al., 1998; Tahirov et al., 1998; Walker and Bradshaw, 1999). In order to characterize the metal ion preferences of MtbMAP A and MtbMAP B, apo-enzymes of these two proteins at concentrations 0.22 μM and 0.275 μM, respectively, were assayed in presence of varying concentrations (1-1000 μM) of divalent metal ions like Co^{2+}, Ni^{2+}, Mn^{2+}, Mg^{2+} and Fe^{2+} while performing standard MAP assay with L-Met-*p*NA as described earlier in 2.4.3.2. Appropriate metal ion blanks were performed to cancel out any background absorbance. The activities were expressed as μM *p*NA released/min/mg protein.

The optimum concentrations of the best activator for each of the enzymes were selected for performing all the further characterizations.

5.2.7.3 MAP activities of MtbMAPs as a function of enzyme concentration

At the optimum concentration of best activating divalent metal ion, MAP activities at various concentrations of MtbMAP A (0.16 to 1.6 μg) and MtbMAP B (0.2 to 2 μg) were studied by performing standard MAP assay against 1 mM L-Met-*p*NA. The metal ion used in case of MtbMAP A was Ni^{2+} and Co^{2+} at 100 μM and 40 μM concentrations respectively and in case of MtbMAP B both these were used at 100 μM concentrations. The activities were represented as μM *p*NA / min at each protein concentrations.

5.2.7.4 Temperature and pH optimum for MtbMAPs

Enzyme activities of MtbMAP A and MtbMAP B were carried out at different temperatures ranging from 10 - 80 ^{o}C and in different pH buffers from pH 3.5 - 10.5 to find out the optimum temperature and pH for their activities. The standard MAP assay was performed at these indicated temperatures at pH 8.0 and in assay buffers of different pH at 37 ^{o}C. The buffers used to set different pH were 50 mM of citrate buffer (pH 4.8), sodium acetate buffer (pH 3.5-5.0), phosphate buffer (pH 5.5- 7.5), Tris-Cl buffer (pH 8- 9.5) and sodium-glycine buffer (pH 9.5-10.5), all of them containing 100 mM KCl.

5.2.7.5 Enzyme kinetics of MtbMAPs

Continuous MAP assay was performed against various concentrations of L-Met-*p*-NA (0-1 mM) at room temperature at pH 8.0 using 0.22 μM MtbMAP A and 0.275 μM MtbMAP B in presence of optimized concentrations of Ni^{2+} and Co^{2+}. Reaction rates of MtbMAP A and MtbMAP B at various concentrations of substrate L-Met-*p*-NA were calculated from linear cure fits of μM *p*-NA released *vs* time data. K_m and V_{max} were

determined from slopes of various concentrations of substrate by applying a non-linear curve fit. Kinetic analysis was performed using Graph Pad Prism version 5.0 (Graph pad software, San Diego CA). The turnover number, K_{cat} value was determined directly from the software by applying the formula $K_{cat} = V_{max} / [E_T]$, where V_{max} is the maximum velocity and E_T is the total enzyme concentration.

5.2.7.6 Thermo-stability of MtbMAPs

Thermo-stabilities of MtbMAPs A were determined as it was described by Karadzic et al., (2002) with necessary modifications. Thermo-stability was assessed by pre-incubating 20 μg purified apo-enzymes of MtbMAP A and MtbMAP B at pH 8.0 at 37 ^{o}C and 55 °C. The enzyme activities were monitored at 37 ^{o}C by adding aliquots of pre incubated 0.22 μM MtbMAP A and 0.275 μM of MtbMAP B in the standard MAP assay in presence of optimized concentrations of Ni^{2+}, over a period of 1 h at every 10 min intervals. The residual activities at each time intervals were represented as percentage relative activities of enzyme activity at time 0.

5.2.7.7 Effect of metallo-protease inhibitors on MtbMAPs

The effects of potential metallo-protease inhibitors such as bestatin, amastatin (Rich et al., 1984), actinonin (Chen et al., 2000) and fumagillin (Lowther et al., 1998) were tested on metal-loaded apo-enzymes of both MtbMAP A and MtbMAP B at three different concentrations (0.1, 1 and 10 μM) in the standard MAP assay. The inhibitors were dissolved in 100% DMSO and 0.22 μM of MtbMAP A and 0.275 μM of MtbMAP B in presence of 100 μM Ni^{2+} was incubated with the above mentioned concentrations of these inhibitors for 15 min at room temperature prior to starting the standard MAP assay with 1 mM L-Met-*p*-NA. Corresponding inhibitor blanks were also performed. The uninhibited reaction in each

case was taken as control and the results were expressed as percentage relative activity of the control.

5.2.7.8 Feedback inhibition of MtbMAPs by L-methionine

In order to check whether multiple MAP enzymes in *M. tuberculosis* have any role to play in methionine metabolism or whether their activities are any way regulated by feedback inhibition by L-methionine, standard MAP assay was performed using MtbMAP A (0.22 μM) and MtbMAP B (0.275 μM) in presence of varying concentrations (0 -100 μM) of L-methionine with 1 mM L-Met-*p*-NA as substrate. Corresponding blank reactions using L-methionine was performed and values were corrected by subtracting appropriate blanks. Results were represented as the percentage relative activities of the uninhibited reactions.

5.3 Result and Discussion

5.3.1 Genome search for *map* gene in *M. tuberculosis* H37Rv

Search for methionine aminopeptidase gene (*map*) in *M. tuberculosis* H37Rv genome returned two putative *map* genes i.e. *map*A (Rv0734) and *map*B (Rv2681c) (**Table 5.1** and **5.2**). The translated nucleotide sequences were also retrieved from the same website and it showed polypeptides of 266 aa (~28 kDa) and 285 aa (~32 kDa) (**Table 5.1** and **5.2**) for MtbMAP A and MtbMAP B proteins respectively.

Table 5.1 Nucleotide and amino acid sequence of *map*A gene of *M. tuberculosis*

➢ ***M. tuberculosis* H37Rv|Rv0734|mapA: 801 bp – PROBABLE METHIONINE AMINOPEPTIDASE MAP A**

```
atgcgcccactggcacggctgcggggtcgcagggtcgtgccgcagcgcagtgccggcgaa
ctcgacgcgatggccgcggcgggcgccgtcgttgccgccgcgctgcgggcgatccgtgcg
gcagcggctcccggcacatccagcctgagtctcgacgagatcgccgagtcggtgatccgc
gaatccggcgccaccccgtcgtttctgggctatcacggctacccggcctcgatctgcgcg
 tcatcaacgaccgggtggttcatggcatcccgtcgaccgccgaggtgctcgcgcccggtg
 atctggtatccatcgactgcggtgcggtgctggacggttggcatggcgatgcggcgatca
 ctttcggggttggcgccctgagcgacgccgacgaagcgctgtcggaggcgacaagggaat
 cgcttcaggccggcatcgccgcgatggtggtcggcaatcggttgaccgacgtcgcgcatg
 ccatcgaaacgggtacccgtgccgccgagctccgttatggacgctcgttcgggatcgtcg
 ccggttacgggggccacggcatcggccgccagatgcatatggatccgttcttgccgaacg
 agggtgcgccggggcgcggtccgctgctggctgccggctcggtgctggccatcgaaccga
 tgctgaccctcggtaccaccaaaacggtggtgctcgacgacaaatggacggtcacgaccg
 ccgatgggtcacgtgcggcacactgggaacacaccgtggcggtaaccgacgacgggcccc
 gaattctgacgctcggttag
```

➢ ***M. tuberculosis* H37Rv|Rv0734|mapA: 801 bp – PROBABLE METHIONINE AMINOPEPTIDASE MAP A**

MRPLARLRGRRVVPQRSAGELDAMAAAGAVVAAALRAIRAAAAPGTSSLSLDEIAESV
RESGATPSFLGYHGYPASICASINDRVVHGIPSTAEVLAPGDLVSIDCGAVLDGWHGDAAI
TFGVGALSDADEALSEATRESLQAGIAAMVVGNRLTDVAHAIETGTRAAELRYGRSFGIV
AGYGGHGIGRQMHMDPFLPNEGAPGRGPLLAAGSVLAIEPMLTLGTTKTVVLDDKWTVTT
ADGSRAAHWEHTVAVTDDGPRILTLG

Table 5.2 Nucleotide and amino acid sequence of *map*B gene of *M. tuberculosis*

***M. tuberculosis* H37Rv|Rv2861c|mapB: 858 bp - PROBABLE METHIONINE AMINOPEPTIDASE MAPB**

```
atgcctagtcgtaccgcgctctcccccggcgtgctgtccccgacacggccggtgcccaac
tggatcgcgcgccccgaatacgtcggcaaaccggccgcccaagagggcagcgagccgtgg
gtgcagacacctgaggtcatcgagaagatgcgcgtggcaggccggatcgccgcaggtgcg
ttggccgaggcgggcaaggcggtcgcgcccggggtaaccaccgacgaactcgaccggatc
gcgcacgaatacctggtcgacaacggcgcctacccatcaacgctgggctacaagggattc
ccgaagtcgtgctgcacgtccctcaacgaggtcatctgccatggaatccccgactcgacg
gtgatcaccgacggcgacatcgtcaacatcgacgtcaccgcctacatcggtggggtgcac
ggtgacaccaacgcgacgtttccggccggcgatgtcgcagacgaacaccggttgctcgtt
gaccggacccgcgaagcgaccatgcgtgcgatcaacaccgtcaagcccgggcgggcgttg
tccgttatcggtcgtgtcatcgagtcgtatgcaaatcggttcgggtacaacgtggttcga
gacttcactggtcatggcatcggcacgacgttccacaacgggctggtcgtcttgcactac
gaccagcccgctgtcgagaccatcatgcagccggggatgaccttcaccatcgagccgatg
atcaacttgggcgcactggactacgaaatctgggacgacggttggacggtggtcaccaag
gaccgcaagtggaccgcacagttcgaacacaccctgctggttaccgataccggcgtcgag
 atcctgacctgtctgtag
```

***M. tuberculosis* H37Rv|Rv2861c|MapB: 285 aa - PROBABLE METHIONINE AMINOPEPTIDASE MAPB**

MPSRTALSPGVLSPTRPVPNWIARPEYVGKPAAQEGSEPWVQTPEVIEKMRVAGRIAAGA
LAEAGKAVAPGVTTDELDRIAHEYLVDNGAYPSTLGYKGFPKSCCTSLNEVICHGIPDST
VITDGDIVNIDVTAYIGGVHGDTNATFPAGDVADEHRLLVDRTREATMRAINTVKPGRAL
VIGRVIESYANRFGYNVVRDFTGHGIGTTFHNGLVVLHYDQPAVETIMQPGMTFTIEPM
INLGALDYEIWDDGWTVVTKDRKWTAQFEHTLLVTDTGVEILTCL

5.3.2 PCR amplification and cloning of *map* genes

*map*A and *map*B genes were amplified from the genomic DNA of *M. tuberculosis* using gene specific primers at annealing temperature of 60 ^{o}C and 59 ^{o}C respectively. **Table 5.3** and **5.4** shows the optimized PCR program for amplification of *map*A and *map*B, respectively. Inclusion of 8% DMSO in the reaction mixture facilitated better amplification of *map*A gene. The amplicons of *map*A and *map*B showed an expected size of 801 bp and 858 bp respectively on 1% agarose gel (**Fig 5.1a** and **5.1b**). The amplified *map*A gene was ligated as blunt/sticky insert into *Nde*I / *Xho*I restriction sites of pET28a vector, where as *map*B was ligated as sticky end inserts into *Nde*I / *EcoR*I sites of pET28a (**Fig 5.2**). The recombinant pET28a: *map*A plasmid was confirmed by double digestion of the plasmid with *EcoR*V and *Xho*I, which released a DNA fragment of size which was approximately 801 bp higher than the release from pET28a plasmid alone (**Fig 5.3a**) and in the case of pET28a: *map*B plasmid, *Nde*I / *EcoR*I digestion released a 858 bp DNA fragment (**Fig 5.3b**). Both these recombinant plasmids were DNA sequenced with T_7 forward primer to confirm the in-frame insertion of *map*A and *map*B genes into pET28a vector without any PCR artifacts (**Fig 5.4a** and **5.4b**).

Table 5.3 PCR conditions for amplification of *map*A gene (Rv0734)

Cycles	Temperature (^{o}C)	Time
1	**94**	**5 min**
30	**94**	**45 sec**
	60	**30 sec**
	72	**1 min**
1	**72**	**10 min**

Table 5.4 PCR conditions for amplification of *map*B gene (Rv2861c)

Cycles	Temperature (^{o}C)	Time
1	**94**	**3 min**
30	**94**	**30 sec**
	59	**2 min**
	72	**1 min**
1	**72**	**10 min**

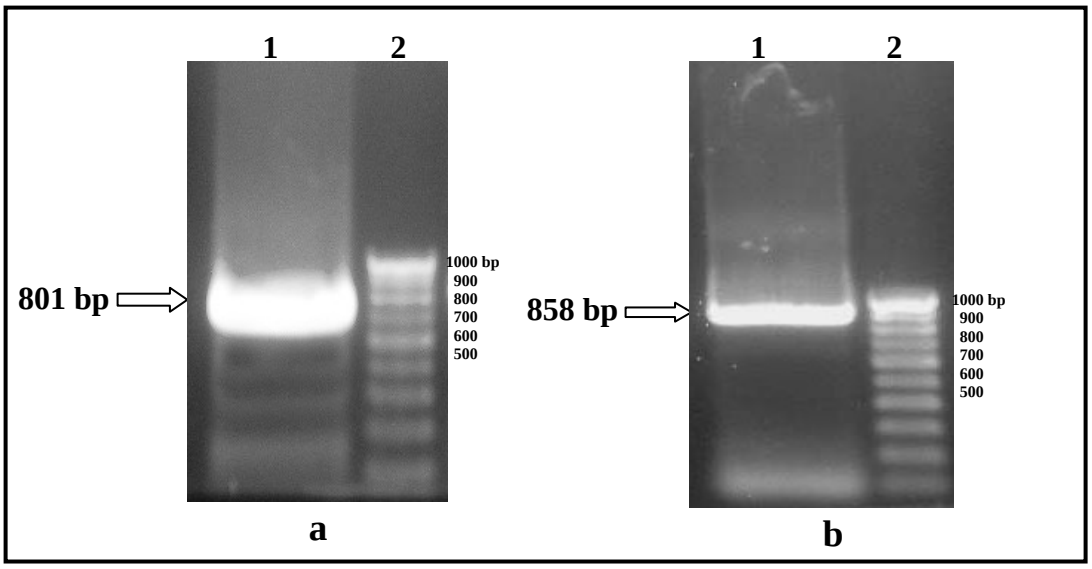

Fig 5.1: PCR amplification of *map* genes of *M. tuberculosis.* (a) *map*A amplification; Lane 1: *map*A amplicons; Lane 2: 100 bp DNA ladder; (**b)** *map*B amplification; Lane 1: *map*B amplicons; Lane 2: 100 bp DNA ladder.

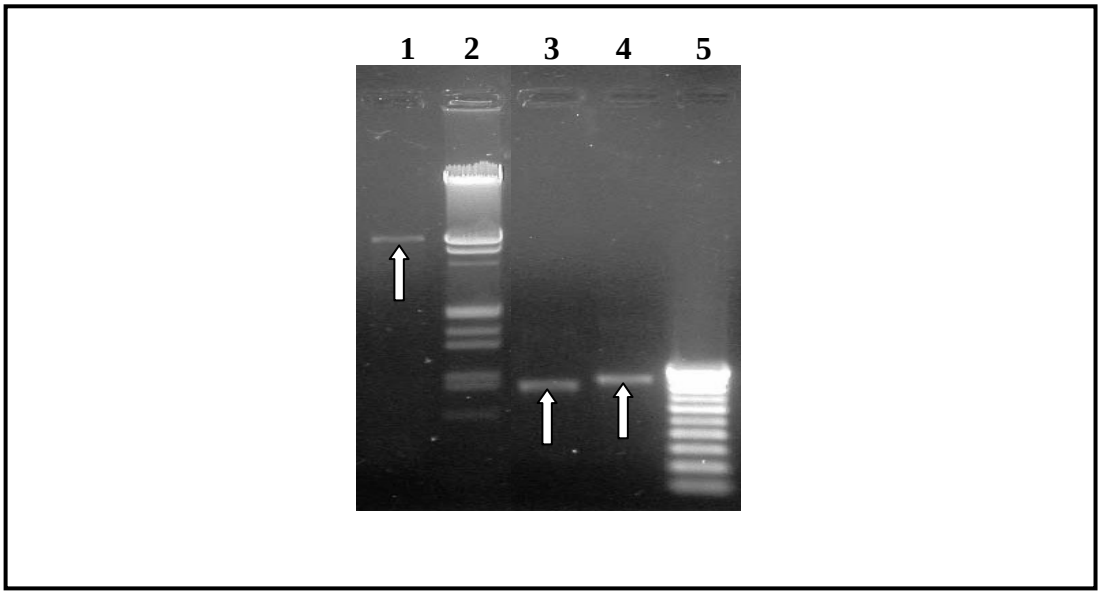

Fig 5.2: Digested pET28a vector and *map* inserts for ligation. Lane 1: pET 28a double digested with *Nde*I / *EcoR*I; Lane 2: λ DNA *EcoR*I/ *Hind* III double digest DNA ladder; Lane 3: *map*A blunt / sticky insert (801 bp) prepared for blunt-sticky ligation into *Nde*I and *Xho*I sites of pET28a; Lane 4: *map*B insert (858 bp) double digested with *Nde* I and *EcoR* I; Lane 5: 100 bp DNA ladder.

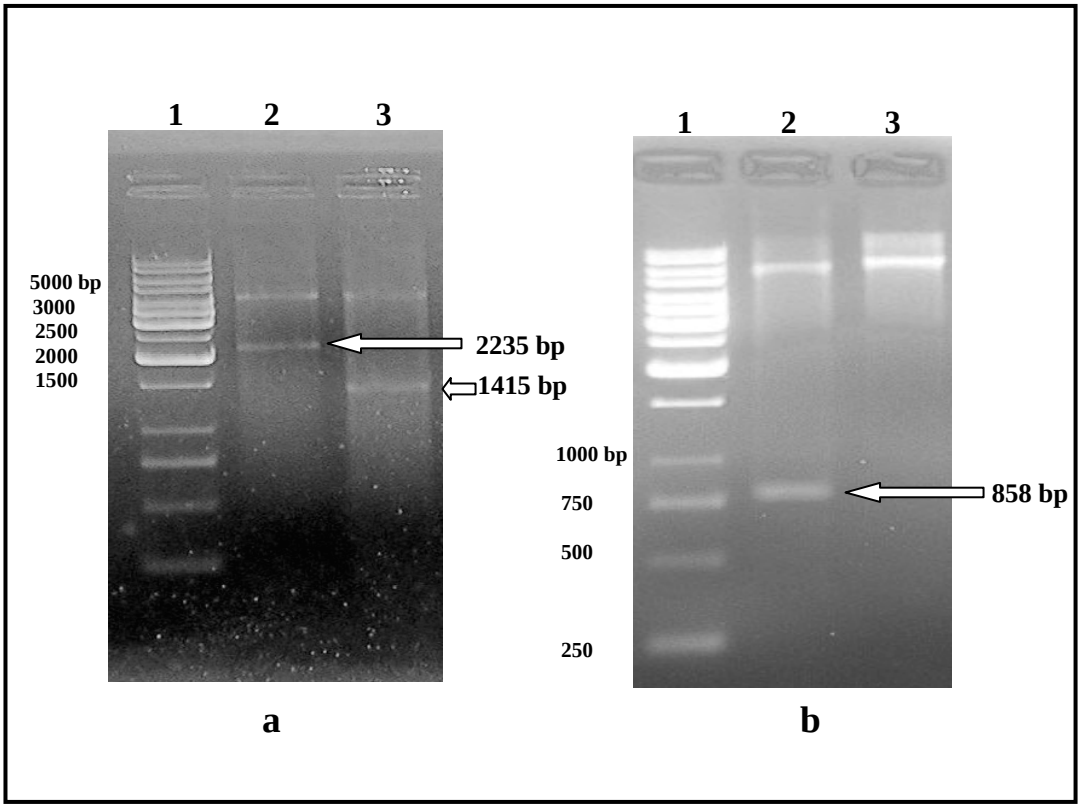

Fig 5.3: Confirmations of pET28a: *map* recombinants by double digestion. **(a)** Confirmation of pET28a: *map*A plasmid by double digestion with *EcoR*V and *Xho*I; Lane 1: 1 kb DNA ladder; Lane 2: pET28a: *map*A *EcoR*V/ *Xho*I double digest releasing a 2235 bp fragment containing *map*A gene; Lane 3: pET28a plasmid *EcoR*V/ *Xho*I double digest. **(b)** Confirmation of pET28a: *map*B plasmid by double digestion with *Nde*I and *EcoR*I; Lane 1: 1 kb DNA ladder; Lane 2: pET28a: *map*B double *Nde*I / *EcoR*I double digest releasing 858 bp fragment of *map*B; Lane 3: pET28a: *map*B single digest with *Nde*I showing the mobility shift with reference to the double digested fragment.

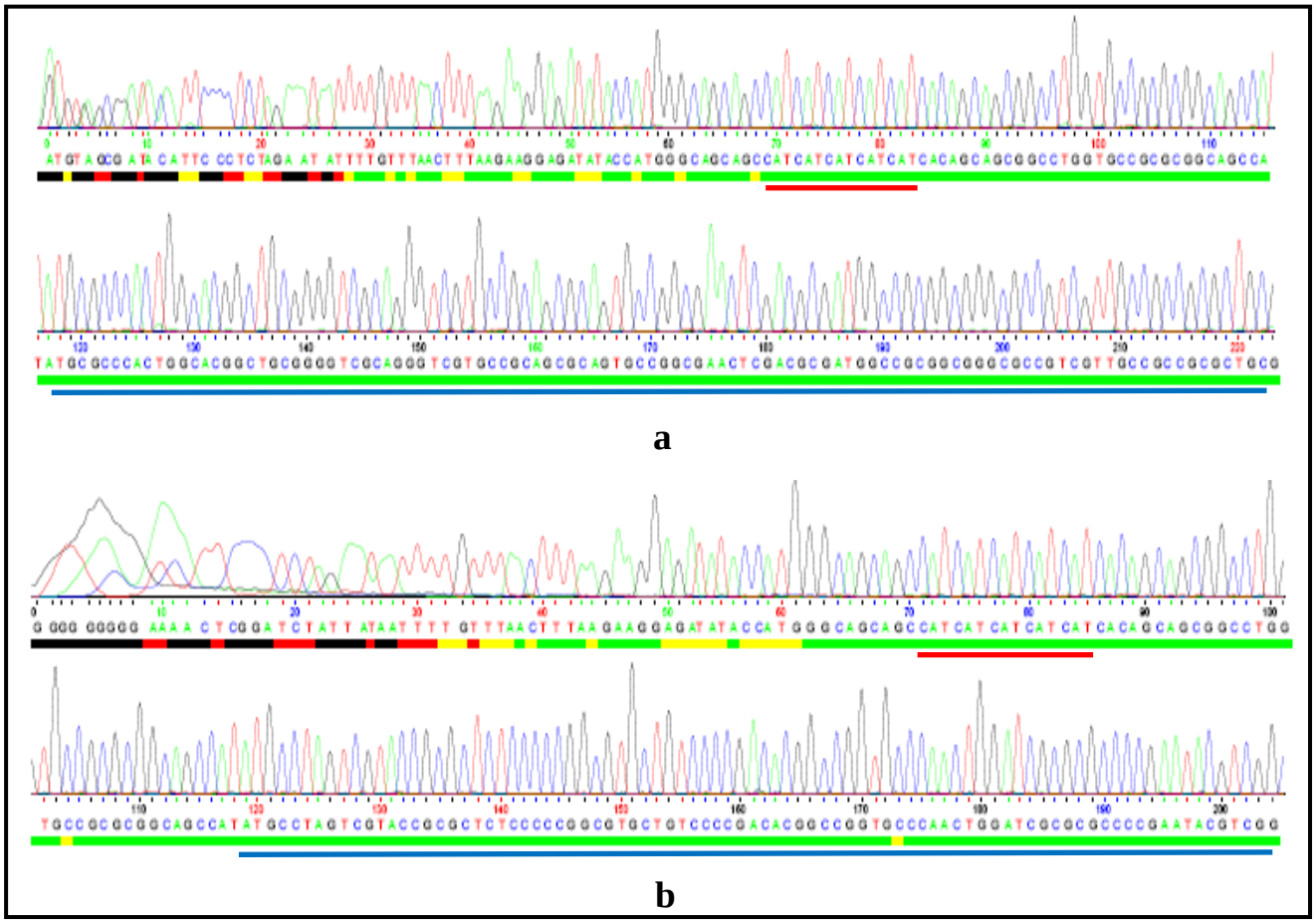

Fig 5.4: DNA sequencing chromatogram of (a) pET28a: *map*A plasmid (b) pET28a: *map*B plasmid using T_7 primer. The in-frame insertion of *map*A and *map*B gene (underlined with blue line) at *Nde* I site was confirmed. Sequences coding for N-terminal penta-His tag is underlined in red in both the cases.

5.3.3 Over expression, purification and Western blotting of recombinant MtbMAPs

Upon over expression in *E. coli*, both MtbMAP A and MtbMAP B got expressed in high levels. Eventhough majority of MtbMAP A, over expressed in *E. coli*, was seen in the insoluble pellet fractions, it could be successfully solublised in high levels with 3 M urea containing lysis buffer. In case of MtbMAP B, majority of the over expressed proteins were seen in the soluble fractions and only small amount were solublised from the insoluble pellet fraction. Recombinant MtbMAP A showed molecular weight of 29 ± 1 kDa, inclusive of the

N-terminal His-tag, on 12% SDS-PAGE. MtbMAP B, along with N-terminal His-tag, showed a molecular weight of 32 ± 1 kDa on 12% SDS-PAGE (**Fig 5.5a** and **5.5b**). Both these molecular weights were in accordance with the calculated theoretical molecular weights. Some of the recent studies on MtbMAPs have reported similar kinds of molecular weights for both MtbMAP A and MtbMAP B (Zhang et al., 2009; Lu et al., 2010; Olaleye et al., 2010; Lu and Ye, 2010). Zhang et al., (2009) confirmed these molecular weights by performing matrix-assisted laser desorption ionization time-of-flight (MALDI-TOF). MtbMAP B was confirmed to be a monomeric protein with approximate molecular weight of 31 kDa in solution by size-exclusion chromatography, even though they showed trimeric state during crystallization (Lu et al., 2010). In another study, we could purify a putative protein showing MAP activity from the cell lysate of *M. smegmatis* mc^2 155 having subunit molecular weight of ~ 37 kDa (Narayanan et al., 2008). The molecular weight of prototype *E. coli* MAP is 29 ± 1 (D'souza and Holz, 1999) and that of N-terminal truncated human type I MAP is 36 ± 1 kDa (Addlagatta et al., 2005a).

Most of the bacterial and eukaryotic recombinant MAPs studied till date has been purified from the soluble fractions of *E. coli* lysate. MtbMAP B was found to express in high level in the soluble fraction as N-terminal His-tagged protein, where as MtbMAP A was expressed in high levels in the insoluble fraction (**Fig 5.5a** and **5.5b**). Complete insoluble expression was observed in case of MtbMAP A expressed without any tag by Lu and Ye (2010). They reported slight improvement in solubility by expressing it with N-terminal His-tag from pET28a vector. In another contemporary study, expressing MtbMAP A with C-terminal His-tag from pET28b vector was reported to further improve the solubility to a slight extent (Olaleye et al., 2010). To best of our knowledge there are no reports on

refolding of any MAP enzymes from inclusion bodies. Since the fixing of metal ions during refolding MAPs could be a tricky task to achieve, we opted to purify both MtbMAP A and MtbMAP B from soluble fractions using Ni-NTA chromatography.

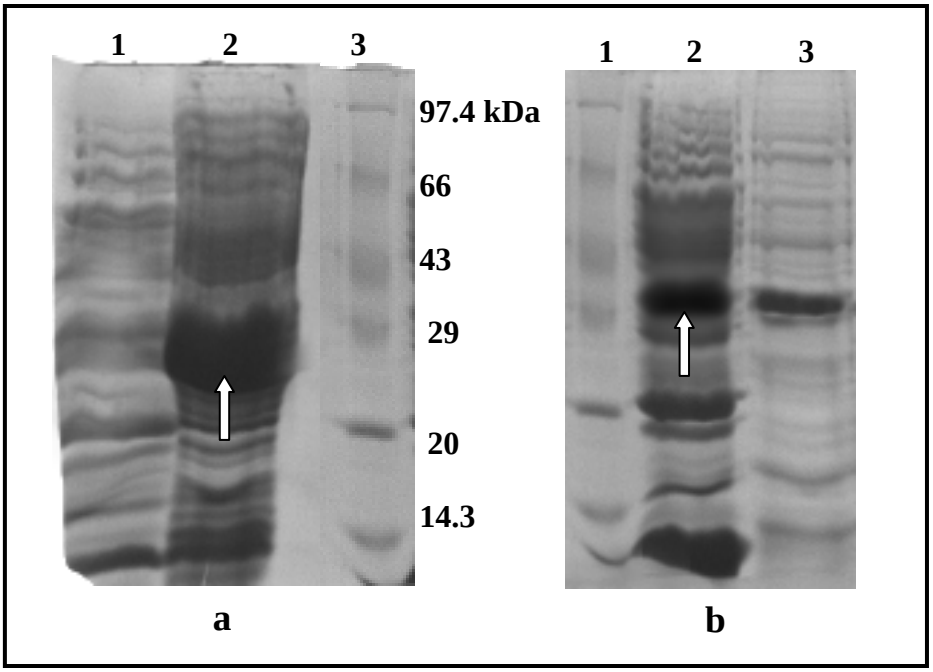

Fig 5.5: 12% SDS-PAGE showing expression of MtbMAPs in different fractions from *E. coli*. (a) Expression of MtbMAP A; Lane 1: Soluble fraction; Lane 2: Insoluble fraction; Lane 3: Protein ladder **(b)** Expression of MtbMAP B; Lane 1: Protein ladder; Lane 2: Soluble fraction; Lane 3: Insoluble fraction.

Both MtbMAP A and MtbMAP B got purified to 99% homogeneity when purified through Ni-NTA column and eluted with 250 mM imidazole containing buffer (Fig **5.6a** and **5.6b**). Both the purified proteins showed the expected molecular size on 12% SDS-PAGE. There were conflicting reports on the effect of retaining N-terminal His-tag on purified MAP enzymes. The removal of His-tag was reported in case of *E. coli* MAP (Lowther et al., 1998; D'souza and Holz, 1999), presuming that the metal ions added during the assay might prefer His-tag than the metal binding site. Report from Zhang et al., (2009) suggested the negative

effect of N-terminal His-tag on the activities of MtbMAP A and not on MtbMAP B. These results were later challenged by studies by Lu and Ye (2010), where they found no difference in activation of MtbMAP A activity by metal ions in presence or absence of N-terminal His-tag. Thus no attempts were made in the present study to remove the N-terminal His-tag.

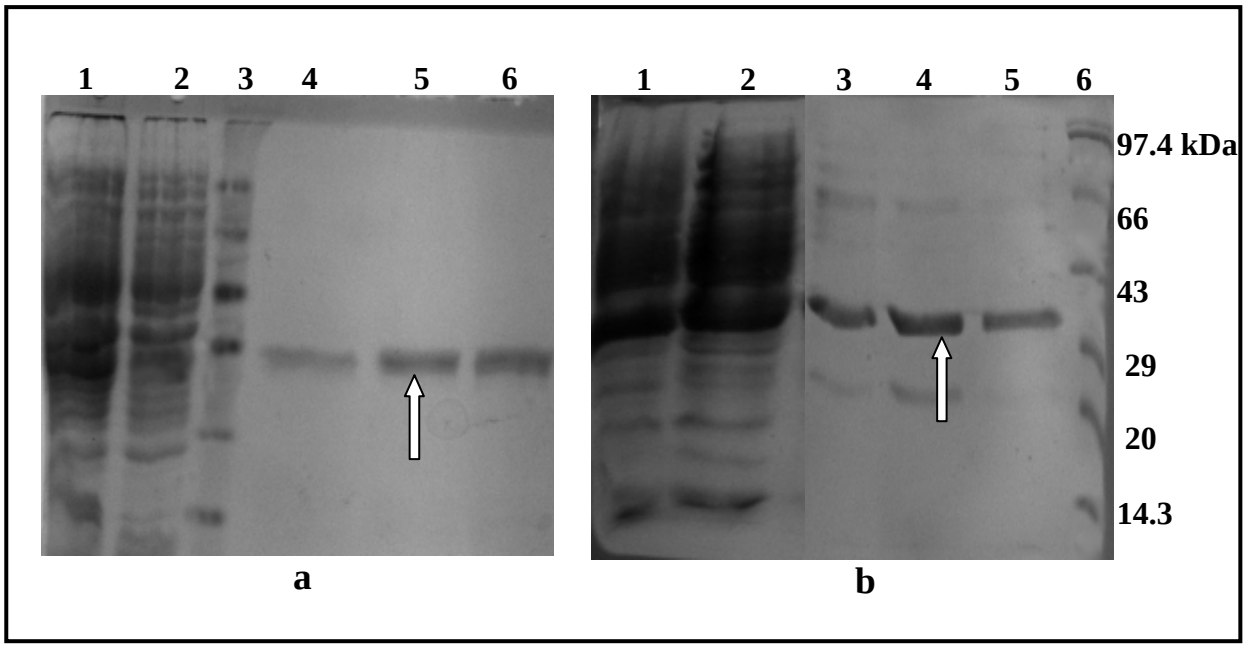

Fig 5.6: Purification of MtbMAPs from soluble fractions. (a) Purification of MtbMAP A; Lane 1: Insoluble fraction; Lane 2: Soluble fraction; Lane 3: Protein ladder; Lane 4-6: MtbMAP A eluted with 250 mM imidazole (29 kDa) ; **(b)** Purification of MtbMAP B; Lane 1: Insoluble fraction; Lane 2: Soluble fraction; Lane 3-5: MtbMAP B eluted with 250 mM imidazole (32 kDa); Lane 6: Protein ladder.

Except for very few studies, majority of the MAP enzymes studied till date has been characterized as apo-enzymes mainly due to the loosely bound metal-cofactor reported in these enzymes. EDTA is most commonly used to remove the metal ions from MAPs (Lowther et al., 1998; D'souza and Holz, 1999). There are reports using 1, 10, phenanthroline for this purpose (Lu and Ye, 2010), but owing to its lower water solubility, EDTA is mostly preferred. From our previous experience in preparing apo-MAP enzyme

(Narayanan et al., 2008), 100 mM EDTA was used to ensure complete removal of divalent metal ions from purified MtbMAP A and MtbMAP B. EDTA was completely removed by extensive dialysis against metal free buffers. The final yield of purified apo-MtbMAP A was 1-2 mg per liter and that of purified apo-MtbMAP B was 6-8 mg per liter.

Western blotting on the soluble fractions of MtbMAP A and MtbMAP B with anti-his-antibodies clearly demonstrated the difference in their soluble expression (**Fig 5.7**). The signals on membrane blot corresponded to the expected molecular size of MtbMAP A and MtbMAP B, proving their recombinant nature further.

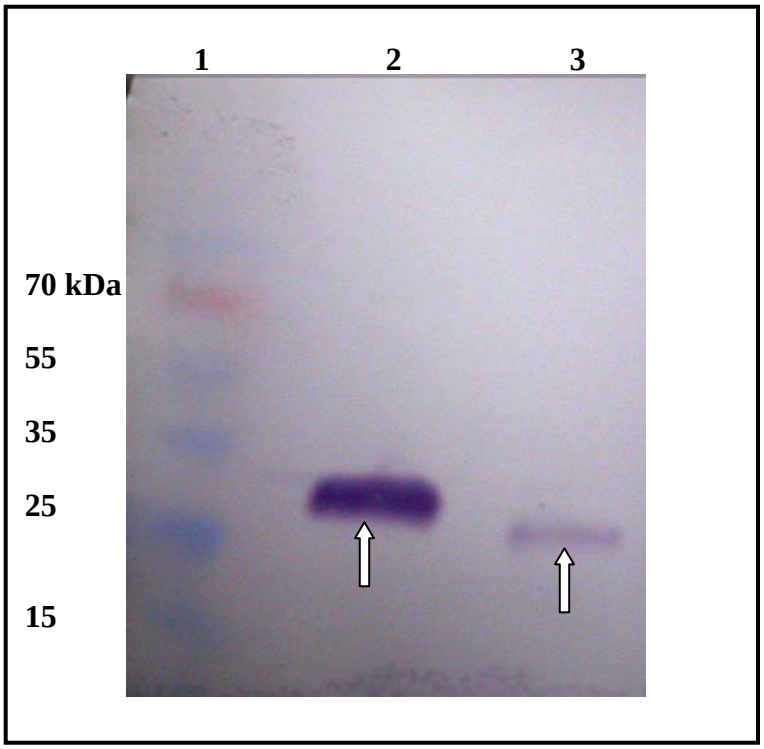

Fig 5.7: Western blotting of MtbMAPs from soluble fractions. Lane 1: Prestained protein ladder; Lane 2: Soluble fraction MtbMAP B; Lane 3: Soluble fraction of MtbMAP A

5.3.4 Enzyme activity of MtbMAPs

The MAP activities of purified apo-MtbMAPs in presence of 0.2 mM $CoCl_2$ were as shown in **Fig 5.8**. In absence of any added metal-ion both the enzymes showed negligible hydrolysis of the substrate, L-Met-*p*NA. The concentration of $CoCl_2$ was selected based on the studies on MtbMAPs by Zhang et al., 2009. At this concentration of 0.2 mM $CoCl_2$, MtbMAP B showed almost twice the activity of MtbMAP A in hydrolyzing the substrate. It was reported recently (Zhang et al., 2009) that at similar assay conditions, MtbMAP B showed 30% more activity compared to MtbMAP A in the previous studies (Zhang et al., 2009). But their studies didn't indicate any removal of native metal ions from both the proteins so it was assumed that it might have done using holo-enzymes of MtbMAPs. Similar trends in activities of MtbMAP A and MtbMAP B were published from the studies by Olaleye et al., (2010), where they used 10 μM Co^{2+} in the assay. L-Met-*p*NA was used in our studies as substrate due to its simplicity in assay procedure and ease of detection. L-Met-*p*NA was proved to be a good substrate in studying type I and type II MAPs and both these types of enzymes had substrate saturation beyond 1 mM of L-Met-*p*NA (Mitra et al., 2006). Hence, throughout this study, 1 mM L-Met-*p*NA was used as substrate for characterising MtbMAPs, unless specified otherwise.

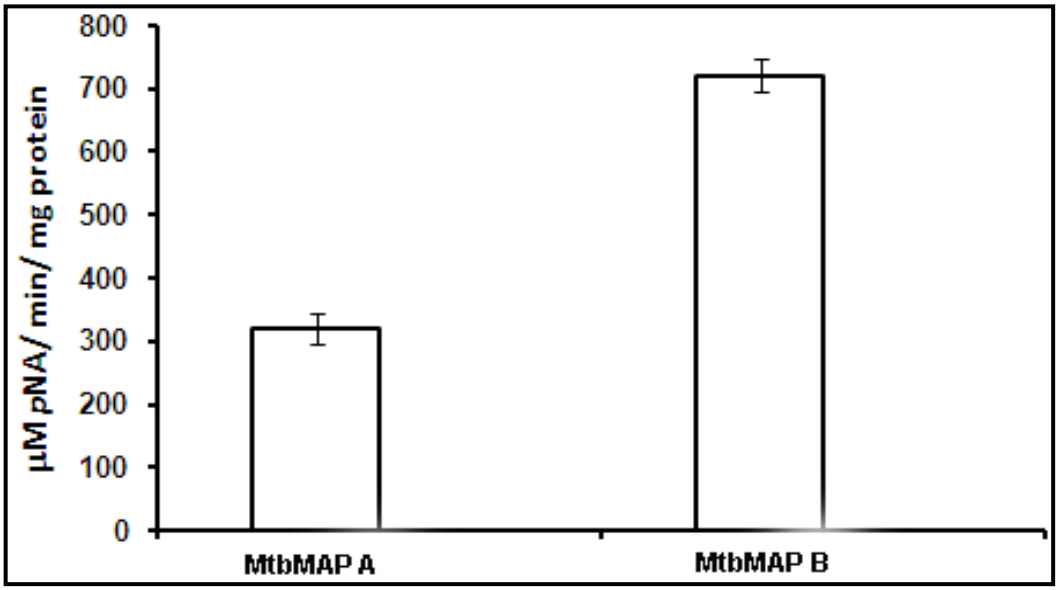

Fig 5.8: MAP assay with apo-MtbMAPs. Assay was performed in Tris-Cl buffer, pH 8.0 with 100 mM KCl using 1 mM L-Met-*p*NA as substrate in presence of 0.2 mM $CoCl_2$. 1.6 µg of each of the proteins were used in the assay and activities are represented as µM *p*NA released/min/mg protein.

5.3.5 Substrate specificities of MtbMAPs

In presence of 0.2 mM $CoCl_2$, both the MtbMAPs had high specificity towards L-Met-*p*NA, compared to all other amino acid-*p*NA substrates used in the study (**Fig 5.9**). Among the two MtbMAPs, MtbMAP B showed high specificity in cleaving methionine. However, MtbMAP A could use *p*NA substrates with uncharged amino acid at N-terminal end to a smaller extent (**Fig 5.9**). This proves MtbMAP A to have slightly broader substrate specificity. From structural studies on MtbMAP B, it was suggested to be associated with the ribosomes with the SH3 binding motif in its N-terminal extension (Addlagatta et al., 2005b). Thus, it was clear that MtbMAP B is assigned to perform post-translational NME in *M. tuberculosis* cytoplasm. No such N-terminal extension is present in MtbMAP A and there are some ambiguities regarding their site of action. The broader substrate specificities of MtbMAP A suggest that this enzyme might be involved in maintaining the methionine or

amino acid pool in the cytoplasm of *M. tuberculosis*. Further studies are required for providing some experimental evidences to assign the true role of MtbMAP A in *M. tuberculosis*.

MAP activities are decided by the nature of penultimate amino acids in a polypeptide. Usually MAPs prefer non-bulky amino acids like Ala, Cys, Gly, Pro, Ser, Thr or Val at the penultimate positions (Sherman et al., 1985). The preferences of MtbMAPs on the penultimate amino acids were studied by Zhang et al., (2009) using oligopeptides and they reported alanine as the preferred amino acid at penultimate position for tri-peptides and glycine and proline in case of tetra-peptides for both MtbMAPs. However, this study didn't characterized the penultimate amino acid preferences of MtbMAPs due to some technical reasons.

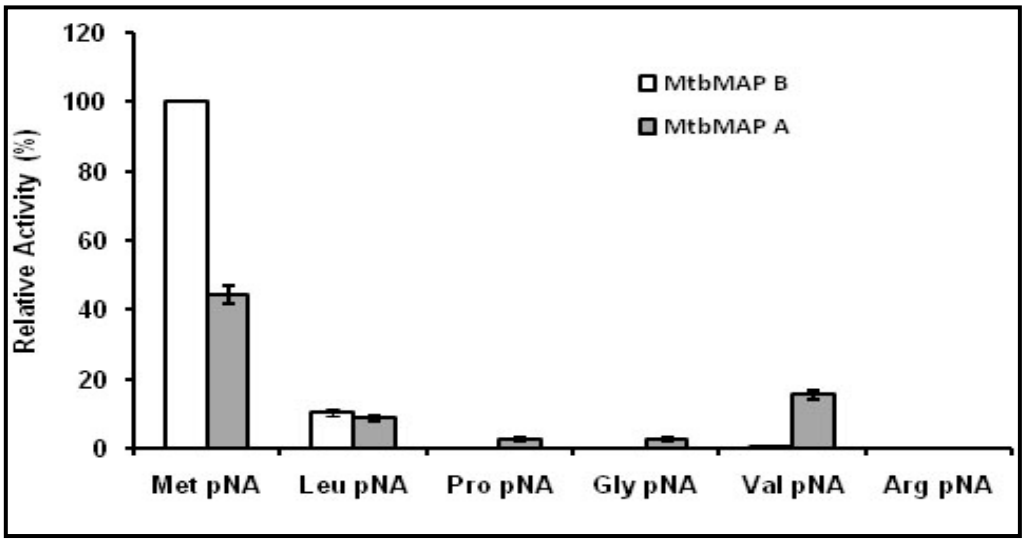

Fig 5.9: N-terminal amino acid preferences of MtbMAPs. Enzyme assay was performed using 1 mM of the indicated amino acyl-*p*NAs in presence of 0.2 mM $CoCl_2$ at pH 8.0 and 37^{o}C.The results are represented as percentage relative activities of MtbMAP B against L-Met-*p*NA.

5.3.6 Metal ion preferences of MtbMAPs

Metal- preferences of MtbMAPs for their *in vitro* MAP activity were as shown in **Fig 5.10a** and **5.10b**. In absence of any added metal ions, there were no MAP activities detected for both MtbMAPs, which proved the efficiency in preparation of apo-enzymes. During metal ion titrations, 0.22 μM MtbMAP A was activated maximum at 100 μM of Ni^{2+} followed by 40 μM of Co^{2+}. Slight activation of MtbMAP A activity was also noted in the entire range by Mn^{2+} and in limited range by Fe^{2+} (**Fig 5.10a**). Metal-ions showed inhibitory effect beyond a threshold concentration and at 1 mM concentration there was no activity in case of Co^{2+}, even though activity was retained in case of Ni^{2+}.

In case of MtbMAP B, both Ni^{2+} and Co^{2+} showed similar trends in activation of enzyme activity (**Fig 5.10b**). Both these at 100 μM produced the maximum activity of MtbMAP B. Beyond this concentration there was a concentration dependent inhibition of MtbMAP B activity with increase in metal-ion concentration. Mn^{2+} triggered significant activity at 400 μM concentrations, but both Fe^{2+} and Mg^{2+} were inefficient activators of MtbMAP B activity.

Studies on MAP enzymes from different prokaryotic and eukaryotic organisms have confirmed the necessity for metal-ions in their catalytic activities. Co^{2+} was recognized as the metal-cofactor for MAPs for many years (Bradshaw et al., 1998; Chang et al., 1990) and many of the crystal structures of Co^{2+} containing MAPs were published and characterized. Walker and Bradshaw (1998) identified Zn^{2+} as the metal co-factor for MAP I in yeast. Apart from these two metal ions Mn^{2+} and Fe^{2+} were also reported to show significant activation of enzyme activities of different MAPs (D'souza and Holz, 1999; Wang et al.,

2003). We have previously reported Mg^{2+} as the best activator of MAP enzyme purified from *M. smegmatis* (Narayanan et al., 2008).

These kinds of bell shaped curve for metal ion activation were previously reported in case of *E. coli* MAP (Li et al., 2003) and *S. cerevisiae* MAP (Chen et al., 2004). Even though activation of MAPs by Co^{2+} was observed in previous cases, Ni^{2+} activation of MAP activities was never reported before for *E. coli* or other bacterial MAPs. Similar to the observation in this study, Lu et al., (2010) and Lu and Ye, (2010) observed Ni^{2+} activation of MtbMAPs, except that they found Ni^{2+} alone as best activator of MtbMAP B. Also the concentrations reported for maximum activation fell in the range of 10-20 μM. These differences might have arised due to the variation in the assay procedure adopted by each group. In many cases, methionyl aminomethylcoumarin (Met-AMC), a flourogenic substrate was used to characterise MAP activities of MtbMAPs. Using this substrate and following the multiple independent binding sites (MIBS) model for metal stoichiometry (Chai and Ye, 2010), the dissociation constants (K_d) for Ni^{2+} for MtbMAP A and MtbMAP B were identified as 2.31 μM and 1.41 μM respectively (Lu et al., 2010; Lu and Ye, 2010). But, K_d values for binding of Co^{2+} was 1.87 μM and 0.13 μM for MtbMAP A and MtbMAP B respectively, proving Co^{2+} to have higher affinity and tight binding relative to Ni^{2+}.

It was notable that Mg^{2+}, which showed maximum activation of MAP enzyme purified from *M. smegmatis* (Narayanan et al., 2008), didn't show any activation of both MtbMAPs. Mg^{2+} was reported to activate MtbMAP A in the studies from Zhang et al., 2009 and based on their study they suggested the native MAP enzyme purified from cell lysate of *M. smegmatis* to be an ortholog of MtbMAP A. However, we didn't find any activation of MtbMAPs in presence of Mg^{2+}. It could be well possible that MAP protein purified from *M.*

smegmatis may not be a bonafied MAP enzyme or it could be one of the other two orthologus MAP proteins which are shorter than MtbMAPs in size.

Based on the metal-ion preferences of MtbMAPs, it could be suggested that both these enzymes may have different sites of action as suggested by their difference in the substrate specificity or that they may play differential role in different phases of infection in *M. tuberculosis*. Based on quantitative real time-PCR it was proved that the expression of Rv0734 transcript was higher in log phase *M. tuberculosis* cultures, where as that of Rv2861c transcript was higher in stationary phase cultures (Zhang et al., 2009). Thus the identified variations in metal-preferences may open up new avenues to design metallo-specific MAP inhibitors for both MtbMAPs in order to inhibit both actively growing and dormant *M. tuberculosis* cultures.

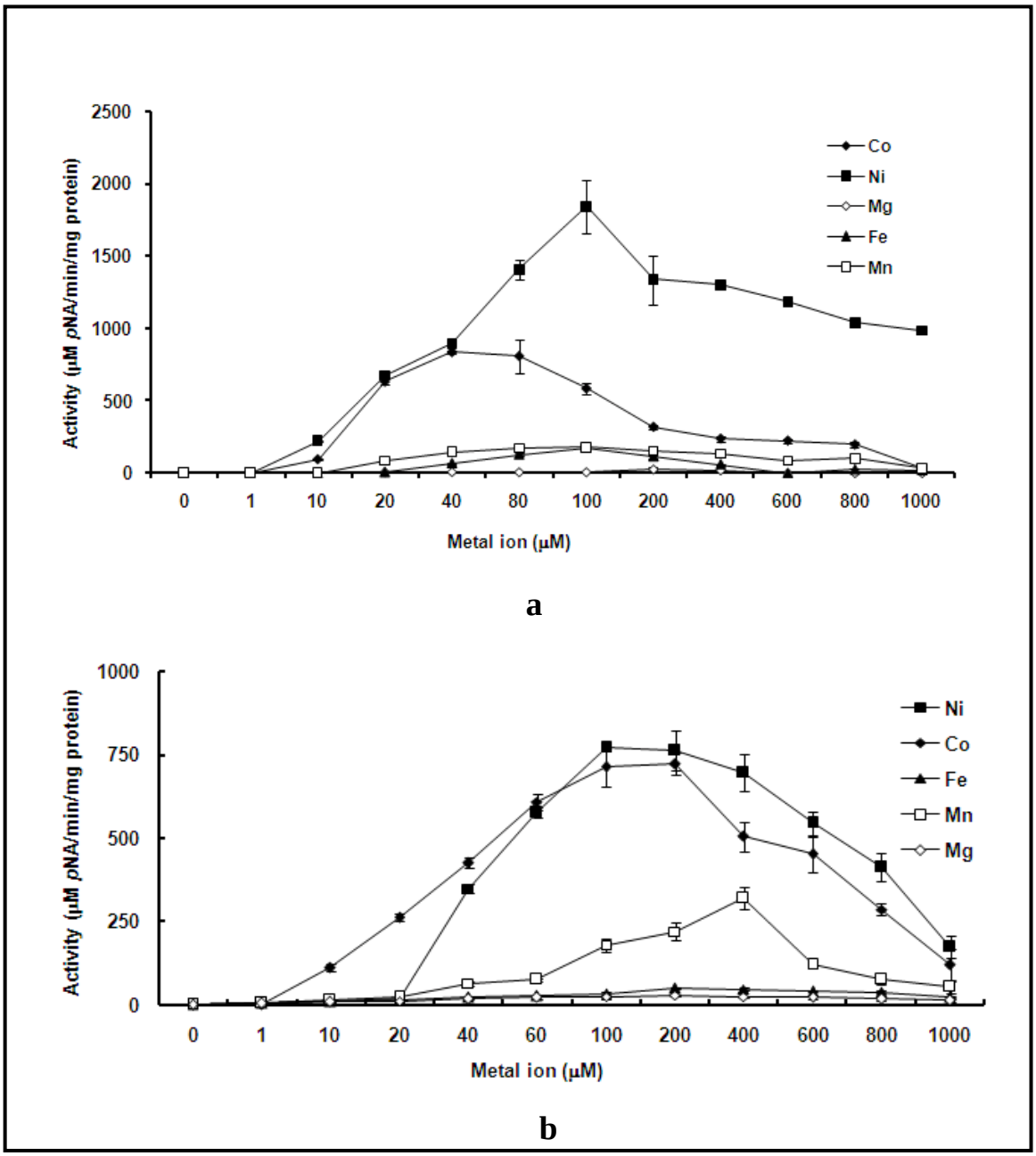

Fig 5.10: Metal ion titrations for MAP activity of (a) MtbMAP A and (b) MtbMAP B. Assay was performed by including 0-1 mM of the indicated cations in standard MAP assay with 1 mM L-Met-*p*NA using 0.22 µM MtbMAP A and 0.275 µM MtbMAP B at pH 8.0 and 37 ^{o}C .

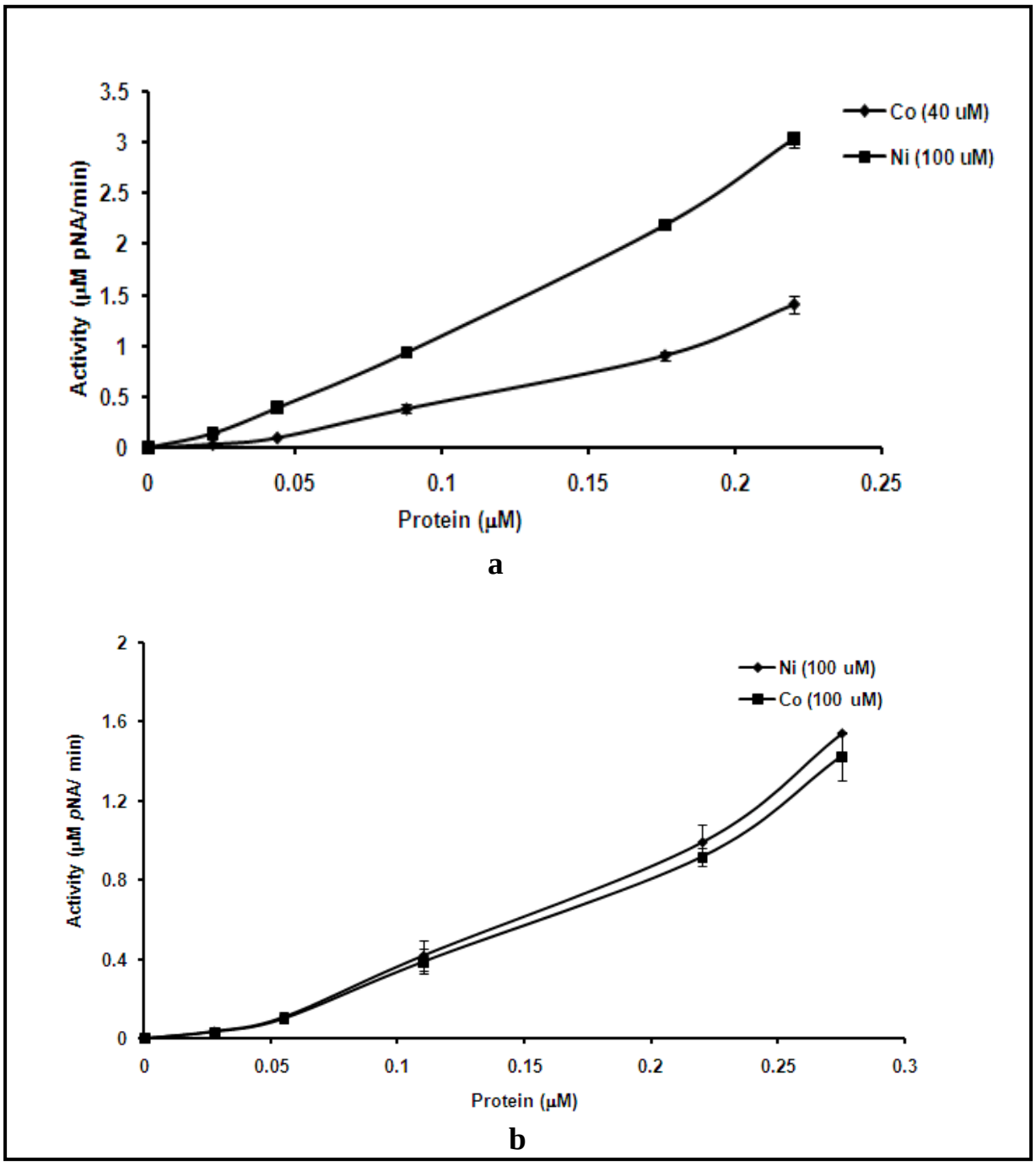

Fig 5.11: Enzyme concentration *vs* MAP activity of MtbMAPs. (a) MtbMAP A **(b)** MtbMAP B; The corresponding optimized concentrations of Ni^{2+} and Co^{2+} for each of these enzymes were used in the assay.

5.3.7 Activities of MtbMAPs *w.r.t* enzyme concentration

MAP activities of MtbMAPs showed an increase with enzyme concentrations, which was not strictly linear (**Fig 5.11**). This deviation from linearity might be due to the difference in optimum metal-ion concentration for activating enzymes at different concentration. How ever, the results confirmed that MtbMAP A is more catalytically active than MtbMAP B at the optimum concentration of metal ion used. Hence, in all further assays we used 0.22 μM MtbMAP A and 0.275 μM MtbMAP B along with optimized concentrations of Ni^{2+} and Co^{2+} for these enzyme concentrations.

5.3.8 Optimum temperature and pH for MtbMAPs

The optimum temperature for enzyme activity of MtbMAP A was 37 ^{o}C and for that of MtbMAP B was 55 ^{o}C (**Fig 5.12a**). MtbMAP B activity increased only in very small increments from 37 ^{o}C to 55 ^{o}C, reaching the maximum activity at 55 ^{o}C. Both the enzymes were not active beyond 65 ^{o}C. Both MtbMAP A and MtbMAP B had maximum activity at pH 8.0, with very low activity in acidic and basic range (**Fig 5.12b**).

In literature, optimum temperature for MtbMAP A activity was reported to be 55 ^{o}C by Zang et al., (2009) and as 42 ^{o}C by Olaleye et al., (2010). In case of MtbMAP B the optimum temperature was reported as 37 ^{o}C and 50 ^{o}C, respectively, by the above workers. Hence, there exists an ambiguity regarding the optimum temperature for activities of MtbMAPs. Results from present study are more similar to that of Olaleye et al., (2010) and could be so because they too have used a *p*-NA based substrate in studying the enzyme activities of MtbMAPs. The optimum temperature for MAP enzyme purified from *M. smegmatis* was 55 ^{o}C (Narayanan et al., 2008), based on which Zhang et al., (2009) proposed it to be an ortholog of MtbMAP A. *E. coli* and yeast MAP enzymes had 37 and 45

^{o}C as their optimum temperature for *in vitro* activity (Lowther et al., 1998; Chang et al., 1990) and the optimum temperatures of MAPs were found to vary slightly depending on the assay procedures adopted.

The pH optimum for MtbMAP activity was similar to the reports of Olaleye et al., (2010). MtbMAP B had a broader range of pH optimum from pH 7- 9.5 compared to MtbMAP A which had a steep decline in activity on either side of pH 8.0. Zang et al., (2009) reported MtbMAP B to have broader pH range, leading to 60% activity retention even at pH 5.0. They correlated this property of MtbMAP B with its higher expression in the dormant phase of *M. tuberculosis* infection, where it survives in the acidic environment in macrophages. But such broader pH optimum for *in vitro* activity of MtbMAP B was not observed in present study or in the studies by Olaleye et al., (2010). The pH optimum for MAP from *M. smegmatis* was 8.5 (Narayanan et al., 2008). The optimum pH for *in vitro* activities of *E. coli* and yeast MAP enzymes was pH 8.0 and pH 7.0 respectively (Lowther et al., 1998; Chang et al., 1990).

Although MtbMAP B had 10% relative increase in activity at 55 ^{o}C, for sake of comparison and for ease of handling their further activity assays were also performed at 37 ^{o}C at pH 8.0, similar to MtbMAP A.

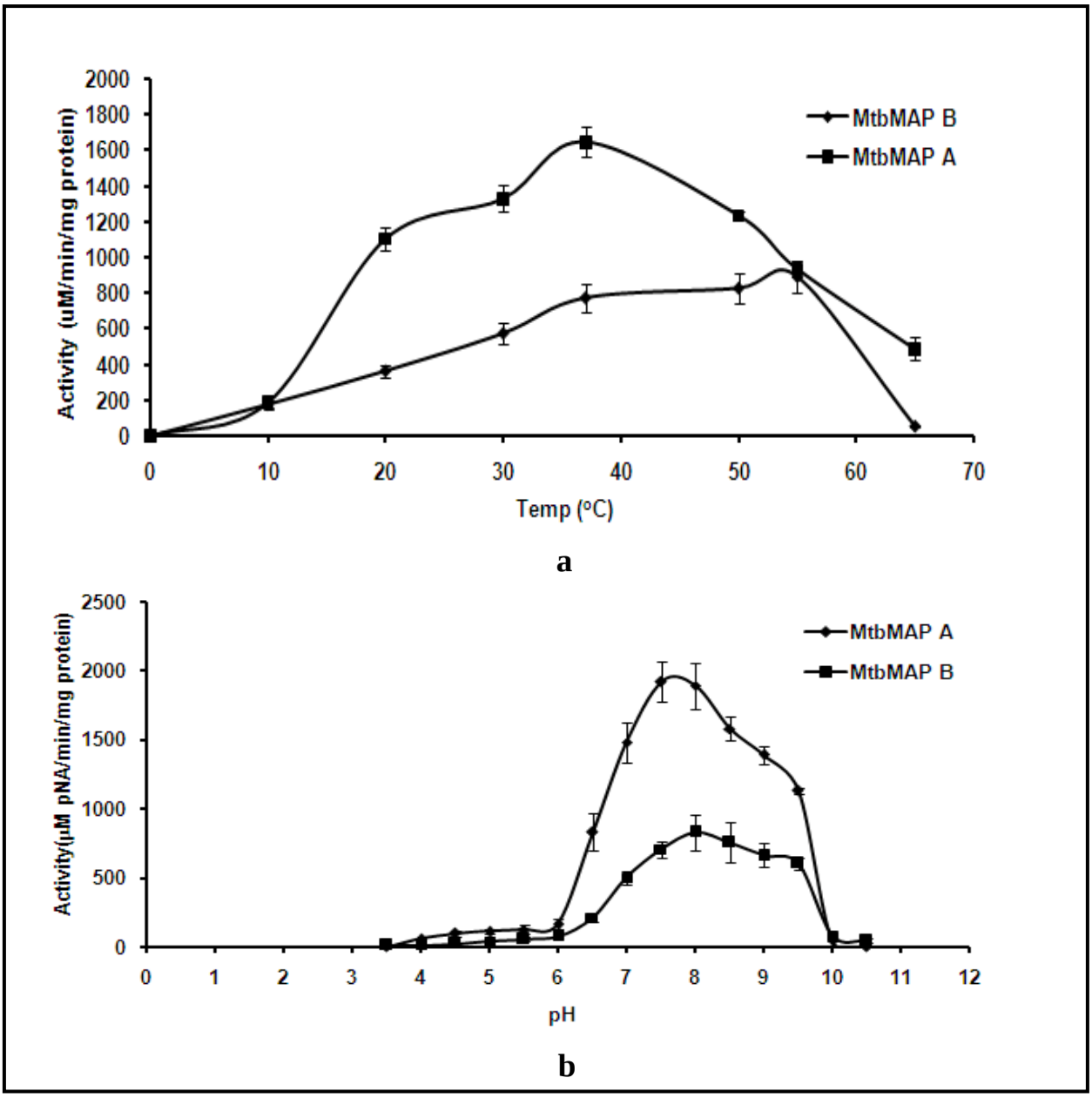

Fig 5.12: Optimum temperature (a) and pH (b) for enzyme activities of MtbMAPs. 100 µM Ni^{2+} was used with 0.22 µM MtbMAP A and 100 µM Co^{2+} was used along with 0.275 µM MtbMAP B in this assay.

5.3.9 Enzyme kinetics of MtbMAPs

MtbMAPs followed typical Michealis-Menten kinetics for catalysis against L-Met-*p*NA (**Fig 5.13**). The V_{max} values as derived from the MM plot for MtbMAP A were 1.763 ± 0.12 and 1.029 ± 0.13 μM *p*NA/min with Ni^{2+} and Co^{2+} respectively. The K_m values of MtbMAP A corresponding to these two metal ions were 154 ± 37 and 193 ± 23 μM (**Table 5.7**). The catalytic efficiency value (K_{cat} /K_m) for MtbMAP A was 867 and 404 $M^{-1}s^{-1}$ for Ni^{2+} and Co^{2+} respectively. The K_{cat} / K_m values of MtbMAP B were 171 and 153 $M^{-1}s^{-1}$ for Ni^{2+} and Co^{2+} respectively, with corresponding V_{max} values of 1.12 ± 0.06 and 1.2 ± 0.06 μM *p*NA/min (**Table 5.5**). The K_m values of MtbMAP B corresponding to these two metal ions were 466 ± 57 and 520.5 ± 59 μM. Kinetic parameters suggests MtbMAP A with Ni^{2+} was nearly six fold catalytically efficient than MtbMAP B, with higher affinity for substrate L-Met-*p*NA and with higher enzyme turnover value.

The K_m values reported for holo-MtbMAP A with substrate Met-Ala-Ser was 18 μM (Zhang et al., 2009) and for Ni^{2+} enzyme with Met-AMC was 11 μM (Lu and Ye, 2010). The K_m value for MtbMAP A from present study was close to the reported range of K_m value, 122 ± 22 μM, with substrate Met-Pro-*p*NA by Olaleye et al., (2010). But the overall catalytic efficiency values reported for MtbMAP A by previous workers were 100 folds higher than what we obtained with L-Met-*p*NA. This could be only due to the different substrate opted in present study compared to the previous reports. It was previously reported that *E. coli* and *Pyrococcus furiosus* MAPs could only cleave L-Met-*p*NA with 500 fold less efficiency compared to a tetra-peptide, Met-Gly-Met-Met (Mitra et al., 2006).

Surprisingly, in one of the previous studies using the substrate Met-Pro-*p*NA, the catalytic efficiency of MtbMAP B was reported to be higher than MtbMAP A (Olaleye et al., 2010). This variation could have arised due to the usage of unoptimized concentrations of metal ions in their studies like our initial MAP activity assay. Apart from the above report, all other reports including this study support MtbMAP A as a better enzyme catalyst than MtbMAP B.

The catalytic efficiencies of yeast and *E. coli* MAPs were 10-20 folds higher than both MtbMAPs, even though their K_m values against tetra-peptide substrates fall in the range with that of MtbMAPs (Chen et al., 2004; Chiu et al., 1999).

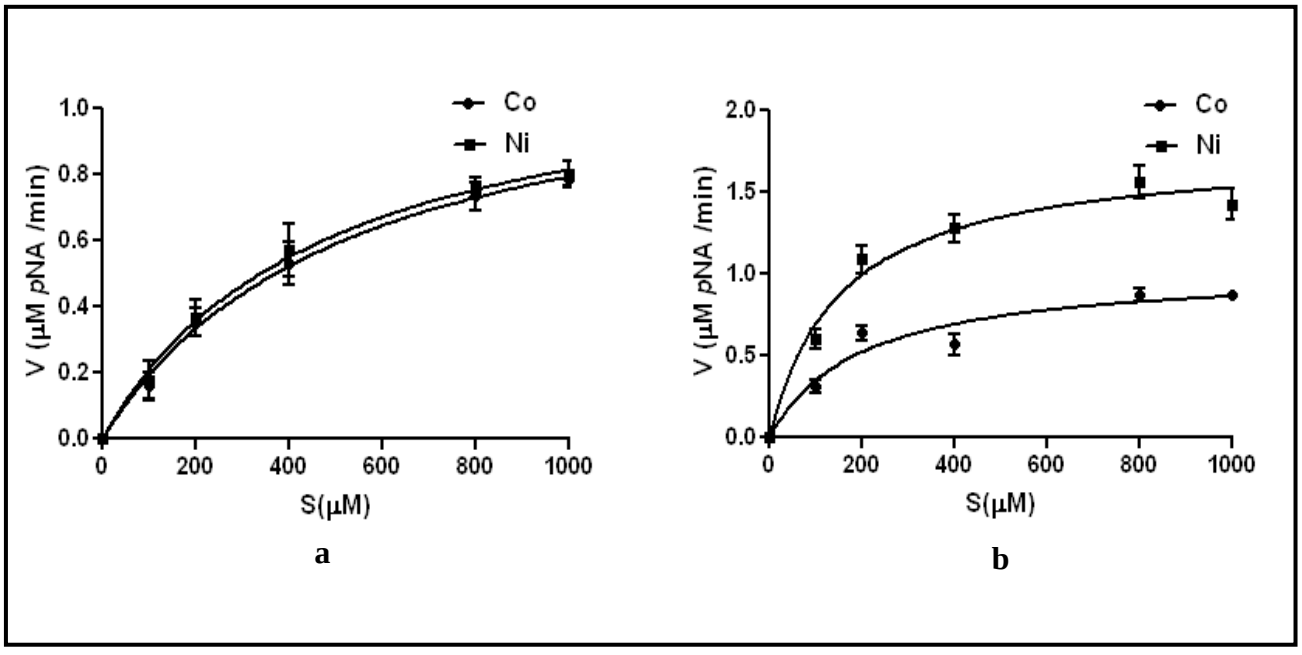

Fig 5.13: Michealis-Menten plot for enzyme kinetics of MtbMAPs against substrate L-Met-*p*NA. (a) MtbMAP B: 0.275 μM of purified apo-MtbMAP B was used in the assay with 100 μM of Co^{2+} or Ni^{2+} against 0-1 mM of L-Met-*p*NA; **(b)** MtbMAP A: 0.22 μM of purified apo-MtbMAP A was used with 100 μM Ni^{2+} and 40 μM Co^{2+} against 0-1mM of L-Met-*p*NA. MM Plot was made with Graph pad prism software.

Table 5.5: Kinetic parameters of MtbMAPs with substrate L-Met-*p*NA

Kinetic Parameters	MtbMAP B		MtbMAP A	
	Ni^{2+} (100 μM)	Co^{2+} (100 μM)	Ni^{2+} (100 μM)	Co^{2+} (40 μM)
V_{max} (μM *p*NA/min)	1.12 ± 0.06	1.2 ± 0.06	1.763 ± 0.12	1.029 ± 0.13
K_m (μM)	466 ± 57	520.5 ± 59	154 ± 37	193 ± 23
K_{cat} (s^{-1})	0.08	0.08	0.133	0.078
K_{cat}/K_m ($M^{-1}s^{-1}$)	171	153	867	404

5.3.10 Thermo-stability of MtbMAPs

Among the two MtbMAPs, MtbMAP B was found to be moderately stable at 37 ^{o}C with a half-life ($t_{1/2}$) more than 1 h. At 55 ^{o}C the enzyme retained only 15% of its original activity after 1 h with $t_{1/2}$ close to 40 min (**Fig 5.14a**). MtbMAP A was found to be less stable compared to MtbMAP B and had a $t_{1/2}$ of 50 min at 37 ^{o}C. The enzyme lost all its activity after incubating at 55 ^{o}C for 1 h. The $t_{1/2}$ for MtbMAP A at 55 ^{o}C was close to 20 min (**Fig 5.14b**). These results go in hand with the temperature optimum for their activity and prove that MtbMAP B is more thermo-stable compared MtbMAP A. Similar results were published by Olaleye et al., (2010) but, the reverse was published by Zhang et al., (2009) for MtbMAPs. MAP enzyme purified from *M. smegmatis* showed thermo-stability like that of MtbMAP B at 55 ^{o}C (Narayanan et al., 2008). MtbMAP B has an N-terminal linker region (Addlagatta et al., 2005b) and MtbMAP A has an internal six amino acid insertions which differentiates them structurally. The stability determinants in the tertiary

structures of MAPs are still not well defined. These structural differences might have led to the differences in thermo-stabilities of the two MtbMAPs.

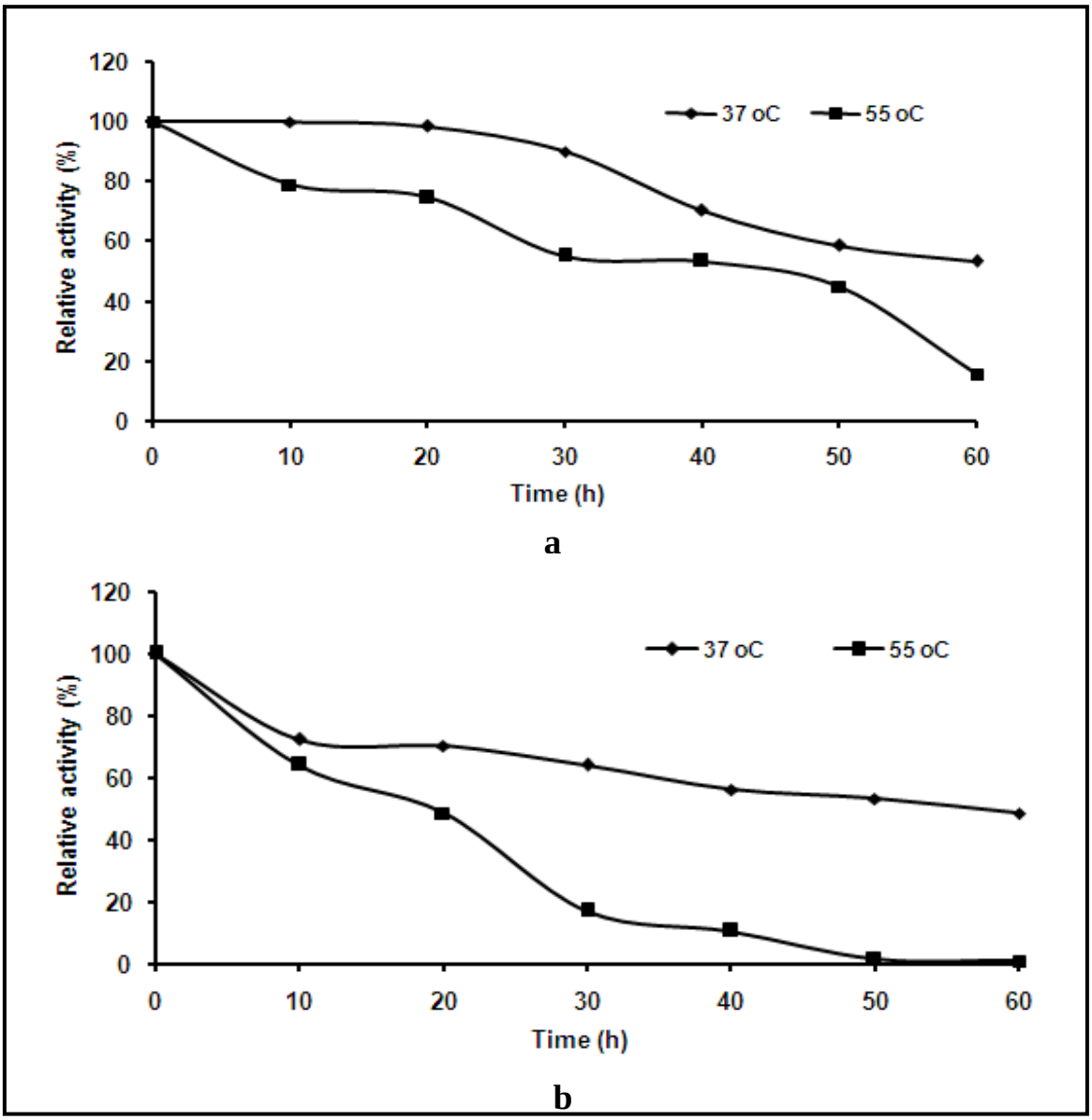

Fig 5.14: Thermo-stabilities of MtbMAPs (a) MtbMAP B **(b)** MtbMAP A**.** 20 µg of each of these apo-enzymes were incubated at the indicated temperatures and residual activities were assayed at every 10 min in presence of 100 µM Ni^{2+}. The residual activities are expressed as percentage relative activities of each enzyme at time 0.

5.3.11 Effect of metallo-protease inhibitors on MtbMAP activity

The effects of four metallo-protease inhibitors studied on MtbMAP activities are shown in **Table 5.6**. Among the four inhibitors studied, only bestatin and actinonin had slight inhibitory activities on MtbMAPs. At 10 μM concentration of bestatin, MtbMAP A lost 25% of its activity and MtbMAP B lost 50% of its activity. Actinonin showed remarkable inhibition of MtbMAPs activity at 10 μM concentration, at which there was only 20% activity retention of MtbMAP B and 60% activity retention of MtbMAP A. In general, there was better inhibition of MtbMAP B compared to MtbMAP A. Not surprisingly, fumagillin, a known inhibitor of type II MAPs didn't show any inhibitory effects on MtbMAPs.

Actinonin, a known PDF inhibitor, was reported to show inhibitory effects on MAP enzyme from *M. smegmatis* (Narayanan et al., 2008). Actinonin contain hydroxamate side-chains as the metal ion chelators. Derivatives of peptidyl hydroxamic acids were previously reported to have inhibitory effects on *E. coli* MAP enzyme (Hu et al., 2004). Similarly, the derivatives of bestatin, a known leucine aminopeptidase inhibitor, with its N-terminal side chain replaced with nor-leucine were reported to inhibit *E. coli* MAP with high efficiencies (Lowther and Matthews, 2000).

Recently, the importance of metallo-form selective inhibitors of MAPs is being recognized for selective inhibition of bacterial MAPs with different metal ions. (Ye et al., 2004; Wang et al., 2008). Many cathecol based inhibitors and triazole based inhibitors of MtbMAP A and MtbMAP B with different metal-form selectivities were reported to be potent inhibitors of these enzymes *in vitro* (Lu et al., 2010; Lu and Ye, 2010). In a separate study, derivatives of 2, 3-dichloro-1, 4-napthoquinone were shown to be potent inhibitors of

in vitro enzyme activities of MtbMAP A and MtbMAP B (Olaleye et al., 2010). Very recently the derivatives of bengamides, known natural inhibitors of human MAP I and MAP II, were reported to produce remarkable inhibition of both MtbMAP A and MtbMAP B activities and modest growth inhibition of *M. tuberculosis* in culture (Lu et al., 2011). Even though the inhibitors in present study were not as potent as reported by others, it suggests actinonin as a possible starting point to develop inhibitors specific for MtbMAP B. It could be an important finding since many derivatives of actinonin are already under clinical trials as deformylase inhibitor and it would be advantageous to identify a single compound which would inhibit both the NME enzymes in bacteria in order to reduce the possibilities of resistant development against these inhibitors.

Table 5.6: Effect of metallo-protease inhibitors on MtbMAP activities

Inhibitor (μM)	Relative Activity (%)	
	MtbMAP A	MtbMAP B
Control		
0	**100**	**100**
Bestatin		
0.1	**92 ± 3**	**92 ± 3**
1.0	**86 ± 7**	**72 ± 7**
10	**75 ± 8**	**52 ± 8**
Amastatin		
0.1	**102 ± 4**	**102 ± 4**
1.0	**98 ± 5**	**98 ± 5**
10	**95 ±7**	**95 ±7**
Actinonin		
0.1	**91 ± 11**	**72± 11**
1.0	**81 ± 6**	**44± 6**
10	**66 ± 9**	**28± 9**
Fumagillin		
0.1	**104 ± 3**	**104 ± 4**
1.0	**99 ± 5**	**99 ± 5**
10	**89 ± 3**	**89 ± 3**

5.3.12 Effect of methionine as a feed- back inhibitor

The effects of methionine as a feed-back inhibitor of MtbMAPs were as shown in **Fig 5.15**. Methionine had no effects on the *in vitro* activity of MtbMAP A, but inhibited MtbMAP B to a greater extent. At the highest concentration of methionine tested, MtbMAP B retained only 30% of its original activity. Thus, it proved that methionine concentration has an inhibitory effect on the *in vitro* activity of MtbMAP B, probably *in vivo* too, which could be a possible reason for lower activity of MtbMAP B compared to MtbMAP A. From studies on substrate specificity, it was clear that MtbMAP B has very strict specificity for cleaving N-terminal methionine, but MtbMAP A could cleave other uncharged amino acids too to a small extent. These differences in substrate specificities and methionine inhibitions points to the fact that there could be slight structural variations between these two enzymes in their substrate binding pocket, even though they show high similarities at amino acid sequence level. In the absence of any structural information about MtbMAP A, it is difficult to explain these variations in properties of MtbMAPs. This also raises questions about the role of MAP enzymes in maintaining the methionine / amino acid pools in the cytoplasm of *M. tuberculosis*.

The essential roles of multiple map genes in bacteria are not yet completely elucidated. Among the two MAP proteins in *S. cerevisiae*, MAP 2 was inhibited in presence of methionine and not MAP 1 (Dummitt et al., 2003**)**. Based on experimental evidences, they proposed the role of MAP 1 in preventing premature activation of *met* genes through MAP function in methionine salvage and suggested this as the reason for the dominant essentiality of MAP 1 over MAP 2 for NME and cell growth in yeast. Among the two MtbMAPs, the essential role of MtbMAP A over MtbMAP B in cell viability of

M. tuberculosis was confirmed by gene knockdown studies (Olaleye et al., 2010). One possible reason for the dominant essentiality of MtbMAP A in *M. tuberculosis* could be that MtbMAP B gets inhibited at higher methionine concentrations and MtbMAP A might be playing essential functions in methionine salvage similar to MAP 1 in *S. cerevisiae* (Dummitt et al., 2003).

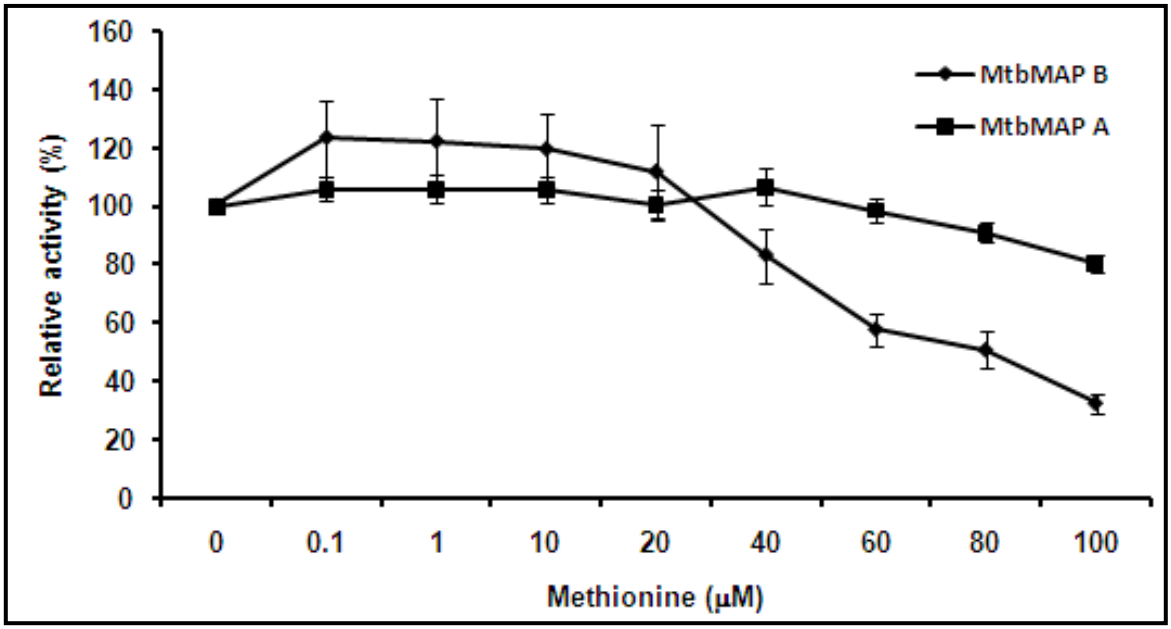

Fig 5.15: Feed-back inhibition of *in vitro* enzyme activities of MtbMAPs by L-methionine. 0-100 μM of L-methionine was included in standard MAP assay with 0.22 μM of MtbMAP A and 0.275 μM of MtbMAP B in presence of 100 μM Ni^{2+} against 1 mM L- Met-*p*NA.

5.4 CONCLUSIONS

Studies on recombinant MtbMAPs provided insights into variations in the biochemical and biophysical properties of these two enzymes. Soluble expressions of recombinant MtbMAP A was not as efficient as that of MtbMAP B and this would further delay the crystallization and structural determinations of MtbMAP A. The differences in the metal ion preferences and catalytic efficiencies of the two MtbMAP enzymes suggest their possible differential role in the active and dormant phase of *M. tuberculosis* growth. The

broader substrate specificities, higher catalytic efficiencies and resistance to product inhibition of MtbMAP A compared to MtbMAP B makes it more suitable NME enzyme in the active phase of *M. tuberculosis* growth. The higher stability shown by MtbMAP B compared to MtbMAP A might be a useful property to support NME in the dormant phase of *M. tuberculosis* growth in order to withstand different kinds of stress responses in macrophages. Among the inhibitors, actinonin was proved to be a good starting point for further improvements in developing specific inhibitors against MtbMAP B. Actinonin based inhibitors which can inhibit both MtbPDF and MtbMAP B, might have great potency in completely arresting the latency during *M. tuberculosis* infection. The variations is the sequence structure and properties of both MtbMAPs with human and other bacterial flora suggest its potential to become an important drug target in future. Further characterizations of the structure and properties of MtbMAPs will provide us opportunities to develop inhibitors which would serve as potent drugs for treating both active and latent TB. Ultimately, combination therapy with inhibitors active against both the enzymes in the NME pathway of *M. tuberculosis* may help to limit the development of further drug resistance problems in TB.

CHAPTER 6

Construction and Characterization of Site-Directed Mutantsof Methionine Aminopeptidases of *M. tuberculosis* H37Rv

CHAPTER 6

Construction and Characterization of Site-Directed Mutants of Methionine Aminopeptidases of *M. tuberculosis* H37Rv

6.1 Introduction

The essentiality of N-terminal methionine excision (NME) process for cell survival has brought the enzymes involved in this pathway into the list of potent drug targets for developing novel drugs against infectious diseases and some diseases like cancer and rheumatoid arthritis. Peptide deformylase (PDF) was initially considered as the better target among the two enzymes in NME for developing drugs against bacterial infections, mainly due to its non-essentiality in eukaryotic NME (Yuan and White, 2006). Some of the PDF inhibitors like LBM-415 have even entered phase II clinical trials as broad spectrum antibacterial drug (Fritsche et al., 2005). However, in recent past, there has been an increase in reports on the essentiality of human mitochondrial PDF in mitochondrial NME (Escobar-Alvarez et al., 2009; Escobar-Alvarez et al., 2010) and also on fast emergence of resistant mutants against various PDF inhibitors (Leeds and Dean, 2006). Like PDF, the equally essential second step in prokaryotic NME has also attracted researchers to focus on to methionine aminopeptidase (MAP) as potent drug target. The essentiality of MAP for cell survival in prokaryotes has been well demonstrated by deletion or inhibition of MAP genes or gene products in *E. coli* and *Salmonella typhimurium* (Chang et al., 1989; Miller et al., 1989).

Several MAPs have been purified and sequenced from a variety of bacterial sources and MAPs from *E. coli* and *P. furiosus* have been crystallographically characterized and extensively studied to define the catalytic and metal binding sites along with other relevant

structural features of these enzymes (Tahirov et al., 1998; Lowther and Matthews, 2000). The mechanism of metal-mediated catalysis was proposed based on the *E. coli* crystal structure and is believed to be universal for different classes of "pita-bread" enzymes including aminopeptidase P and creatinase (Lowther et al., 1999a; Ye et al., 2006). The catalytic residue in case of *E. coli* MAP is E204, supported by the hydrogen bonding interactions on substrates by H178 and H79 along with the metal – bound hydroxide on the metal ions. Apart from the data from crystal structures of MAPs with substrate – analogues and inhibitors, site-directed mutagenesis of the critical residues have also contributed in defining the mechanism of catalysis and inhibition of MAPs. The defined roles of H178, H79 and E204 in catalysis of *E. coli* MAP were confirmed by creating site-directed mutants of these residues and studying their *in vitro* catalytic properties (Lowther et al., 1999b). The corresponding residues were confirmed as important catalytic residues in human type II MAP also by performing similar mutagenesis experiments (Griffith et al., 1998). Additionally, site-directed mutagenesis defined the H231 in human MAP2, a structural equivalent of H79 in *E. coli*, as the residue which gets covalently modified by the MAP2 specific inhibitor fumagillin (Griffith et al., 1998; Addlagatta et al., 2005a).

The key residues involved in the formation of metal binding pocket and substrate binding pockets of MAPs were defined based on extensive site-directed mutagenesis studies on *E. coli* MAP (Chiu et al., 1999). This study confirmed the universality of residues involved in metal binding in case of all MAPs. The residues deciding the substrate specificities of MAPs were identified similarly using site-directed mutagenesis on human and *E. coli* type I MAPs. From these studies C70 in *E. coli* MAP or C202 in human MAP was defined as the residue which decides the specificities of MAP enzyme towards the N-

terminal and penultimate amino acids of peptide substrates (Li et al., 2004). They proved that an alanine mutation of this cystein leads to loss of stringent specificity of MAP enzymes towards N-terminal methionine. The substrate specificities of yeast type I MAP enzyme was altered similarly by M329A and Q356A mutation in the recombinant enzyme, which allowed it to utilize substrates with bulkier amino acids like leucine, methionine, phenylalanine and tryptophan at the penultimate positions (Walker and Bradshaw, 1999). An important molecular discrimination between type I and type II MAPs were defined by site-directed mutagenesis studies on C59 residue in type I MAPs. The C59 residue was characteristic to type I MAPs and absent from type II MAPs and using site-directed mutagenesis, this residue alone was identified as molecular targets for thiol-specific modifiers and inhibitors in case of type I MAPs (Swierczek et al, 2005).

Apart from these substrate binding and metal binding residues, the role of many other residues present in the vicinities of these regions were also defined using site-directed mutagenesis. Characterizing the role of residues in this region has a lot of implications in designing inhibitors towards MAPs. The adaptability of a surface-exposed loop bearing Y62, H63, G64 and Y65 (YHGY loop) in bacterial type I MAPs for accommodating substrates and inhibitors of different sizes have been defined by structural studies and site-directed mutagenesis (Ma et al., 2007). This loop was either buried in human type I MAP or was replaced by a unique insert in human type II MAP, which makes its adaptability less feasible in case of human MAPs. This loop region is believed to provide opportunities for selective inhibition of bacterial MAPs. The role of H63 in this YHGY loop of *E. coli* MAP was further characterized by site-directed mutagenesis to reveal its importance in hydrolysis of small peptides (Mitra et al., 2009). Similarly, an A362T mutation in type I MAP compared

to type II MAP in case of human and yeast in a loop near to the substrate binding site was identified as the reason behind the selectivity of inhibitor ovalicin towards type II MAPs (Brdlik and Crews, 2004). In light of the newly proposed mono-metal mediated catalysis of *E. coli* MAP based on structural evidences (Ye et al., 2006), site-directed mutagenesis of the second metal-binding residue D97 was performed to recognize the role of the second metal ion in restoring complete activity of this enzyme *in vitro* (Mitra et al., 2008).

Structure-based drug design against bacterial MAPs takes advantage of the structural information especially at the active site, to guide the design and development of inhibitors to achieve desired potencies and selectivity. Since there is a high level of sequence homology between bacterial and human type I MAPs within the catalytic domain, it is desirable to identify the differences between the two in order to improve selectivity of bacterial MAP inhibitors as antibiotics. Currently, the variations in the metal-ion specificities between bacterial and human MAPs are being explored to improve the specificities of MAP inhibitors by improving their metallo-selectivity (Li et al., 2003; Chai and Ye, 2009). Moreover, it is highly important to characterize the variations at the catalytic pockets of type I MAPs between pathogenic and non-pathogenic bacterial MAPs so as to reduce the toxicity towards the indigenous gut-microbial populations.

MAP is now identified as a promising target for the development of novel drugs against TB causing drug-resistant bacteria. The recent works on inhibitor designing against MtbMAPs have only taken into account the *in vitro* metallo-specificity of these enzymes (Olaleye et al., 2010; Lu and Ye, 2010; Lu et al., 2010, Lu et al., 2011). But none of these works have proved the specificities of these inhibitors towards MtbMAPs and their lack of inhibition on human or other bacterial MAPs. It is desirable to identify the uniqueness at the

sequence and structural level of MtbMAPs with other type I MAPs in order to further fine tune these inhibitors to improve their specificities towards *M. tuberculosis* enzymes. The present work attempts to identify and characterize some of these variations in MtbMAPs at the sequence level by constructing appropriate site-directed mutants of both the MtbMAP enzymes and characterizing these mutants.

6.2 Materials and Methods

6.2.1 Multiple sequence alignment of MtbMAPs with other type I MAPs

In order to compare the protein sequences of MtbMAPs with other characterized type I MAPs, multiple sequence alignments of MtbMAP sequences were performed along with bacterial and human type I MAP sequences using ClustalW program (Thompson et al., 1997). *E. coli* MAP I represents prokaryotic type I MAPs and *H. sapiens* MAP I represents the eukaryotic type I MAPs. Amino acid sequences of MAPs were retrieved from the annotated genome data base Kyoto Encyclopedia for Genes and Genomes (KEGG) (*www.genome.jp/kegg*). The alignment file generated was visualized and edited using the Genedoc software (*http://www.nrbsc.org/gfx/genedoc/*) (Nicholas et al., 1997).

6.2.2 Design and construction of site-directed mutants of MtbMAPs

Based on multiple sequence alignment, residues corresponding to those reported to be involved in the formation of substrate binding S1' pocket and metal binding pockets in *E. coli* and human MAPs were identified (Chiu et al., 1999; Li et al., 2004). In the present study, seven sites from these identified positions were selected for constructing nine site-substitution mutants (C105S, C105I, K98A, K98H, T94C, H114A, D142A, W255L and E269V) in MtbMAP B. A specific insertion region was recognized in the catalytic domain of MtbMAP A which was absent from the other type I MAPs in the study. This insertion region

was selected for creating a deletion mutant in MtbMAP A (Δ164-176), in order to analyse the relevance of residues in this region for *in vitro* enzyme activity, metal-binding ability and stability of MtbMAP A.

Mutagenic primers were designed by incorporating the corresponding mutations in them using the primer designing program from Stratagene (QuickChange® Primer design software) (**Table 6.1**). The primers were custom synthesised from IDT, USA and mutagenesis was performed on pET28a: *map*A and pET28a: *map*B plasmids according to the manufacturer's protocol (2.3.4). For creating deletion mutant, the number of cycling in PCR during site-directed mutagenesis was performed for 18 cycles (**Table 2.2**). Individual mutations were confirmed by DNA sequencing of both the strands of mutated plasmids using T_7 primers (Scigenomics, India). The confirmed mutated plasmids were transformed into *E. coli* BL21 (DE3) cells for expression of mutant recombinant proteins of MtbMAPs.

6.2.3 Over expression and purification of site-directed mutants of MtbMAPs

Over expression of substitution mutants of MtbMAP B and deletion mutant construct of MtbMAP A in *E. coli* BL21 (DE3) was done similar to the wild type enzymes as described in 5.2.4. Those mutants which got expressed in the soluble fractions were purified through Ni-NTA column as native enzymes, similar to wild type enzyme (5.2.5), and apo-enzymes were prepared and stored at -20 ^{o}C until analysis. Attempts were also made to improve the soluble expression of deletion mutant (MtbMAP A-Δ164 -176)

Table 6.1 List of mutagenic primers used to construct MtbMAPs mutants

Mutagenic Primer	Sequence (5' to 3')[#]
T94C FP	GGCGCCTACCCATCA**TGC**CTGGGCTACAAGGGA
T94C RP	TCCCTTGTAGCCCAG**GCA**TGATGGGTAGGCGCC
K98A FP	ATCAACGCTGGGCTAC**GCG**GGATTCCCGAAGTCG
K98A RP	CGACTTCGGGAATCC**CGC**GTAGCCCAGCGTTGAT
K98H FP	CATCAACGCTGGGCTAC**CAT**GGATTCCCGAAGTCGTG
K98H RP	CACGACTTCGGGAATCC**ATG**GTAGCCCAGCGTTGATG
C105S FP	CCCGAAGTCGTGC**AGC**ACGTCCCTCAA
C105S RP	TTGAGGGACGT**GCT**GCACGACTTCGGG
C105I FP	ATTCCCGAAGTCGTGC**ATC**ACGTCCCTCAACGAG
C105I RP	CTCGTTGAGGGACGT**GAT**GCACGACTTCGGGAAT
H114A FP	CAACGAGGTCATCTGC**GCT**GGAATCCCCGACTCG
H114A RP	CGAGTCGGGGATTCC**AGC**GCAGATGACCTCGTTG-
D142AFP	GGGTGCACGGT**GCC**ACCAACGCGAC
D142ARP	GTCGCGTTGGT**GGC**ACCGTGCACCC
W255LFP	GAAATCTGGGACGACGGT**TTG**ACGGTGGTCAC
W255LRP	GTGACCACCGT**CAA**ACCGTCGTCCCAGATTTC
E269VFP	GACCGCACAGTTC**GTA**CACACCCTGCTGG
E269VRP	CCAGCAGGGTGTG**TAC**GAACTGTGCGGTC
del164-176FP	GACCGACGTCGCGCATGCCATCGAATTCGGGATCGTCGCCGGTTA
del164-176 RP	TAACCGGCGACGATCCCGAACGTTATGGCATGCGCGACGTCGGTC

6.2.4 Optimization of the conditions for soluble expression of MtbMAP A- Δ164-176

During the expression studies, it was observed that recombinant MtbMAP A Δ164-176 was expressed almost completely in the insoluble fractions. Hence, attempts were made to bring the over expressed MtbMAP A-Δ164-176 proteins into the soluble fraction by varying the IPTG concentrations, incubation temperatures and by co-expressing with molecular *E.coli* chaperonins.

6.2.4.1 IPTG concentration

The effect of different IPTG concentrations (0.1, 0.25, 0.5, 0.75 and 1 mM) on soluble expression of MtbMAP A-Δ164-176 were studied as described for MtbPDF in chapter 3 (3.2.6.1). The induction was carried out at 30 ^{o}C for a time period of 12 h. Soluble expression at 0.5 mM IPTG was taken as control.

6.2.4.2 Induction temperature

The effect of induction temperatures were also done similar to MtbPDF (3.2.6.2). After the OD_{600} of cells reached 0.6, they were induced with 0.5 mM IPTG and left for incubation at various temperatures (16 ^{o}C, 30 ^{o}C and 37 ^{o}C) for a period of 12 h. Soluble expression at 30 ^{o}C was taken as control.

6.2.4.3 Co-expression of chaperonin GroEL/ GroES

Co-expression of molecular chaperone GroEL/GroES along with recombinant MtbMAP A and MtbMAP A-Δ164-176 was done essentially as described for MtbPDF in chapter 3 (3.2.6.3). The soluble fractions from chaperon co-expression studies were passed through Ni-NTA column in order to purify his-tagged recombinant enzymes expressed in soluble fractions. The improvement in soluble expression was confirmed by analyzing the corresponding purified protein bands on SDS-PAGE.

6.2.5 Solubilisation and purification of MtbMAP A -Δ164-176 from inclusion bodies

Since the attempts to express MtbMAP A-Δ164-176 in the soluble fraction were not successful, the mutant and wild type MtbMAP A proteins expressed in the insoluble fractions as inclusion bodies were extracted in 3 M urea or 6 M guanidium chloride containing lysis buffer as described in chapter 5 (5.2.4). The solubilised inclusion bodies were passed through Ni-NTA column in the denaturing conditions (2.3.3) in order to purify MtbMAP A or MtbMAP A -Δ164-176 expressed in the insoluble fractions. The proteins were eluted in 250 mM imidazole containing buffer and were processed similar to the wild type enzyme (5.2.5) for preparation of apo-enzymes. Urea in the purified fractions was removed along with EDTA during dialysis. The purified apo-enzymes of MtbMAP A-Δ164-176 thus prepared were stored at -20 ^{o}C until analysis.

6.2.6 Refolding of MtbMAP A from solubilised inclusion bodies

Inclusion body formation is a major obstacle in obtaining active recombinant proteins from *E. coli* and is particularly severe in case of *M. tuberculosis* proteins expressed with his-tag (Vincentelli et al., 2003). Proteins lose their native structure in the inclusion bodies and forms insoluble aggregates. Developing efficient protein native structure recovery procedures based on inclusion body refolding is an important challenge. There is no "universal" refolding buffer and studies showed that refolding buffer suitable for one protein may not work well with other (Mukhopadhyay, 1997). Methods have been designed to recover correctly folded proteins from inclusion bodies. These include dilution, dialysis and on-column refolding methods (De Bernardez-Clark, 1998), all of which involve an initial solubilisation of inclusion bodies using highly concentrated solutions of chaotropic agents such as guanidinium chloride or urea. The subsequent step in all these methods

consists of removing the denaturing agent and restoring the protein to its native shape from the unfolded soluble state.

In absence of soluble expression and purification of MtbMAP A-Δ164-176 in its native form, it was difficult to study the effects of deletion of the insertion region from MtbMAP A. It was decided to standardize the refolding protocol for the wild type MtbMAP A in order to bring it into active form from solublised inclusion bodies. It was assumed that the same strategy could be used to refold the deletion construct for comparing its properties. Refolding metallo-proteins by restoring both metal-binding and substrate binding pockets was the real challenge in this approach. In present study, four strategies were adopted for refolding MtbMAP A i.e., dilution, dialysis, on-column refolding and arginine solublisation.

6.2.6.1 Dilution

MtbMAP A inclusion bodies solubilised with 3 M urea buffer was used for refolding using dilution. Dilution screen was performed in a total volume of 200 µl in 96 well microtiter plates. Initially, for choosing a suitable protein concentration for dilution, precipitation of the protein at different concentrations during dilution was monitored by a method described by Vincentelli et al., (2004). The precipitation of proteins at 50,100,150 and 200 µg/ml concentration was studied by measuring the optical density at 340 nm. The lists of buffers used for dilution are shown in **Table 6.2**. For all the buffers, the effect of two refolding temperatures, 25 ^{o}C and 4 ^{o}C, were studied. Protein was left diluted in the refolding buffer overnight at the chosen temperature to allow equilibration with the buffer.

Pro-matrix protein refolding kit (Pierce Biotech) (Qoronfleh, 2004) has refolding buffers designed based on a fractional factorial approach and these buffers can be supplemented with additives. This kit consists of denaturing agent guanidine hydrochloride

and solubilising agent arginine. 0.55 mM Tris, 21 mM NaCl, 0.88 mM KCl remains as constant ingredients in all the buffers. The pH of all the buffers provided in the kit was maintained at 8.0. The protein samples for carrying out the experiments using buffers of Pro-matrix kit were extracted using 6 M guanidium hydrochloride as per the manufacture's instruction. The sample was extracted in denaturing lysis buffer (50 mM Tris-Cl, 5 mM DTT, 6 M guanidium hydrochloride, pH 8.0) from the inclusion body state. The lists of buffers from Pro-matrix kit used in the study are shown in **Table 6.3**. The refolding temperature was maintained at 4^{o}C for overnight.

Table 6.2 List of dilution buffers screened for refolding MtbMAP A

S.No	Buffer composition	References
1	50 mM Tris-Cl (pH 8.0)	Cherish Babu et al., 2008
2	50 mM Tris-Cl,1% Triton-X 100,10%glycerol (pH 8.0)	,,
3	50 mM Tris-Cl,100 mM NaCl,10%glycerol (pH 8.0)	,,
4	50 mM Tris-Cl,10 mM glycine, 10 mM EDTA (pH 8.0)	,,
5	50 mM Tris-Cl, 220 mM arginine (pH 8.0)	,,
6	50 mM Tris-Cl, 440 mM arginine (pH 8.0)	,,
7	50 mM Tris-Cl, 1mg/ml BSA (pH 8.0)	,,
8	50 mM Tris-Cl, 500 mM KCl (pH 8.0)	,,
9	50 mM Tris-Cl, 500 mM KCl, 1 mM methionine (pH 8.0)	,,
10	50 mM Tris-Cl, 500 mM KCl, 5 mM methionine (pH 8.0)	,,
11	50 mM Tris-Cl, 5 mM $CoCl_2$ (pH 8.0)	Dong et al.,2008
12	50 mM Tris-Cl, 10 mM $CoCl_2$ (pH 8.0)	,,
13	50m M Tris-Cl, 500 mM KCl, 5 mM $CoCl_2$, 5 mM methionine (pH 8.0)	,,

Table 6.3 List of Pro-matrix kit buffers screened for refolding MtbMAP A

S. No	Buffer base composition	Additives used
1	0 M guanidine-Cl,0 M arginine	5 mM DTT
2	0 M guanidine-Cl,0.44 M arginine	,,
3	0 M guanidine-Cl, 0.88 M arginine.	,,
4	0.55 M guanidine-Cl, 0 M arginine.	,,
5	0.55 M guadinine-Cl, 0.44 M arginine.	,,
6	0.55 M guanidine-Cl, 0.88 M arginine.	,,
7	1.1 M guanidine-Cl, 0 M arginine.	,,
8	1.1 M guanidine-Cl,0.44 M arginine	,,
9	1.1 M guanidine-Cl, 0.88 M arginine	,,
10	0.55 M guanidine-Cl,0 M arginine	2 M GSH,0.2 M GSSG*
11	0.55 M guanidine-Cl, 0.44 M arginine.	2 MGSH,0.2 M GSSG
12	0.55 M guanidine-Cl, 0.88 M arginine.	2MGSH,0.2 M GSSG
13	0.55 M guanidine-Cl,0 M arginine	5 mM $CoCl_2$
14	0.55M guanidine-Cl, 0.44 M arginine.	5 mM $CoCl_2$
15	0.55 M guanidine-Cl, 0.88 M arginine.	5 mM $CoCl_2$
16	0.55 M guanidine-Cl,0M arginine	5 mM $CoCl_2$ 5 mM methionine.
17	0.55M guanidine-Cl, 0.44 M arginine.	5 mM $CoCl_2$ 5 mM methionine.
18	0.55 M guanidine-Cl, 0.88 M arginine.	5 mM $CoCl_2$ 5 mM methionine.

*GSH- Reduced glutathione; GSSG-Oxidized glutathione.

6.2.6.2 Dialysis

The protein content was diluted to final concentrations of 50 µg/ml, 100 µg/ml and 200 µg/ml, in presence or absence of 0.2 mg/ml BSA in 50 mM Tris-Cl (p H 8.0) in a total volume of 2 ml. All these dilutions were dialysed against 500 ml dialysis buffer (50 mM Tris-Cl (p H 8.0), 150 mM KCl +/- 5 mM $CoCl_2$) in a dialysis membrane (8 kDa cutoff) for 14 h at 4 ^oC with two buffer exchanges. Prior to purification, the MAP activity of the refolded proteins after dialysis was performed against 1 mM L-Met-*p*NA in presence of 100 µM Ni^{2+}.

6.2.6.3 On-column refolding

Another alternative successful refolding strategy is by refolding the proteins while they are immobilized on to a matrix. Most widely adopted method for refolding his-tagged recombinant proteins is refolding on Ni-NTA column (D'Alatri et al., 1998; Rogl et al., 1998).

1 ml of 3 M urea extract (3mg) was loaded onto the column pre-equilibrated with the binding buffer (50 mM Tris-Cl, 0.5 M KCl, 3 M urea, 10 mM imidazole, pH 8.0) and column was washed with 10 ml of 3 M urea containing wash buffer I (50 mM Tris-Cl, 0.5 M KCl, 3 M urea, 20 mM imidazole, pH 8.0). To employ a decreasing urea gradient, the column was further washed with 10 ml of 2 M urea containing buffer (50 mM Tris-Cl, 0.5M KCl, 20 mM, imidazole, 2 M urea, pH 8.0) and then with 1 M urea containing buffer. A final wash was given with a buffer without urea (50 mM Tris-Cl, 0.5 M KCl, 20 mM imidazole, pH 8.0). Elution of the recombinant protein from the column was done in buffers containing 250 mM imidazole. The protein contents in all the eluted fractions were analyzed on SDS-PAGE to check their purity. The activity of the on-column refolded MtbMAP A was assayed

by performing standard MAP assay with 1 mM L-Met-*p*NA as described in previous sections.

6.2.7 Solubilisation of inclusion bodies using L-arginine

Among the different additives studied so far for improving solubility of recombinant proteins from inclusion bodies, the positive effects of L-arginine in reducing protein aggregation and improving refolding process has been demonstrated for many proteins (Yasuda et al., 1998; Ramos et al., 2003). Interaction of guanidine structure in arginine with tryptophan residues in the proteins have been suggested as the possible mechanism of action in reducing protein aggregation (Arakawa and Tsumoto, 2003). Some of these studies have suggested arginine at 2 M concentration as less denaturing for extraction of inclusion bodies at near native structure, replacing urea or guanidium hydrochloride (Arakawa and Tsumoto, 2003). Recently, there have been some reports on fine-tuning the inclusion bodies to contain a high percentage of correctly folded protein precursors, termed as "non-classical inclusion bodies", by varying the cultural conditions (Jevsevar et al., 2005; Peternel et al., 2008a). LB-glucose medium (2.5% glucose in LB broth) has been reported for production of non-classical inclusion bodies of many proteins like human granulocyte colony stimulating factor, green fluorescent proteins and human tumor necrosis factor TNF-α (Peternel et al., 2008b). We have combined non-classical inclusion body approaches along with arginine extraction for solublisation of MtbMAP A and MtbMAP A-Δ164-176 from inclusion bodies.

Briefly, the recombinant expression was done in 100 ml of LB-glucose (2.5% glucose) broth instead of LB broth and rest was followed as in chapter 5 (5.2.4). During protein extraction, after sonication and clarification by centrifugation, the insoluble pellet was collected and extracted with 50 mM Tris-Cl, pH 8.0 containing 2 M L-arginine.

The arginine extract was diluted to a protein concentration of 0.2 mg / ml and dialysed against 50 mM Tris-Cl, 0.5 M NaCl and 10 mM imidazole, pH 8 at 4 ^{o}C for overnight to facilitate complete removal of arginine. The dialysed proteins were further used for native purification through Ni-NTA column and were processed to produce apo-enzymes as described in chapter 5 (5.2.5). The refolding efficiency was tested by performing standard MAP assay with L-Met-*p*NA. The structural variations in arginine extracted - refolded MtbMAP A was compared with the native MtbMAP A purified from soluble fraction by performing CD-spectroscopy, as described in chapter 3 (3.2.9.12), using 0.1 mg /ml of both the proteins in 20 mM phosphate buffer pH 7.4. The enzyme activities of refolded apo-MtbMAP A and apo-MtbMAP A -Δ164-176 were studied against 1 mM L-Met-*p*NA in presence of 100 μM Ni^{2+}.

6.2.8 Comparison of MAP activity of MtbMAP B mutants with wild type

Those mutants of MtbMAP B which were expressed in the soluble fractions and purified by Ni- affinity chromatography were used to study the effects of mutations on MAP activity against L-Met-*p*NA. MAP assay of MtbMAP B in comparison with the mutants were performed as described in chapter 5 (5.2.6) using 2 μg and 4 μg of purified apo-enzymes in presence of 100 μM Co^{2+} against 1 mM L-Met-*p*NA at pH 8.0 and 37 ^{o}C.

6.3 Results and Discussion

6.3.1 Multiple sequence alignment of MtbMAP

Multiple sequence alignment of MtbMAPs with representatives of bacterial and human type I MAPs are shown in **Fig 6.1**. The two MtbMAPs share about 33% of sequence identity between themselves. Both MtbMAPs have less than 45% of similarity with *E. coli*

MAP 1 and 48% similarity with human MAP 1. Both have less than 30% similarity with human type II MAP.

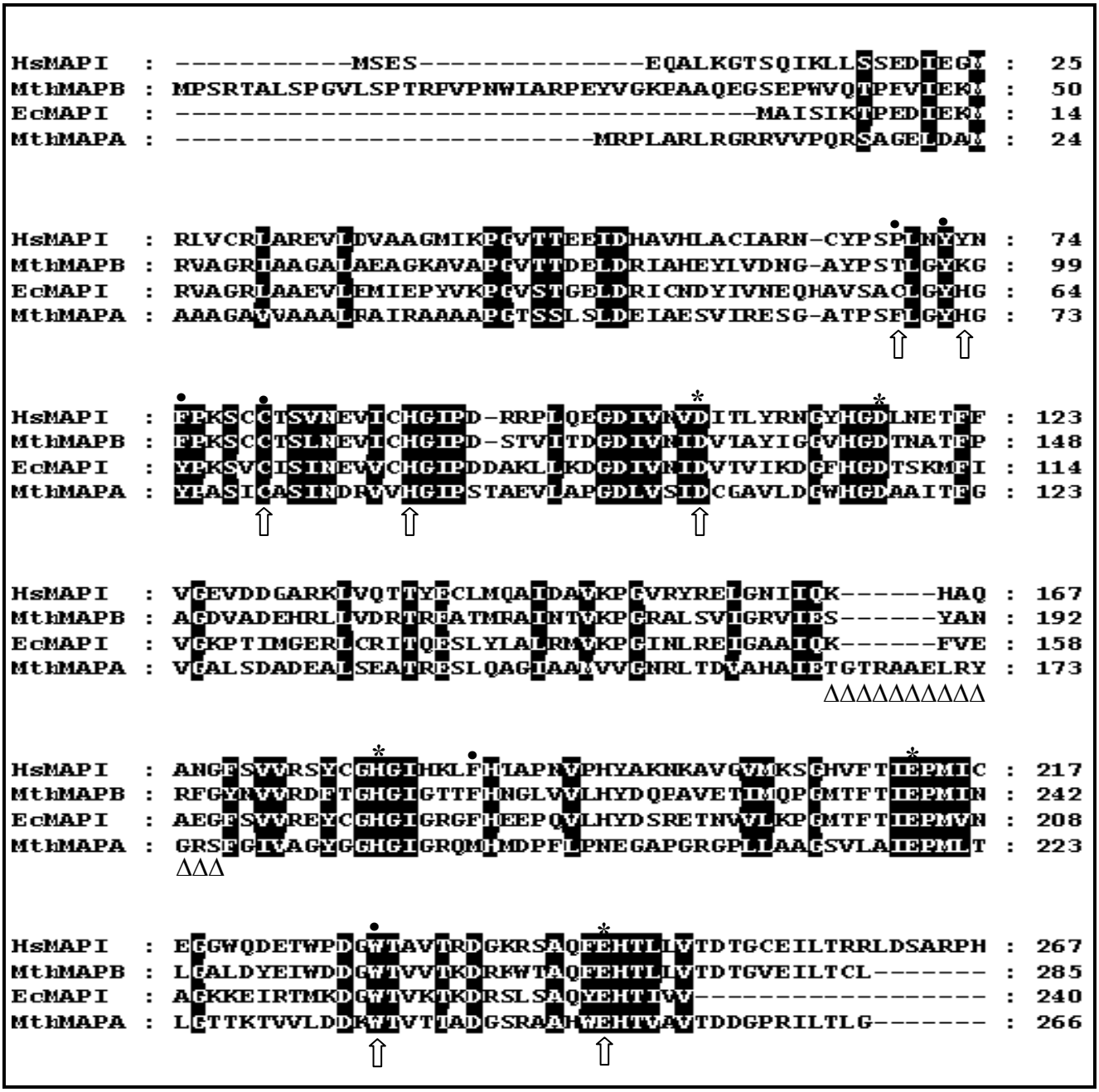

Fig 6.1: Multiple sequence alignment of MtbMAPs with type I MAP sequences from *E. coli* and *H. sapiens*. The conserved residues involved in metal-binding in MAP Is are denoted with an asterisk (*) above them. The residues involved in formation of substrate binding S1' pockets in *E. coli* are denoted with filled circle (•) above them. The sites selected for creating substitution mutants in MtbMAP B are denoted by arrow heads (⇧) below them. The residues deleted from the insertion region of MtbMAP A in creating deletion mutants are denoted by triangles (Δ) below them.

With in these differences, there is a high level of conservation of all the five metal binding residues in all these MAPs (Chiu et al., 1999; Li et al., 2004). The metal binding residues in case of MtbMAP A are D106, D117, H186, E219 and E250. The corresponding residues in MtbMAP B are D131, D142, H205, E238 and E269 (**Fig 6.1**). The residues forming S1' pocket in case of MtbMAPs showed variations from those of *E. coli* and human type I MAPs (Chiu et al., 1999; Li et al., 2004). Important variations between residues of S1' pocket of MtbMAP A with *E. coli* MAP were, F68 instead of C59 and M192 instead of F177. The variations between S1' pocket of MtbMAP B and *E. coli* MAP were T94 instead of C59 and F100 instead of Y65 (**Fig 6.1**).Apart from this a lysine replaces the conserved H63 of *E. coli* (Mitra et al., 2009) in case of MtbMAP B. Thus, even though there is low similarity between MtbMAPs and *E. coli* MAP, there is a high level of conservation of metal binding and S1' pocket in both the cases.

Structurally, there was an extended N-terminal in case of MtbMAP B, which led to classification of this enzyme under MAP type Ic. This N-terminal extension was reported to contain a surface exposed Pro-x-x-Pro (PxxP) motif in the crystal structure (PDB ID: 1YJ3) which allows Src-homology (SH3) binding within the ribosome (Addlagatta et al., 2005b). In case of MtbMAP A, there was a specific 8 amino acid insertion region with in the catalytic domain between the 2^{nd} and 3^{rd} metal binding residues, which was absent from all other type I MAPs (**Fig 6.1**). This unique insertion sequences in type I MAPs are not reported earlier. In case of eukaryotic and archaebacterial type II MAPs, insertion sequences are reported between 4^{th} and 5^{th} metal binding residues (Tahirov et al., 1998; Addlagatta et al., 2005a). In case of *Streptococcus salivarius* and *Lactococcus lactis* MAP 1s, a 24 amino acid insertion was reported between 1^{st} and 2^{nd} a metal binding residue, which was not

reported in other type I MAPs (Boufous and Vadeboncoeur, 2003). However, the importance of this insertion region was not analysed in these organisms. Analysing MAP sequences from other members in the Mycobacterium families too showed this insertion in homologs of MtbMAP A (data not included). Thus, the insertion region in MtbMAP A is specific for Mycobacterium MAP type 1a. Since this differentiates MtbMAP A from human type I MAPs structurally, characterizing the structural role of this insertion region would be of great advantage in improving specificity of inhibitors against Mtb MAP A. Moreover, similar insertion regions in MtbPDF, proved to be essential for enzyme activities, have been identified as specific targets for targeting anti-sense oligos to arrest the growth of *M. smegmatis* in culture (Saxena et al., 2008). From the studies of Zhang et al., (2009) and Olaleye et al., (2010), it is now clear that MtbMAP A is the most essential MAP during the active phase of growth in *M. tuberculosis*. Thus identifying and characterizing structural variations between human MAP 1 and MtbMAP A will have a great relevance in improving the specificities of MAP inhibitors against *M. tuberculosis.*

Based on the multiple sequence alignment, construction of a deletion mutant, removing the residues from insertion region (169-176), was attempted in MtbMAP A. This deletion construct would reveal structural and functional roles of the residues of insertion region in MAP activity and stability of MtbMAP A.

In case of MtbMAP B, nine substitution mutants were proposed at seven sites. Among this, T94C and K98H were created to explore the effects of substituting these two residues of S1' pockets of MtbMAP B with those of *E. coli*. K98A was created to study the catalytic role of lysine residue in the exterior loop in the vicinity of active site in MtbMAP B. H63 at this position in *E. coli* MAP was reported to have important role to play in

substrate recognition (Mitra et al., 2009). C105S corresponds to substitution of a conserved cystein in the S1' pocket of type I MAPs. In case of human type II, instead of cystein there is an isoleucine at this position. The effect of this substitution was studied by C105I mutation. H114A mutant was created to study the role of this histidine in the catalysis of MtbMAP B. Substitution of corresponding residue, H79, in *E. coli* MAP was reported to affect the catalysis and this residue was proposed to be involved in positioning the substrate in the binding pocket for effective catalysis in *E. coli* MAP (Watterson et al., 2008). W255L substitutes this conserved tryptophan residue in the S1' binding pocket of MtbMAP B. This mutation was adopted from the studies of Chiu et al., 1999 on *E. coli* MAP. D142A and E269V substitutes two of the conserved metal binding residues in MtbMAP B. From the crystal structure of MtbMAP B it was understood that both these residues are important in binding the first metal ion in the dinuclear metal centre (Lu et al., 2010).

6.3.2 Construction of site-directed mutants of MtbMAPs

The nine substitution mutants of MtbMAP B (T94C, K98H, K98A, C105S, C105I, H114A, D142A, W255L and E269V) and deletion mutant of MtbMAP A (MtbMAP A-Δ164-176) were constructed and the recombinant plasmids bearing these mutations were confirmed by DNA sequencing of the mutated plasmids (**Fig 6.2** and **Fig 6.3**). The mutant plasmids were transformed into *E. coli* BL 21 (DE3) cells for over expression studies.

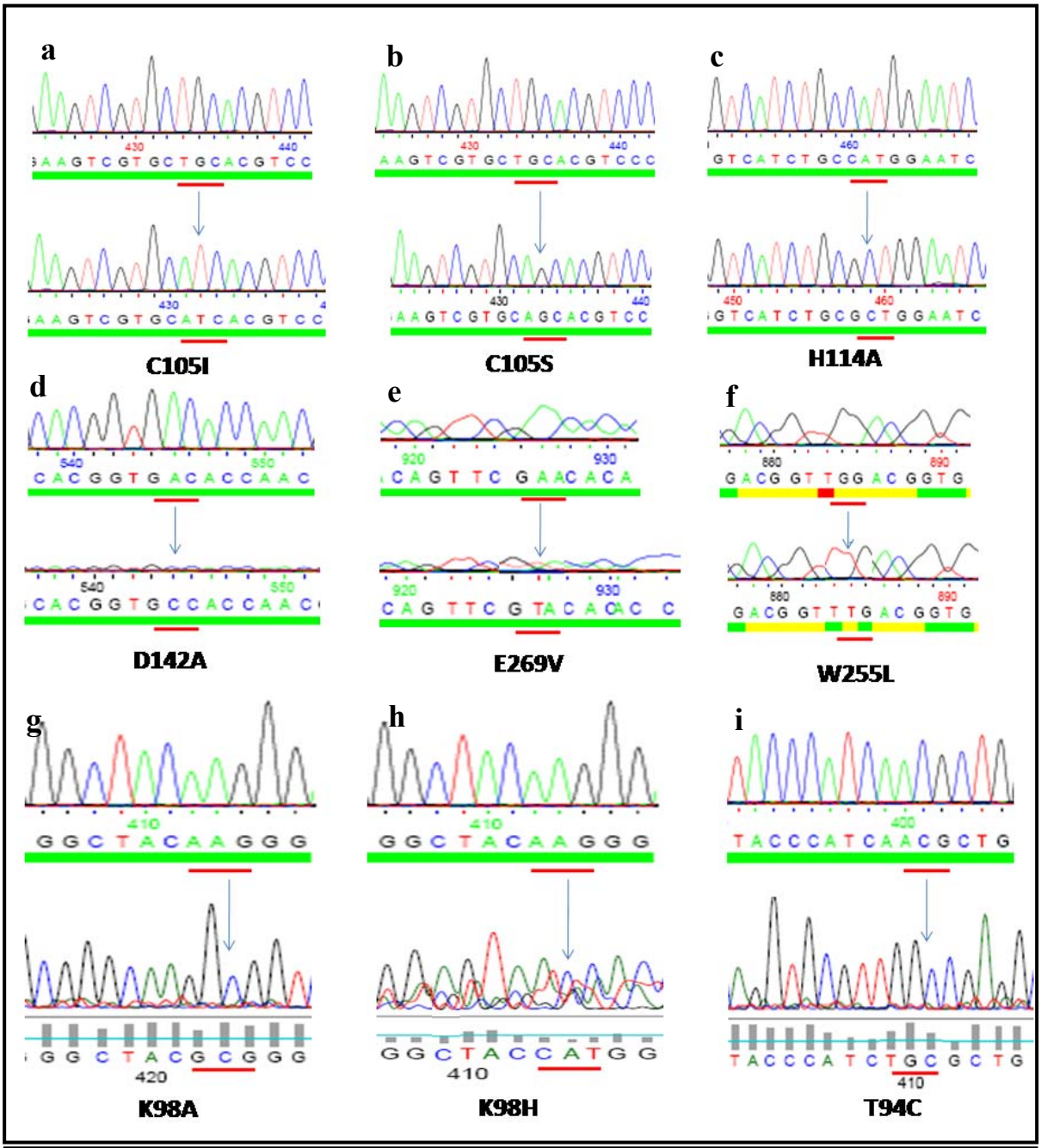

Fig 6.2: (a-i) Confirmation of site-specific mutations on pET28a. *map*B plasmid by DNA sequencing. The upper chromatogram in each figure shows the wild type sequence and the lower one shows the mutated sequence. The codons mutated are underlined in red in each case and the corresponding amino acids replaced at those sites are denoted at the bottom of each figure.

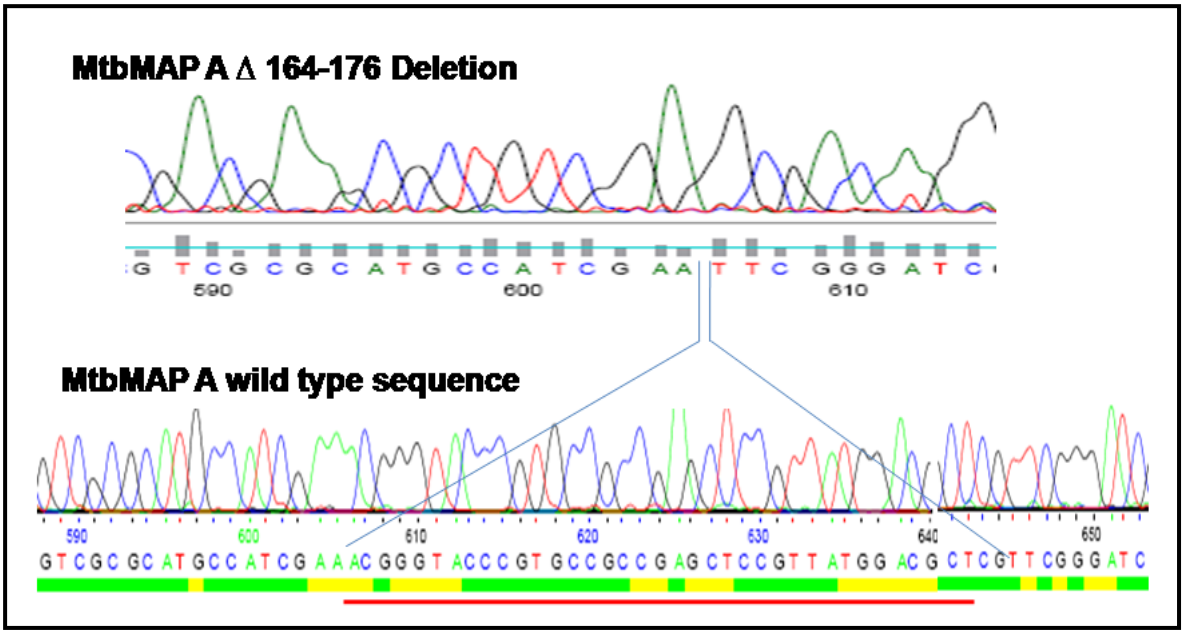

Fig 6.3: Confirmation of deletion mutagenesis on pET28a. *map*A plasmid by DNA sequencing. The upper chromatogram shows the plasmid DNA sequences with 39 bases (13 codons) deleted corresponding to amino acids 164-176 in MtbMAP A. The deleted sequences are shown in the chromatogram of wild type MtbMAP A sequence, underlined in red.

6.3.3 Over expression and purification of MtbMAP A-Δ164-176

Upon over expression from *E. coli* BL21 (DE3), whole of the MtbMAP A-Δ164-176 proteins got expressed in the insoluble fractions as inclusion bodies (**Fig 6.4**). In case of wild type MtbMAP A, even though there was an increased expression in the insoluble fraction, only small amounts could be purified from soluble fraction (5.3.3). Western blot analysis further confirmed the lack of soluble expression in case of MtbMAP A-Δ164-176. This could be due the fact that the deletion of the insertion region has affected the tertiary structure and folding of MtbMAP A, which led to its complete expression in the insoluble fraction. Deletion of similar insertion region in case of MtbPDF too has led to complete insoluble expression, but could easily be refolded from the inclusion bodies by simple

dialysis (Saxena et al., 2008). Attempts to purify recombinant proteins from soluble fractions through Ni-NTA column have turned positive only in case of wild type MtbMAP A, as described in chapter 5 (**Fig 5.6 A**).

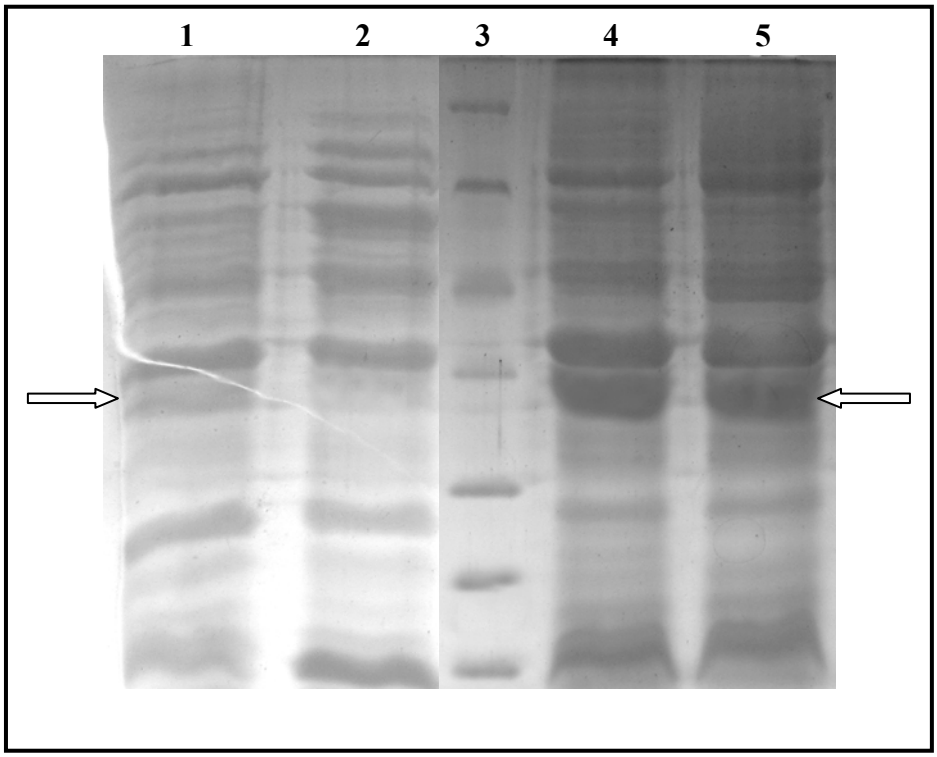

Fig 6.4: 12% SDS-PAGE showing expression of MtbMAP A and MtbMAP A-Δ164-176 in different fractions from *E. coli*. Lane 1: Soluble fraction MtbMAP A; Lane 2: Soluble fraction MtbMAP A-Δ164-176; Lane 3: Protein ladder; Lane 4: Insoluble fraction of MtbMAP A; Lane 5: Insoluble fraction of MtbMAP A-Δ164-176.

6.3.4 Optimization of conditions for soluble expression of MtbMAP A-Δ164-176

Optimization of parameters like induction at varying temperature and IPTG concentrations had no positive effect in bringing either MtbMAP A or MtbMAP A-Δ164-176 into soluble fractions. Upon co-expression with chaperone GroEL/S, the wild type enzyme alone could be co-purified by Ni-NTA column chromatography (**Fig 6.5**) as in the case of MtbPDF (chapter 3, Fig **3.10**). This suggested a possible alteration in the overall

structure of deletion mutant, which might have led to disturbances in the sites for chaperone-binding to assist proper folding and solubilisation of these proteins similar to wild type MtbMAP A.

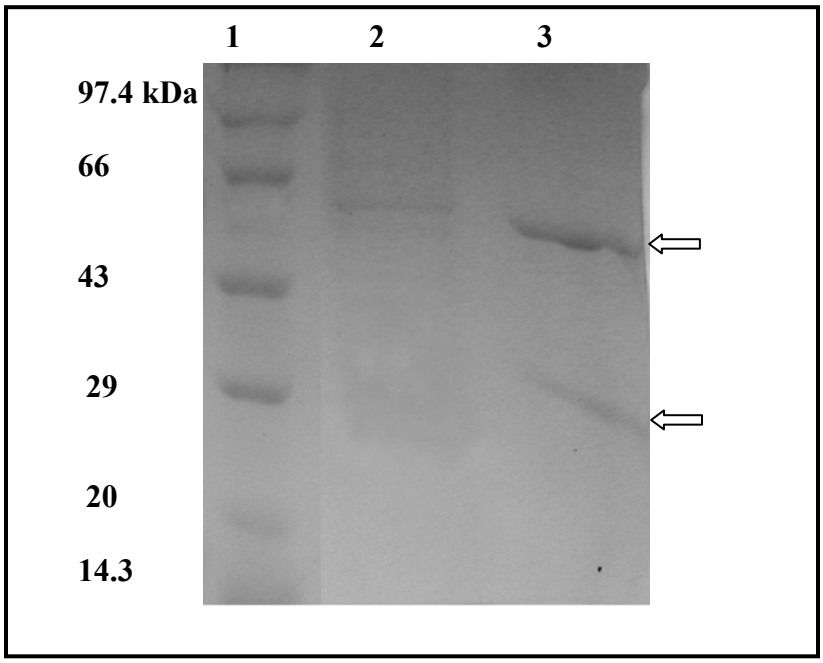

Fig 6.5: Co-purification MtbMAP A and MtbMAP A -Δ164-176 with chaperone GroEL/S through Ni-NTA column. Lane 1: Protein ladder; Lane 2: Co-purification MtbMAP A -Δ164-176 from soluble fractions of GroEL/S co-expression. Lane 3: Co-purification MtbMAP A from soluble fractions of GroEL/S co-expression; GroE (60 kDa) and purified on MtbMAP A (29kDa) are marked with arrows. MtbMAP A -Δ164-176 didn't get purified from the soluble fractions by this strategy.

6.3.5 Purification of MtbMAP A -Δ164-176 from inclusion bodies

Since the soluble expression and purification of MtbMAP A-Δ164-176 was not achieved, it was decided to solublise and purify the deletion mutant protein expressed in the inclusion bodies. Similarly, the wild type MtbMAP A was also solubilised and purified from the inclusion bodies. Both the wild type and mutant proteins got purified to near homogeneity producing a final yield of 13 mg and 8 mg respectively, per liter culture (**Fig**

6.6). The proteins purified from inclusion bodies didn't show any variations in the molecular weight on 12% SDS-PAGE compared to the wild type enzyme purified from soluble fractions. Since only 13 amino acids were deleted to construct deletion mutant, the difference in the molecular weights between wild type and mutant enzyme was not that significance to recognize on SDS-PAGE.

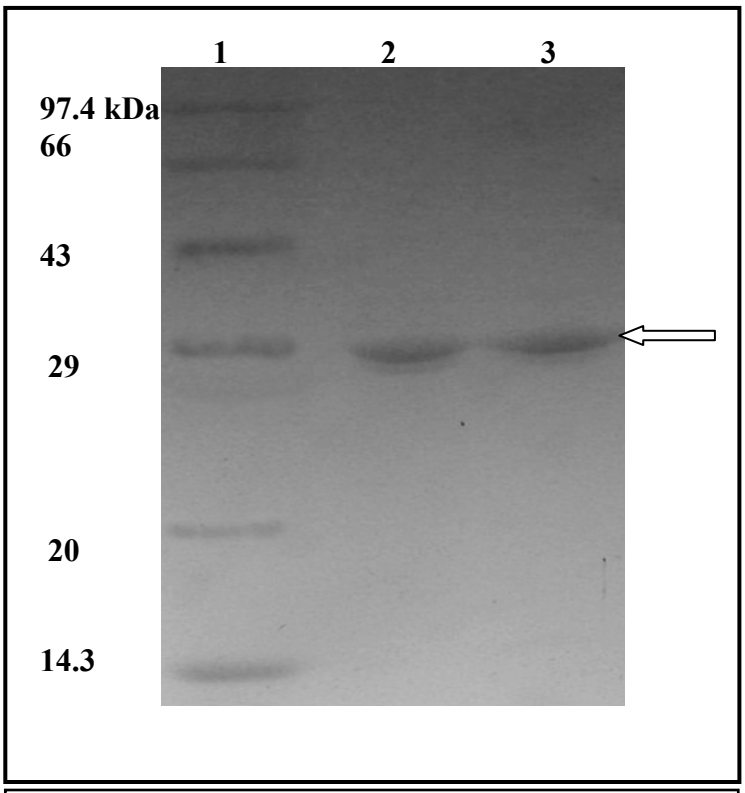

Fig 6.6: Purification of MtbMAP A and MtbMAP A-Δ164-176 from solublised inclusion bodies. Lane 1: Protein ladder; Lane 2: Purified MtbMAP A; Lane 3: Purified MtbMAP A -Δ164-176; Proteins were solublised in presence of 3 M urea and were purified under denaturing condition through Ni-NTA column.

6.3.6 Refolding of MtbMAP A from solubilised inclusion bodies

In order to standardize the refolding process of deletion mutant, attempts were made to standardize refolding of wild type MtbMAP A from solubilised inclusion bodies.

Complete refolding of MtbMAP A into active enzyme from solubilised inclusion bodies was not achieved by any of the attempted refolding methods.

6.3.6.1 Refolding by dilution

During dilution it was found that the recombinant proteins precipitated out when the concentration was greater than 100 μg/ml as indicated by their absorbance at 340 nm and visualization of precipitation (data not shown). So a protein concentration of 50 μg/ml was used for all the dilution experiments. Among the different refolding buffers used in dilution of MtbMAP A, none produced completely refolded proteins as indicated by their activity against 1 mM L-Met-*p*NA in any of the refolding temperatures studied (data not included).

Pro-matrix protein refolding kit has been used for refolding many of the heterogenous proteins from inclusion bodies. Successful refolding has been reported for proteins like lysozyme, a novel immunotoxin (Wan et al., 2006), a novel mannose binding protein from *Acanthamoeba* (Garate et al., 2004). However, in our study with MtbMAP A, the use of Pro-matrix refolding buffers proved to be unsuccessful in refolding this protein to their active state, as indicated by the failure in hydrolyzing the substrate L-Met-*p*NA.

6.3.6.2 Refolding by dialysis

One-step dialysis method has successfully been employed for the refolding MtbPDF in this study. During dialysis, the concentration of denaturant decreases with time to the concentration of refolding solvent. As the denaturant concentration is decreased, the rate of folding into native and near-native structures of proteins increases. Dialysis has been successfully used previously to refold many antibodies and lysozyme (Tsumoto et al., 1998; Maeda et al., 1995).

Dialysis of MtbMAP A at concentrations 100 and 200 μg/ml led to

visible precipitation. So dialysis was attempted by keeping the protein concentration at 50 µg/ml. After overnight dialysis, it was found that the protein at this concentration remained soluble against all the dialysis buffers tested. But, none of the dialysis buffers, with or without metal ions, produced active enzymes and hence it was concluded that dialysis method using the buffers tested was not effective in refolding MtbMAP A from inclusion bodies.

6.3.6.3 On-column refolding

On-column refolding or matrix assisted refolding methods have been successfully used in refolding some of the recombinant proteins like yeast dehydrodolichyl phospholipase and some membrane proteins of *E. coli* from inclusion bodies (Chang et al., 2001; Rogl et al., 1998). This method has the advantage of combining refolding and purification step. The gradient washing of the immobilized protein on the Ni-NTA column with buffers containing decreasing concentrations of urea was found ineffective in refolding MtbMAP A. Moreover, there was loss of bound proteins at each step of washing due to the change in urea concentration (data not included). Since the substrate, L-Met-*p*NA was also not hydrolysed, it was assumed that the method was not effective in bringing active MtbMAP A from inclusion bodies.

6.3.7 Solubilisation of inclusion bodies with arginine

MtbMAP A expressed in the insoluble fractions of recombinant *E. coli* BL21 (DE3) cells grown in LB-glucose medium got extracted in 2 M arginine. Analysis on SDS-PAGE showed over expressed bands corresponding to the size of MtbMAP A (**Fig 6.7a**). The inclusion bodies solublised by arginine and purified through Ni-NTA column showed purified bands corresponding to MtbMAP A (**Fig 6.7b**). The yield in case of arginine

extraction was lower compared to 3 M urea extracted inclusion bodies and the final yield of arginine extracted-purified MtbMAP A from 1 liter of culture was 2-3 mg.

Applying the same strategy to refold MtbMAP A-Δ164-176 resulted in purification of deletion mutant from the arginine solubilised inclusion bodies through Ni-NTA column (**Fig 6.7b** and **6.7c**). The final yield of the apo-MtbMAP A-Δ164-176 from arginine extract was 0.8-1 mg per liter culture.

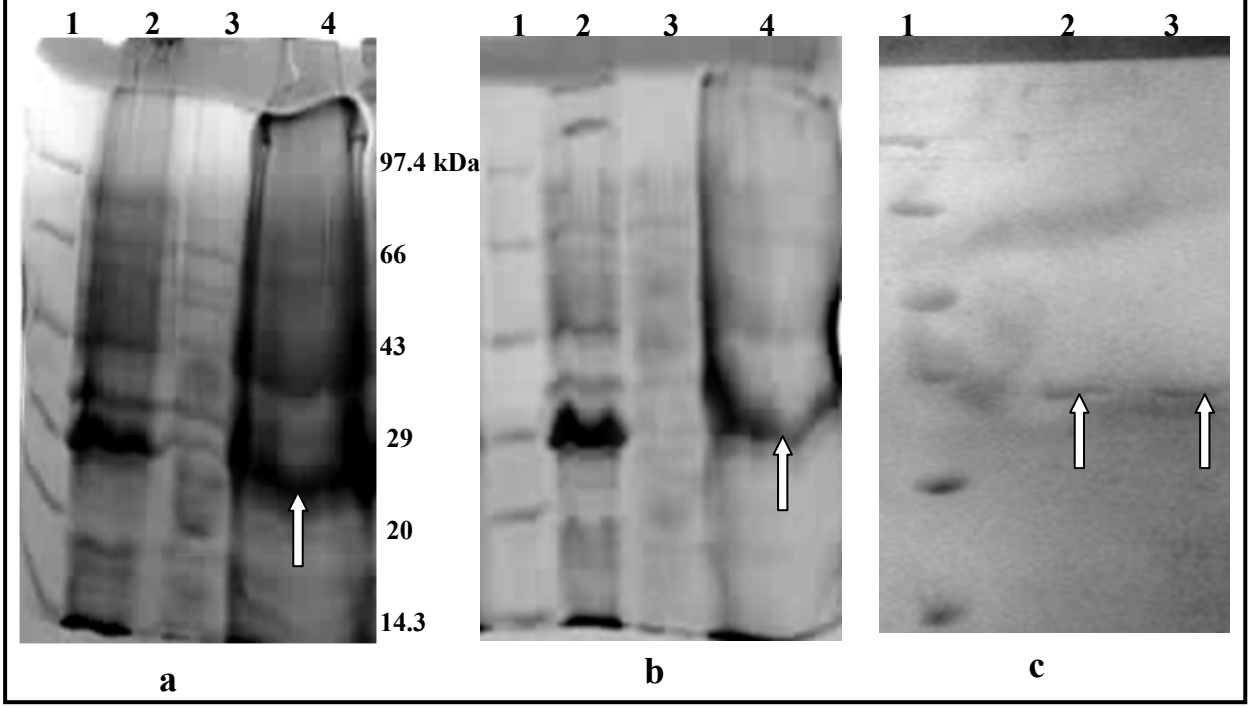

Fig 6.7: Solublisation of inclusion bodies with arginine and purification of solublised inclusion bodies. (a) MtbMAP A **(b)** MtbMAP A -Δ164-176; Lane 1: Protein ladder; Lane 2: Induced total protein; Lane 3: Soluble fraction; Lane 4: 2 M arginine extract of insoluble fractions; **(c)** Purification arginine solublised MtbMAP A and MtbMAP A -Δ164-176 through Ni-NTA column; Lane 1: Protein ladder; Lane 2: MtbMAP A; Lane 3: MtbMAP A -Δ164-176.

The purified apo-enzymes of MtbMAP A from the arginine solubilised inclusion bodies showed specific activity of 110 ± 17 μM *p*NA/min/mg proteins against 1 mM L-Met-*p*NA in standard MAP assay in presence of 100 μM of Ni^{2+} against a specific activity of

1406 ± 37 μM/min/mg protein in case of MtbMAP A proteins purified from soluble fraction. The arginine extracted proteins from inclusion bodies showed less than 10% activity compared to those purified from soluble fraction. Nevertheless, there was visible enzyme activity from the solublised inclusion bodies of MtbMAP A by following arginine extraction.

While comparing the CD spectrum of MtbMAP A purified from soluble fractions and those purified from arginine extract of inclusion bodies, visible secondary structure alterations were evident (**Fig 6.8**). There were two negative minima in both the cases at 222 nm and 208 nm corresponding to the helical structures. The low mean residue ellipticity (θ) values (~ -3) in the native structure at 222 nm clearly suggests the presence of β-sheets in addition to the helical structures. The θ values were comparatively higher in case of the arginine solublised MtbMAP A with a shift in the negative minima at 208 nm to 212 nm. Also the crossing point for arginine solublised MtbMAP A was at 203 nm instead of 198 nm in case of the native MtbMAP A. These differences in the CD spectrum suggest slight variations in the total β-sheet contents and loop contents between the two structures. These structural differences could be due to the presence of mixtures of native and near-native structures in case of arginine solublised MtbMAP A. These structural differences might have led to the variations in the enzyme activities between the two structures.

The MAP activity assay for MtbMAP A-Δ164-176 in standard conditions in presence of Ni^{2+} showed no detectable hydrolysis of L-Met-*p*NA. This suggests that the deletion mutant MtbMAP A-Δ164-176 could possibly be an inactive one. Further optimizations of the refolding conditions are required for producing completely active

MtbMAP A from inclusion bodies in order to compare the enzyme activities of wild type and deletion mutant and to comment on the activity status of the deletion mutant.

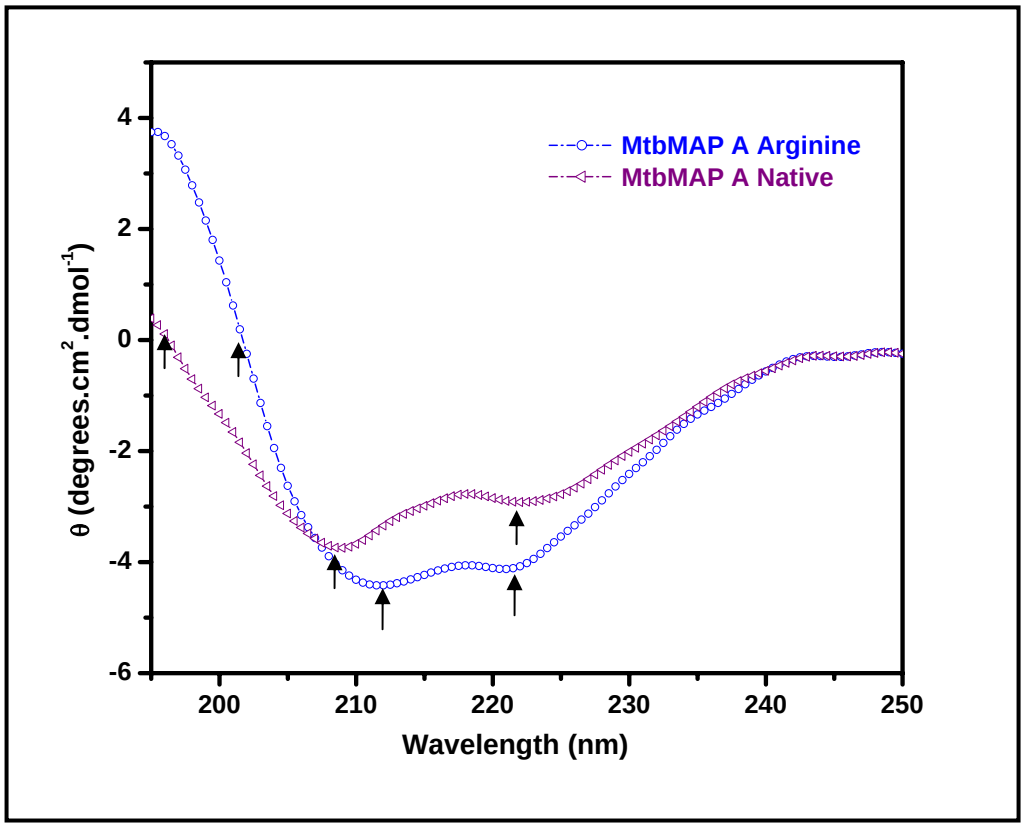

Fig 6.8: CD spectrum apo-MtbMAP A purified from soluble fraction and from arginine solublised inclusion bodies. 0.1 mg / ml of protein concentration was used in 20 mM phosphate buffer, pH 7.4: The negative minima at 222 nm, 208 nm and 198 nm are indicated by arrow heads.

6.3.8 Over expression and purification of MtbMAP B mutants

Upon induction, all the nine mutants of MtbMAP B got expressed in *E coli*, showing similar molecular mass of wild type MtbMAP B on SDS-PAGE (**Fig 6.9**). Fractionating the proteins expressed showed that only six mutants (T94C, K98H, K98A, C105S, C105I and D142A) were expressed similar to the wild type enzyme in the soluble fraction (**Fig 6.9a**). The other three mutants (H114A, E269V and W255L) were completely expressed in insoluble fractions as inclusion bodies (**Fig 6.9b**). Attempts to purify these mutants from

soluble fractions through Ni-NTA columns didn't yield any purified bands at the corresponding size on SDS-PAGE. No further attempts were made to solublise these three mutants and they were not considered for further studies. Among all the mutants of MtbMAP B, D142A was expressed in high levels similar to the wild type enzymes. It was surprising to note that while D142A got expressed in high levels, the other mutation on metal binding residue, E269V produced completely insoluble proteins. Both these are residues involved in binding the first metal ion in MtbMAP B, as seen from the crystal structure of MtbMAP B (Lu et al., 2010). The differences in expression could possibly be due to the substitution of E269 with a valine residue instead of alanine as for D142. Substitutions of conserved residue W255 from the S1' pocket and H114 from the flexible exterior loops too resulted in complete insoluble expression. Corresponding mutants of *E.coli* MAP have been successfully expressed and characterized by previous workers (Chiu et al., 1999; Mitra et al., 2009).

The mutants expressed in soluble fractions similar to wild type enzymes were purified to near homogeneity as seen from their SDS-PAGE analysis (**Fig 6.9c**).They were processed similar to the wild type enzymes to produce their corresponding apo-enzymes.

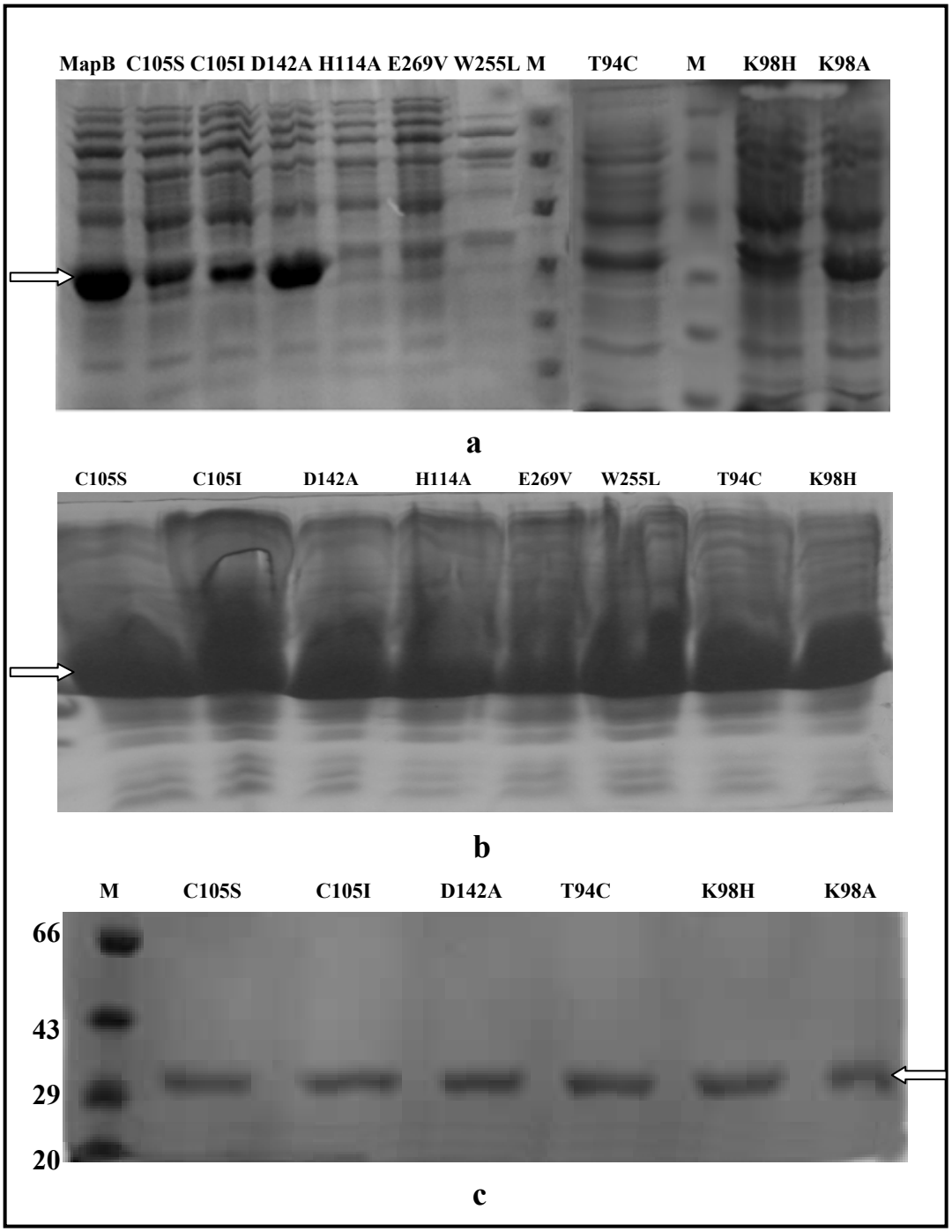

Fig 6.9: Overexpression and purification of site-directed mutants of MtbMAP B. (a) Soluble fractions from expression of mutants **(b)** Insoluble fractions from expression of mutants **(c)** Purification of the mutants expressed in soluble fractions. The mutants are denoted above in each lane and lane M represents the protein ladder in each case.

6.3.9 Enzyme activities of MtbMAP B mutants

The enzyme activities of mutants purified from soluble fractions as apo-enzymes against 1 mM L-Met-*p*NA in presence of 100 μM of Co^{2+} are shown in **Fig 6.10**. The results showed that two of the mutants T94C and K98H, substituting the MtbMAP B residues with corresponding residues from *E. coli* MAP, had increased the MAP activity by a small extent. But K98A substitution has led to slight reduction in the MAP activity. T94 corresponds to the C59 residue in *E. coli* MAP, which was suggested to be involved in the formation of S1' hydrophobic pocket (Chiu et al., 1999). This cystein residue was reported to be characteristic for all bacterial type I MAPs studied and offers discrimination with the type II MAPs lacking it at this position (Swierczek et al, 2005). But in case of MtbMAP A and MtbMAP B, this cystein was replaced by phenylalanine and threonine respectively (**Fig 6.1**). K98 in MtbMAP B corresponds to H79 in case of *E. coli* MAP which was previously reported to be involved in the positioning of substrate in the hydrophobic pocket by formation of hydrogen bonding with them (Watterson et al., 2008). From the slight decrease in activity of K98A mutant and increase in activity of K98H mutant, it was evident that K98 plays an important role in maintaining the catalytic activities of MtbMAP A. Since histidine was able to play the role of lysine at this position better in case of K98H mutant, we assume this evolutionary substitution of histidine to be one of the reasons for low catalytic activities of MtbMAP B. C105S mutation was reported in *E. coli* MAP previously and this has led to reduction of MAP activities by 50% (Chiu et al., 1999). In case of human type I MAP the mutations at corresponding cystein residues at this position (C202) was proven to be responsible for deciding the N-terminal substrate specificities of the enzyme (Li et al., 2004). In our studies too we found nearly 50% of activity loss by C105S mutation. Mutating the residue at this

position with iso-leucine residue found in human type II MAP, decreased the MAP activity against L-Met-*p*NA. One probable reason for this decrease in MAP activities might be due to the variation in substrate specificities between the two types of MAP enzyme. In our study we have used only L-Met-*p*NA as the substrate to screen MAP activities. Using tri or tetra peptides as substrates will throw more light into the effects of each of the above described mutations. As expected, the substitution of metal binding D142 reduced the enzyme activities of MtbMAP B drastically. Characterizing the metal-binding properties and kinetic properties against substrates with varying lengths will provide more insights into the effects of each of the above described mutations on catalysis and substrate binding properties of MtbMAP B.

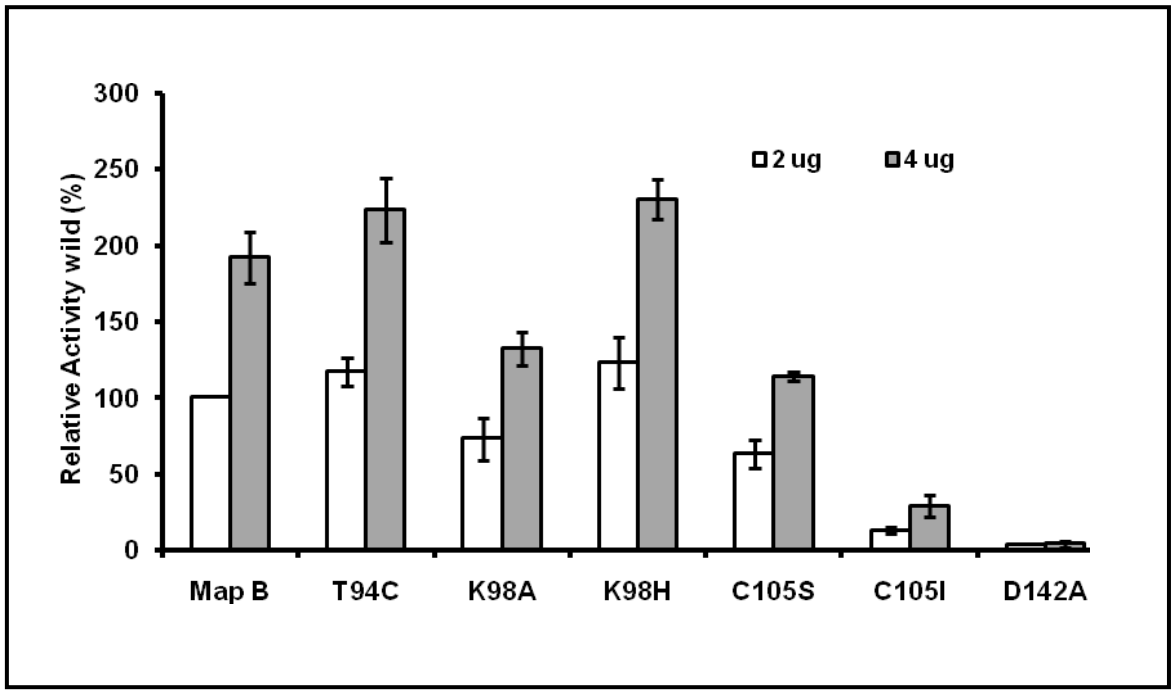

Fig 6.10: Enzyme activities of mutants of MtbMAP B. Activity assay was done against 1 mM L-Met-*p*NA in presence of 100 μM Co^{2+} at pH 8.0 and 37 ^{o}C. The results are represented as percentage relative activities of the activity of MtbMAP B at 2 μg.

6.4 CONCLUSIONS

The studies on mutants of MtbMAPs, revealed the importance of some critical regions and residues in MtbMAPs that determine the enzyme activity. Both MtbMAP A and MtbMAP B showed high level of conservation of residues in the metal-binding and substrate binding pockets compared to other type I MAPs. The insertion region in the amino acid sequences between 2^{nd} and 3^{rd} metal-binding residues of MtbMAP A was found to be specific for Mycobacterium MAP A. Deleting this region had adverse effect on the soluble expression of MtbMAP A. Refolding of MtbMAP A from inclusion bodies was not successful by traditional refolding strategies. But changing the expression conditions to produce non-classical inclusion bodies and extracting with arginine proved to be effective in renaturing MtbMAP A to a certain extent. Characterizing the relevance of this insertion region in MtbMAP A activity and stability might help in identifying this region as potential targets for designing anti-sense oligos against *M. tuberculosis*. In the absence of the crystal structure of MtbMAP A, this study could be further extended to create the sequence based homology model of MtbMAP A and MtbMAP A-Δ164-176 and to perform molecular dynamics on these structures to compare the differences in stability of the mutant structure and variations at the substrate and metal-binding pockets. The present study also identifies some uncharacterized mutations such as T94C and K98H in MtbMAP B to produce preliminary information on their relevance in the enzyme activities.

CHAPTER 7

Summary and Conclusions

CHAPTER 7

Summary and Conclusions

Analysis of *Mycobacterium tuberculosis* H37Rv genome for genes encoding enzymes involved in the N-terminal methionine excision (NME) pathway revealed one *def* gene (Rv0429c) coding for peptide deformylase and two *map* genes; *map*A (Rv0734) and *map*B (Rv2681c) coding for methionine aminopeptidases. All these three genes were essential for the viability and survival of the pathogen either in its active phase of growth or in stationary phase. In the present study, an attempt was made to characterize these gene products as recombinant proteins by cloning the respective genes in pET28a expression vector and expressing them as N-terminal 6x-histidine tagged proteins in *E. coli*.

Over expression of *def* gene in *E coli* yielded high amounts of recombinant MtbPDF in the form of insoluble inclusion bodies, which got easily refolded and purified into their active form by simple dilution and dialysis. Recombinant MtbPDF was active against the tested N-formylated substrates and showed specificities towards substrates with non-bulkier amino acids at their P2' position. The catalytic and kinetic properties of this enzyme revealed it to be catalytically less efficient, compared to the previously characterised bacterial PDFs. Fe was identified as the major metal ion in the purified MtbPDF. MtbPDF was moderately thermo-stable with optimum activity at or below the ambient temperature at neutral pH. Biochemical characterizations revealed the enzyme to be highly resistant towards H_2O_2, which was unusual for Fe-containing PDFs. MtbPDF was inhibited by micro molar concentrations of competitive PDF inhibitor actinonin. Over expression of MtbPDF in *E. coli* rendered the host cells resistant towards actinonin, proving that MtbPDF can function

in *E. coli* cytoplasm and complement the *E. coli* PDF activity. Based on this observation, a cell-based inhibitor screening assay protocol was developed and tested for screening natural MtbPDF inhibitors using *E. coli* cells expressing MtbPDF.

Site-substitution mutations of the key amino acid residues from the three conserved motifs of MtbPDF revealed their importance in the activity and stability of the enzyme. Lack of enzyme activities in two of the MtbPDF mutants (G49C and L107E) bearing mutations corresponding to the residues of human mitochondrial PDF, suggested these evolutionary mutations as the possible reason for loss of enzyme activity in later. Substitution of a unique glycine residue in MtbPDF to an otherwise conserved aspartate (G151D) altered the enzyme activity and stability of MtbPDF. G151D mutation improved the overall catalytic efficiency of the enzyme in addition to broadening the substrate specificities of the enzymes towards substrates with bulkier amino acids at P2' positions. This mutant had an improved thermo-stability with its optimum temperature for activity shifted to higher range similar to other characterised PDFs. On the contrary, this mutation adversely affected the stability of MtbPDF towards H_2O_2. Molecular modeling and molecular dynamics simulations of this mutant structure revealed an improved structural stability and increased size in the peptide binding pocket compared to the wild type enzyme. The destabilization of a surface exposed loop containing three arginines in the mutant structure, reported as oxygen scavengers in MtbPDF, was proposed as the reason for the observed reduction in oxidative stress stability in G151D mutant. Molecular docking studies on mutant structure clearly demonstrated the improvement in substrate binding and catalysis compared to the wild type enzyme.

Over expression of *map*B gene in *E. coli* produced high amounts of soluble recombinant MtbMAP B compared to the soluble expression of recombinant MtbMAP A

protein. Both these MtbMAPs, purified in their native form, could hydrolyse the *N*-terminal methionine from the substrate, L-Met-*p*-Nitro anilide. MtbMAP A was optimally activated by Ni^{2+} followed by Co^{2+}, whereas MtbMAP B was equally activated by both these metal ions. Both the enzymes showed metal-depended inhibition at higher concentrations of metal-ions. MtbMAP A was catalytically more efficient compared to MtbMAP B, but the later had stringent specificity towards hydrolyzing methionine. MtbMAP B was comparatively more thermo-stable than MtbMAP A and both showed optimum enzyme activities at near neutral pH. At higher concentrations, actinonin and bestatin had slight inhibitory effects on MtbMAPs, more pronounced in case of MtbMAP B. MtbMAP B also showed product inhibition in presence of higher concentrations of L-methionine.

MtbMAP A possesses a unique eight amino acid insertion in its catalytic domain which is absent in other type I MAPs. Attempts to study the properties of deletion construct of MtbMAP A (Δ 164-176) was hampered by its complete expression in the insoluble fraction. Attempts to refold either MtbMAP A or the deletion mutant protein from the insoluble fractions proved ineffective in restoring the complete enzyme activity. Nevertheless, a refolding strategy was successfully formulated to refold MtbMAP A with very low activity. Six substitution mutants of MtbMAP B which got expressed in soluble fraction as active proteins were studied further to reveal their importance in metal binding and catalysis of the enzyme.

In conclusion, this study proved that the annotated genes for putative enzymes of NME pathway in the genome of *M. tuberculosis* actually code for active enzymes. It was concluded that MtbPDF is a Fe-containing enzyme with stability towards oxidizing agents, which might be an important property of this enzyme to counter the possible oxidative stress

within the macrophages during infection. The unique glycine in motif III of MtbPDF was responsible for the lower catalytic activity and lower thermo-stability of the enzyme. But, the study revealed that this glycine is important for maintaining the oxidative-stress resistance of MtbPDF. Thus, we propose this glycine, instead of aspartate, in motif III of MtbPDF as a structural adaptation for maintaining the oxidative stress resistance at the cost of activity and thermo-stability of the enzyme. Studies on mutation at this site also revealed the subtle variations it induced in the substrate binding pocket of MtbPDF, especially at the S2' position, compared to other PDFs. This variation in the S2' position in the substrate binding site of MtbPDF could be further explored to modify the current PDF inhibitors so as to improve their specificities towards MtbPDF (**Fig 7.1**).

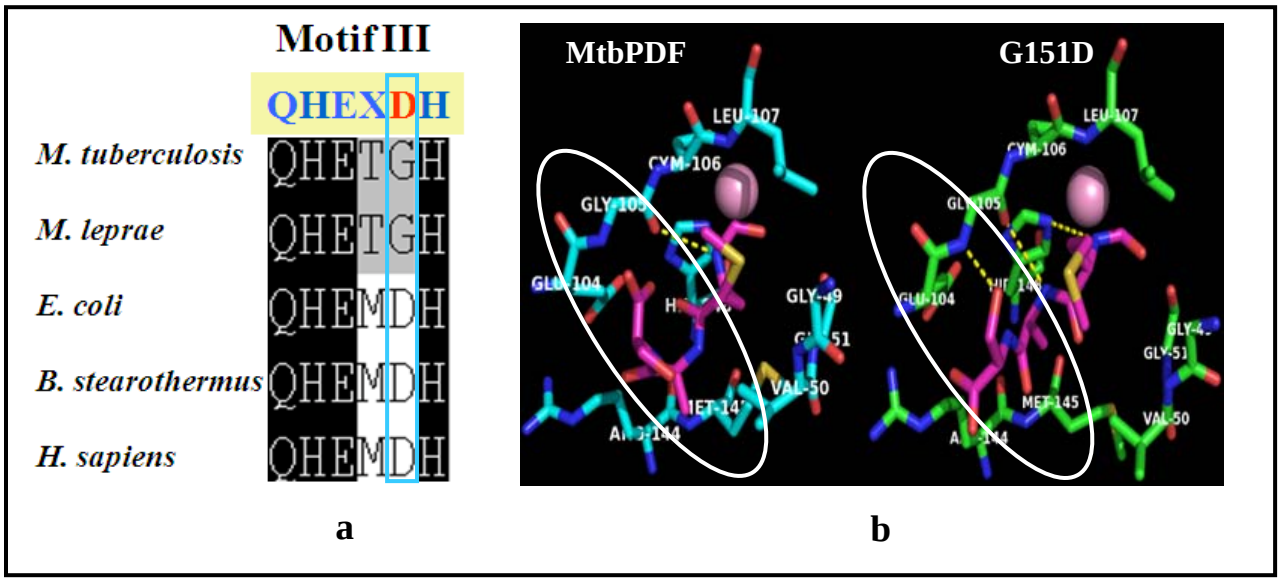

Fig 7.1: Variation in the space availability at P2' position of substrate binding site of MtbPDF, by virtue of presence of glycine in motif III (a) Presence of glycine in motif III is specific to Mycobacterium PDF **(b)** Substituting this glycine with otherwise conserved aspartate increases space in substrate binding site at P2' position. MtbPDF has smaller space availability at P2' position which can be explored to modify the side chains of inhibitor at S2' position, to suit only MtbPDF pocket.

The differences in metal-preferences and catalytic efficiencies of the two MtbMAPs clearly suggest their differential role in the different stages of growth and infection of *M.*

tuberculosis. The higher activity of MtbMAP A suggest that this enzyme might be involved in NME during the active growth phase of *M. tuberculosis*, while the MtbMAP B with its better stability suits the dormant phase to overcome the various stress responses from the host macrophages. The difference in substrate specificities and resistance to feed back inhibition also suggested their differential role in NME and in methionine salvage in *M. tuberculosis*. The insertion region in the catalytic domain of MtbMAP A, identified in this study, is very specific with no counterparts in other known bacterial or eukaryotic MAPs. Even though we couldn't characterize it fully, this region could have some importance in the activity and stability of the enzyme. Since crystallization of MtbMAP A has not been successful yet, the future works should focus on molecular modeling and dynamics studies on deletion mutant, MtbMAP A Δ 164-176, to define the role of this deleted region in MtbMAP A. Once proved essential for the enzyme activity of MtbMAP A, this unique insertion region might have implications in designing MtbMAP A selective structure-based mechanistic inhibitors, which can arrest the active growth of *M. tuberculosis*. Alternatively, this region would very well serve as a site for designing anti-sense oligos against MtbMAP A to arrest mycobacterial growth.

This unique insertion sequence in MtbMAP A distinguishes it from all the type I and type II MAPs reported till date. Thus a new sub-classification based on the insertion sequences in the catalytic region of MAPs is proposed from the present study (**Fig 7.2**).Thus type I MAPs can be classified in to five sub types Type Ia- *E.coli* MAP I (catalytic domain); Type Ib- Human MAP I (N-terminal extension with zinc-finger domain); Type Ic- *M. tuberculosis* MAP B (N-terminal extension with no zinc-finger domain); Type Id- *Streptococcal salivarius* MAPI (Insertion between R_1 and R_2 residues of metal binding

pocket); Type Ie- *M tuberculosis* MAP A (Insertion between R_2 and R_3 residues of metal binding pocket); Type II- Human MAP II (N-terminal extension with acid/ base domain and Insertion between R_4 and R_5 residues of metal binding pocket).

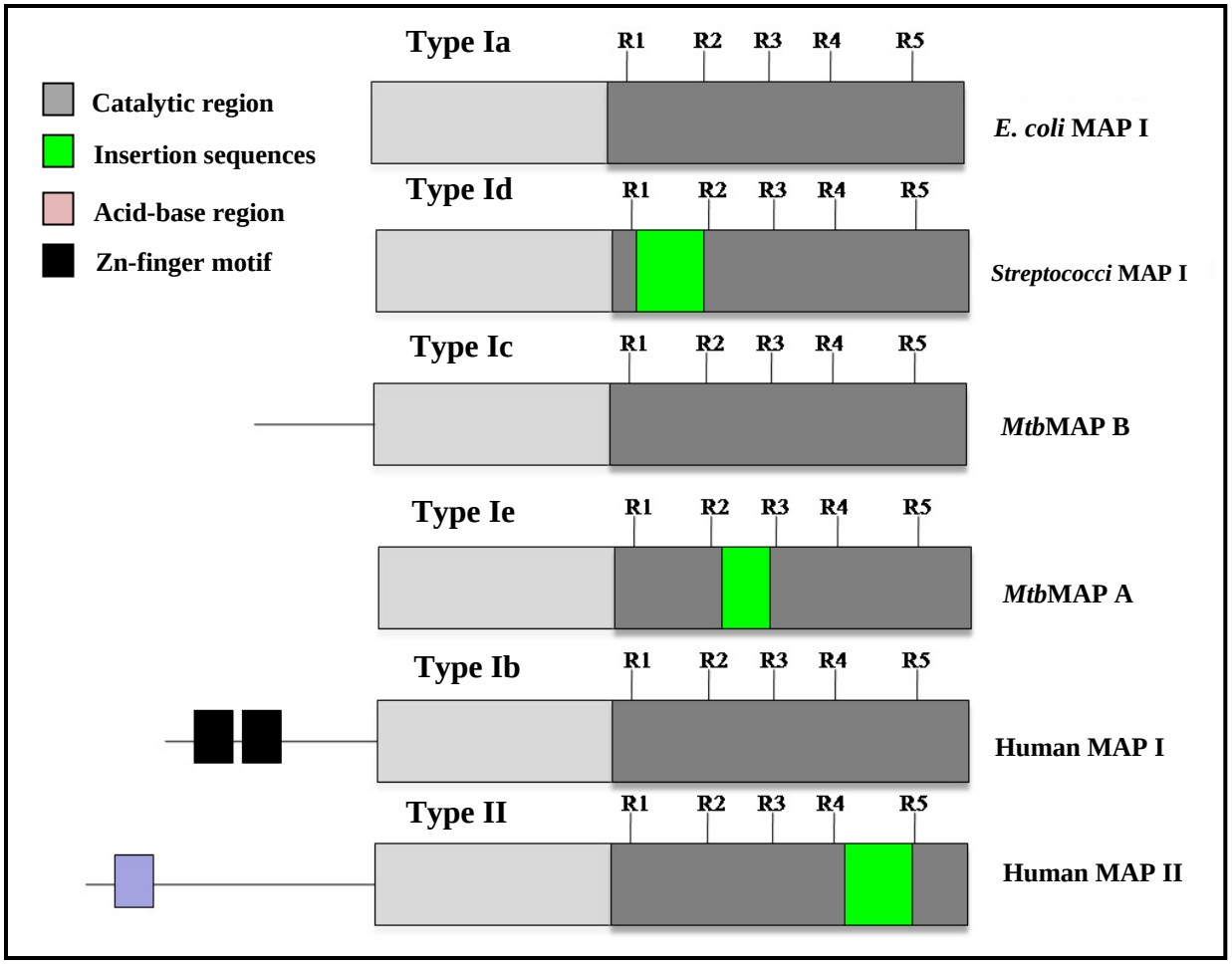

Fig 7.2: Proposed classification of MAPs based on their unique insertion sequences. (-) N-terminal extension**; R1-R5:** Metal binding residues.

To conclude, the study brought out unique structural and biochemical aspects of N-terminal methionine excision (NME) enzymes, such as peptide deformylase and methionine aminopeptidases, of *M. tuberculosis*. The future works on these enzymes should exploit

these variations revealed in order to develop these enzymes as potent drug targets for developing novel antimycobacterial drugs.

Bibliography

Bibliography

Adams JM, On the release of the formyl group from nascent protein. *Journal of Molecular Biology* 33, 571–589 [1968]

Addlagatta A, Hu X, Liu JO and Matthews BW, Structural basis for the functional differences between type I and type II human methionine aminopeptidases *Biochemistry* 44, 14741-14749 [2005a]

Addlagatta A, Quillin ML, Omotoso O, Liu JO and Matthews BW, Identification of an SH3-binding motif in a new class of methionine aminopeptidases from *Mycobacterium tuberculosis* suggests a mode of interaction with the ribosome. *Biochemistry* 44, 7166-7174 [2005b]

Anishetty S, Pulimi M and Pennathur G, Potential drug targets in *Mycobacterium tuberculosis* through metabolic pathway analysis. *Computational Biology and Chemistry* 29, 368–378 [2005]

Antczak C, Shum D, Escobar S, Bassit B, Kim E, Seshan VE and Djaballah H, High-throughput identification of inhibitors of human mitochondrial peptide deformylase. *Journal of. Biomolecular Screening* 12, 521–535 [2007]

Apfel CM, Banner DW, Bur D, Dietz M, Hirata T, Hubschwerlen C, Locher H, Page MG, Pirson W, Rosse G and Specklin JL, Hydroxamic acid derivatives as potent peptide deformylase inhibitors and antibacterial agents. *Journal of Medicinal Chemistry* 43, 2324-233 [2000]

Apfel CM, Locher H, Evers S, Takács B, Hubschwerlen C, Pirson W, Page MGP and Keck W, Peptide deformylase as an antibacterial drug target: Target validation and resistance development. *Antimicrobial Agents and Chemotherapy*

45, 1058-1064 [2001]

Arakawa T and Tsumoto K, Effects of arginine on refolding of aggregated proteins: not facilitate refolding, but suppress aggregation. *Biochemical and Biophysical Research Communication* 304, 148-152 [2003]

Arfin SM and Bradshaw RA, Co- translational processing and protein turnover in eukaryotic cells. *Biochemistry* 27, 7979–7984 [1988]

Arfin SM, Kendall RL, Hall L, Weaver LH, Stewart AE, Matthews BW and Bradshaw RA, Eukaryotic methionyl aminopeptidases: two classes of cobalt-dependent enzymes. *Proceedings of National Academy of Science USA* 92, 7714–7718 [1995]

Atanassova A, Sugita M, Sugiura M, Pajpanova T and Ivanov I, Molecular cloning, expression and characterization of three distinctive genes encoding methionine aminopeptidases in cyanobacterium *Synechocystis* sp. strain PCC6803. *Archives in Microbiology* 180, 185-193 [2003]

Auld DS, Use of chelating agents to inhibit enzymes. *Methods in Enzymology* 158, 110-114 [1988]

Baldwin ET, Harris MS, Yem AW, Wolfe CL, Vosters AF, Curry KA, Murray RW, Bock JH, Marshall VP, Cialdella JI, Merchant MH, Choi G, and Deibel, Jr MR, Crystal Structure of Type II Peptide Deformylase from *Staphylococcus aureus*. *Journal of Biological Chemistry* 277, 31163–31171 [2002]

Ball LA and Kaesberg P, Cleavage of the N-terminal formylmethionine residue from a bacteriophage coat protein *in vitro*. *Journal of Molecular Biology* 79, 531–537 [1973]

Barkan D, Liu Z, Sacchettini JC and Glickman MS, Mycolic acid cyclopropanation is essential for viability, drug resistance, and cell wall integrity of *Mycobacterium*

tuberculosis. *Chemical Biology* 29, 499-509 [2009]

Barry CE, Boshoff HI, Dartois V, Dick T, Ehrt S, Flynn J, Schnappinger D, Wilkinson RJ, and Young D, The spectrum of latent tuberculosis: rethinking the biology and intervention strategies *Nature Review in Microbiology* 7, 845-855 [2009]

Bashiri G, Squire CJ, Baker EN and Moreland NJ, Expression, purification and crystallization of native and selenomethionine labeled *Mycobacterium tuberculosis* FGD1 (Rv0407) using a *Mycobacterium smegmatis* expression system. *Protein Expression and Purification* 54, 38–44 [2007]

Bazan JF, Weaver LH, Roderick SL, Huber R and Matthews BW, Sequence and structure comparison suggest that methionineaminopeptidase, prolidase, aminopeptidase P, and creatinase share a common fold. *Proceedings of National Academy of Sciences USA* 29, 2473–2477 [1994]

Becker A, Schlichting I, Kabsch W, Groche D, Schultz S and Wagner AF, Iron center, substrate recognition, and mechanism of peptide deformylase. *Nature Structural Biology* 5, 1053-1058 [1998b]

Becker A, Schlichting I, Kabsch W, Schultz S and Wagner AFV, Structure of peptide deformylase and identification of the substrate binding site. *Journal of Biological Chemistry* 273, 11413-11416 [1998a]

Ben-Bassat A, Bauer K, Chang SY, Myambo K, Boosman A and Chang S, Processing of the initiation methionine from proteins properties of the *Escherichia coli* methionine aminopeptidase and its gene structure. *Journal of Bacteriology* 169, 751–757 [1987]

Bernier SG, Taghizadeh N, Thompson CD, Westlin WF and Hannig G, Methionine aminopepidases Type I and Type II are essential to control cell proliferation. *Journal of Cellular Biochemistry* 95, 1191–1203 [2005]

Bingel-Erlenmeyer R, Kohler R, Kramer G, Sandikci A, Antolic S, Maier T, Schaffitzel C, Wiedmann B, Bukau B and Ban N, A peptide deformylase–ribosome complex reveals mechanism of nascent chain processing, *Nature* 452, 108-111 [2008]

Birnboim HC and Doly J, A rapid alkaline extraction procedure for screening recombinant plasmid DNA. *Nucleic Acids Research* 24, 1513-1523 [1979]

Bloom JD, Labthavikul ST, Otey CR and Arnold FH, Protein stability promotes evolvability. *Proceedings of National Academy of Science* 103, 5869–5874 [2006]

Blumberg HM, Burman WJ, Chaisson RE, Daley CL, Etkind SC, Friedman LN, Fujiwara P, Grzemska M, Hopewell PC, Iseman MD, Jasmer RM, Koppaka V, Menzies RI, O'Brien RJ, Reves RR, Reichman LB, Simone PM, Starke JR, and Vernon AA, American Thoracic Society/Centers for Disease Control and Prevention/Infectious Diseases Society of America: treatment of tuberculosis. *American Journal of Respiratory and Critical Care Medicine* 167, 603-662 [2003]

Boufous EH and Vadeboncoeur C, Purification and characterization of the *Streptococcus salivarius* methionine aminopeptidase (MetAP). *Biochimie* 85, 993–997[2003]

Boularot A, Giglione C, Petit S, Duroc Y, Alves de Sousa R, Larue V, Cresteil T, Dardel F, Artaud I and Meinnel T, Discovery and refinement of a new structural class of potent peptide deformylase inhibitors. *Journal of Medicinal Chemistry* 11, 10-20 [2007]

Bowie JU, Reidhaar-Olson JF, Lim WA and Sauer RT, Deciphering the message in protein sequences: Tolerance to amino acid substitutions. *Science* 247, 1306–1310 [1990]

Boxem M, Tsai CW, Zhang Y, Saito RM and Liu JO, The *C. elegans* methionine aminopeptidase-2 analog (map-2) is required for germ cell proliferation. *FEBS Letters* 576, 245–250 [2004]

Bracchi-Ricard V, Nguyen KT, Zhou Y, Rajagopalan PT, Chakrabarti D and Pei D, Characterization of an eukaryotic peptide deformylase from *Plasmodium falciparum*. *Archives in Biochemistry and Biophysics* 396, 162-170 [2001]

Bradford MM, Rapid and sensitive method for the quantitation of microgram quantities of protein utilizing the principle of protein-dye binding. *Analytical Biochemistry* 72, 248–254 [1976]

Bradshaw RA, Brickey WW and Walker KW, N-terminal processing: the methionine aminopeptidase and N alpha-acetyl transferase families. *Trends in Biochemical Sciences* 23, 263–267 [1998]

Bradshaw RA and Yi E, Methionine aminopeptidases and angiogenesis. *Essays in Biochemistry* 38, 65–78 [2002]

Bradshaw RA, Brickey WW and Walker KW, N-Terminal processing: the methionine aminopeptidase and N^{α}-acetyl transferase families. *Trends in Biochemical Sciences 23*, 263-267 [1998]

Brdlik CM and Crews CM, A single amino acid residue defines the difference in ovalicin sensitivity between Type I and II methionine aminopeptidases. *Journal of Biological Chemistry* 279, 9475–9480 [2004]

Burley SK, David PR, Sweet RM, Taylor A and Lipscomb WN, Structure determination and refinement of bovine lens leucine aminopeptidase and its complex with bestatin. *Journal of Molecular* Biology 224, 113-140 [1992]

Burman WJ, Rip Van Winkle Wakes Up: Development of Tuberculosis Treatment in the 21st Century. *Clinical Infectious Diseases* 50, S165-S172 [2010]

Capecchi MR, Initiation of *E. coli* proteins. *Proceedings of National Academy of Sciences USA* 55, 1517–24 [1966]

Cardenas ME, Cruz MC, Poeta MD, Chung N, Perfect JR, and Heitman J, Antifungal activities of antineoplastic agents: *Saccharomyces cerevisiae* as a model system to study drug action. *Clinical Microbiology Reviews* 12, 583-611 [1999]

Chai SC and Ye QZ, Analysis of the stoichiometric metal activation of methionine *BMC Biochemistry* 10, 32 [2009]

Chai SC and Ye QZ, Metal-mediated inhibition is a viable approach for inhibiting cellular methionine aminopeptidase. *Bioorganic & Medicinal Chemistry Letters* 19, 6862–6864 [2009]

Chai SC, Lu JP and Ye QZ, Determination of binding affinity of metal cofactor to the active site of methionine aminopeptidase based on quantitation of functional enzyme. *Analytical Biochemistry* 395, 263–264 [2009]

Chai SC, Wang WL and Ye QZ, Fe(II) is the native cofactor for *Escherichia coli* methionine aminopeptidase, *Journal of Biological Chemistry*, 283, 26879-85 [2008]

Chan MK, Gong W, Rajagopalan PTR, Hao B, Tsai CM and Pei D, Crystal structure of the *Escherichia coli* peptide deformylase, *Biochemistry* 36, 13904–13909 [1997]

Chang SY, McGary EC and Chang S, Methionine aminopeptidase gene of *Escherichia coli* is essential for cell growth. *Journal of Bacteriology* 171, 4071-4072 [1989]

Chang SY, Tsai PC, Tseng CS and Liang PH, Refolding and characterization of a yeast dehydrodolichyl diphosphate synthase overexpressed in *Escherichia coli*. *Protein Expression and Purification* 23, 432-439 [2001]

Chang YH, Teichert U and Smith JA, Molecular cloning, sequencing, deletion and overexpression of a eukaryotic methionine aminopeptidase gene from *Saccharomyces cerevisiae. Journal of Biological Chemistry* 267, 8007-8011 [1992]

Chen DZ, Patel DV, Hackbarth CJ, Wang W, Dreyer G, Young DC, Margolis PS, Wu C, Ni Z, Trias J, White R J, and Yuan Z, Actinonin, a naturally occurring antibacterial agent, is potent deformylase inhibitor. *Biochemistry* 39, 1256–62 [2000]

Chen LL, Li J, Li JY, Luo QL, Mao WF, Shen Q, Nan FJ and Ye QZ, Type I methionine aminopeptidase from *Saccharomyces cerevisiae* is a potential target for antifungal drug screening. *Acta Pharmacologica Sinica* 25, 907-914 [2004]

Chen X, Chong CR, Shi L, Yoshimoto T, Sullivan DJ, and Liu JO, Inhibitors of *Plasmodium falciparum* methionine aminopeptidase 1b possess antimalarial activity. *Proceedings of National Academy of Sciences USA* 103, 14548–14553 [2006]

Chen X, Xie S, Bhat S, Kumar N, Shapiro TA, and Liu JO, Fumagillin and fumarranol interact with *P. falciparum* methionine aminopeptidase 2 and inhibit malaria parasite growth *in vitro* and *in vivo. Chemistry and Biology* 16, 193-202 [2009]

Cherish Babu PV, Srinivas VK, Krishna Mohan V and Krishna E, Renaturation, purification and characterization of streptokinase expressed as inclusion body in recombinant *E. coli*. *Journal of Chromatography, B Analytical Technologies in Biomedical Life Sciences* 861,218-226 [2008]

Chiu CH, Lee CZ, Lin KS, Tam MF and Lin LY, Amino acid residues involved in the functional integrity of *Escherichia coli* methionine aminopeptidase. *Journal of Bacteriology* 181, 4686–4689 [1999]

Cho HD, Sood VD, Baker D and Weiner AM, On the role of a conserved, potentially helix-breaking residue in the tRNA-binding α-helix of archaeal CCA-adding enzymes *RNA* 14, 1284-1289 [2008]

Chopra P, Meena LS, and Singh Y, New drug targets for *Mycobacterium tuberculosis*. *Indian Journal of Medical Research* 117, 1-9 [2003]

Chu M, Mierzwa R, He L and Xu L, Isolation and structure elucidation of two novel deformylase inhibitors produced by *Streptomyces* sp. *Tetrahedron Letters* 42, 3549-3551[2001]

Chung JM, Chung IY and Lee YS, The purification and characterization of a *Bacillus stearothermophilus* methionine aminopeptidase (MetAP). *Journal of Biochemistry and Molecular Biology* 35, 228-235 [2002]

Clements JM, Beckett RP, Brown A and Catlin G, Antibiotic activity and characterization of BB-3497, a novel peptide deformylase inhibitor. *Antimicrobial Agents and Chemotherapy* 45, 563-570 [2001]

Cole ST, Brosch R, Parkhill J, Garnier T, Churcher C, Harris D, Gordon SV, Eiglmeier K, Gas S, Barry CE 3rd, Tekaia F, Badcock K, Basham D, Brown D, Chillingworth T, Connor R, Davies R, Devlin K, Feltwell T, Gentles S, Hamlin N, Holroyd S, Hornsby T, Jagels K, Krogh A, McLean J, Moule S, Murphy L, Oliver K, Osborne J, Quail MA, Rajandream MA, Rogers J, Rutter S, Seeger K, Skelton J, Squares R, Squares S, Sulston JE, Taylor K, Whitehead S and Barrell BG, Deciphering the biology of Mycobacterium tuberculosis from the complete genome sequence. *Nature* 393, 537-544 [1998]

Cosper NJ, D'Souza VM, Scott RA and Holz RC, Structural evidence that the methionyl aminopeptidase from *Escherichia coli* is a mononuclear metalloprotease. *Biochemistry* 40, 13302–13309 [2001]

Cynamon MH, Alvirez-Freites E and Yeo AE, BB-3497, a peptide deformylase inhibitor, is active against *Mycobacterium tuberculosis*. *Journal of Antimicrobial Chemotherapy* 53,403-405 [2004]

D'souza VM and Holz RC, The methionyl aminopeptidase from *Escherichia coli* can function as an iron (II) enzyme. *Biochemistry* 38, 11079-11085[1999]

D'Souza VM, Swierczek SI, Cosper NJ, Meng L, Ruebush S, Copik AJ, Scott RA and Holz RC Kinetic and structural characterization of manganese(II)-loaded methionyl aminopeptidases. *Biochemistry* 41, 13096–13105 [2002]

Dahl JL, Kraus CN, Boshoff HIM, Doan B, Foley K, Avarbock D, Kaplan G, Mizrahi V, Rubin H and Barry CE, The role of Rel_{Mtb}-mediated adaptation to stationary phase in long-term persistence of *Mycobacterium tuberculosis* in mice. *Proceedings of National Academy of Sciences USA* 100, 10026–10031 [2003]

D'Alatri L, Di-Massimo AM, Anastasi AM, Pacilli A, Novelli S,. Saccinto MP, De-Santis R, Mele A and Parente D, Production and characterisation of a recombinant single-chain anti ErbB2-clavin immunotoxin, *Anticancer Research* 18, 3369-3373 [1998]

Dardel F, Ragusa S, Lazennec C, Blanquet S and Meinnel T. Solution structure of nickel peptide deformylase. *Journal of Molecular Biology* 280, 501-513[1998]

Datta R, Choudhury P, Bhattacharya M, Leon SF, Zhou Y and Datta B, Protection of translation initiation factor eIF2 phosphorylation correlates with eIF2-associated glycoprotein p67 levels and requires the lysine-rich domain I of p67. *Biochimie* 83, 919–931[2001]

De Bernardez-Clark E, Refolding of recombinant proteins. *Current Opinion in Biotechnology* 9, 157–163 [1998]

Dean CR, Narayan S, Richards J, Daigle DM, Esterow S, Leeds JA, Kamp H, Puyang X, Wiedmann B, Mueller D, Voshol H, van Oostrum J, Wall D, Koehn J, Dzink-Fox J and Ryder NS, Reduced susceptibility of *Haemophilus influenzae* to the peptide deformylase inhibitor LBM415 can result from target protein overexpression due to amplified chromosomal def gene copy number. *Antimicrobial Agents and Chemotherapy* 51, 1004-1010 [2007]

Diacon AH, Pym A, Grobusch M, Patientia R, Rustomjee R, Page-Shipp L, Pistorius C, Krause R, Bogoshi M, Churchyard G, Venter A, Allen J, Palomino JC, De Marez T, van Heeswijk RP, Lounis N, Meyvisch P, Verbeeck J, Parys W, de Beule K, Andries K and Mc Neeley DF, The diarylquinoline TMC207 for multidrug-resistant tuberculosis. *New England Journal of Medicine* 360, 2397-405 [2009]

Dirk LM, Schmidt JJ, Cai Y, Barnes JC, Hanger KM, Nayak NR, Williams MA, Grossman RB, Houtz RL and Rodgers DW, Insights into the substrate specificity of plant peptide deformylase, an essential enzyme with potential for the development of novel biotechnology applications in agriculture. *Biochemical Journal* 413, 417-427[2008]

Dirk LM, Williams MA and Houtz RL, Eukaryotic peptide deformylases. Nuclear-encoded and chloroplast-targeted enzymes in Arabidopsis. *Plant Physiology* 127, 97-107 [2001]

Dong XY, Fu MN and Sun Y, Refolding of recombinant homodimeric malate dehydrogenase expressed in *Escherichia coli* as inclusion bodies. *Biochemical Engineering Journal* 38, 341–348 [2008]

Drath M, Baier K and Forchhammer K, An alternative methionine aminopeptidase, MAP-A, is required for nitrogen starvation and high-light acclimation in the cyanobacterium *Synechocystis* sp. PCC 6803. *Microbiology* 155, 1427-1439 [2009]

Dummitt B, Micka WS and Chang YH, N-terminal methionine removal and methionine metabolism in *Saccharomyces cerevisiae*. *Journal of Cell Biochemistry* 89, 964–974 [2003]

Duroc Y, Giglione C and Meinnel T, Mutations in three distinct loci cause resistance to peptide deformylase inhibitors in *Bacillus subtilis*. *Antimicrobial Agents and Chemotherapy* 53, 1673-1678 [2009]

Dye C and Williams BG, The population dynamics and control of tuberculosis. *Science* 328, 856–861 [2010]

Escobar-Alvarez S, Gardner J, Sheth A, Manfredi G, Yang G, Ouerfelli O, Heaney ML and Scheinberg DA, Inhibition of human peptide deformylase disrupts mitochondrial function. *Molecular Cell Biology* 30, 5099-5109 [2010]

Escobar-Avarez S, Goldgur Y, Yang G, Querfelli O, Li Y and Sceinberg DA, Structure and activity of human mitochondrial peptide deformylase, a novel cancer target. *Journal of Molecular Biology* 17, 1211-1228 [2009]

Evans VJ, Liyanage H, Ravagnani A, Young M and Kashket ER, Truncation of peptide deformylase reduces the growth rate and stabilizes solvent production in *Clostridium beijerinckii* NCIMB 8052. *Applied Environmental Microbiology* 64**,** 1780-1785 [1998]

Evdokimov AG, Pokross M, Walter RL, Mekel M, Barnett BL, Amburgey J, Seibel WL, Soper SJ, Djung JF, Fairweather N, Diven C, Rastogi V, Grinius L, Klanke C, Siehnel R,Twinem T, Andrews R, and Curnow A, Serendipitous discovery of

novel bacterial methionine aminopeptidase inhibitors. *Proteins* 66, 538-546 [2007]

Fang G, Rocha E and Danchin A, How Essential Are Nonessential Genes? *Molecular Biology and Evolution* 22, 2147–2156 [2005]

Fersht AR and Serrano L, Principles in protein stability derived from protein engineering experiments. *Current Opinion in Structural Biology* 3, 75–83 [1993]

Fieulaine S, Juillan-Binard C, Serero A, Dardel F, Giglione C, Meinnel T and Ferrer JL, The crystal structure of mitochondrial (Type 1A) peptide deformylase provides clear guidelines for the design of inhibitors specific for the bacterial forms. *Journal of Biological Chemistry* 280, 42315-42324 [2005]

Fiser A and Sali A, Modeller: generation and refinement of homology-based protein sequence models. *Methods in Enzymol*ogy 374**,** 461– 491 [2003]

Fleischmann RD, Alland D, Eisen JA, Carpenter L, White O, Peterson J, DeBoy R, Dodson R, Gwinn M, Haft D, Hickey E, Kolonay JF, Nelson WC, Umayam LA, Ermolaeva M, Salzberg SL, Delcher A, Utterback T, Weidman J, Khouri H, Gill J, Mikula A, Bishai W, Jacobs Jr WR Jr, Venter JC and Fraser CM, Whole-genome comparison of *Mycobacterium tuberculosis* clinical and laboratory strains, *Journal of Bacteriology* 184, 5479-5490 [2002]

Flinta C, Persson B, Jornvall H and von Heijne G, Sequence determinants of cytosolic N-terminal protein processing. *European Journal of Biochemistry* 154, 193–196 [1986]

Flynn JL and Chan J, Tuberculosis: latency and reactivation. *Infection and Immunology* 69, 4195–201[2001]

Fox W, Ellard GA and Mitchison DA Studies on the treatment of tuberculosis undertaken by the British Medical Research Council tuberculosis units, 1946-

1986, with relevant subsequent publications. *International Journal of Tuberculosis and Lung Diseases* 3, S231–279 [1999]

Fritsche TR, Sader HS, Cleeland R, and Jones RN, Comparative antimicrobial characterization of LBM415 (NVP PDF-713), a new peptide deformylase inhibitor of clinical importance. *Antimicrobial Agents and Chemotherapy* 49, 1468–1476 [2005]

Fry KT and Lamborg MR, Amidohydrolase activity of *Escherichia coli* extracts with formylated amino acids and dipeptides as substrates. *Journal Molecular Biology* 28, 423–433 [1967]

Garate M, Cao Z, Batemana E and Panjwam N, Novel mannose binding protein of *Acanthamoeba. Journal of Biological Chemistry* 279, 29849-29856 [2004]

Gerlt JA, Protein engineering to study enzyme catalytic mechanisms. *Current Opinion in Structural Biology* 4, 593–600 [1994]

Gey van Pittius NC, Sampson SL, Lee H, Kim Y, van Helden1 PD and Warren RM, Evolution and expansion of the *Mycobacterium tuberculosis* PE and PPE multigene families and their association with the duplication of the ESAT-6 (*esx*) gene cluster regions. *BMC Evolutionary Biology* 6, 95[2006]

Ghosh M, Grunden AM, Dunn DM, Weiss R and Adams MWW, 1998.Characterization of native and recombinant forms of an unusual cobalt- dependent proline dipeptidase (prolidase) from the hyperthermophilic archaeon *Pyrococcus furiosus*. *Journal of Bacteriology* 180, 4781-4789 [1998]

Giglione C and Meinnel T, Organellar peptide deformylases: universality of the N-terminal methionine cleavage mechanism. *Trends in Plant Science* 6, 566-572 [2001]

Giglione C, Boularot A, and Meinnel T, Protein N-terminal methionine excision, *CMLS Cell and Molecular Life Sciences* 61, 1455–1474 [2004]

Giglione C, Pierre M and Meinnel T, Peptide deformylase as a target for new generation, broad spectrum antimicrobial agents. *Molecular Microbiology* 36, 1197-1205 [2000b]

Giglione C, Serero A, Pierre M, Boisson B and Meinnel T, Identification of eukaryotic peptide deformylases reveals universality of N-terminal protein processing mechanisms. *EMBO Journal* 19, 5916–5929 [2000a]

Giglione C, Vallon O and Meinnel T, Control of protein life-span by N-terminal methionine excision. *The EMBO Journal* 22, 13-23 [2003]

Glickman MS, Cox JS and Jacobs WR Jr, A novel mycolic acid cyclopropane synthetase is required for cording, persistence and virulence of *Mycobacterium tuberculosis*. *Molecular Cell* 5, 717-727 [2000]

Global Alliance for Tuberculosis Drug Development*:* Executive Summary of the Scientific Blueprint for TB Drug Development. *Tuberculosis* 81, 1–52 [2001]

Goldstone RM, Moreland NJ, Bashiri G, Baker EN and Lott JS, A new Gateway® vector and expression protocol for fast and efficient recombinant protein expression in *Mycobacterium smegmatis. Protein Expression and Purification* 57, 81-87 [2008]

Gomez JE and McKinney J, Persistence and drug tolerance. In *Tuberculosis*, Ed. Rom W and Garay S, 101–14. New York: *Lippincott*. 2nd ed. [2003]

Gordon JC, Myers JB, Folta T, Shoja V, Heath LS and Onufriev A, H++: a server for estimating pKas and adding missing hydrogens to macromolecules. *Nucleic Acids Research* 33**,** 368–371 [2005]

Gordon JJ, Kelly BK and Miller GA. Actinonin: an antibiotic substance produced by an Actinomycete. *Nature* 195, 701–702 [1962]

Greenfield NJ, Using circular dichroism spectra to estimate protein secondary structure. *Nature protocols* 1**,** 2876–2890 [2006]

Griffith EC, Su Z, Niwayama S, Ramsay CA, Chang YH and Liu JO, Molecular recognition of angiogenesis inhibitors fumagillin and ovalicin by methionine aminopeptidase 2. *Proceedings of National Academy of Sciences USA 95*, 15183–15188 [1998]

Griffith EC, Su Z, Turk BE, Chen S, Chang YH, Wu Z, Biemann K, and Liu JO, Methionine aminopeptidase (type 2) is the common target for angiogenesis inhibitors AGM-1470 and ovalicin. *Chemistry and Biology* 4, 461-471 [1997]

Groche D, Becker A, Schlichting I, Kabsch W, Schultz S and Wagner AF, Isolation and crystallization of functionally competent *Escherichia coli* peptide deformylase forms containing either Iron or Nickel in the active site, *Biochemical and Biophysical Research Communication* 246 , 342–346, [1998]

Guillon JM, Mechulam Y, Schmitter JM, Blanquet S, and Fayat G, Disruption of the gene for Met-tRNA(fMet) formyltransferase severely impairs growth of *Escherichia coli. Journal of Bacteriology* 174, 4294-4301 [1992]

Guilloteau J, Mathieu M, Giglione C, Blanc V, Dupuy A, Chevrier M, Gil P,Famechon A, Meinnel T and Mikol V, The crystal structures of four peptide deformylases bound to the antibiotic actinonin reveal two distinct types: A platform for the structure-based design of antibacterial agents. *Journal of Molecular Biology* 320, 951–962 [2002]

Gupta R, Lavollay M, Mainardi JL, Arthur M, Bishai WR and Lamichhane G, The *Mycobacterium tuberculosis* gene, ldt_{Mt2}, encodes a non-classical

transpeptidase required for virulence and resistance to amoxicillin. *Nature Medicine* 16, 466–469 [2010]

Haas M, Beyer D, Gahlmann R and Freiberg C, YkrB is the main peptide deformylase in *Bacillus subtilis*, a eubacterium containing two functional peptide deformylases. *Microbiology* 147, 1783–1791 [2001]

Hackbarth CJ, Chen DZ, Lewis JG, Clark K, Mangold JB, Cramer JA, Margolis PS, Wang W, Koehn J, Wu C, Lopez S, Withers G ,Gu H, Dunn E, Kulathila R, Pan SH, Porter WL, Jacobs J, Trias J, Patel DV, Weidmann B, White RJ and

Yuan Z, N-alkyl urea hydroxamic acids as a new class of peptide deformylase inhibitors with antibacterial activity. *Antimicrobial Agents and Chemotherapy* 46, 2752-2764 [2002]

Han C, Wang Q, Dong L, Sun H, Peng S, Chen J, Yang Y, Yue J, Shen X and Jiang H, Molecular cloning and characterization of a new peptide deformylase from human pathogenic bacterium *Helicobacter pylori*. *Biochemical and Biophysical Research Communications* 319, 1292–1298 [2004]

Hao B, Gong W, Rajagopalan PTR, Zhou Y, Pei D and Chan MK, Structural basis for the design of antibiotics targeting peptide deformylase. *Biochemistry* 38, 4712-4719 [1999]

Hasan S, Daugelat S, Rao PSS and Schreiber M, Prioritizing genomic drug targets in pathogens: Application to *Mycobacterium tuberculosis*. *PLoS Computational Biology* 2, 539-550 [2006]

Hengen P, Purification of His-Tag fusion proteins from *Escherichia coli. Trends in biochemical sciences* 20, 285–286 [1995]

Hirel PH, Schmitter MJ, Dessen P, Fayat G and Blanquet S, Extent of N-terminal methionine excision from *Escherichia coli* proteins is governed by the side-chain

length of the penultimate amino acid. *Proceedings of National Academy of Sciences USA* 86**,** 8247–8251 [1989]

Holmes MA and Matthews BW, Structure of thermolysin refined at 1.6 A resolution. *Journal of Molecular Biology* 160, 623–639 [1982]

Hooper NM, Families of zinc metalloproteases. *FEBS Letters* 354, 1-6 [1994]

Hu X, Addlagatta A, Lu J, Matthews BW and Liu JO, Elucidation of the function of type 1 human methionine aminopeptidase during cell cycle progression. *Proceedings of National Academy of Sciences USA* 103, 18148–18153 [2006]

Hu X, Zhu J, Srivathsan S and Pei D, Peptidyl hydroxamic acids as methionine aminopeptidase inhibitors. *Bioorganic & Medicinal Chemistry Letters* 14, 77–79 [2004]

Hu X, Nguyen KT, Verlinde CL, Hol WG and Pei D, Structure-based design of a macrocyclic inhibitor for peptide deformylase. *Journal of Medicinal Chemistry* 28, 3771-3774 [2003]

Hu YJ, Wei Y, Zhou Y, Rajagopalan PT and Pei D, Determination of substrate specificity for peptide deformylase through the screening of a combinatorial peptide library. *Biochemistry* 38, 643-650 [1999]

Huang J, Van Aller GS, Taylor AN, Kerrigan JJ, Liu WS, Trulli JM., Lai, Z., Holmes, D., Aubart, K.M., Brown, J.R., and Zalacain, M, Phylogenomic and biochemical characterization of three *Legionella pneumophila* polypeptide deformylases. *Journal of Bacteriology* 188, 5249-5257 [2006]

Humphrey W, Dalke A and Schulten K, VMD-visual molecular dynamics. *Journal of Molecular Graphics* 14, 33–38 [1996]

Hutchison CA, Peterson SN, Gill SR, Cline RT, White O and Fraser CM, Global transposon mutagenesis and a minimal Mycoplasma genome. *Science* 286, 2165–2169 [1999]

Hutschison CA, Philipps S, Edgell MH, Gillham S, Jahnke P and Smith M, Mutagenesis at a Specific Position in a DNA Sequence. *Journal of Biological Chemistry* 253, 6551-6560 [1978]

Inoue H, Nojima H, and Okayama H, High efficiency transformation of *Escherichia coli* with plasmids. *Gene* 96, 23-28 [1990]

International Human Genome Sequencing Consortium, Initial sequencing and analysis of the human genome. *Nature* 409, 860-921 [2001]

Ioerger TR and Sacchettini JC, Structural genomics approach to drug discovery for *Mycobacterium tuberculosis*. *Current Opinion in Microbiology* 12, 318–325[2009]

Jain R, Chen D, White RJ, Patel DV and Yuan Z, Bacterial peptide deformylase inhibitors: a new class of antibacterial agents. *Current Medicinal Chemistry* 12, 1606–1621 [2005]

Javadpour MM, Eilers M, Groesbeek M and Smith SO, Helix packing in polytopic membrane proteins: role of glycine in transmembrane helix association. *Biophysical Journal* 77, 1609–1618 [1999]

Jeong HJ, Shin JS and Ok SH, Barley DNA-binding methionine aminopeptidase, which changes the localization from the nucleus to the cytoplasm by low temperature, is involved in freezing tolerance. *Plant Science* 180, 53-60 [2011]

Jevsevar S, Gaberc-Porekar V, Fonda I, Podobnik B, Grdadolnik J and Menart V, Production of nonclassical inclusion bodies from which correctly folded protein can be extracted. *Biotechnology Progress* 21, 632-639 [2005]

Johnson KW, Lofland D and Moser HE, PDF inhibitors: An emerging class of antibacterial drugs. *Current Drug Targets – Infectious Disorders* 5, 39-52 [2005]

Kalscheuer R, Syson K, Veeraraghavan U, Weinrick B, Biermann KE, Liu Z, Sacchettini JC, Besra G, Bornemann S and Jacobs WR Jr, Self-poisoning of *Mycobacterium tuberculosis* by targeting GlgE in an alpha-glucan pathway. *Nature Chemical Biology* 6, 376-384 [2010]

Kanehisa M, Goto S, Kawashima S and Nakaya A, The KEGG databases at Genome Net. *Nucleic Acids Research* 30, 42–46 [2002]

Karadzic I, Izrael L, Gojgic-Cvijovic G, and Vujcic Z, Leucine aminopeptidase from *Streptomyces hygroscopicus* is controlled by a low molecular weight inhibitor. *Journal of Bioscience and Bioengineering* 94, 309–314 [2002]

Keding SJ, Dales NA, Lim S, Beaulieu D and Rich DH, Synthesis of (3*R*)-amino-(2*S*)-hydroxy amino acids for inhibition of methionine aminopeptidase 1. *Synthetic Communications* 28, 4463–4470 [1998]

Kendall RL and Bradshaw RA, Isolation and characterization of the methionine aminopeptidase from porcine liver responsible for the co-translational processing of proteins. *Journal of Biological Chemistry* 267, 20667–20673 [1992]

Khasnobis S, Escuyer VE and Chatterjee D, Emerging therapeutic targets in tuberculosis: post-genomic era. *Expert Opinion on Therapeutic Targets* 6, 21–40 [2002]

Kim HW, Han BW, Yoon HJ, Yang JK, Lee BI, Lee HH, Ahn HJ and Suh SW, Crystallization and preliminary X-ray crystallographic analysis of peptide deformylase from *Pseudomonas aeruginosa*. *Acta Crystallography D. Bioloical Crystallography* 58, 1874-1875 [2002]

Kinnings SL, Xie L, Fung KH, Jackson RM, Xie L and Bourn PE, The *Mycobacterium tuberculosis* Drugome and Its Polypharmacological Implications. *PLoS Computational Biology* 6, e1000976 [2010]

Kobayashi K, Ehrlich SD, Albertini A, Amati G, Andersen KK and Arnaud M, Essential *Bacillus subtilis* genes. *Proceedings of National Academy of Science USA* 100, 4678–4683 [2003]

Kobayashi M and Shimizu S, Cobalt proteins. *European Journal of Biochemistry* 261, 1-9 [1999]

Koul A, Dendouga N, Vergauwen K, Molenberghs B, Vranckx L, Willebrords R, Ristic Z, Lill H, Dorange I, Guillemont J, Bald D and Andries K, Diarylquinolines target subunit c of mycobacterial ATP synthase. *Nature Chemical Biology* 3, 323 - 324 [2007]

Koul A, Arnoult E, Lounis N, Guillemont J and Andries K, The challenge of new drug discovery for tuberculosis. *Nature* 27, 483-490 [2011]

Kozak M, Comparison of initiation of protein synthesis in procaryotes, eucaryotes and organelles. *Microbiology Reviews* 47, 1–45 [1983]

Kreusch A, Spraggon G, Lee C, Klock H, McMullan D, Ng K, Shin T, Vincent J, Warner I, Ericson C and Lesley SAStructure Analysis of Peptide Deformylases from *Streptococcus pneumoniae*, *Staphylococcus aureus*, *Thermotoga maritima* and *Pseudomonas aeruginosa*: Snapshots of the Oxygen Sensitivity of Peptide Deformylase. *Journal of Molecular Biology* 330, 309–321 [2003]

Kwon YJ, Sohn MJ, Zheng CJ and Kim WG, Fumimycin: a peptide deformylase inhibitor with an unusual skeleton produced by *Aspergillus fumisynnematus*. *Organic letters* 9, 2449-2451 [2007]

Laemmli UK, Cleavage of structural proteins during assembly of the head of the bacteriophage T4. *Nature* 227, 680-685 [1970]

Lamichhane G, Novel targets in *M. tuberculosis*: search for new drugs. *Trends in Molecular Medicine* 17, 1471-491 [2011]

Lass AA, Suessenbacher G, Wolkart BM and Brunner F, Functional and analytical evidence for scavenging of oxygen radicals by L-arginine. *Molecular Pharmacology* 61, 1081–1088 [2002]

Lavollay M, Arthur M, Fourgeaud M, Dubost L, Marie A, Veziris N, Blanot D, Gutmann L and Mainardi JL, The peptidoglycan of stationary-phase *Mycobacterium tuberculosis* predominantly contains cross-links generated by L,D-transpeptidation. *Journal of Bacteriology* 190, 4360-4366 [2008]

Lazennec C and Meinnel T, Formate dehydrogenase-coupled spectrophotometric assay of peptide deformylase. *Analytical Biochemistry* 244, 180–182 [1997]

Lee MD, She Y, Soskis MJ, Borella CP, Gardner JR, Hayes PA, Dy BM, Heaney ML, Philips MR, Bornmann WG Sirotnak FM and Scheinberg DA, Human mitochondrial peptide deformylase, a new anticancer target of actinonin-based antibiotics. *Journal of Clinical Investigation* 114, 1107-1116 [2004]

Leeds JA and Dean CR, Peptide deformylase as an antibacterial target: a critical assessment. *Current Opinion in Pharmacology* 6, 445–452 [2006]

Leszczyniecka M, Bhatia U, Cueto M, Nirmala NR, Towbin H, Vattay A, Wang B, Zabludoff S and Phillips PE, MAP1D, a novel methionine aminopeptidase family member is overexpressed in colon cancer. *Oncogene* 25, 3471–3478 [2006]

Li JY, Chen LL, Cui YM, Luo QL, Li J, Nan FJ, Ye QZ, Specificity for inhibitors of metal-substituted methionine aminopeptidase. *Biochemical and Biophysical Research Communication* 307, 172–179 [2003]

Li JY, Cui YM, Chen LL, Gu M, Li J, Nan FJ and Ye QZ Mutations at the S1 sites of methionine aminopeptidases from *Escherichia coli* and *Homo sapiens* reveal the residues critical for substrate specificity, *Journal of Biological Chemistry* 279, 21128–21134 [2004]

Li X and Chang YH, Amino-terminal protein processing in *Saccharomyces cerevisiae* is an essential function that requires two distinct methionine aminopeptidases. *Proceedings of National Academy of Sciences USA* 92, 12357-12361 [1995]

Li X and Chang YH, Evidence that the human homologue of a rat initiation factor-2 associated protein (p67) is a methionine aminopeptidase. *Biochemical and Biophysical Research Communication.* 227, 152–159 [1996]

Li Y, Chen Z and Gong W, Enzymatic properties of a new peptide deformylase from pathogenic bacterium *Leptospira interrogans*. *Biochemical and Biophysical Research Communications* 295, 884–889 [2002]

Lin P, Hu T, Hu J, Yu W, Han C, Zhang J, Qin G, Yu K, Götz F, Shen X, Jiang H and Qu D, Characterization of peptide deformylase homologues from *Staphylococcus epidermidis. Microbiology* 156, 3194-3202 [2010]

Liu S, Widom J, Kemp CW and Clardy J, Structure of human methionine aminopeptidase-2 complexed with fumagillin. *Science* 282, 1324–1327 [1998]

Livingston DM and Leder P, Deformylation and protein synthesis. *Biochemistry* 8, 435–443 [1969]

Lowther WT and Matthews BW, Metalloaminopeptidases: common functional themes in disparate structural surroundings. *Chemical Reviews* 102, 4581-4608 [2002]

Lowther WT and Matthews BW, Structure and function of the methionine aminopeptidases. *Biochimica et Biophysica Acta* 1477, 157-167 [2000]

Lowther WT, Mcmillen DA, Orville AM and Matthews BW, The anti-angiogenic agent fumagillin covalently modifies a conserved active-site histidine in the *Escherichia coli* methionine aminopeptidase. *Proceedings of National Academy of Sciences USA* 95, 12153–12157 [1998]

Lowther WT, Orville AM, Madden DT, Lim S, Rich DH and Matthews BW, *Escherichia coli* Methionine Aminopeptidase: Implications of crystallographic analyses of the native, mutant and inhibited enzymes for the mechanism of catalysis. *Biochemistry* 38, 7678–7688 [1999b]

Lowther WT, Zhang Y, Sampson PB, Honek JF and Matthews BW, Insights into the mechanism of *Escherichia coli* methionine aminopeptidase from the structural analysis of reaction products and Phosphorus-based transition-state analogues. *Biochemistry* 38, 14810-14819 [1999a]

Lu JP and Ye QZ, Expression and characterization of *Mycobacterium tuberculosis* methionine aminopeptidase type 1a. *Bioorganic & Medicinal Chemistry Letters* 20, 2776–2779 [2010]

Lu JP, Chai SC and Ye QZ, Catalysis and inhibition of *Mycobacterium tuberculosis* methionine aminopeptidase. *Journal of Medical Chemistry* 53, 1329-1337 [2010]

Lu JP, Yuan XH, Yuan H, Wang WL, Wan B, Franzblau SG and Ye QZ, Inhibition of *Mycobacterium tuberculosis* Methionine Aminopeptidases by Bengamide Derivatives. *ChemMedChem* 6, 1041-1048 [2011]

Luo QL, Li JY, Liu ZY, Chen LL, Li J, Qian Z, Shen Q, Li Y, Lushington GH, Ye QZ and Nan FJ, Discovery and structural modification of inhibitors of methionine aminopeptidases from *Escherichia coli* and *Saccharomyces cerevisiae*. *Journal of Medicinal Chemistry* 46: 2631-2640 [2003]

L'vov BV, Fifty years of atomic absorption spectrometry. J*ournal of Analytical Chemistry* 60, 382-392 [2005]

Ma ZQ, Xie SX, Huang QQ, Nan FJ, Hurley TD and Ye QZ, Structural analysis of inhibition of *E. coli* methionine aminopeptidase: implication of loop adaptability in selective inhibition of bacterial enzymes. *BMC Structural Biology* 7, 84 [2007]

Maeda Y, Koga H, Yamada H, Ueda T and Imoto T, Effective renaturation of reduced lysozyme by gentle removal of urea. *Protein Engineering* 8, 201–205 [1995]

Mamelli L, Petit S, Chevalier J, Giglione C, Lieutaud A, Meinnel T, Artaud I and Pagès JM, New antibiotic molecules: bypassing the membrane barrier of gram negative bacteria increases the activity of peptide deformylase inhibitors. *PLoS One* 30, e6443 [2009]

Margolis PS, Hackbarth CJ, Lopez S, Maniar M, Wang W, Yuan Z, White R and Trias J, Resistance of *Streptococcus pneumonia* to deformylase inhibitors is due to mutations in defB. *Antimicrobial Agents and Chemotherapy* 45, 2432–2435 [2001]

Margolis PS, Hackbarth CJ, Young DC, Wang W, Chen D, Yuan Z, White R and Trias J, Peptide deformylase in *Staphylococcus aureus*: resistance to inhibition is mediated by mutations in the formyltransferase gene. *Antimicrobial Agents and Chemotherapy* 44, 1825-1831 [2000]

Mazel D, Coic E, Blanchard S, Saurin W, and Marliere P, A survey of polypeptide deformylase function throughout the eubacterial lineage. *Journal of Molecular Biology* 266, 939-949 [1997]

Mazel D, Pochet S and Marliere P, Genetic characterization of polypeptide deformylase, a distinctive enzyme of eubacterial translation. *EMBO J* 13, 914-923 [1994]

McKinney JD, Bentrup HZK, Munoz -Elias EJ, Miczak A, Chen B, Chan WT, Swenson D, Sacchettini JC, Jacobs WR Jr and Russell DG, Persistence of *Mycobacterium tuberculosis* in macrophages and mice requires the glyoxylate shunt enzyme isocitrate lyase. *Nature* 406, *735*-738 [2000]

Mechulam Y, Meinnel T and Blanquet S, A family of RNA-binding enzymes: the aminoacyl-tRNA synthetases. *Subcellular Biochemistry* 24, 323–376 [1995]

Meinnel T, Blanquet S and Dardel F, A new subclass of the zinc metalloproteases superfamily revealed by the solution structure of peptide deformylase. *Journal of Molecular Biology* 262,375-386 [1996a]

Meinnel T and Blanquet S, Characterization of the Thermus thermophilus locus encoding peptide deformylase and methionyltRNA (fMet) formyltransferase. *Journal of Bacteriology* 176, 7387-7390 [1994]

Meinnel T and Blanquet S, Enzymatic properties of *Escherichia coli* peptide deformylase *Journal of Bacteriology* 177, 1883–1887 [1995]

Meinnel T and Blanquet S, Evidence that peptide deformylase and methionyl-tRNA(fMet) formyltransferase are encoded within the same operon in *Escherichia coli*. *Journal of Bacteriology* 175, 7737-7740 [1993a]

Meinnel T, Lazennec C and Blanquet S, Mapping of the active site zinc ligands of peptide deformylase. *Journal of Molecular Biology* 254, 175–183 [1995]

Meinnel T, Lazennec C, Dardel F, Schmitter J and Blanquet S, The C-terminal domain of peptide deformylase is disordered and dispensable for activity. *FEBS Letters* 385, 91-95 [1996b]

Meinnel T, Lazennec C, Villoing S and Blanquet S, Structure-function relationships within the peptide deformylase family. Evidence for a conserved architecture of

the active site involving three conserved motifs and a metal ion. *Journal of Molecular Biology* 267, 749–761 [1997]

Meinnel T, Mechulam Y and Blanquet S, Methionine as translation start signal: a review of the enzymes of the pathway in *Escherichia coli*. *Biochimie* 75, 1061-1075 [1993b]

Meinnel T, Peptide deformylase of eukaryotic protists: a target for new antiparasitic agents? *Parasitology Today* 16, 165-168 [2000]

Meng L, Ruebush S, D'Souza VM, Copik AJ, Tsunasawa S and Holz RC, Overexpression and divalent metal binding properties of the methionyl aminopeptidase from *Pyrococcus furiosus*. *Biochemistry* 41, 7199-7208 [2002]

Menten L and Michaelis MI, Die Kinetik der Invertinwirkung. *Biochemistry* 49, 333–369 [1913]

Miller CG, Kukral AM, Miller JL and Movva NR, pepM is an essential gene in *Salmonella typhimurium*. *Journal of Bacteriology* 171, 5215-5217 [1989]

Miller CG, Protein degradation and proteolytic modification. In: *Escherichia coli* and *Salmonella typhimurium*. *Cellular and Molecular Biology*, 680–691 [1987a]

Miller CG, Strauch KL, Kukral AM, Miller JL, Wingfield PT, Mazzei GJ, Werlen RC, Graber P and Movva NR, N-terminal methionine-specific peptidase in *Salmonella typhimurium*. *Proceedings of National Academy of Sciences USA* 84, 2718-2722 [1987b]

Mitchison D, Basic mechanisms of chemotherapy. *Chest* 76, 771–781 [1979]

Mitra S, Bennett B and Holz RC, Mutation of H63 and its catalytic affect on the methionine aminopeptidase from *Escherichia coli*. *Biochimica et Biophysica Acta* 1794, 137–143 [2009]

Mitra S, Dygas-Holz AM, Jiracek J, Zertova M, Zakova L and Holz RC, A new colorimetric assay for methionyl aminopeptidases: Examination of the binding of a new class of pseudopeptide analog inhibitors. *Analytical Biochemistry* 357, 43–49 [2006]

Mitra S, Job KM, Meng L, Bennett B and Holz RC, Analyzing the catalytic role of Asp97 in the methionine aminopeptidase from *Escherichia coli*. *FEBS Journal* 275, 6248–6259 [2008]

Mogk A, Mayer MP and Deuerling E, Mechanisms of protein folding: molecular chaperones and their application in biotechnology. *Chembiochem* 3, 807-814 [2002]

Morris GM, Goodsell DS, Halliday RS, Huey R, Hart WE, Belew RK and Olson AJ, Automated docking using a Lamarckian genetic algorithm and an empirical binding free energy function. *Journal of Computational Chemistry* 19, 1639–1662 [1998]

Mukhopadhyay A, Inclusion bodies and purification of proteins in biologically active forms. *Advances in Biochemical Engineering and Biotechnology* 56, 61–109 [1997]

Munoz-Elias EJ and McKinney JD, *Mycobacterium tuberculosis* isocitrate lyases 1 and 2 are jointly required for *in vivo* growth and virulence. *Nature Medicine* 11, 638–644 [2005]

Nam KH, Kim KH, Kim EEK and Hwang KY, Crystal structure of an EfPDF complex with Met-Ala-Ser based on crystallographic packing. *Biochemical and Biophysical Research Communications* 381, 630-633 [2009]

Nampoothiri KM, Rubex R, Patel AK, Narayanan SS, Krishna S, Das SM and Pandey A, Molecular cloning, overexpression and biochemical characterization of

hypothetical β-lactamases of *Mycobacterium tuberculosis* H37Rv. *Journal of Applied Microbiology* 105, 59-67 [2008]

Narayanan SS, Ramanujam A, Krishna S and Nampoothiri KM, Purification and biochemical studies on Methionine aminopeptidaes from *Mycobacterium smegmatis* mc^2 155. *Applied Biochemistry and Biotechnology* 151, 512-521 [2008]

Nguyen K, Mechanism, function, and inhibition of peptide deformylase. Ph.D Dissertation, *Ohio State University* [2005]

Nguyen KT, Hu X, Colton C, Chakrabarti R, Zhu MX and Pei D. Characterization of a human peptide deformylase: implications for antibacterial drug design. *Biochemistry* 42, 9952–9958 [2003]

Nguyen KT, Wu JC, Boylan JA, Gherardini FC and Pei D, Zinc is the metal cofactor of *Borrelia burgdorferi* peptide deformylase. *Archives of Biochemistry and Biophysics* 468, 217–225 [2007]

Nicholas KB, Nicholas H B Jr, and Deerfield DW II, GeneDoc: Analysis and Visualization of Genetic Variation. *EMBNEW.NEWS* 4, 14 [1997]

Nishihara K, Kanemori M, Kitagawa M, Yanagi H and Yura T, Chaperone co-expression plasmids: Differential and synergistic roles of Dnak-Dnaj-GroE and GroEL-GroES in assisting folding of an allergen of Japanese cedar pollen, cryj2, in *Escherichia coli*. *Applied Environmental Microbiology* 64, 1694-1699 [1998]

O'brien RJ and Nunn PP, The need for new drugs against Tuberculosis: Obstacles, Opportunities, and Next Steps. *American Journal of Respiratory and Critical Care Medicine* 162, 1055–1058 [2001]

Oefner C, Douangamath A, D'Arcy A, Hafeli S, Mareque D. Mac Sweeney A, Padilla J, Pierau S, Schulz H, Thormann M, Wadman S and Dale GE, The 1.15A crystal

structure of the *Staphylococcus aureus* methionyl-aminopeptidase and complexes with triazole based inhibitors. *Journal of Molecular Biology* 332**,** 13–21 [2003]

Olaleye O, Raghunand TR, Bhat S, He J, Tyagi S, Lamichhane G, Gu P, Zhou J, Zhang Y, Grosset J, Bishai WR and Liu JO, Methionine aminopeptidases from *Mycobacterium tuberculosis* as novel antimycobacterial targets. *Chemistry and Biology* 29, 86-97 [2010]

Olaleye OA, Bishaie WA and Liu JO, Targeting the role of N-terminal methionine processing enzymes in *Mycobacterium tuberculosis*. *Tuberculosis* 89, S55–S59 [2009]

Oyenbujoh P, Zumla A, Ribeiro I, Rustomjee R, Mwaba P, Gomes M and Grang JM, Treatment of tuberculosis: Present status and future prospects. *Bulletin of the World Health Organization* 83, 857-865 [2005]

Palma M, Worgall S and Quadri LE, Transcriptome analysis of the *Pseudomonas aeruginosa* response to iron. *Archives in Microbiology* 180**,** 374–379 [2003]

Parida SK and Kaufmann SH, The quest for biomarkers in tuberculosis, *Drug Discovery Today* 15, 148-57 [2010]

Park JK, Kim KH, Moon JH and Kim EE, Characterization of Peptide Deformylase2 from *Bacillus cereus*. *Journal of Biochemistry and Molecular Biology* 40, 1050-1057 [2007]

Pei D, Peptide deformylase: a target for novel antibiotics? *Emerging Therapeutic Targets* 5, 23–40 [2001]

Perez-Iratxeta C and Andrade-Navarro MA, K2D2: Estimation of protein secondary structure from circular dichroism spectra *BMC Structural Biology* 8, 25 [2008]

Peternel S, Grdadolnik J, Gaberc-Porekar V and Komel R, Engineering inclusion bodies for non denaturing extraction of functional proteins. *Microbial Cell Factories* 7, 34 [2008a]

Peternel S, Jevsevar S, Bele M, Gaberc-Porekar V and Menart V, New properties of inclusion bodies with implications for biotechnology. *Biotechnology and Applied Biochemistry* 49, 239-246 [2008b]

Phillips JC, Braun R, Wang W, Gumbart J, Tajkhorshid E, Villa E, Chipot C, Skeel RD, Kale L and Schulten K, Scalable molecular dynamics with NAMD. *Journal of Computational Chemistry* 26, 1781–1802 [2005]

Pichota A, Duraiswamy J, Yin Z, Keller TH, Alam J, Liung S, Lee G, Mukharjee K, Nanjundappa M, Teo, JWP, Thayalan P, Yap A, Dick T, Meng W, Koehn J, Pan S, Clark K, Xie X, Soen C and Cynamon M, Peptide deformylase inhibitors of Mycobacterium tuberculosis: synthesis, structural investigations, and biological results. *Bioorganic and Medicinal Chemistry Letters* 18, 6568–6572 [2008]

Pohlmann J and Brotz-Oesterhelt H, New aminoacyl-tRNA synthetase inhibitors as antibacterial agents. *Current Drug Targets*: *Infectious Disorders* 4, 261–272 [2004]

Qoronfleh W, "Misfolded proteins? Inclusion bodies? Restoring protein function with the Pro-Matrix protein refolding system." Paper presented at the PEPTALK-Protein Expression meeting, San Diego, CA. http://www.chi-peptalk.com [2004]

Ragusa S, Blanquet S and Meinnel T, Control of peptide deformylase activity by metal cations *Journal of Molecular Biology* 280, 515-523 [1998]

Rajagopalan PTR and Pei D, Oxygen-mediated inactivation of peptide deformylase. *Journal of Biological Chemistry* 273, 22305–22310 [1998]

Rajagopalan PTR, Datta A and Pei D, Purification, characterization, and inhibition of peptide deformylase from *Escherichia coli*. *Biochemistry* 36, 13910–13918 [1997a]

Rajagopalan PTR, Grimme S and Pei D, Characterization of cobalt (II)-substituted peptide deformylase: Function of the metal ion and the catalytic residue Glu-133. *Biochemistry* 39, 779-790 [2000]

Rajagopalan PTR, Yu XC and Pei D, Peptide deformylase: a new type of mononuclear iron protein. *Journal of American Chemical Society* 119, 12418–12419 [1997b]

Ramanathan-Girish S, McColm J, Clements JM, Taupin P, Barrowcliffe S, Hevizi J, Safrin S, Moore C, Patou G, Moser H, Gadd A, Hoch U, Jiang V, Lofland D and Johnson KW, Pharmacokinetics in animals and humans of a first-in-class peptide deformylase inhibitor *Antimicrobial Agents and Chemotherapy* 48, 4835-4842 [2004]

Ramırez-Zavala B, Mercado-Flores Y, Hernandez-Rodrıguez C and Villa-Tanaca L, Purification and characterization of a lysine aminopeptidase from *Kluyveromyces marxianus*. *FEMS Microbiology Letters* 235, 369–375 [2004]

Ramos OHP, Carmona AK and Selistre-de-Araujo HS, Expression, refolding, and *in vitro* activation of a recombinant snake venom pro-metalloprotease *Protein Expression and Purification* 28, 34–41[2003]

Reed SG, Alderson MR, Dalemans W, Lobet Y and Skeiky YAW, Prospects for a better vaccine against tuberculosis. *Tuberculosis* 83, 213–219 [2003].

Rengarajan J, Bloom BR and Rubin EJ, Genome-wide requirements for Mycobacterium tuberculosis adaptation and survival in macrophages. *Proceedings of National Academy of Sciences USA* 102, 8327-8332 [2005]

Rich DH, Moon BJ and Harbeson S, Inhibition of aminopeptidases by amastatin and bestatin derivatives. Effect of inhibitor structure on slow-binding processes. *Journal of Medicinal Chemistry* 27, 417-422 [1984]

Robertson JG, Mechanistic basis of enzyme-targeted drugs. *Biochemistry* 44, 5561-5571 [2005].

Roderick SL and Matthews BW, Structure of the cobalt dependent methionine aminopeptidase from *Escherichia coli*: a new type of proteolytic enzyme. *Biochemistry* 32, 3907-3912 [1993]

Rogl H, Kosemund , Kuhlbrandt W and Collinson I, Refolding of Escherichia coli produced membrane protein inclusion bodies immobilised by nickel chelating chromatography, *FEBS Letter* 432, 21-26 [1998]

Sambrook J, Fritsch FE and Maniatis T Eds, Molecular Cloning: A Laboratory Manual, Cold Spring Harbor Laboratory Cold Spring Harbor, New York [1989]

Sasaki J and Nakashima N, Methionine-independent initiation of translation in the capsid protein of an insect RNA virus. *Proceedings of National Academy of Science USA* 97, 1512–1515 [2000]

Sassetti CM, Boyd DH and Rubin EJ, Genes required for mycobacterial growth defined by high density mutagenesis. *Molecular Microbiology* 48, 77-84 [2003]

Saxena R and Chakraborti PK, Identification of regions involved in enzymatic stability of peptide deformylase of *Mycobacterium tuberculosis*. *Journal of Bacteriology* 187, 8216–8220 [2005b]

Saxena R and Chakraborti PK, The carboxy-terminal end of the peptide deformylase from *Mycobacterium tuberculosis* is indispensable for its enzymatic activity. *Biochemical and Biophysical Research Communications* 332, 418-425 [2005a]

Saxena R, Kanudia P, Datt M, Dar HH, Karthikeyan S, Singh B and Chakraborti PK, Three consecutive arginines are important for the mycobacterial peptide deformylase enzyme activity. *Journal of Biological Chemistry* 238, 23754–23764 [2008]

Schein CH, Production of soluble recombinant proteins in bacteria. *Biotechnology* 7, 1141-1148 [1989]

Schlieker C, Bukau B and Mogk A, Prevention and reversion of protein aggregation by molecular chaperones in the *E. coli* cytosol: implications for their applicability in biotechnology. *Journal of Biotechnology* 96, 13-21 [2002]

Schmidt J, Herfuth E and Subramanian AR, Purification and characterization of seven chloroplast ribosomal proteins; evidence that organelle ribosomal protein genes are functional and that NH_2- terminal processing occurs via multiple pathways in chloroplasts *Plant Molecular Biology* 20, 459-465 [1992]

Schmitt E, Guillon JM, Meinnel T, Mechulam Y, Dardel F and Blanquet S, Molecular recognition governing the initiation of translation in *Escherichia coli*. A review. *Biochimie* 78, 543–554 [1996]

Schwarz E, Lilie H and Rudolph R, The effect of molecular chaperones on in vivo and in vitro folding processes. *Biological Chemistry* 377, 411-416 [1996]

Selvakumar P, Lakshmikuttyamma A, Dimmock JR, Sharma RK, Methionine aminopeptidase 2 and cancer. *Biochimica et Biophysica Acta* 65, 148-154 [2006]

Serero A, Giglione C and Meinnel T, Distinctive features of the two classes of eukaryotic peptide deformylases. *Journal of Molecular Biology* 314, 695–708 [2001]

Serero A, Giglione C, Sardini A, Martinez-Sanz J and Meinnel T, An unusual peptide deformylase features in the human mitochondrial N-terminal methionine excision pathway. *Journal of Biological Chemistry* 278, 52953-52963 [2003]

Sharma A, Sharma S, Khuller GK and Kanwar AJ, In vitro and ex vivo activity of peptide deformylase inhibitors against *Mycobacterium tuberculosis* H37Rv. *International Journal of Antimicrobial* 34, 226-230 [2009]

Sherman F, Stewart JW and Tsunasawa S, Methionine or not methionine at the beginning of a protein. *Bioessays* 3, 27–31 [1985]

Sikorski J, Lapidus A, Copeland A, Misra M, Johannes Sikorski1, Alla Lapidus, Alex Copeland, Monica Misra, Del-Rio TG , Nolan M, Lucas S, Chen F, Tice H, Cheng J, Jando M, Schneider S, Bruce D, Goodwin L, Pitluck S, Liolios K, Mikhailova N, Pati A, Ivanova N, Mavromatis K, Chen A , Palaniappan K , Chertkov O, Land M, Hauser L , Chang Y, Jeffries CD, Brettin T, Detter JC , Han C, Rohde M, Göker M , Bristow J, Eisen JA, Markowitz V, Hugenholtz P, Kyrpides NC and Klenk H, Complete genome sequence of *Segniliparus rotundus* type strain (CDC 1076T). *Standard Genomic Sciences* 2, 203-211 [2010]

Sin N, Meng L, Wang MQ, Wen JJ, Bornmann WG and Crews CM, The anti-angiogenic agent fumagillin covalently binds and inhibits the methionine aminopeptidase, MetAP-2. *Proceedings of National Academy of Science USA* 94, 6099–6103 [1997]

Smith KJ, Petit CM, Aubart K, Smyth M, McManus E, Jones J, Fosberry A, Lewis C, Lonetto M and Christensen SB, Structural variation and inhibitor binding in polypeptide deformylase from four different bacterial species. *Protein Science* 12, 349-60 [2003]

Smith HK, Beckett RP, Clements JM, Doel S, East SP, Launchbury SB, Pratt LM, Spavold ZM, Thomas W, Todd RS and Whittaker M, Structure-activity relationships of the peptide deformylase inhibitor BB-3497: modification of the metal binding group. *Bioorganic and Medicinal Chemistry Letters* 12, 3595-3599 [2002]

Snyder SL and Sobocinski PZ, An *improved 2, 4, 6-trinitrobenzenesulfonic acid method for the determination of amines*. *Analytical Biochemistry 64*, *284-288 [*1975]

Solbiati J, Chapman-Smith A, Miller JL, Miller CG and Cronan JE Jr, Processing of the N termini of nascent polypeptide chains requires deformylation prior to methionine removal. *Journal of Molecular Biology* 290, 607-614 [1999]

Sørensen HP and Mortensen KK, Soluble expression of recombinant proteins in the cytoplasm of *Escherichia coli*. *Microbial Cell Factories* 4, 1 [2005]

Stallings CL, Stephanou NC, Chu L, Hochschild A, Nickels BE and Glickman MS, CarD is an essential regulator of rRNA transcription required for *Mycobacterium tuberculosis* persistence. *Cell* 138, 146-159 [2009]

Styblo K and Meijer J, Impact of BCG vaccination programmes in children and young adults on the tuberculosis problem. *Tubercle* 57, 17–43 [1976]

Sutcliffe JA, Improving on nature: antibiotics that target the ribosome. *Current Opinion in Microbiology* 8, 534–542 [2005]

Swierczek K, Copik AJ, Swierczek SI and Holz RC, Molecular Discrimination of Type-I over Type-II Methionyl Aminopeptidases, *Biochemistry* 44, 12049-12056 [2005].

Tahirov TH, Oki H, Tsukihara T, Ogasahara S, Yutani K, Ogata K, Izu Y, Tsunasawa S and Kato I, Crystal structure of Methionine Aminopeptidase from hyperthermophile *Pyrococcus furiosus. Journal of Molecular Biology* 284, 101-124 [1998]

Tahirov TH, Oki H, Tsukihara T, Ogasahara S, Yutani K, Ogata K, Izu Y, Tsunasawa S and Kato I, Crystal structure of Methionine Aminopeptidase from hyperthermophile *Pyrococcus furiosus. Journal of Molecular Biology* 284, 101-124 [1998]

Takeda M and Webster RE, Protein chain initiation and deformylation in *B. subtilis* homogenates. *Proceedings of National Academy of Sciences USA* 60, 1487–1494 [1968]

Takeuchi N, Kawakami M, Omori A, Ueda T, Spremulli LL and Watanabe K, Mammalian mitochondrial methionyl-tRNA transformylase from bovine liver; Purification, characterization, and gene structure. *Journal of Biological Chemistry* 273,15085-15090 [1998].

Tang XB, Si SY and Zhang YQ, Identification of a new peptide deformylase gene from *Enterococcus faecium* and establishment of a new screening model targeted on PDF for novel antibiotics. *Biomedical Environmental Sciences* 17,350-358 [2004]

Teo JWP, Thayalan P, Beer D, Yap ASL, Nanjundappa M, Ngew X, Duraiswamy J, Liung S, Dartois V, Schreiber M, Hasan S, Cynamon M, Ryder NS, Yang X, Weidmann B, Bracken K, Dick T and Mukherjee K, Peptide deformylase inhibitors as potent antimycobacterial agents. *Antimicrobial Agents and Chemotherapy* 50, 3665–3673 [2006]

Thompson JD, Gibson TJ, Plewniak F, Jeanmougin F and Higgins DG, The CLUSTAL-X windows interface: flexible strategies for multiple sequence alignment aided by quality analysis tools. *Nucleic Acids Research* 25, 4876–4882 [1997]

Thongboonkerd V, Luengpailin J, Cao J, Pierce WM, Cai J and Klein JB, Fluoride exposure attenuates expression of *Streptococcus pyogenes* virulence factors. *Journal of Biological Chemistry* 277, 16599–16605 [2002]

Towbin H, Staehelin T and Gordon J, Electrophoretic transfer of proteins from polyacrylamide gels to nitrocellulose sheets: procedure and some applications. *Proceedings of the National Academy of Sciences USA* 76, 4350–54 [1979]

Tsumoto K, Shinoki K, Kondo H, Uchikawa M, Juji T and Kumagai I, Highly efficient recovery of functional single-chain Fv fragments from inclusion bodies overexpressed in *Escherichia coli* by controlled introduction of oxidizing reagents—application to a human single-chain Fv fragment. *Journal of Immunology Methods* 219, 119–129 [1998]

Tsunasawa S, Izu Y, Miyagi M and Kato I, Methionine aminopeptidase from the hyperthermophilic Archaeon *Pyrococcus furiosus*: molecular cloning and overexpression in *Escherichia coli* of the gene, and characteristics of the enzyme. *Journal of Biochemistry* 122, 843–850 [1997]

Van Aller GS, Nandigama R, Petit CM, DeWolf WE,, Quinn CJ, Aubart KM, Zalacain M,. Christensen SB, Copeland RA, and Lai Z Mechanism of time-dependent inhibition of polypeptide deformylase by actinonin. *Biochemistry* 44, 253-260 [2005]

Varshavsky A, The N-end rule pathway of protein degradation. *Genes to Cells* 2, 13-28 [1997]

Vasina JA and Baneyx F, Expression of aggregation prone recombinant proteins at low temperatures: a comparative study of the *Escherichia coli* cspA and tac promoter systems. *Protein Expression and Purification* 9, 211-218 [1997]

Vetro JA and Chang YH, Yeast methionine aminopeptidase type 1 is ribosome-associated and requires its N-terminal zinc finger domain for normal function *in vivo*. *Journal of Cellular Biochemistry* 85, 678-88 [2002]

Vincentelli R, Bignon C, Gruez A, Canaan S, Sulzenbacher G, Tegoni M, Campanacci V and Cambillau C, Medium-scale structural genomics: Strategies for protein expression and crystallization. *Accounts of Chemical Research* 36, 165–172 [2003]

Vogt VM, Purification and properties of an aminopeptidase from *Escherichia coli*. *Journal of Biological Chemistry* 245, 4760–4769 [1970]

Walker JE, Lutter R, Dupuis A and Runswick MJ, Identification of the subunits of F1F0-ATPase from bovine heart mitochondria. *Biochemistry* 30, 5369-5378 [1991].

Walker KW and Bradshaw RA, Yeast methionine aminopeptidase I can utilize either Zn^{2+} or Co^{2}+ as a cofactor: A case of mistaken identity? *Protein Science* 7, 2684-2687 [1998]

Walker KW and Bradshaw RA, Yeast Methionine Aminopeptidase I: Alteration of Substrate specificity by site-directed mutagenesis. *Journal of Biological Chemistry* 274, 13403–13409 [1999]

Waller JP, The NH2 terminal residue of the proteins from cell-free extract of *E. coli*. *J*ournal of *Mol*ecular *Biol*ogy 7, 483-496 [1963]

Wan L, Zing L, Chen L, Huang Q, Li S, Lu Y, Li Y, Ching J and Lu X .Immunotoxin containing humanized single chain fragment variable antibody against CTLA4 and the N terminal fragment of a human perforin, *Protein expression and purification* 48**,**307-313 [2006]

Wang J, Sheppard GS, Lou P, Kawai M, Park C, Egan DA, Schneider A, Bouska J, Lesniewski R and Henkin J, Physiologically relevant metal cofactor for methionine aminopeptidase-2 is manganese. *Biochemistry* 42, 5035-5042 [2003]

Wang WL, Chai SC, Huang M, He HZ, Hurley TD, Ye QZ, Discovery of inhibitors of *Escherichia coli* methionine aminopeptidase with the Fe(II)-form selectivity and antibacterial activity. *Journal of Medicinal Chemistry* 51, 6110–6120 [2008]

Warner DF and Mizrahi V, Mycobacterial genetics in target validation. *Drug Discovery Today: Technologies* 1, 93-98 [2004]

Watterson SJ, Mitra S, Swierczek SI, Bennett B, Holz RC, Kinetic and spectroscopic analysis of the catalytic role of H79 in the methionine aminopeptidase from *Escherichia coli*. *Biochemistry* 47, 11885-11893 [2008]

Wei Y and Pei D, Continuous spectrophotometric assay of peptide deformylase. *Analytical Biochemistry* 250, 29–34 [1997]

Weng M, Zheng ZL, Bao W, Cai YJ, Yin Y, and Zou GL, Enhancement of oxidative stability of the subtilisin nattokinase by site-directed mutagenesis expressed in *Escherichia coli*. *Biochimica et Biophysica Acta* 1794, 1566–1572 [2009]

White TA and Kell DB, Comparative genomic assessment of novel broad-spectrum targets for antibacterial drugs. *Computational and Functional Genomics* 5, 304-327 [2004]

Whitmore L and Wallace BA, Protein secondary structure analyses from circular dichroism spectroscopy: methods and reference databases. *Biopolymers* 89, 392–400 [2008]

WHO,Global map and information on XDR-TB, [2009]

WHO,GlobalTuberculosisControl:Epidemiology,Strategy,Financing, [2009]

WHO, Global tuberculosis control—Surveillance, planning, financing,[2005]

Wingfield P, Graber P, Turcatti G, Movva NR, Pelletier M, Craig S, Rose K and Miller CG, Purification and characterization of a methionine-specific aminopeptidase

from *Salmonella typhimurium European Journal of Biochemistry* 180, 23-32 [1989]

Winograd E, Pulido MA and Wasserman M, Production of DNA-recombinant polypeptides by Tac inducible vectors using micromolar concentrations of IPTG. *Biotechniques* 14, 886-887, [1993]

Wirth T, Hildebrand F, Allix-Béguec C, Wölbeling F, Kubica T, Kremer K, van Soolingen D, Rüsch-Gerdes S, Locht C, Brisse S, Meyer A, Supply P and Niemann S, Origin, Spread and Demography of the *Mycobacterium tuberculosis* Complex. *PLoS Pathogens* 4, e1000160 [2008]

Wong C, Essentiality of methionine aminopeptidase in *staphylococcus aureus*, M.Phil Dissertation, *University of Honkong* [2005]

Woycechowsky KJ, Choutko A, Vamvaca K and Hilvert D, Relative tolerance of an enzymatic molten globule and its thermostable counterpart to point mutation. *Biochemistry* 47, 13489–13496 [2008]

Yan C, Lunjiang L, Runsheng C, Ongchuan B, Jiangang Y and Boqin Q, Molecular dynamics simulation of site-directed mutagenesis of HIV-1 Tat *trans* –activator. *Chinese Science Bulletin* 44,708-711 [1999]

Yang G, Kirkpatrick RB, Ho T, Zhang GF, Liang PH and Johanson KO, Steady-state kinetic characterization of substrates and metal-ion specificities of the full-length and N-terminally truncated recombinant human methionine aminopeptidases (type 2). *Biochemistry* 40, 10645–10654 [2001]

Yasuda M, Murakami Y, Sowa A, Ogino H and Ishikawa H, Effects of additives on refolding of a denatured protein. *Biotechnology progress* 14, 601-606 [1998]

Ye QZ, Xie SX, Huang M, Huang WJ, Lu JP and Ma ZQ, Metalloform-selective inhibitors of *Escherichia coli* methionine aminopeptidase and X-ray structure of a

Mn(II)-form enzyme complexed with an inhibitor. *Journal of American Chemical Society* 126, 13940–13941 [2004]

Ye QZ, Xie SX, Ma ZQ, Huang M and Hanzlik RP, Structural basis of catalysis by monometalated methionine aminopeptidase. *Proceedings of National Academy of Sciences USA* 103, 9470-9475 [2006]

Yeh I, Hanekamp T, Tsoka S, Karp PD and Altman RB, Computational analysis of *Plasmodium falciparum* metabolism: Organizing genomic information to facilitate drug discovery. *Genome Research* 14, 917–924 [2004]

Yildir C, Onsan ZI and Kirdar B, Optimization of starting time and period of induction and inducer concentration in the production of the restriction enzyme *EcoRI* from recombinant *Escherichia coli* 294. *Turkish Journal of Chemistry* 22, 221-226 [1998]

Yoo JS, Zheng CJ, Lee S, Kwak JH and Kim WG, Macrolactin N, a new peptide deformylase inhibitor produced by *Bacillus subtilis*. *Bioorganic and Medicinal Chemistry Letters* 15, 4889-4892 [2006]

Yoon HJ, Kim HL, Lee SK, Kim HW, Kim HW and Lee JY, Crystal structure of peptide deformylase from *Staphylococcus aureus* in complex with actinonin, a naturally occurring antibacterial agent. *Proteins: Structure and Function and Genetics* 57, 639–642 [2004]

You C, Lu H, Sekowska A, Fang G, Wang Y, Gilles AM and Danchin A, The two authentic methionine aminopeptidase genes are differentially expressed in *Bacillus subtilis*. *BMC Microbiology* 5, 57 [2005]

You CH, Lu HY, Sekowska A, Fang G, Wang YP, Gilles A and Danchin A, The two authentic methionine aminopeptidase genes are differentially expressed in *Bacillus subtilis*. *BMC Microbiology* 5, 57 [2005]

Yuan H, Chai SC, Lam CK, Howard Xu H and Ye QZ, Two methionine aminopeptidases from *Acinetobacter baumannii* are functional enzymes. *Bioorganic and Medicinal Chemistry Letters* 21, 3395-3398 [2011]

Yuan Z and White RJ, The evolution of peptide deformylase as a target: contribution of biochemistry, genetics and genomics. *Biochemical pharmacology* 30, 1042-1047 [2006]

Zhang X, Chen S, Hu Z, Zhang L and Wang H, Expression and characterization of two functional methionine aminopeptidases from Mycobacterium tuberculosis H37Rv. *Current Microbiology* 59, 520-525 [2009b]

Zhang Y and Amzel L M, Tuberculosis Drug Targets. *Current Drug Targets* 3, 131-154 [2002]

Zhang Y and Yew, Mechanisms of drug resistance in *Mycobacterium tuberculosis* State of the art series. Drug-resistant tuberculosis. *The International Journal of Tuberculosis and Lung Disease* 13, 1320-1330 [2009a]

Zhang Y, Griffith EC, Sage J, Jacks T and Liu JO, Cell cycle inhibition by the anti-angiogenic agent TNP-470 is mediated by p53 and p21WAF1/CIP1. *Proceedings of National Academy of Sciences USA* 97, 6427–6432 [2000]

Zhang Y, Persistent and dormant tubercle bacilli and latent tuberculosis. *Frontiers in Bioscience* 9, 1136–1156 [2004]

Zhang Y, The magic bullets and tuberculosis drug targets. *Annual Reviews on Pharmacology and Toxicology* 45, 529–564 [2005]

Zhou Z, Song X, Li Y and Gong W, Unique structural characteristics of peptide deformylase from pathogenic bacterium *Leptospira interrogans*. *Journal of Molecular Biology* 339, 207–215 [2004]

Zuo S, Guo Q, Ling C and Chang YH, Evidence that two zinc fingers in the methionine aminopeptidase from *Saccharomyces cerevisiae* are important for normal growth, *Molecular General Genetics* 246, 247–253 [1995]

Annexure I

List of major instruments used in the study

Equipment	Model
PCR machine	ep*gradient*- Eppendorf, India
Gel documentation system	G-box-Syngene, India
Electrophoresis unit	Genei, India
Western blotting unit	Genei, India
Microtiterplate reader	Biorad-680XR, India
Sonicator	VCX-750, Sonics, USA
Nanodrop	Thermo Scientific, USA
Vacuum concentrator	5301-Eppendorf, India
Lyophiliser	hDB-5503, Operon, Korea
Laminar Air Flow Chamber	Clean Air System, India
UV-VIS Spectrophotometer	UV-160A, Shimadzu, Japan
CD-Spectropolarimeter	Jasco-J810, Japan
Atomic absorption spectrophotometer	Varian -AA775, USA
Centrifuge	Eppendorf, Germany; Kuboto, Japan
Autoclave	Tomy, Japan
Incubator	New Brunswick Scientific, USA
Weighing Balance	Mettler Toledo, Mumbai, India
pH meter	Systronics, India
Deep freezer	Operon, Korea
Incubating water bath	Julabo, Germany

Annexure II

A. List of Publications

I. Scientific publications in SCI journals

1. **Sai Shyam Narayanan** and Kesavan Madhavan Nampoothiri (2011) Molecular cloning, over expression and characterization of two methionine aminopeptidases (MAP) from *M. tuberculosis* H37Rv (manuscript communicated)
2. **Sai Shyam Narayanan,** Pandian Sokkar, Murugesan Ramachandran and Kesavan Madhavan Nampoothiri (2011) Glycine in the conserved motif III modulates the thermo-stability and oxidative stress resistance of peptide deformylase in *Mycobacterium tuberculosis*. *FEMS Microbiology Letters***,** 320(1), 40-47.doi: 10.1111/j.1574-6968.2011.02289.x.
3. **Sai Shyam Narayanan**, Ajeena Ramanujan, Shyam Krishna, Kesavan Madhavan Nampoothiri (2008) Purification and biochemical characterization of Methionine Aminopeptidase (MetAP) from *Mycobacterium smegmatis* mc^2155, *Applied Biochemistry and Biotechnology*, 151 (2-3) , 512-521. DOI: 10.1007/s12010-008-8227-y (Cited 4 times in SCI journals).
4. K.M. Nampoothiri, R. Rubex, A.K. Patel, **S.S. Narayanan**, S. Krishna, S.M. Das and A. Pandey (2008) Molecular cloning, over-expression and biochemical characterization of hypothetical β-lactamase of *Mycobacterium tuberculosis* H37Rv, *Journal of Applied Microbiology*, 105 (1), 59-67.DOI:10.1111/j. 13652672. 2007. 03721.x. (Cited 2 times in SCI journals)

II. Posters presented at National / International conferences

1. **Sai Shyam N** and K. Madhavan Nampoothiri (2011) Molecular studies on N-terminal Methionine excision enzymes of *Mycobacterium tuberculosis.* Proceedings of 23rd Kerala Science Congress. January 29-31. P 57 (**Kerala State Young Scientist Award for Biotechnology , 2011**)
2. **Sai Shyam N** and K. Madhavan Nampoothiri (2010) Molecular discrimination of Mycobacterium peptide deformylase from other prokaryotic and eukaryotic deformylases. Proceedings of 7th Convention of Biotech Research Society of India (BRSI) and International conference on genomic sciences-Recent trends, November 12-14, at Madurai Kamaraj University, Madurai, India P 142.
3. **Sai Shyam N**, Shyam Krishana and K.Madhavan Nampoothiri (2008) Peptide processing enzymes of *Mycobacterium tuberculosis* as potential drug targets, Proceedins of International symposium on "emerging trends in tuberculosis research" December 1-3, at International Center for Genetic Engineering and Biotechnology (ICGEB), New Delhi, India. P 68.
4. **Sai Shyam N** and K. Madhavan Nampoothiri (2008) Studies on MAP A, the hypothetical methionine aminopeptidases from *M. tuberculosis* H37Rv, Proceedings of 5th Convention of Biotech Research Society of India (BRSI) and International congress on "bioprocesses in food industries" November 6-8, at Osmania University, Hyderabad, India.P 183.
5. **Sai Shyam N**, Ajeena Ramanujam, Shyam Krishna and K.Madhavan Nampoothiri (2007) Methionine aminopeptidases: Unique peptide processing enzyme from Mycobacterium, at "Mycobacterium mini-symposium",

proceedings of 4th Convention of Biotech Research Society India (BRSI) and International conference on "new horizons in biotechnology" at National Institute for interdisciplinary Science and Technology (NIIST), Trivandrum, India. P.69

6. **Sai Shyam N**, K.Madhavan Nampoothiri and Ashok Pandey (2006) Cloning and Over expression of the peptide deformylase from *Mycobacterium tuberculosis* H37 Rv, Proceedings of the 3rd Convention of Biotech Research Society India (BRSI) and international conference on "Exploring Horizons in biotechnology: a global venture" November 2-4, at Sardar Patel University and Charutar Vidyamandal, Vallabh Vidyanagar -388 120, Gujarat, India. p 288. (**Best poster award in Medical Biotechnology**).

III. Nucleotide submission in GenBank

1. Mohandas SP, Ravikumar S, **Narayanan SS** and Nampoothiri KM (2011) *Streptomyces yunnanensis* strain NII716, 16S ribosomal RNA gene, partial sequence GenBank Accession No: JF732920.

B. Awards / Honours

1. Kerala State-Young Scientist Award for Biotechnology (2011), at 23rd Kerala Science Congress, Trivandrum January 29-31.
2. UGC-NRCBS Visiting fellowship (2009) to visit and utilize NRCBS facility at School of biological sciences, Madurai Kamaraj University, Madurai.
3. Best poster presentation award in Medical Biotechnology (2006) at 3rd convention of Biotech Research Society of India (BRSI), Gujarat November 2-4.
4. CSIR-Senior Research Fellowship- 2008-2011.